5.0 CONCEPTUAL MODEL OF GROUNDWATER FLOW IN THE AQUIFER

The conceptual model for groundwater flow in the Southern Carrizo-Wilcox GAM area is based on the hydrogeologic setting, described in Section 4. The conceptual model is a simplified representation of the hydrogeological features which govern groundwater flow in the aquifer. These include the hydrostratigraphy, hydraulic properties, and stresses such as pumping and recharge, and the boundaries. Each of the elements of our conceptual model is described below. The schematic diagram in Figure 5.1 depicts the conceptual hydrogeologic model of groundwater flow in the Carrizo-Wilcox aquifer. Figure 5.1 represents the aquifer under predevelopment conditions. With the addition of pumping as the resource is developed, an additional discharge from each aquifer layer would occur. The pumping discharge would be depicted by an additional arrow from each pumped layer in Figure 5.1.

The conceptual model distinguishes four layers in the Carrizo-Wilcox aquifer, consisting of the lower, middle, and upper Wilcox layers in addition to the Carrizo Sand. These layers tie in with the subdivision of the aquifer in the Central Carrizo-Wilcox GAM, except for the top of the middle Wilcox. The Carrizo-Wilcox aquifer is overlain by the Reklaw Formation, representing the confining unit downdip of the Carrizo outcrop, separating the major Carrizo-Wilcox aquifer from the shallower Queen City and Sparta minor aquifers. For the Southern Carrizo-Wilcox GAM, the Reklaw confining unit and the overlying Queen City aquifer unit are represented as separate layers in the model to properly account for vertical flow across the Reklaw. Southeast, and down dip of the Queen City outcrop, a wedge of younger sediments overly the aquifer. In this part of the study area, vertical flow between the Queen City aquifer and the water table is approximated using general-head boundary conditions.

In addition to identifying the hydrostratigraphic layers of the aquifer, the conceptual model also defines the mechanisms of recharge and discharge, as well as groundwater flow through the aquifer. Recharge occurs mainly in the outcrop areas of the Carrizo-Wilcox layers along the northwestern edge of the study area. Similarly, recharge to the shallow Queen City aquifer occurs through infiltration in the outcrop area. Additional recharge to the Carrizo-Wilcox aquifer may occur by cross-formational flow from the Queen City aquifer through the Reklaw confining unit (Figure 5.1) in areas where the vertical gradient has been reversed by Carrizo

pumping. However, in the confined section, vertical gradients are naturally upward from the Carrizo-Wilcox aquifer to the overlying Queen City. Cross-formational flow between the different layers within the Carrizo-Wilcox aquifer may redistribute groundwater, recharged in the outcrops, into different aquifer layers as a result of variations in hydraulic properties and topography (Figure 5.1).

Most of the precipitation falling on the outcrop runs off into the small creeks, which discharge through major streams out of the model area. In addition to runoff, a significant portion of the precipitation is lost by evapotranspiration (ET), leaving only a small fraction of the precipitation to infiltrate into the subsurface and recharge the aquifer. Diffuse recharge occurs preferentially in topographically higher interstream areas within the outcrops. Focused recharge along streams can occur when the water table in the aquifer is below the stream-level elevation. If stream levels are lower than surrounding groundwater levels, groundwater discharges to the streams resulting in gaining streams. In this case, water levels in the valley are typically close to land surface and some of the shallow groundwater in this area can be lost to evapotranspiration.

Recharge is a complex function of precipitation, soil type, geology, water level and soil moisture, topography, and ET. Precipitation, ET, water-table elevation, and soil moisture vary spatially and temporally, whereas soil type, geology, and topography vary spatially. In addition to natural phenomena, water levels are affected by pumping and man-made surface-water reservoirs, which may in turn affect recharge. Under undisturbed conditions (e.g., prior to pumping), groundwater recharge is balanced by natural discharge of groundwater. To maintain a state of dynamic equilibrium, groundwater withdrawal by pumping must be balanced by (1) an increase in recharge, (2) a decrease in natural discharge, (3) a loss of storage, (4) or a combination of these factors. Balancing pumping by increased recharge implies that recharge was rejected prior to the onset of pumpage (Theis, 1940; Domenico and Schwartz, 1990). This occurs primarily in outcrop areas of aquifers where the water table is near land surface.

The onset of pumpage and the concomitant water-level decline induces an increase in recharge, because less water is captured by evapotranspiration as the water table declines below the root zone and vertical gradients in the recharge zone increase. Freeze (1971) showed for an unconfined aquifer that the increase in recharge occurs initially without affecting the natural discharge even though pumpage continues to increase (Figure 5.2a). After some time, the

recharge stabilizes as the increased pumpage is offset by a decrease in the natural discharge (i.e., gaining streams). With continued increase in pumpage and concomitant decrease in basin discharge, the conditions could become 'unstable', whereby the decrease in natural discharge can no longer feed the increased pumpage (Figure 5.2b). Water levels decline to a depth below which the maximum recharge rate can no longer be sustained, because of consistently drier conditions in the unsaturated zone and increased evapotranspiration during redistribution (Freeze, 1969). Compared to the hypothetical system described by Freeze (1971), the unconfined-confined system of the Carrizo-Wilcox aquifer will exhibit a more complex response, whereby the water-table response in the outcrop to pumpage in the confined section would be delayed.

Our conceptual model for the southern Carrizo-Wilcox aquifer is considered to represent a stable groundwater basin, as indicated in Figure 5.2b, though with a limited rejected recharge potential particularly toward the southwest. That is, depth to water during predevelopment conditions is typically at or below the root zone and a further water-level decline due to pumpage does not decrease evapotranspiration. This implies that effective recharge during predevelopment conditions is expected to be at or slightly less than current average recharge as a result of pumpage over the last several decades.

In the eastern portion of the study area, groundwater from the aquifer discharges to local creeks and major streams throughout the area, contributing to the baseflow of the major streams. In addition, discharge from the Carrizo-Wilcox aquifer occurs by cross-formational flow through the overlying Reklaw Formation into the Queen City. Similarly, discharge from the Queen City aquifer is to the streams in the Queen City outcrop area or through leakage across the younger formations above the Queen City aquifer in the downdip section of the aquifer.

Groundwater flow within the aquifers is controlled by the topography, the structure, and the permeability variation within the different layers. The available data suggest that the Carrizo has the highest average hydraulic conductivity, whereas the underlying Wilcox layers have significantly lower conductivities. Groundwater flow in the Carrizo-Wilcox aquifer is generally downdip to the southeast turning more to the east farther downdip owing to the lower topographic elevations in the northeastern part of the model.

The heterogeneity and structure of the aquifer affect the water quality. The structural dip of the aquifer layers affects the extent of the fresh-water section, which is greater in the southern part compared to the northeastern part, where the dip of the strata increase (Hamlin, 1988). Fault zones may limit downdip flow of fresh groundwater, as indicated by higher total dissolved solids (TDS) southeast of the strike-oriented faults updip of the growth fault zone (Hamlin, 1988). Even though delineating high-TDS groundwater is important for water availability determinations, water quality assessment is not an explicit requirement of the current GAM. However, a preliminary characterization of water quality for the Carrizo-Wilcox aquifer in the study area is given in Appendix F.

The vertical boundary along the southern edge of the model corresponds to the updip limit of the growth faults, displacing mainly Wilcox and deeper strata downward (Figure 5.1). This boundary is represented by a no-flow boundary in the model, representing the stagnant zone associated with the overall downdip hydraulic gradient of the Carrizo-Wilcox aquifer system and the general updip gradient of the geopressured zone southeast of the growth fault zone. As a result, discharge from the confined section of the Carrizo-Wilcox aquifer is through upward cross-formational flow or pumping.

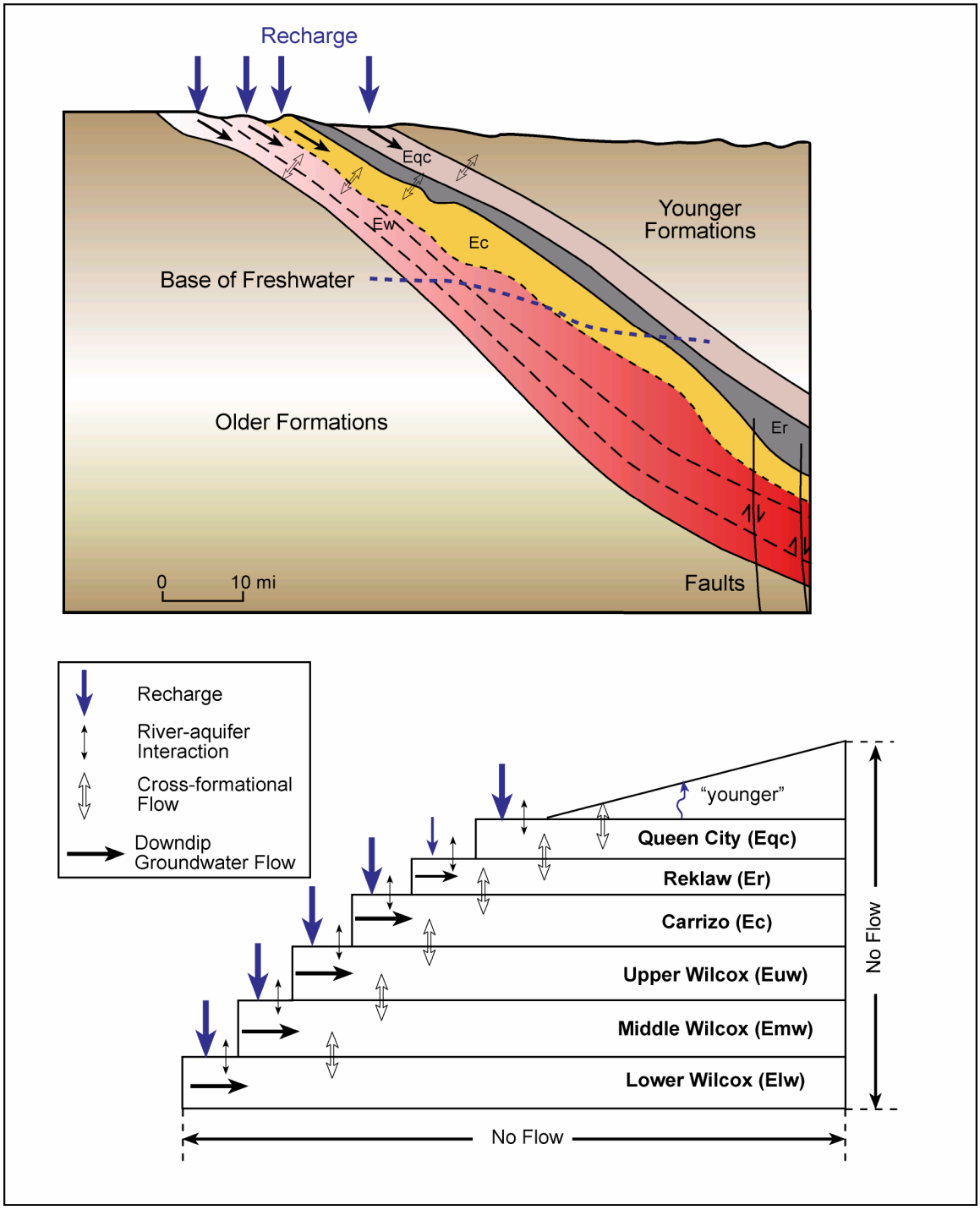

Figure 5.1 **Conceptual groundwater flow model for the Southern Carrizo-Wilcox GAM.**

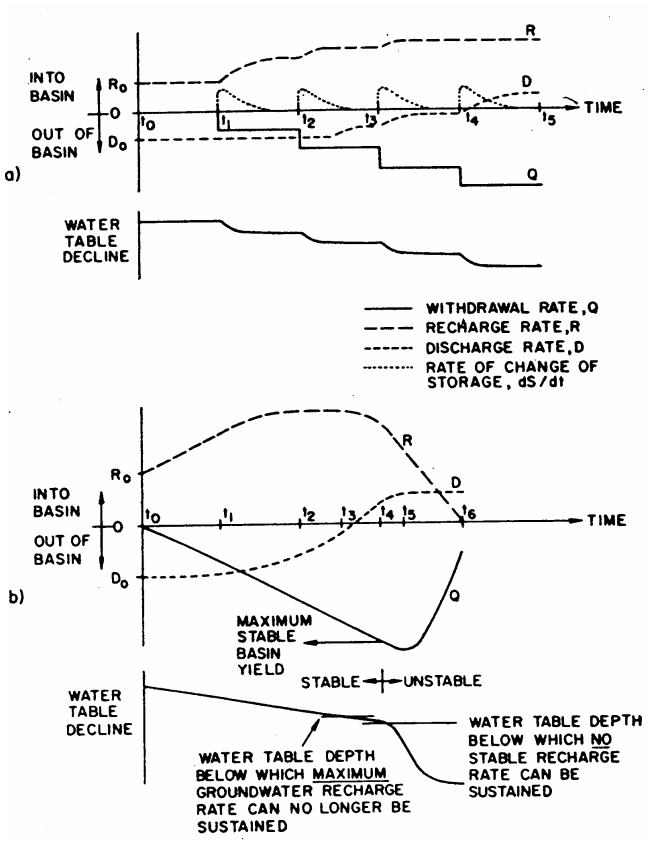

Figure 5.2 Schematic diagram of transient relationships between recharge rates, discharge rates, and withdrawal rates (from Freeze, 1971).

6.0 MODEL DESIGN

Model design represents the process of translating the conceptual model for groundwater flow in the aquifer (Section 5) into a numerical representation which is generally described as the model. The conceptual model for flow defines the required processes and attributes for the code to be used. In addition to selection of the appropriate code, model design includes definition of the model grid and layer structure, the model boundary conditions, and the model hydraulic parameters. Each of these elements of model design and their implementation are described in this section.

6.1 Code and Processor

The code selected for the Southern Carrizo-Wilcox GAM and for all GAMs developed by or for the TWDB is MODFLOW-96 (Harbaugh and McDonald, 1996). MODFLOW-96 is a multi-dimensional, finite-difference, block-centered, saturated groundwater flow code which is supported by enhanced boundary condition packages to handle recharge, ET, streams (Prudic, 1988), and reservoirs (Fenske et al., 1996).

The benefits of using MODFLOW for the Southern Carrizo-Wilcox GAM include; (1) MODFLOW incorporates the necessary physics represented in the conceptual model for flow described in Section 5 of this report, (2) MODFLOW is the most widely accepted groundwater flow code in use today, (3) MODFLOW was written and is supported by the United States Geological Survey (USGS) and is public domain, (4) MODFLOW is well documented (McDonald and Harbaugh, 1988; Harbaugh and McDonald, 1996), (5) MODFLOW has a large user group, and (6) there are a plethora of graphical user interface programs written for use with MODFLOW.

To the extent possible, we have developed the MODFLOW data sets to be compatible with Processing MODFLOW for Windows (PMWIN) Version 5.3 (Chiang and Kinzelbach, 1998). The size of the GAM and the complexity of our application precludes 100-percent compatibility with PMWIN, as well as many other interfaces.

We have executed the model on x86 compatible (i.e. Pentium or Athlon) computers equipped with the Windows 2000 operating system. MODFLOW is not typically a memory-

intensive application in its executable form. However, if any preprocessor (such as PMWIN) is used for this size and complexity of model, at least 256MB of RAM is recommended.

6.2 Model Layers and Grid

Consistent with the model hydrostratigraphy described in Section 4.1 and the conceptual flow model detailed in Section 5, we have divided the Southern Carrizo-Wilcox GAM into six model layers. MODFLOW-96 numbers layers from top (nearest to ground surface) to bottom and this is the order by which each layer will be introduced. Layer 1 is the Queen City Formation east of the Frio River and the El Pico Clay west of the Frio River. Layer 2 is the Reklaw Formation east of the Frio River and the equivalent Bigford Formation west of the Frio River. Layer 3 is the Carrizo Sand, the primary aquifer in the study area (Klemt et al., 1976). Layer 4 is the upper Wilcox, which is present only in the confined portion of the aquifer. Layer 5 is the middle Wilcox and Layer 6 is the lower Wilcox. The middle and lower Wilcox are primarily used as a water resource in their outcrops. The model layers are shown with the model hydrostratigraphy in Figures 4.1.1 and 5.1.

The Southern Carrizo-Wilcox GAM model area is bounded laterally on the northeast by the surface water basin divide between the Guadalupe and Colorado rivers and to the southwest by the Rio Grande. The updip limit of the model is defined by the outcrop of the Carrizo-Wilcox aquifer at the contact with the Midway Formation. The southern boundary of the model is defined by the updip limit of the Wilcox growth fault zone (Bebout et al., 1982). MODFLOW-96 requires a rectilinear grid and also requires an equal number of rows for all columns. As a result, the model area is constrained to being a rectangular grid. Typically, one axis of the model grid is aligned parallel to the primary direction of flow (this is to the southeast for the Southern Carrizo-Wilcox GAM). The model area was determined by imposing the preceding constraints with the additional constraint of minimizing the number of model grid cells. The model grid origin is located at GAM Coordinates (5,062,000, 18,280,000), with the x-axis rotated positive 0.641 radians (E 36.727° N). The GAM standard requires that grid cells be square of a uniform dimension of 1 mile (area of 1 square mile). The model has 217 columns and 112 rows for a total number of grid cells per layer of 24,304. As discussed below, not all of these grid cells are active in the model. Figure 6.2.1 shows the entire model grid. Included on

this figure is an inset with an enlargement of Frio County to show the model grid at the county scale.

Not all model grid cells are active grid cells. We defined the active area of each model layer by intersecting the layer grid with the geologic map and the growth fault boundaries to the south. Cells extending past the outcrop or downdip of the growth fault boundary were defined as inactive in the IBOUND array. If a cell was 50% or more in the outcrop, it was defined as active. Cells west of the Rio Grande on the southwestern boundary of the model were also made inactive on the assumption that the Rio Grande is a regional sink for the aquifer being modeled. After clipping the layers to their proper dimensions, Layers 1 through 6 had the following number of grid cell respectively, 11682, 12848, 13781, 13911, 14910, and 15674. The total number of active grid cells in the model grid is 82896.

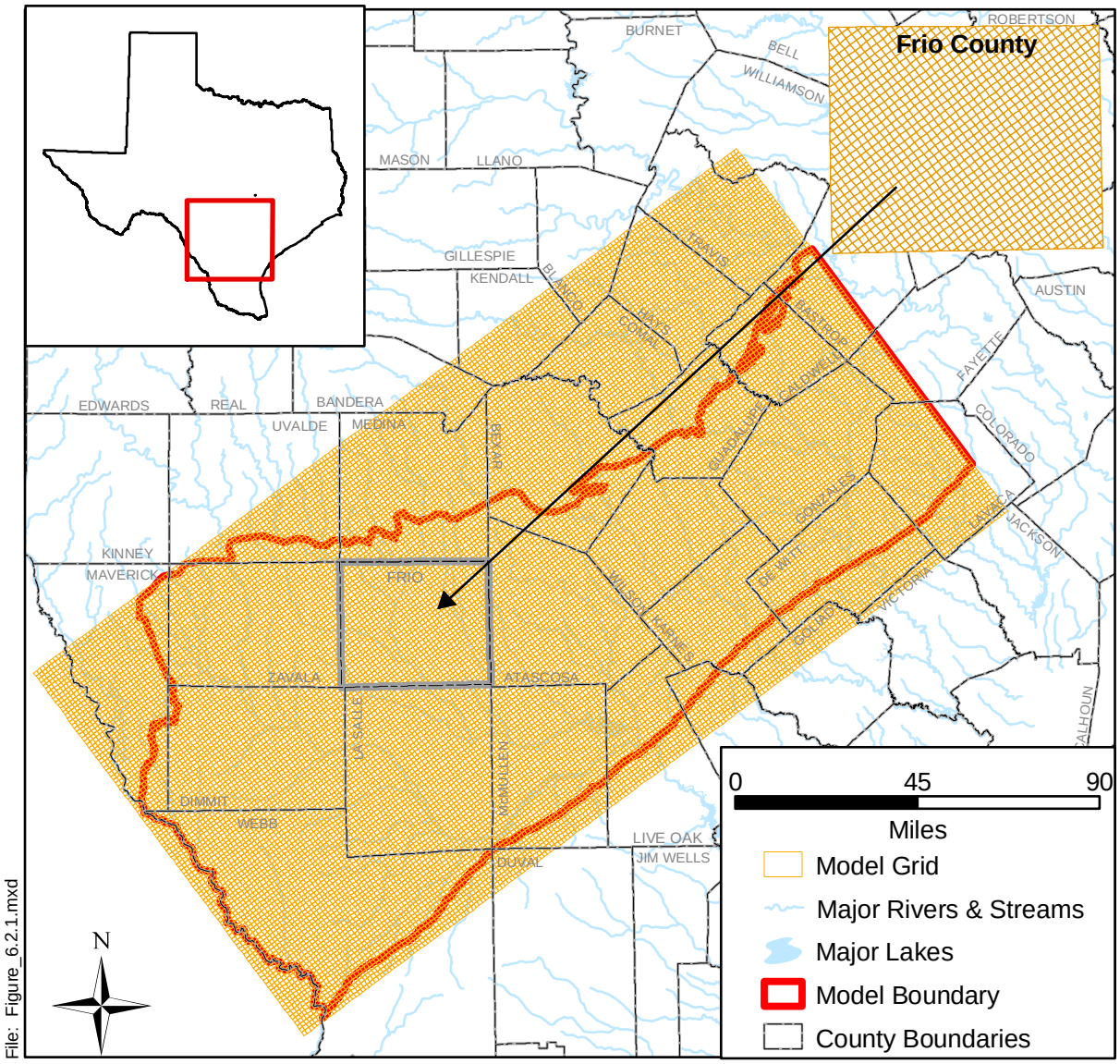

Figure 6.2.1 Southern Carrizo-Wilcox GAM model grid.

6.3 Boundary Condition Implementation

A boundary condition can be defined as a constraint put on the active model grid to characterize the interaction between the active simulation grid domain and the surrounding environment. There are generally three types of boundary conditions; specified head (First Type or Dirichlet), specified flow (Second Type or Neumann), and head-dependent flow (Third Type or Cauchy). The no-flow boundary condition is a special case of the specified flow boundary condition.

Boundaries can be defined as being time independent or time dependent. An example of a time dependent boundary might be a pumping flow boundary or a reservoir stage elevation. Because many boundaries require time dependent (transient) specification, the stress periods used by MODFLOW must be specified. A stress period in MODFLOW defines the minimum time period over which a boundary or model stress may remain constant. Each stress period may have a number of computational time steps which are some fraction of the stress period but over which boundaries remain constant. For this model, the stress periods have been set at one month. Therefore, all transient boundaries in the model cannot change over a period of less than one month.

Boundaries requiring specification include: layer lateral and vertical boundaries, surface water boundaries, recharge boundaries, and discharge boundaries caused by pumping. Lateral and vertical boundaries will be a combination of specified flow (no-flow, Second Type) or head-dependent flow boundaries (general head boundaries, Third Type). Surface water boundaries are head-dependent flow boundaries (Third Type). Recharge is a specified flow boundary (Second Type). Evapotranspiration (ET) is a head-dependent flow boundary (Third Type). Pumping discharge is a specified flow boundary (Second Type).

Figures 6.3.1 through 6.3.6 show the active and inactive grid cells along with the model boundary conditions for each of the six model layers, respectively. Implementation of the boundary conditions for the Southern Carrizo-Wilcox GAM is described below. Unless otherwise specified below, the boundary between the active and inactive cells is a no-flow boundary.

6.3.1 Lateral Model Boundaries

The lateral model boundaries have been defined to occur on the northeast at the drainage divide between the Guadalupe and Colorado rivers and to the southwest along the Rio Grande. Both of these boundaries are assumed to be groundwater divides which are equivalent to no-flow boundaries (Second Type). From a review of the predevelopment hydraulic head map, we concluded that the eastern model boundary is coincident with the groundwater flow direction and reasonably mimics a no-flow boundary. A no-flow boundary was also assigned to the southwestern model boundary with the assumption of insignificant underflow of the Rio Grande in the model area.

The applicability of no-flow boundaries was investigated further for the simulated historical period (1980 through 1999). A no-flow boundary was maintained at the Rio Grande during the transient and predictive model periods (1980-2050). For the northeastern model boundary, water levels were reviewed for the period from 1980 through 1999. Water levels were found to be reasonably constant given the scale of the model with a head decrease observed from a few feet up to 30 feet. Because specification of boundary heads across the northeastern model boundary is inherently uncertain, and because head decreases along the boundary are within the model head error, the northeastern boundary was maintained as a no-flow boundary throughout the transient historical simulation period. If pumping east of the boundary is equal or less than pumping west of the boundary, the assumed boundary is conservative. The northeastern boundary was also investigated for the predictive simulation period (2000-2050). Preliminary maps of drawdown provided by the Central Carrizo-Wilcox GAM team indicated that drawdowns over the predictive period were on the order of historical drawdowns and the no-flow boundary was maintained.

6.3.2 Vertical Boundaries

The model has a no flow boundary on the bottom of Layer 6 (the lower Wilcox) representing the marine shales of the Midway Formation. The upper model boundary is the free-water surface calculated in the outcrops of Layers 1 through 6. In downdip portions of the model where younger sediments overlie the Queen City, these sediments are represented by a general head boundary condition (Third Type). The initial vertical conductances of the general head boundaries were based upon a harmonic average of the hydraulic conductivities of the overlying units. The 1998 model of LBG-Guyton and HDR (1998) was used to estimate the hydraulic

conductances of the overlying younger units. The hydraulic heads associated with the general head boundaries were set equal to the water table as estimated using the regression equations of Williams and Williamson (1989).

6.3.3 Surface Water Implementation

Surface water acts as a head-dependent flow (Third Type) boundary condition for the top boundary of the active model grid cells (outcrop). The stream package (Prudic, 1988) and reservoir package (Fenske et al., 1996) are head-dependent flow boundary conditions that offer a first-order approximation of surface water/groundwater interaction. The stream-routing package will allow for stream-related recharge to be rejected during gaining conditions and for stream-related recharge to be induced during losing conditions. When pumping affects water levels near stream/aquifer connections, recharge will be included through stream loss.

The stream routing package requires designation of segments and reaches. A reach is the smallest division of the stream network and is comprised of an individual grid cell. A segment is a collection of reaches which are contiguous and do not have contributing or diverting tributaries. In MODFLOW, physical properties must be defined describing the hydraulic connection (conductance) between the stream and the aquifer. Stream flow rates are defined at the beginning of each segment for each stress period.

INTERA developed a GIS-based method for developing the reach and segment data coverages for MODFLOW. Figures 6.3.1 through 6.3.6 show the model grid cells which contain stream reaches in the model domain. Required physical properties of the reaches including stream width, bed thickness, and roughness are taken from the EPA River Reach data set (http://www.epa.gov/region02/gis/atlas/rf1.htm). The hydraulic conductivity used to define the hydraulic conductance between the aquifer and the stream was initially approximated based on the hydraulic conductivity of the underlying formation. Hibbs and Sharp, (1991) studied the hydraulic connection between the Colorado River and the alluvium and Carrizo-Wilcox aquifer near a Bastrop well field. They concluded that the connection between the river and the aquifer was very good and did not see hydraulic evidence for a low permeability river bed. Our initial approach was to keep the hydraulic conductivity of the stream bed high and relatively constant and allow the stream width taken from the EPA River Reach data set (RFI) to control the streambed conductance.

The stream routing package also requires specification of stream flow rate for each starting reach at each stress period. For predevelopment conditions, and for the historical period, no representative stream gage data exist for the majority of the stream segments. To handle this for the pre-development simulation, we have used mean flow rates from the EPA RF1 data set to specify the flow rate entering each model segment. The EPA RF1 data set contains mean flow rates estimated along the entire stream and coinciding with all of the modeled stream segments.

For the transient simulations, stream flows were based on historical records. However, because the stream gage coverage is sparse, stream flow rates required estimation at the majority of stream segments. The approach we employed to develop ungaged stream segment flow rates has the following assumptions: (1) gages in close proximity behave similarly, (2) the RF1 average stream segment stream flow estimates are accurate, (3) a gage's distribution of monthly stream flow is lognormal, and (4) the standard deviation of the log of monthly flow rate at an ungaged location is equal to the standard deviation of the log of monthly flow rate at a nearby ungaged location. We have checked assumptions 1 through 3 and have found they generally do hold for the model region. Assumption 4 cannot be definitively established in the current domain, due to lack of data for cross-validation.

To calculate the ungaged stream segment flow rates at each monthly stress period, we first constructed the monthly distribution of log flow rate at our gaged stream locations and calculated the standard deviation of that distribution. From the EPA RF1 data set we have the mean flow rates for all segments. For example, if for a given stress period the gaged monthly stream flow was equal to the 75^{th} percentile of the distribution, we would use the mean flow rate from the EPA RF1 data set with the standard deviation borrowed from the actual gaged flow distribution to estimate the 75^{th} percentile flow rate at the ungaged segment. This technique maintains the proper magnitude of flows at ungaged locations as constrained by the EPA RF1 mean flow estimates while superposing the flow variability based upon the nearest gaged data.

The MODFLOW reservoir package (Fenske et al., 1996) has been used to model reservoirs and lakes. Modeled reservoir properties include the hydraulic conductance between the lake and the aquifer and the reservoir stage as a function of stress period. Because reservoirs are in river valleys, the reservoir package must be integrated with the stream routing package. This is done by starting a new segment at the downstream side of each reservoir. The hydraulic

conductivity used to estimate the reservoir/aquifer hydraulic conductance was initially set to a constant, approximately based on the hydraulic conductivity of the underlying formation. Lake stage records were developed by reviewing records in the literature and by contacting various river authorities in the study area. These stage histories are provided in the data model delivered with this modeling report. Only two reservoirs were modeled in the GAM, Calaveras Lake and Victor Braunig Lake, both located in southern Bexar County.

Spring discharge records were reviewed for application in the Southern Carrizo-Wilcox GAM as drain boundary conditions (Type 3). However, as discussed in Section 4 of this report, there are no significant springs still flowing in the model area that are not coincident with stream reach cells (which provide a sufficiently similar boundary condition).

6.3.4 Implementation of Recharge

Because an evaluation of groundwater availability is largely dependent upon recharge (Freeze, 1971), it is an important model input parameter warranting careful examination and meaningful implementation. In typical model applications, recharge is either homogeneously defined as a percentage of the yearly average precipitation or calibrated as an unknown parameter. Unfortunately, recharge and hydraulic conductivity can be correlated parameters preventing independent estimation when using only head data constraints. Another compounding problem is that recharge is a complex function of precipitation rate and volume, soil type, water level and soil moisture, topography, and ET (Freeze, 1969). Precipitation, ET, water table elevation, and soil moisture are areally and temporally variable. Soil type, geology, and topography are spatially variable. For the GAM, recharge requires specification for steady-state conditions, for transient conditions from 1980 until 2000, for the transient drought of record, and for average conditions. Reliable tools for specification of recharge at watershed scale, or the regional model scale (1000s of square miles for the GAMs) do not currently exist.

As a tractable approach to dealing with recharge at the scale of this model, we have used SWAT (Soil Water Assessment Tool) to estimate diffuse recharge rates. SWAT was developed for the USDA Agricultural Research Service by the Blacklands Research Center in Temple, Texas. SWAT is a public-domain model. The SWAT Website where downloads and code-specific documentation can be found is http://www.brc.tamus.edi/swat/. SWAT provides a GIS-driven, watershed scale tool to estimate regional soil water balances, incorporating soils data

(USDA/NRCS STATSGO) with the USGS Multi-Resolution Land Characteristics (MRLC) data. SWAT uses standard techniques to track water after it reaches the ground as precipitation. SWAT uses the NRCS Curve Number Method (accounting for antecedent moisture conditions) to partition precipitation into runoff and infiltration. Infiltrating water either increases the soil moisture, is lost through ET, or continues down to the water table. We used the Hargreaves Method for estimating potential ET because it only requires estimates of monthly mean minimum and maximum temperatures which are available for the study area. Average daily net radiation is available within SWAT for month and degrees of latitude. The Hargreaves method is considered accurate for simulation periods that are equal to, or larger than, one month. This is consistent with one month stress periods and the assumptions underlying the NRCS curve-number method for estimating runoff. The potential ET is converted to an actual ET based on the vegetation size and type (determines maximum ET) and soil water availability (determines actual ET).

SWAT is used in an uncoupled mode to estimate several model inputs for MODFLOW. Consistent with the transient MODFLOW stress periods of one month, SWAT results were output in one month increments. However, SWAT simulations were carried out using daily time steps and precipitation/temperature data. Daily time steps (or less) are necessary for approximating runoff during precipitation events. SWAT was simulated for the time period from 1975 through 1999 to coincide with the spinup, calibration and transient model simulation periods.

For each MODFLOW stress period, SWAT calculates: (1) the recharge rate for the recharge package, (2) the ET max for the ET package, and (3) the extinction depth for the ET package. The SWAT estimate of shallow recharge is used as a recharge flux in MODFLOW. SWAT accounts for ET which may occur in the vadose zone. However, in our method of application, SWAT does not account for groundwater transpiration. To account for groundwater ET, the "surplus" ET from SWAT (ET max – ET actual) was applied as ET max in the groundwater ET package in MODFLOW. For each month simulated, SWAT calculates a rooting depth representative of the season, vegetative cover, and soil type. This rooting depth is passed through to MODFLOW as the extinction depth required by the MODFLOW ET Package. As a result, ET from groundwater will occur when the water table (as simulated by MODFLOW) is above the extinction depth and there is surplus ET potential for that particular stress period.

Appendix E provides a more detailed explanation of our use of SWAT in an uncoupled mode with MODFLOW.

For the predevelopment model, the SWAT estimates for recharge were averaged values taken from the 1975 to 1999 simulation. The ET max estimates were also averaged for this same time period for input into the MODFLOW ET package. The maximum soil rooting depth was used for the predevelopment model. In the transient simulation, recharge varies as a function of time as well as location.

SWAT was also used for implementing recharge in the predictive simulation period (2000-2050). Recharge was varied seasonally in the predictive simulations based upon monthly average recharge from the 1975 to 1999 simulation. For example, all of the January outputs for the period from 1975 through 1999 were averaged, all of the February outputs were averaged, etc. Predictive simulations end with a drought-of-record. Recharge conditions for the drought-of-record were developed by running SWAT through the drought-of-record climatic conditions. A discussion of the drought-of-record will be held until discussion of the predictive simulations in Section 10.

6.3.5 Implementation of Pumping Discharge

Pumping discharge is not considered in the predevelopment model because the model is meant to be representative of times prior to significant resource use. However, pumping discharge is the primary stress on the model during the historical (1980-1999) and the predictive (2000-2050) model periods. Pumping discharge is a cell dependent specified flow boundary.

The procedural techniques used to estimate and allocate pumping are provided in Section 4.7 and Appendices B and C. For details of how the historical or predictive pumping was derived, the reader is referred to those appendices. Once the pumping had been estimated for each of the seven user groups, it was summed across all user groups for a given model cell (row, column) and a given model layer. This process was repeated for all active model cells in the model domain for each transient stress period. As discussed above, the stress period used in the transient simulations is 1 month. Therefore, the MODFLOW well-package data set has a specified flow boundary condition for each month of simulation, for each active grid cell within which pumping is occurring.

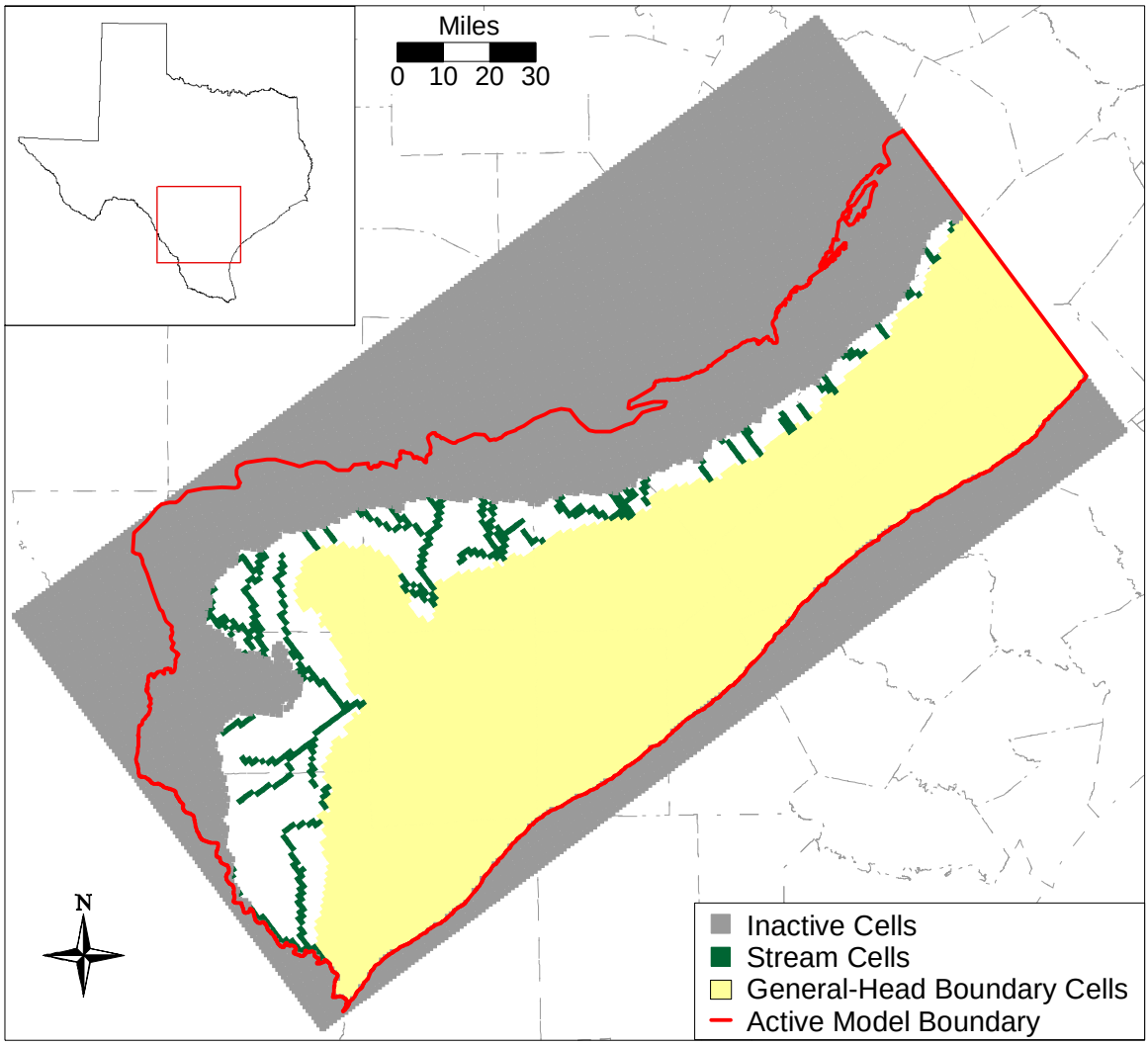

Figure 6.3.1 Layer 1 (Queen City) boundary conditions and active/inactive cells.

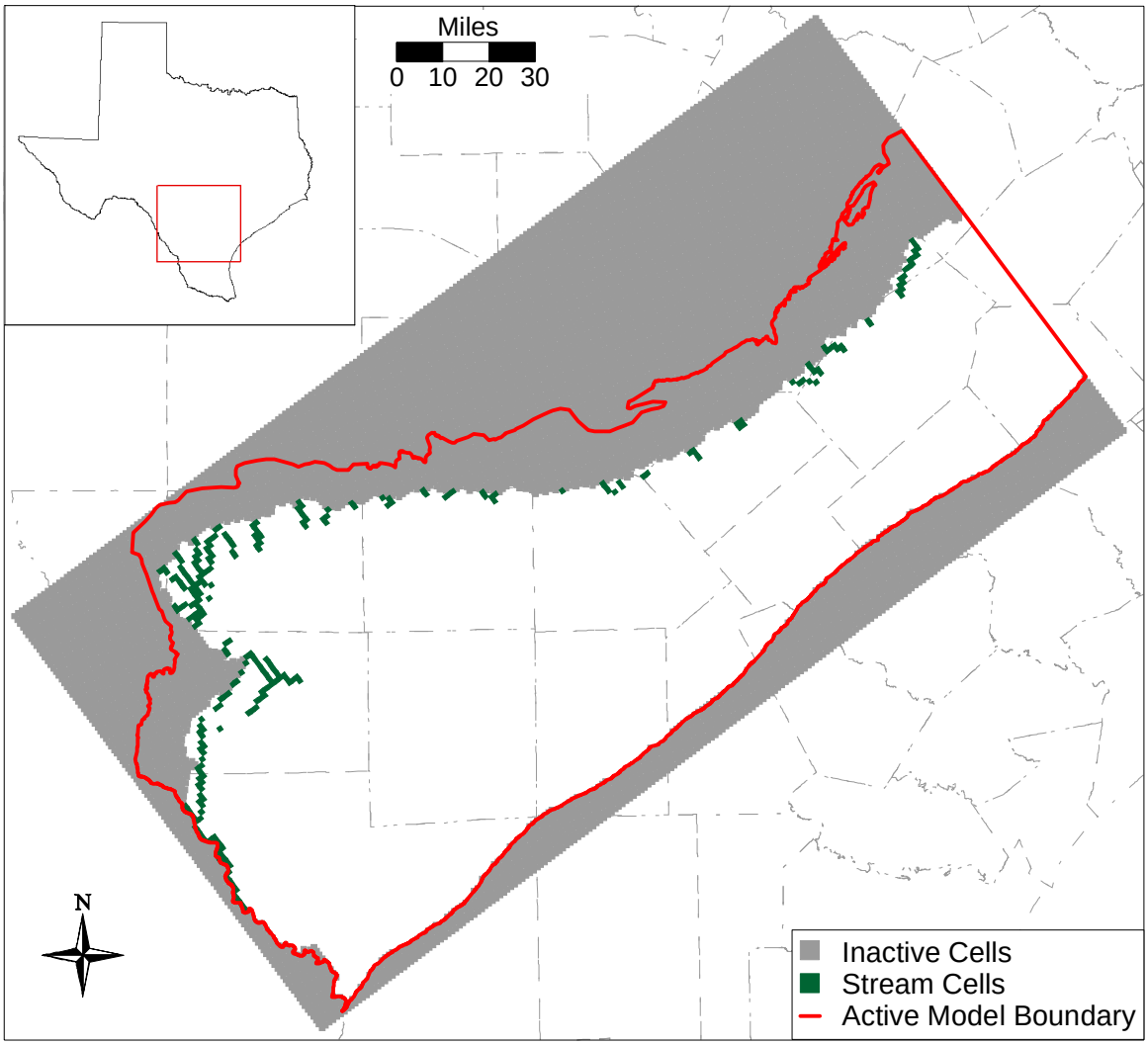

Figure 6.3.2 Layer 2 (Reklaw) boundary conditions and active/inactive cells.

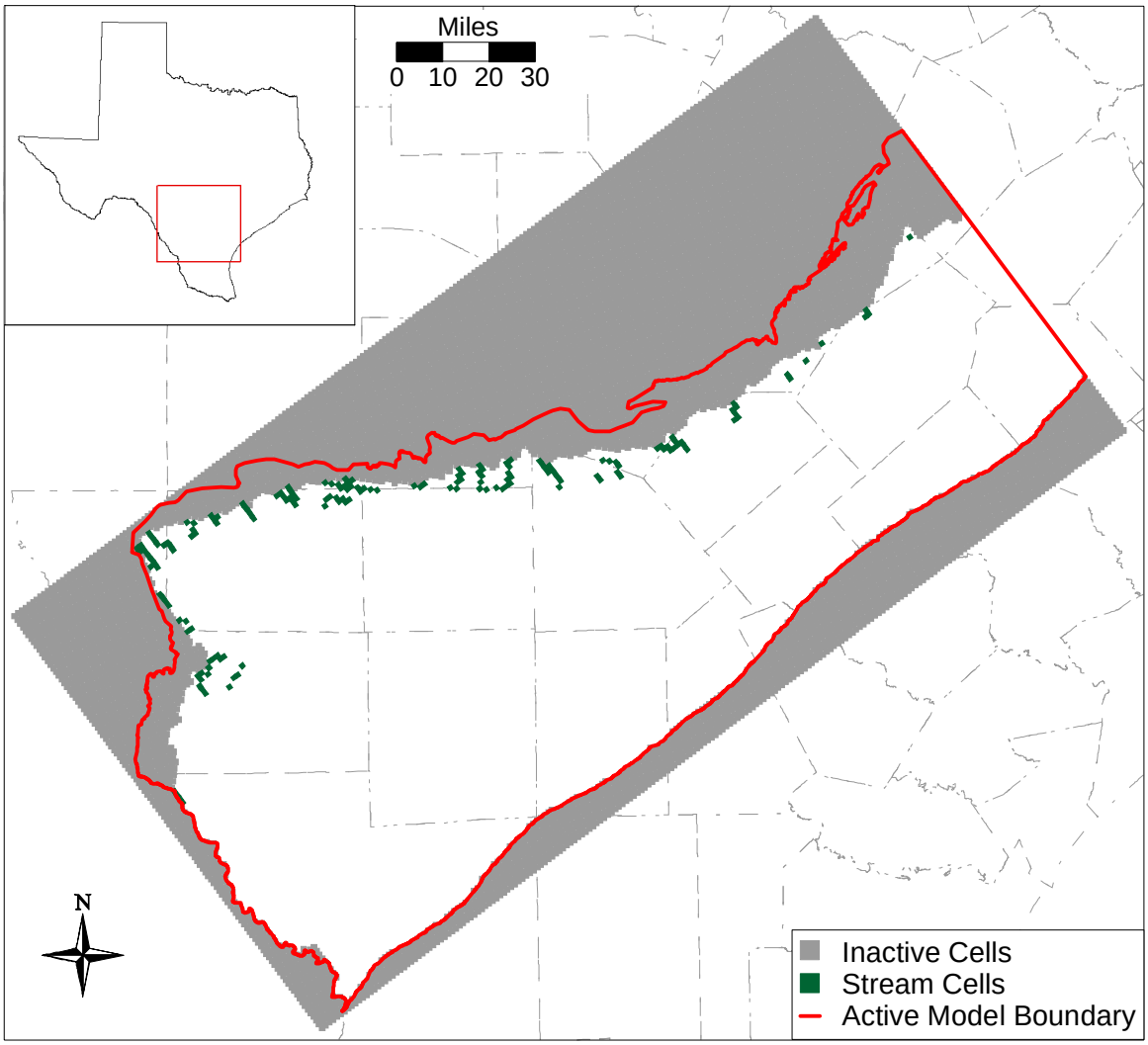

Figure 6.3.3 Layer 3 (Carrizo) boundary conditions and active/inactive cells.

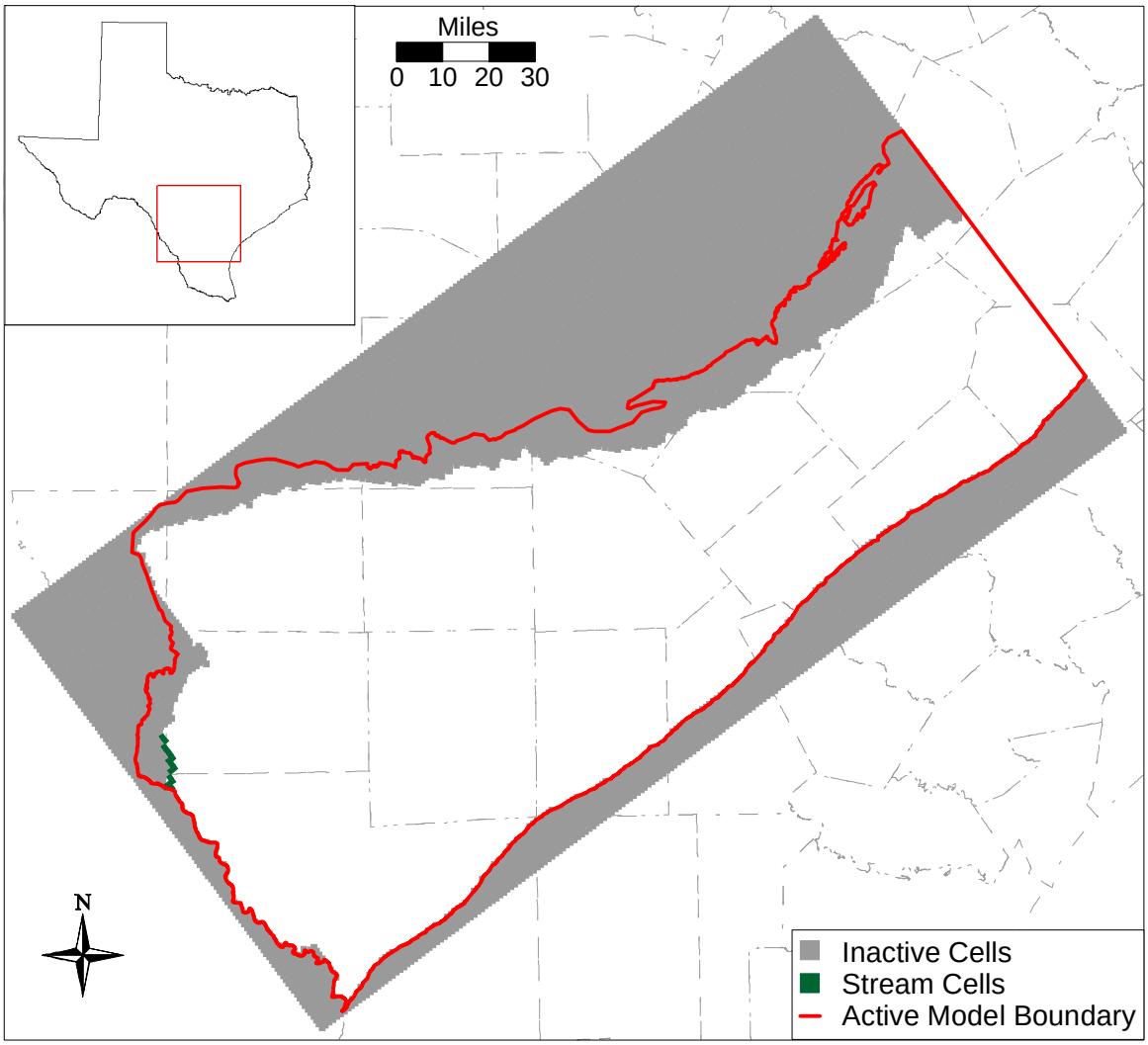

Figure 6.3.4 Layer 4 (upper Wilcox) boundary conditions and active/inactive cells.

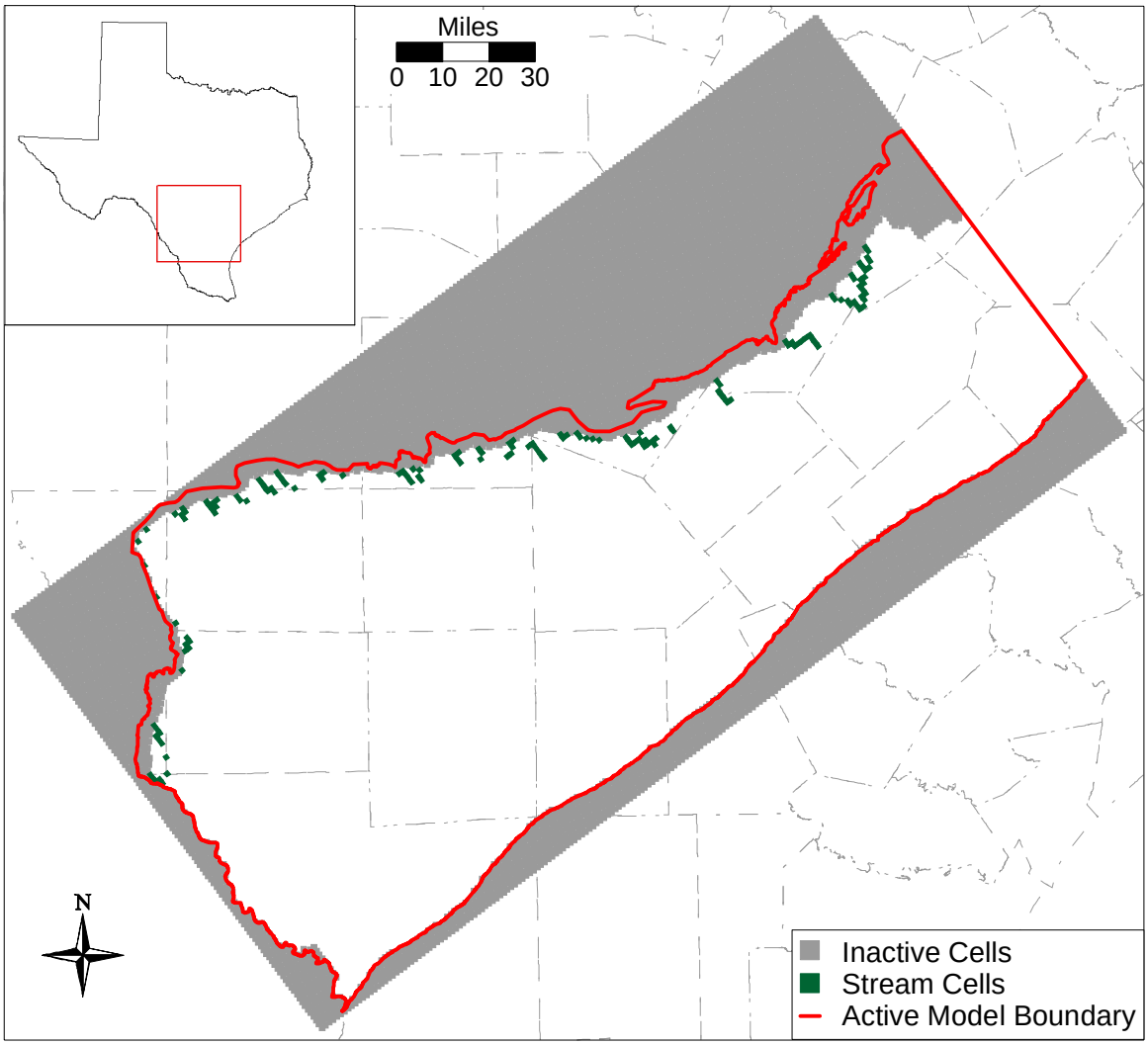

Figure 6.3.5 Layer 5 (middle Wilcox) boundary conditions and active/inactive cells.

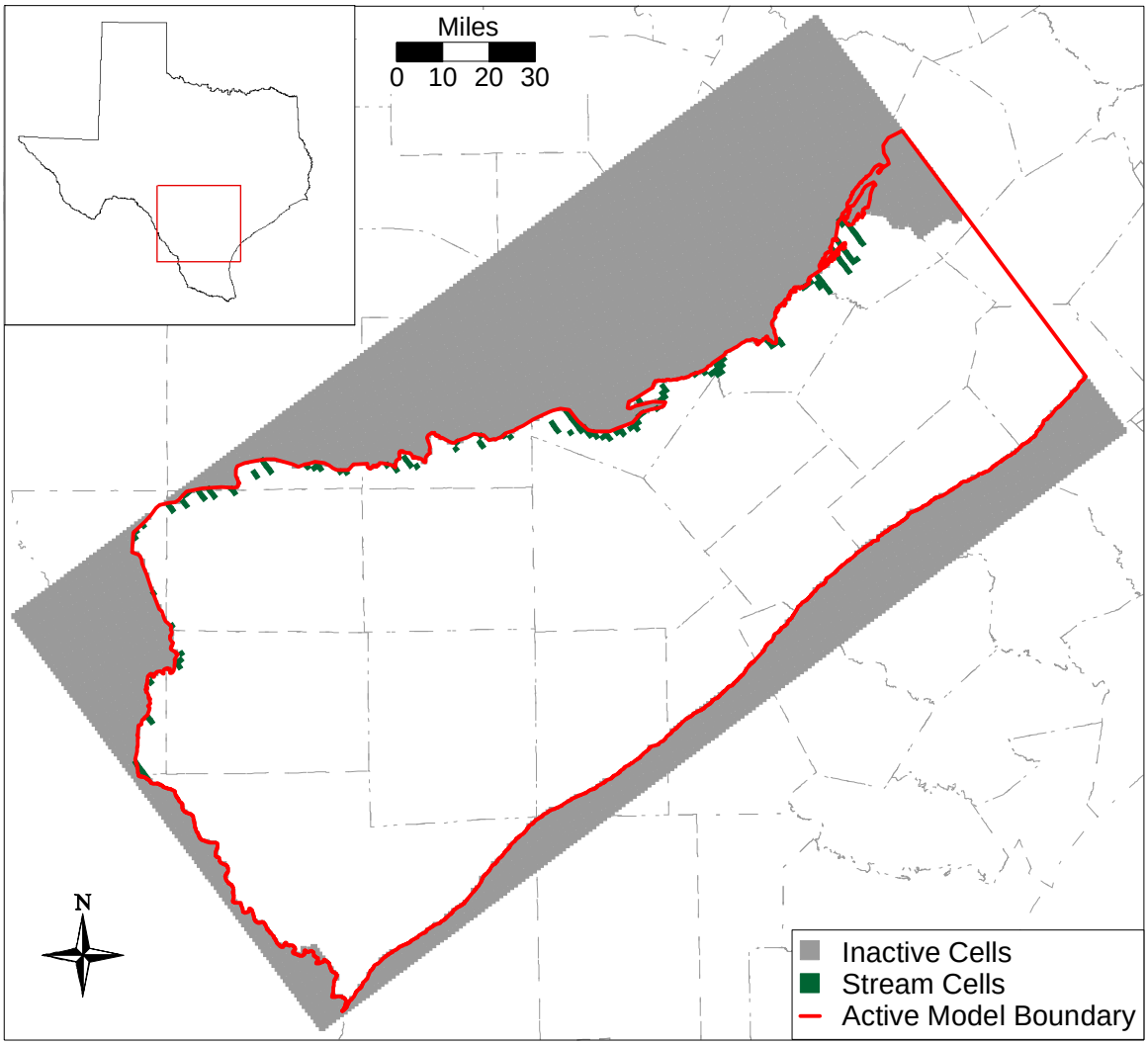

Figure 6.3.6 Layer 6 (lower Wilcox) boundary conditions and active/inactive cells.

6.4 Model Hydraulic Parameters

For the steady state model, the primary parameter to be estimated and distributed across the model grid is hydraulic conductivity. For the transient model, the storage coefficient becomes important. The method used for distributing hydraulic conductivity and storage in the model domain is described in the following.

6.4.1 Hydraulic Conductivity

In the GAM, model properties are constant within a given grid block which is one square mile in area and varies in thickness from a minimum of 20 feet to hundreds of feet. The challenge in constructing a regional model at this scale is in the development of an accurate "effective" hydraulic conductivity that is representative of the grid block scale, and thus represents the different lithologies present in each grid cell. The effective hydraulic conductivity depends on the geometry, hydraulic conductivity, and the correlation scale relative to the grid scale and simulation scale of the various lithologies present in the grid cell (Freeze, 1975).

There have been many investigations on estimating an average effective hydraulic conductivity given assumptions for flow dimension, layer geometry, and correlation scales (Warren and Price, 1961; Gutjahr et al., 1978, Fogg, 1989). For one-dimensional flow in lithologies combined in parallel (i e., layered), the appropriate effective hydraulic conductivity would be the weighted arithmetic mean. For one-dimensional flow in lithologies combined in series, the effective hydraulic conductivity is the harmonic mean. Hydraulic conductivity has been found to be a log-normally distributed parameter. In two-dimensional uniform flow, assuming that the hydraulic conductivity is log-normally distributed and randomly juxtaposed, the effective-hydraulic conductivity is exactly the geometric mean (deMarsily, 1986). Fogg (1989) has studied effective hydraulic conductivity for a model of the Carrizo-Wilcox aquifer in Freestone and Anderson counties in East Texas. His study concluded that for the case when the individual lithologic layers vary in dimension from smaller and larger than the model grid scale, the effective hydraulic conductivity in the horizontal dimension is between the geometric mean and the arithmetic mean. In the vertical dimension, he found that the effective hydraulic conductivity should vary from the geometric to the harmonic mean.

In Section 4.3 we discussed the distribution of hydraulic conductivities available for the Carrizo-Wilcox aquifer in Mace et al. (2000a). Hydraulic parameterization of coastal plain

sediments is often correlated to sand body thickness, geometry, and depositional facies (e.g., Payne, 1975; Henry et al., 1980; Fogg, 1986; Thorkildsen and Price, 1991). From the analysis provided in Section 4.3 of this report, hydraulic conductivity has been distributed within the model regions where data were available. Likewise, sand thickness and sand fraction (%) distributions for the modeled aquifers were developed where data were available. However, as discussed earlier in Section 4.3, correlations between sand thickness (sand fraction) and hydraulic conductivity were not successful.

There are two key assumptions that underlie the method which we used to estimate horizontal and vertical hydraulic conductivity. First, it was assumed that the available transmissivity data, or interpreted hydraulic conductivity data, are representative of the higher permeability strata encountered in the borehole. The higher permeability strata were also assumed to be dominated by a sand lithology. Second, it was assumed that the measured hydraulic conductivities are representative of horizontal hydraulic conductivity, not vertical hydraulic conductivity. Vertical hydraulic conductivity data at a scale representative of this model were not available. Based upon these assumptions, the method we used to distribute horizontal and vertical hydraulic conductivity is discussed below.

The model used the geostatistical analysis (kriging) presented in Section 4.3 as the initial sand hydraulic conductivities for a given block. In areas lacking hydraulic conductivity measurements, we used depositional models, lithofacies zones, and sparse hydraulic data to estimate hydraulic conductivity within zones. Data tends to be biased towards the outcrop and shallow subcrop. Previous investigators have found, both theoretically and empirically, that the hydraulic conductivity of unconsolidated sediments decreases with depth (Helm, 1976; Prudic, 1991). This is thought to be a result of sediment compaction with increased overburden pressure. In the Texas Gulf Coastal Plain, this could also be a result of low-energy depositional environments as one moves downdip towards the depocenter. Regardless, we considered decreasing hydraulic conductivity as a function of overburden when data were not available.

With the sand hydraulic conductivity estimated at the grid scale by kriging, we used the sand fraction to estimate an effective horizontal hydraulic conductivity adjusted for the percent of the formation that is not sand (i e., silt or clay). That is:

$$K_h \text{ effective} = K_{sand} \times (\text{net sand b} / \text{layer b}) \qquad (6.1)$$

where: K_h effective is the effective grid block horizontal hydraulic conductivity, K_{sand} is the hydraulic conductivity of the sand as interpreted from hydraulic test data and interpolated to the grid scale, net sand b is the net sand thickness in feet in a given layer, and layer b is the total layer thickness. This equation assumes horizontal flow and also assumes that the horizontal hydraulic conductivity of the non-sand lithologies is unimportant to grid-scale horizontal flow relative to the sands. MODFLOW combines total layer thickness (layer b) and the effective horizontal hydraulic conductivity to calculate grid block transmissibilities which govern flow rates within the model. Equation 6.1 above essentially corrects MODFLOW's calculation of transmissibility to account for the lower permeability strata in the individual layers.

As noted in Section 4.3, the model layers had varying amounts of available supporting data for assigning effective horizontal hydraulic conductivity to model grid cells in the layer. The Carrizo layer (Layer 3) had the most data available. The kriged horizontal hydraulic conductivity field shown in Figure 4.3.6 and the percent sand map shown in Figure 4.3.10 were combined using equation 6.1 to yield an effective horizontal hydraulic conductivity field. This field was then sampled at model grid cell centers to yield effective horizontal hydraulic conductivity for each cell.

Data coverage was far less complete for the remaining layers. Effective hydraulic conductivity was estimated for cells in these layers by dividing each layer into large zones of constant effective horizontal hydraulic conductivity, based on "soft" data -- depositional models, lithofacies zones, etc. as noted above. The properties in these zones could then be scaled during calibration if necessary. In the Queen City/El Pico (Layer 1), four main zones were created. The area was divided first by the outcrop and downdip sections, and then further subdivided at the facies change along the Frio River. Note that in the eastern outcrop zone, the effective horizontal hydraulic conductivity varies according to the kriged data shown in Figure 4.3.7. The Bigford/Reklaw (Layer 2) was also subdivided into four zones. The upper Wilcox (Layer 4) was zoned in the southern downdip portion according to net sand maps from Hamlin (1988) and Klemt et al. (1976). Three downdip zones were created based on cuts in sand fraction of 0.33 and 0.66. In the updip portion where the upper Wilcox has pinched out, this layer takes on the properties (and thus zonation) of the middle Wilcox. The middle Wilcox (Layer 5) was divided into three zones. The outcrop was the first zone and it took on the properties from the kriged data shown in Figure 4.3.5. The downdip section was divided into two large zones of constant

effective horizontal hydraulic conductivity, with the expectation that hydraulic conductivity should decrease moving downdip. The lower Wilcox (Layer 6) was divided into three zones. The outcrop was the first zone and it took on the properties from the kriged data shown in Figure 4.3.4. The downdip section was divided into two large zones of constant effective horizontal hydraulic conductivity, based on the net sand map of Bebout et al. (1982). The calibrated conductivity fields with the zonation discussed above are further discussed in Section 8.1 and shown in Figures 8.1.1 through 8.1.6.

Vertical hydraulic conductivity is not measurable on a model grid scale and is therefore generally a calibrated parameter. Typical vertical anisotropy ratios are on the order of 1 to 1000 determined from model applications (Anderson and Woessner, 1992). However, Williamson et al. (1990) reported that vertical resistance to flow could be significant in the Gulf Coast Aquifer system in Texas and Louisiana which is composed of similar types of coastal plain sediments as encountered in the Carrizo-Wilcox aquifer. Previous regional modeling studies in the Carrizo-Wilcox aquifer have documented vertical anisotropy ratios as high as 50,000 (Williamson et al., 1990).

Because vertical hydraulic conductivity of an aquifer is expected to be controlled by depositional environment and lithofacies, we used percent sand, maximum sand, depositional environment, lithofacies, and depth of burial in zoning vertical hydraulic conductivity to the degree practical.

The final calibrated property values (both effective hydraulic conductivity and anisotropy ratio) for each zone can be found in Section 8: Calibration.

6.4.2 Storativity

For unconfined aquifer conditions, the storativity was assigned homogeneously equal to a value of 0.25. Grid cells which represented outcrop (land surface), are modeled as either confined or unconfined depending upon the elevation of the simulated water table in that grid cell. The confined storativity assigned to outcrop cells was one to account for the condition of ponding water on the ground surface and to help prevent non-physical heads from being computed and used in the equations governing groundwater flow.

For confined aquifer conditions, the storativity was calculated as a function of aquifer thickness based upon a constant specific storage of $3x10^{-6}$ 1/ft. This results in a potential range in storativity from $2x10^{-4}$ to $2x10^{-3}$ in the downdip portions of the Carrizo-Wilcox aquifer.

7.0 MODELING APPROACH

In the context of groundwater modeling, model calibration can be defined as the process of producing agreement between model simulated water levels and aquifer discharge, and field measured water levels and aquifer discharge through the adjustment of independent variables (typically hydraulic conductivity, storativity, and recharge). Generally accepted practice for groundwater calibration usually includes performance of a sensitivity analysis and, if the model is going to be used for predictive purposes, a verification analysis. A sensitivity analysis entails a systematic variation of the calibrated parameters and stresses and the re-simulation of the aquifer conditions. Those parameters which strongly change the simulated aquifer heads and discharges would be important parameters to the calibration. It is important to note, that the "one-off" standard sensitivity analysis does not estimate parameter uncertainty as limited parameter space is investigated and parameter correlation is not accounted for. A verification analysis is a test to determine if the model is suitable for use as a predictive tool. This is performed by using the model to predict aquifer conditions during a period which was not used in the model calibration. Consistent with the approach outlined above, we calibrated the model, verified the model, performed sensitivity analyses, and performed predictive simulations.

7.1 Calibration

Groundwater models are inherently non-unique, meaning that multiple combinations of hydraulic parameters and aquifer stresses can reproduce measured aquifer water levels. To reduce the impact of non-uniqueness, we employed a method described by Ritchey and Rumbaugh (1996). This method includes (1) calibrating the model using parameter values (i.e., hydraulic conductivity, storativity, recharge) that are consistent with measured values, (2) calibrating to multiple hydrologic conditions, and (3) using multiple calibration performance measures such as hydraulic heads and discharge rate to assess calibration. Each of these elements is discussed below.

We used measured hydraulic conductivity and storativity data to initially estimate our parameters. The analysis of hydraulic parameters in Section 4.3 of this report indicates that there is a large amount of hydraulic conductivity data that is available for use as initial model values. Vertical hydraulic conductivity is not measurable at the model scale and thus cannot be well

constrained. Storativity is a parameter which is not well defined on the scale of the model. However, storativity is estimated from measured specific storage data in combination with the aquifer thickness. Recharge has not been directly measured in the study area and is arguably not measurable at the model scale. As described earlier in the report, we used SWAT to provide an initial estimate of shallow recharge. Adjustment of all model parameters were held to within plausible ranges based upon the available data and relevant literature. Adjustments to aquifer parameters from initial estimates were minimized to the extent possible to meet the calibration criteria. As a general rule, parameters that have few measurements were adjusted preferentially as compared to properties that have a good supporting database.

The model was calibrated over two time periods, one representing steady-state conditions and the other representing transient conditions. Because the confined section of the Carrizo-Wilcox aquifer in south Texas has been extensively developed since the turn of the century, portions of the aquifer have not been at steady-state conditions through most of the historical record. Therefore, we have chosen to use "predevelopment" conditions as our steady-state model. Section 4.4.1 describes the process used to estimate aquifer water levels for the steady-state predevelopment model. No pumping stresses were applied to the predevelopment model consistent with the assumption of steady-state conditions prior to significant resource development. The transient model was started in 1975 to allow any initialization effects to dampen by 1980, the start of the calibration period. This period from 1975 to 1980 was considered a "ramp up" period, and was not used for calibration. The transient calibration period ran from 1980 through 1989 consistent with the GAM model requirements. The initial heads used for the transient model were based upon 1980 observations (see Section 4.4.4). Section 4.4.4 describes the aquifer water levels and how they were derived to be used for the transient calibration period. Pumping estimates based upon historical records were applied on a monthly time scale in the transient calibration period. Likewise, recharge, stream flow, and reservoir stage were estimated on a monthly time basis and set as input through the transient calibration period. The time period from 1990 until 1999 was used as the verification period to assess the predictive ability of the model. Like the calibration period, transient stresses or boundary conditions were determined on a monthly time step. Unlike the calibration period, parameters were not adjusted in the verification process.

The model was calibrated through a wide range of hydrological conditions. The steady-state predevelopment model represents a period of equilibrium where recharge and aquifer discharge through streams and cross-formational flow are in balance. Under these conditions, the aquifer rejects the maximum amount of recharge and, as was detailed in Section 5, a minimum amount of recharge is expected under stable basin conditions (Freeze, 1971). The steady-state model is sensitive to recharge. The calibration and verification period (1980 through 1999) represents a significantly different period. By this time, portions of the aquifer have been extensively developed resulting in loss of storage and declining heads. Some of the recharge being rejected under steady-state predevelopment conditions may be captured as a result of losing streams and increased vertical gradients. The calibration and verification period also helps constrain the model parameterization because a wide variety of hydrologic conditions are encountered and simulated. The transient model may be sensitive to parameters that are not sensitive parameters for the steady-state model.

Calibration requires development of calibration targets and specification of calibration measures. To address the issue of non-uniqueness, it is best to use as many types of calibration targets as possible. The primary type of calibration target is hydraulic head (water level). However, we also used stream flows and gain-loss estimates. Simulated heads were compared to measured heads at specific observation points through time (hydrographs) and head distributions (maps) for select time periods (see Section 4.4) to ensure that model head distributions are consistent with hydrogeologic interpretations and accepted conceptual models for flow within the aquifer.

Stream calibration targets were derived from two types of data. First, we compared model simulated stream flow rates to observed flow rates at key stream gages in the model area. Because stream flow rates greatly exceed aquifer/stream fluxes for local cells, available gain/loss estimates were also used for the major streams crossing the outcrop.

Traditional calibration measures (Anderson and Woessner, 1992) such as the mean error, the mean absolute error, and the root mean square error quantify the average error in the calibration process. The mean error (ME) is the mean of the differences between measured heads (h_m) and simulated heads (h_s):

$$ME = \frac{1}{n} \sum_{i=1}^{n} \left(h_m - h_s\right)_i \tag{7.1}$$

where n is the number of calibration measurements. The mean absolute error (MAE) is the mean of the absolute value of the differences between measured heads (h_m) and simulated heads (h_s):

$$MAE = \frac{1}{n} \sum_{i=1}^{n} \left|\left(h_m - h_s\right)_i\right| \tag{7.2}$$

where n is the number of calibration measurements. The root mean square (RMS) error is the square root of the average of the squared differences between measured heads (h_m) and simulated heads (h_s):

$$RMS = \left[\frac{1}{n} \sum_{i=1}^{n} \left(h_m - h_s\right)_i^2\right]^{0.5} \tag{7.3}$$

where n is the number of calibration measurements. The difference between the measured hydraulic head and the simulated hydraulic head is termed a residual.

We used the RMS as the basic measure of calibration for heads. The required calibration criterion for heads is an RMS that is equal to or less than 10 percent of the observed head range in the aquifer being simulated. To provide information on model performance with time, the RMS was calculated for the calibration period (1980-1989) and the verification period (1990-1999). The RMS is useful for describing model error on an average basis but, as a single measure, it does not provide insight into spatial trends in the distribution of the residuals.

An examination of the distribution of residuals is necessary to determine if they are randomly distributed over the model grid and not spatially biased. Post plots of head residuals were used to check for spatial bias by indicating the magnitude and direction of mis-match between observed and simulated heads. Simulated head distributions were also compared to the head distributions developed from the field measurements. Finally, scatter plots were used to determine if the head residuals are biased based on the magnitude of the observed head surface.

For streams, the calibration criteria were defined to be within 10% of the measured values where uncertainty in these targets is proven to be acceptable for such a criteria.

7.2 Calibration Target Uncertainty

Calibration targets are uncertain. In order to not "over-calibrate" a model, which is a stated desire for the GAM models, calibration criteria should be defined consistent with the uncertainty in calibration targets. The primary calibration target in groundwater modeling is hydraulic head. Uncertainty in head measurements can be the result of many factors including, measurement error, scale errors, and various types of averaging errors, both spatial and temporal. The calibration criteria for head is an RMS less than or equal to 10% of head variation within the aquifer being modeled. Head differences across the aquifers in the study area are on the order of 400 to 500 feet. This leads to an acceptable RMS of between 40 and 50 feet. We can compare this RMS to an estimate of the head target errors and see what level of calibration the underlying head targets can support.

Measurement errors are typically on the order of tenths of feet, and at the GAM scale can be insignificant. However, measuring point elevation errors can be significant. Our analysis of differences between the reported land-surface datum (LSD) and the ground surface elevation as determined from a digital elevation map determined that the average difference was -5 feet with a standard deviation of 28 feet. Add to this error in averaging ground surface elevations available on a 30 m grid to a one mile grid, and the resulting errors can average 10 to 20 feet and may greatly exceed 20 feet in areas with higher topographic slopes. Additional error is caused by combining multiple lithologies into a single grid block representing one simulated head. Horizontal to vertical hydraulic conductivity ratios have been proven to be high in the Coastal Plain aquifers of Texas (Fogg et al., 1983; Williamson et al., 1990). As a result, significant vertical gradients can occur within individual model layers. Vertical gradients near pumping centers are quite large and approach 0.1 (Williamson et al., 1990). This implies that portions of the aquifer can have head variations within a single model layer on the order of 10 to 50 feet. On average, in areas away from large pumping centers, this scale effect is expected to be on the order of 10 to 20 feet. Horizontal gradients relative to the grid scale also account for an additional one to five feet error with even greater errors near pumping centers. When these errors are added up, the average error in model heads could easily equal our calibration criteria of 40 to 50 feet. The nugget observed on kriged head maps within the modeled aquifers equals from 20 to 30 feet. This nugget captures both uncertainty and variability in the observed heads being rationalized above. Calibrating to RMS values significantly less than 30 feet would

constitute over calibration of the model and parameter adjustments to reach that RMS are not supported by the hydraulic head uncertainty.

7.3 Sensitivity Analyses

A sensitivity analysis was performed on the steady-state and transient calibrated models to determine the impact of changes in a calibrated parameter on the predictions of the calibrated model. A standard "one-off" sensitivity analysis was performed. This means that hydraulic parameters or stresses were adjusted from their calibrated "base case" values one by one while all other hydraulic parameters were unperturbed.

7.4 Predictions

Once the model satisfied the calibration criteria for both the calibration and verification periods, the model was used to make predictive simulations. The predictive simulations have different simulation periods. Simulations were run from 1999 to 2010, 2020, 2030, 2040, and 2050. Average climatic conditions were applied for each predictive simulation with the simulation ending with a drought of record. Stream flow rates and recharge were applied with seasonal variation in the average conditions period. Pumping stresses were based upon the Regional Water Plans as described in Section 4.7 and Appendix C.

8.0 STEADY-STATE MODEL

The steady-state model is representative of predevelopment conditions. In predevelopment, aquifer inflow from recharge and streams is balanced by groundwater to surface-water discharge and cross-formational flow from the Carrizo-Wilcox aquifer upwards to the younger overlying units. This section provides the details of the calibration of the steady-state model and presents the steady-state model results. This section also describes the results of a sensitivity analysis identifying the model parameters to which the steady-state model calibration is most sensitive.

8.1 Calibration

As was discussed in Section 7, calibration is the process of adjusting model parameters to produce agreement between model simulated water levels and aquifer discharges and measured water levels and aquifer discharges. The calibration process for the steady-state model is described below.

8.1.1 Horizontal and Vertical Hydraulic Conductivities

Section 6.4.1 describes the determination of initial horizontal and vertical hydraulic conductivities for the model. Figures 8.1.1-8.1.6 show the final calibrated effective horizontal hydraulic conductivity fields for the steady-state model. Table 8.1.1 includes the calibrated range of horizontal hydraulic conductivity for each model layer. The horizontal hydraulic conductivities did not require modification from their initial estimates. Queen City (Layer 1) heads were relatively insensitive to changes in horizontal hydraulic conductivity, partially due to the general head boundary that is attached to this layer in the downdip (confined) section. This insensitivity is also the result of the large number of stream cells which act as head boundaries in the Queen City/El Pico outcrop. The Reklaw and Bigford formations (Layer 2) are aquitards in the model area and as a result horizontal hydraulic conductivity had little importance for flow. The Carrizo (Layer 3) has relatively good data coverage for horizontal hydraulic conductivity based upon aquifer tests. We did not have to alter this initial distribution to calibrate. The Wilcox Group (Layers 4-6) lacked significant targets, and horizontal hydraulic conductivity in these layers did not affect heads in the Carrizo, or the model in general, to a significant degree.

Table 8.1.1 shows the calibrated anisotropy ratios (K_h/K_v) for the steady-state model. Downdip heads in the Carrizo (Layer 3) were sensitive to the vertical hydraulic conductivity in the Reklaw (Layer 2, east of the Frio River), due to the change in head gradient across the Reklaw. This sensitivity was consistent with the conceptual model which predicts that groundwater in the Carrizo discharges through cross-formational flow across the Reklaw to the Queen City Formation in the downdip confined portions of the aquifer. Decreasing the vertical hydraulic conductivity of the Reklaw resulted in less groundwater discharge across the Reklaw. The decreased discharge results in increased heads in the downdip portions of the Carrizo.

The anisotropy ratio for the Bigford Formation (Layer 2, west of the Frio River) had much less effect on downdip heads in the Carrizo than did the ratio for the Reklaw east of the Frio River. This difference could result from the fact that lateral downdip flow in the Carrizo extends over a much larger model area in the west than in the east, providing greater surface area for cross-formational flow in the west relative to the east. Hamlin (1988) noted that, as a result of the dip of the Carrizo-Wilcox aquifer, the bad water line encroaches much closer to the outcrop in the eastern model area than in the west. The steady-state model was also insensitive to changes in the anisotropy ratio in the Wilcox layers. This is likely because the Wilcox head targets were confined to the outcrop portions of the model with no predevelopment downdip targets available in these layers. For these reasons, the steady-state model could be calibrated with several different anisotropy ratios for the Bigford Formation and the Wilcox Group.

As a result of the steady-state model's insensitivity to vertical hydraulic conductivity in the Bigford and the Wilcox, these parameters are poorly constrained by the steady-state model. Our initial estimates of anisotropy for these formations during steady-state model calibration were much lower than the final calibrated values. For example, our initial estimate of vertical anisotropy for the Bigford Formation was 300, while the value after transient calibration (and steady-state recalibration) was 10,000. The initial estimate of anisotropy for the upper Wilcox was 100, while the final value after transient calibration was 1,000. These examples illustrate the value of calibrating to multiple hydrologic conditions as discussed in Section 7. We were able to greatly improve the uniqueness of the calibrated parameters by iteratively calibrating between steady-state and transient models.

8.1.2 Recharge

Recharge estimates were based upon forward simulations using SWAT for the time period 1975 through 1999 (see Section 6.3.4). For the steady-state model, recharge was input as an average recharge rate estimated over the transient simulation period. Some modifications were required to the recharge estimates calculated from SWAT. The transient recharge results were adjusted slightly from the SWAT outputs in the eastern model region, due to anomalously high recharge rates estimated by SWAT in this area (Section 9.1). In the steady-state model, recharge was reduced at a few outcrop cells where heads were rising significantly above ground surface. These cells usually had the combined characteristics of high recharge and low hydraulic conductivity or they were thin edge cells with no flow boundaries both below and to the east or west. Figure 8.1.7 shows a histogram comparison of steady-state recharge, before and after calibration. Note that the number of high values of recharge is reduced. The median recharge rate decreased from 0.64 inches per year to 0.51 inches per year. Figure 8.1.8 shows a post plot of the calibrated recharge rates over the modeled outcrop. The spatial variation of recharge did not change significantly during steady-state calibration. In general, Figure 8.1.8 shows recharge increasing from the western portion of the model to the eastern portion. This trend is consistent with the overall trend of increasing precipitation from the west to the east across the model area.

The steady-state model is sensitive to recharge for two reasons: (1) recharge is the primary input source for water and (2) the model is at steady-state where inflow balances outflow with no change in storage or time dependence. In a transient model, recharge to the outcrop can be added to storage over decades without significantly affecting downdip heads. In a steady-state model, where there is no net change in storage, a balance must be found between the input recharge and all other flows in the model. This implies that the behavior of the whole model will be sensitive to the input recharge rate. We believe that SWAT performed well in generating an overall average recharge distribution for the Southern Carrizo-Wilcox GAM because we had to make only minor adjustments to recharge during calibration of the steady-state model.

8.1.3 Groundwater Evapotranspiration

Steady-state groundwater evapotranspiration (ET) was averaged from SWAT transient results and applied as ET maximum in the MODFLOW ET package (see Section 6.3.4). Naturally, ET occurs above the ground surface, within the vadose zone, and within the saturated

zone. Note that the ET maximum taken from SWAT and applied in MODFLOW is groundwater ET, not vadose zone ET (which was already considered in the SWAT recharge results). Appendix E provides further details regarding the application of SWAT with MODFLOW. The maximum rooting depths were taken from the SWAT results and input as the extinction depth in the MODFLOW ET package. The ET surface was set to ground surface, so groundwater ET varied linearly starting from a maximum at ground surface and going down to the root depth. These parameters were fixed during calibration. Figure 8.1.9 shows how the average groundwater ET maximum varies across the model region. The median groundwater ET maximum for the region was 1.2 inches/year. The median rooting depth for the region was 6 feet.

The ET package in MODFLOW added considerable instability to the steady-state model. A model that would previously converge in several minutes without the ET package, would either take much longer or diverge completely when ET was activated. The final calibrated model with ET has a relatively slow convergence for a steady-state model, but is stable for the calibrated parameter set.

8.1.4 General Head Boundaries

The heads assigned to the general head boundaries (GHBs) were estimated from the surficial water table (Section 6.3.2). The initial hydraulic conductances of the GHBs were estimated from the vertical conductivities of the LBG-Guyton and HDR (1998) model "Younger" layers. Heads in the El Pico/Queen City Formation (Layer 1) were very sensitive to the conductance of the GHBs. The heads in the El Pico/Queen City Formation affect the gradient across the Reklaw Formation (Layer 2) to the underlying Carrizo, and therefore affect heads in the Carrizo. As a result, conductance of the GHBs was significant to steady-state calibration in Layers 1 and 3. Figure 8.1.10 shows the conductances for the calibrated GHBs. During calibration, hydraulic conductances of the GHBs were adjusted from their initial estimates by decreasing the conductance west of the Frio River, and slightly increasing the conductance east of the Frio River. These changes are in agreement with the adjustments made to the vertical hydraulic conductivity of Layer 2, where vertical hydraulic conductivity in the Bigford Formation (west of the Frio River) was decreased relative to the vertical hydraulic conductivity of the Reklaw Formation (east of the Frio River). In the process of calibration, heads in the Queen City/El Pico were calibrated through adjustments to the GHBs. When

satisfactory heads were simulated, the vertical hydraulic conductivity of the Reklaw was varied until heads in the Carrizo were close to calibration. Modifications to the GHB conductance and the Reklaw vertical conductivity were made iteratively until the gradient across the Reklaw was matched.

8.1.5 Streams

Our initial approach for the estimation of streambed conductance was to calculate them based upon the hydraulic conductivity of the underlying formation. However, we had some difficulty with this approach because the stream segments could cross multiple outcrops, and the conductivities within the outcrops were widely varying. To simplify the initial estimates, we set a constant streambed conductivity of 1 ft/day and let the overall streambed conductance vary with the streambed width as specified in the EPA RF1 dataset (Section 6.3.3). During the initial steady-state calibration, the streambed conductances were decreased in the western portion of the model (including the Rio Grande, Nueces, and Frio rivers) in order to match heads in the Carrizo outcrop. This resulted in heads increasing in the outcrop with water exiting less freely from the unconfined section to the streams. However, after transient calibration the vertical hydraulic conductivity of the Bigford Formation (Layer 2, west of the Frio River) was decreased (Section 8.1.1 above), increasing heads in the Carrizo and necessitating a return to the original streambed conductivities. Therefore in the final calibration, the streambed conductivities were not modified from their initial estimates.

Table 8.1.1 Calibrated hydraulic conductivity values for the steady-state model (ft/day).

	Outcrop		**Downdip**	
Horizontal Hydraulic Conductivity (ft/day)	*West of Frio River*	*East of Frio River*	*West of Frio River*	*East of Frio River*
El Pico / Queen City	0.5	1 – 30*	0.5	2
Bigford / Reklaw	2	3	2	1
Carrizo	0.3 – 100*			
Upper Wilcox	--		0.3 – 3	
Middle Wilcox	1 – 30*		0.3 - 1	
Lower Wilcox	1 – 30*		1 - 3	
Anisotropy (Kh/Kv)				
El Pico / Queen City	30	30	300	30
Bigford / Reklaw	10000	1000	10000	1000
Carrizo	30			
Upper Wilcox	--		1000	
Middle Wilcox	10000			
Lower Wilcox	3000			

* These ranges are approximate – the Kh in these areas was kriged from well tests. Please see Figure 8.1.1 - 8.1.6 for specific values.

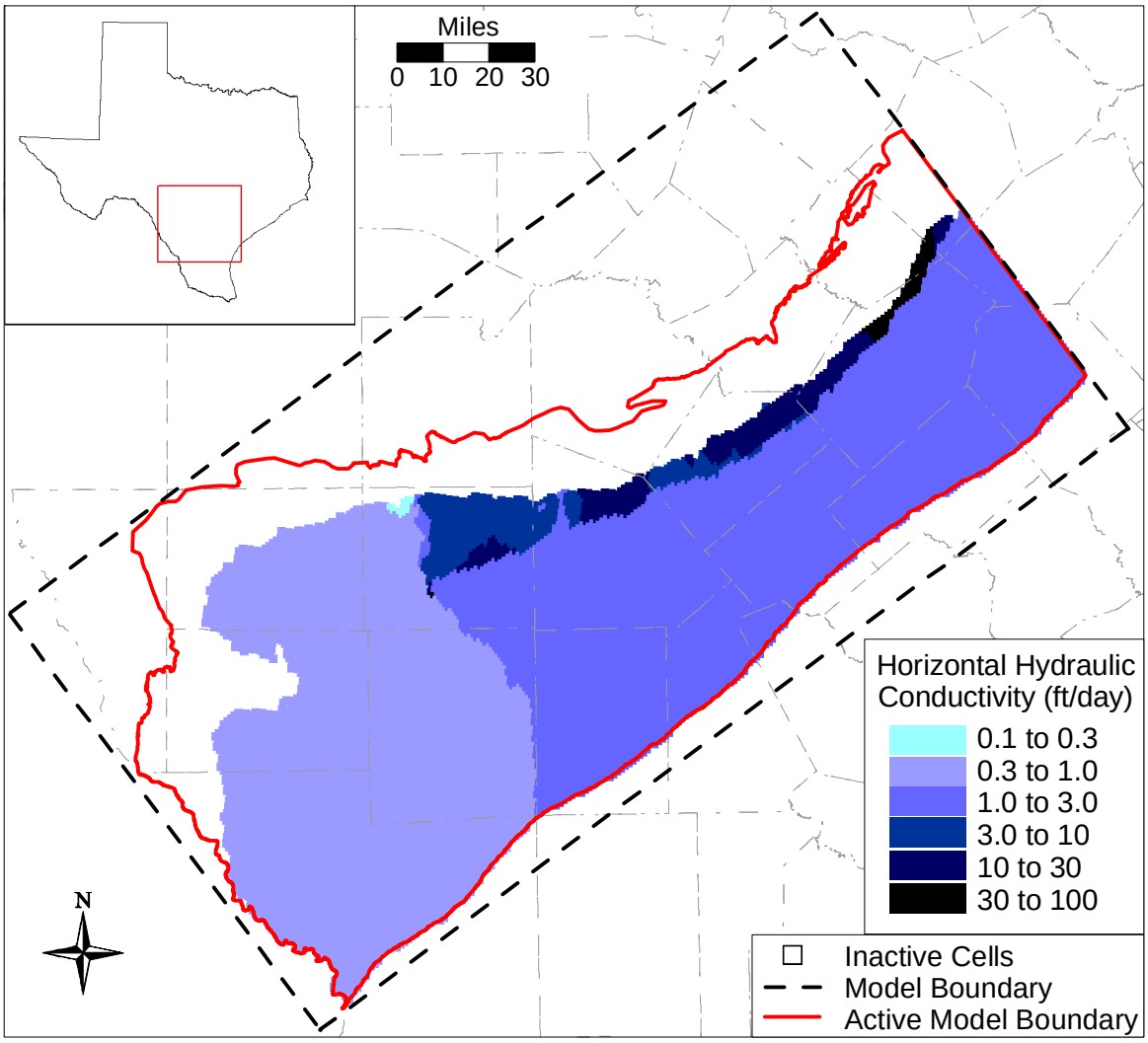

Figure 8.1.1 Calibrated horizontal hydraulic conductivity field for the El Pico/Queen City (Layer 1).

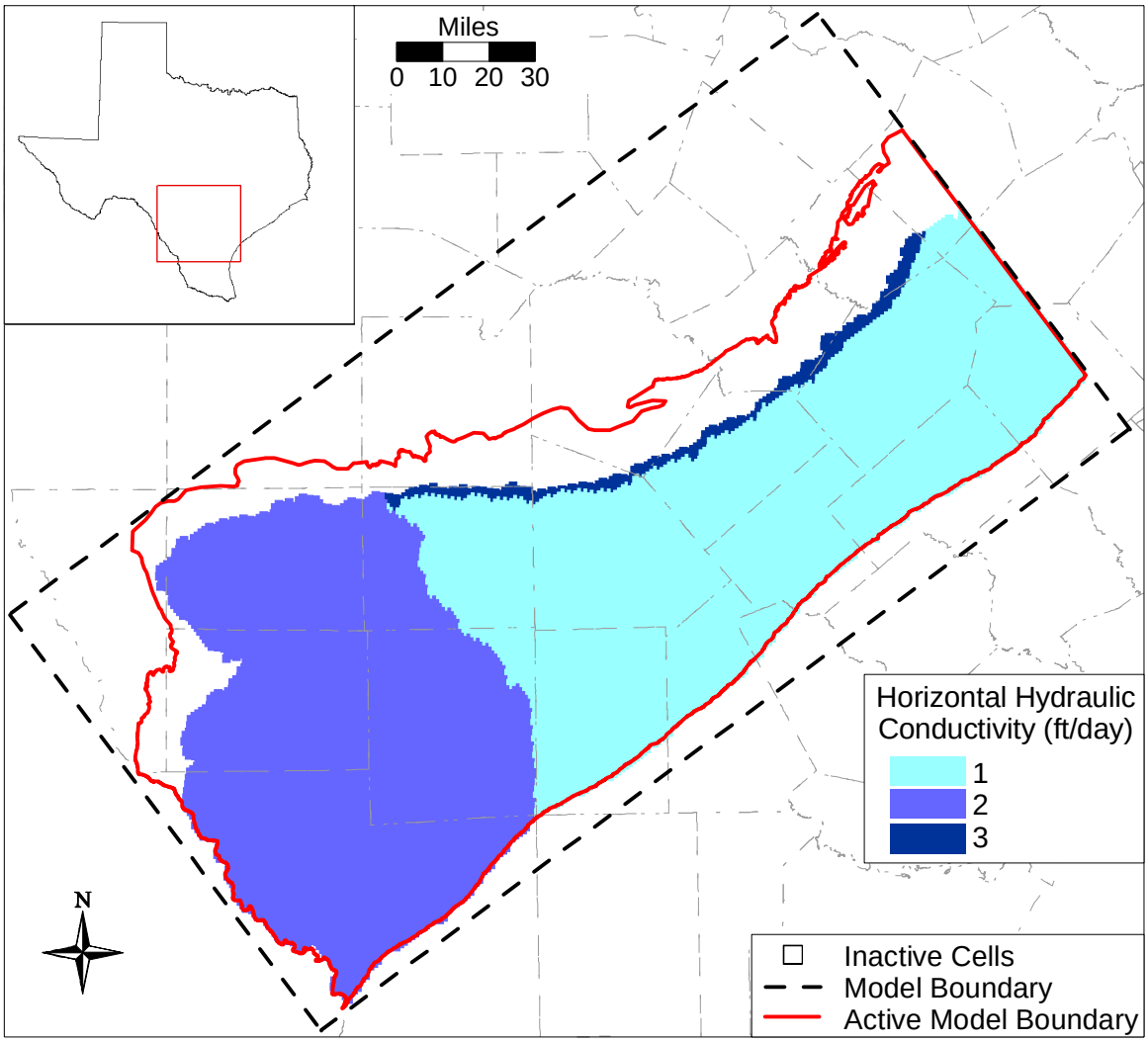

Figure 8.1.2 Calibrated horizontal hydraulic conductivity field for Bigford/Reklaw (Layer 2).

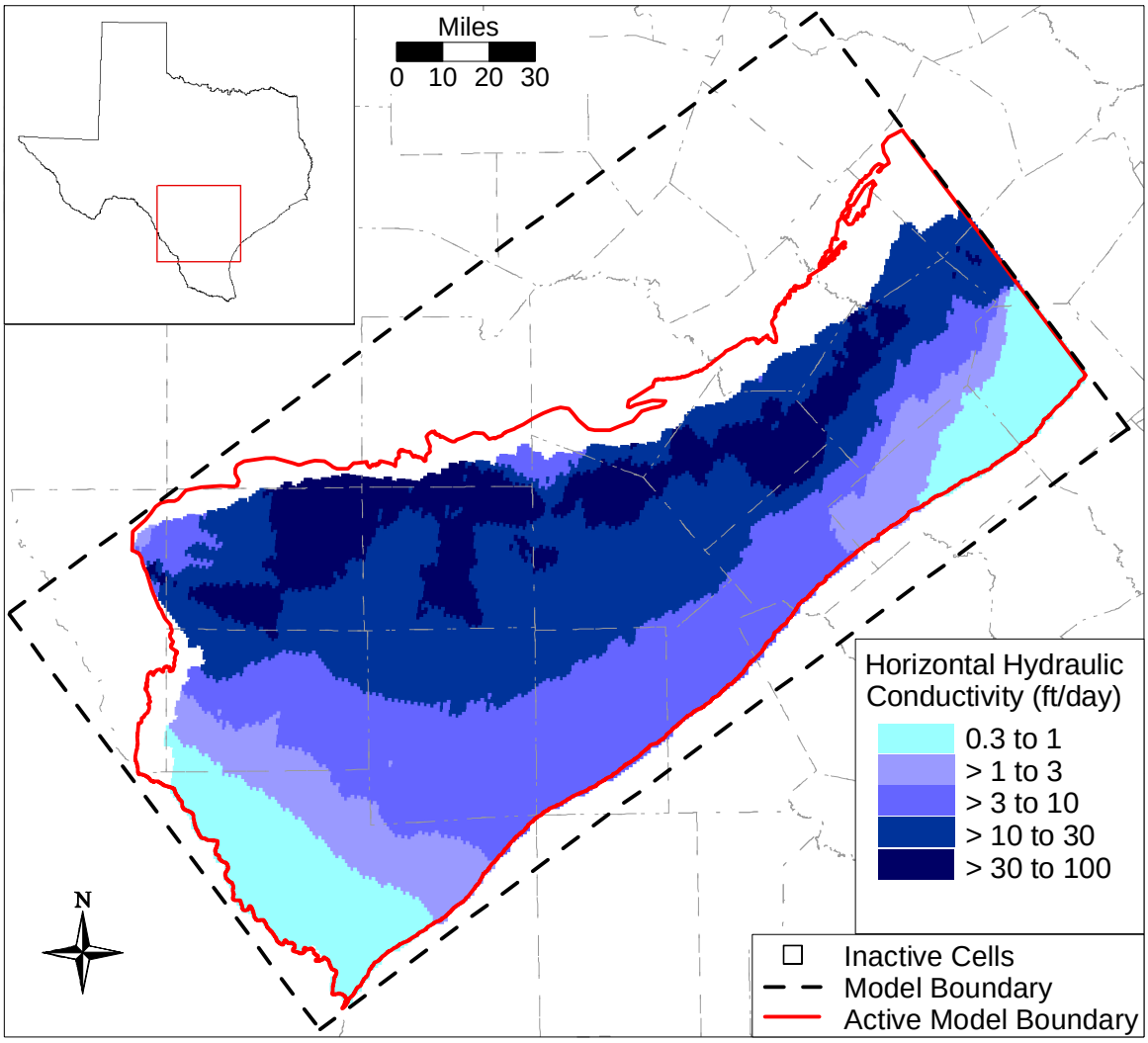

Figure 8.1.3 Calibrated horizontal hydraulic conductivity field for the Carrizo (Layer 3).

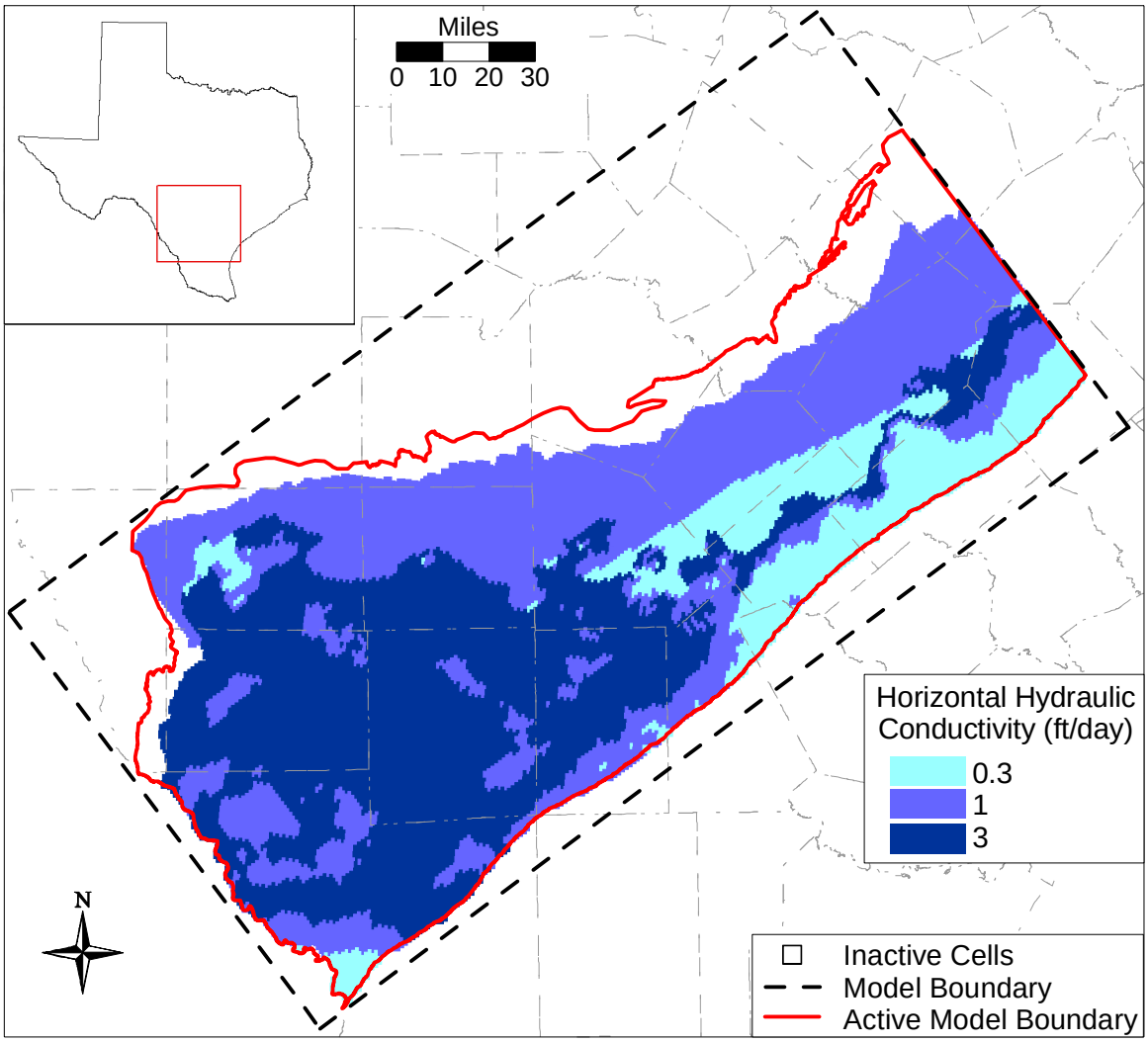

Figure 8.1.4 Calibrated horizontal hydraulic conductivity field for the upper Wilcox (Layer 4).

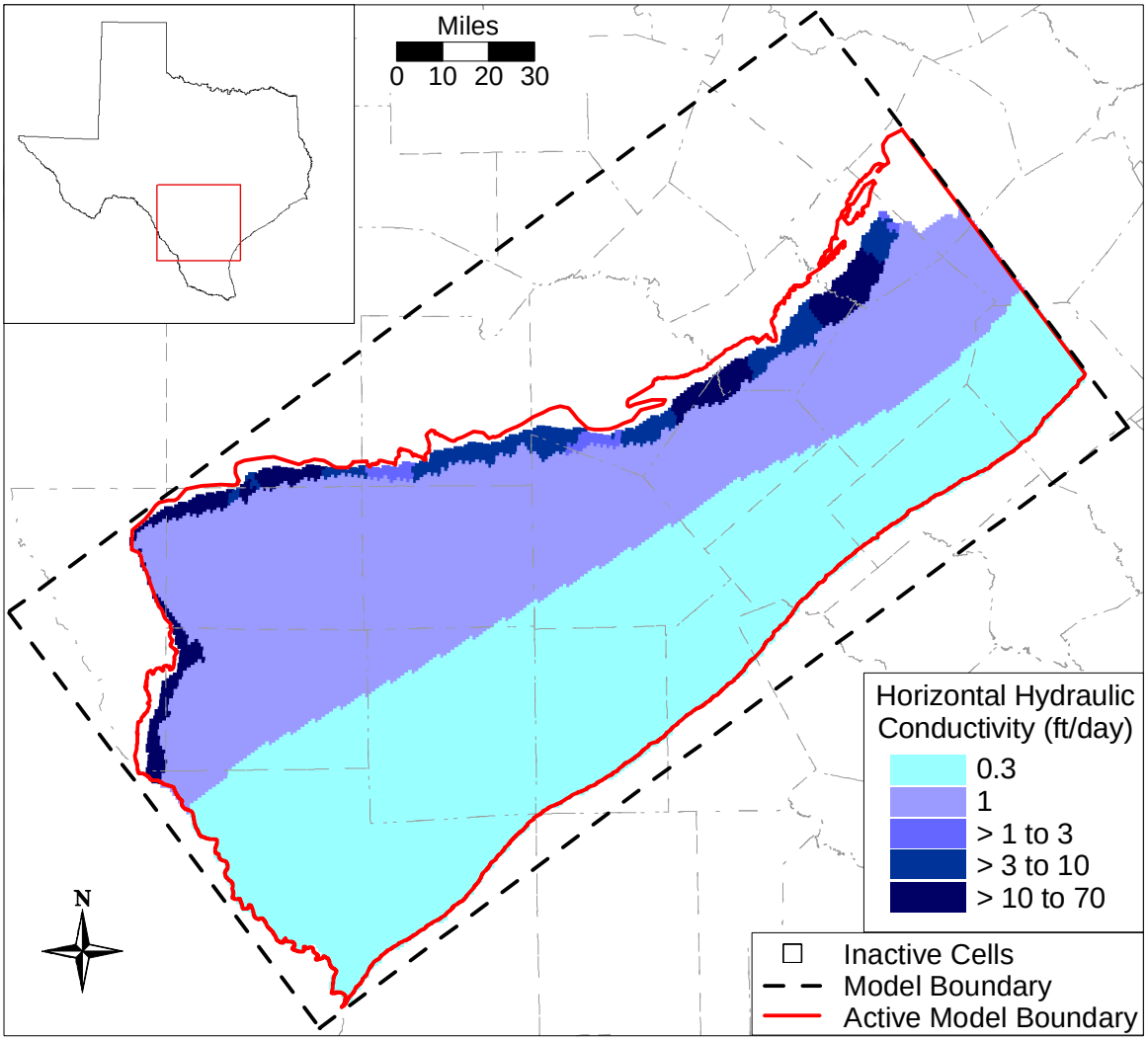

Figure 8.1.5 Calibrated horizontal hydraulic conductivity field for middle Wilcox (Layer 5).

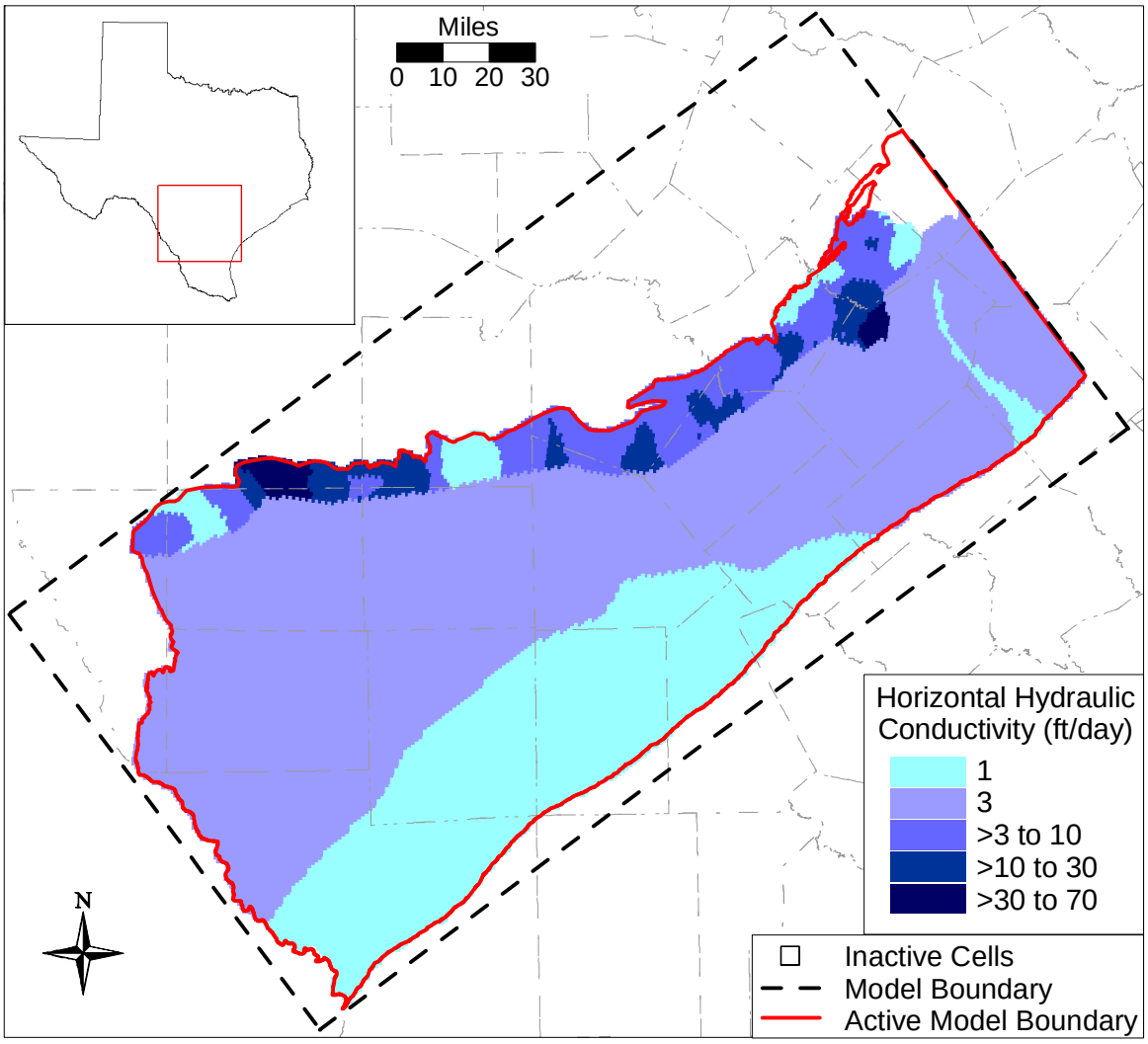

Figure 8.1.6 Calibrated horizontal hydraulic conductivity field for the lower Wilcox (Layer 6).

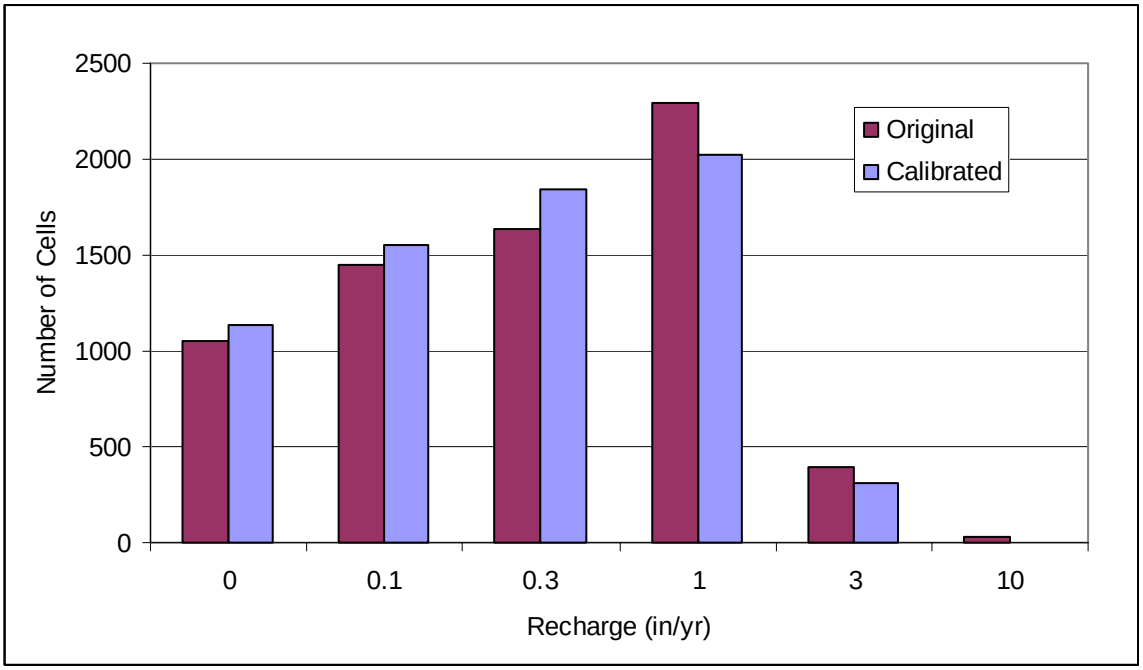

Figure 8.1.7 Comparison between initial recharge and the calibrated recharge.

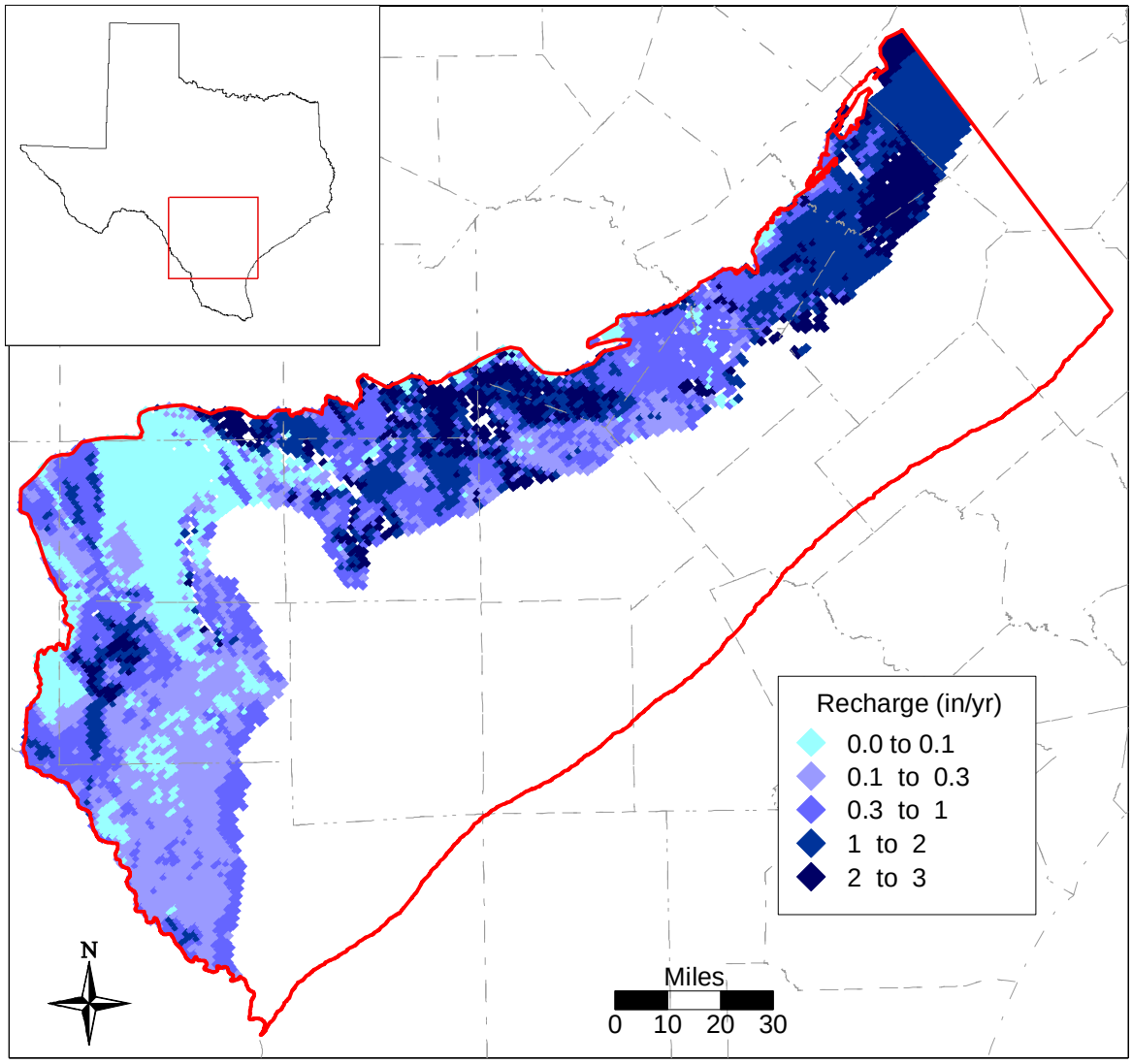

Figure 8.1.8 Steady-state calibrated recharge (in/year).

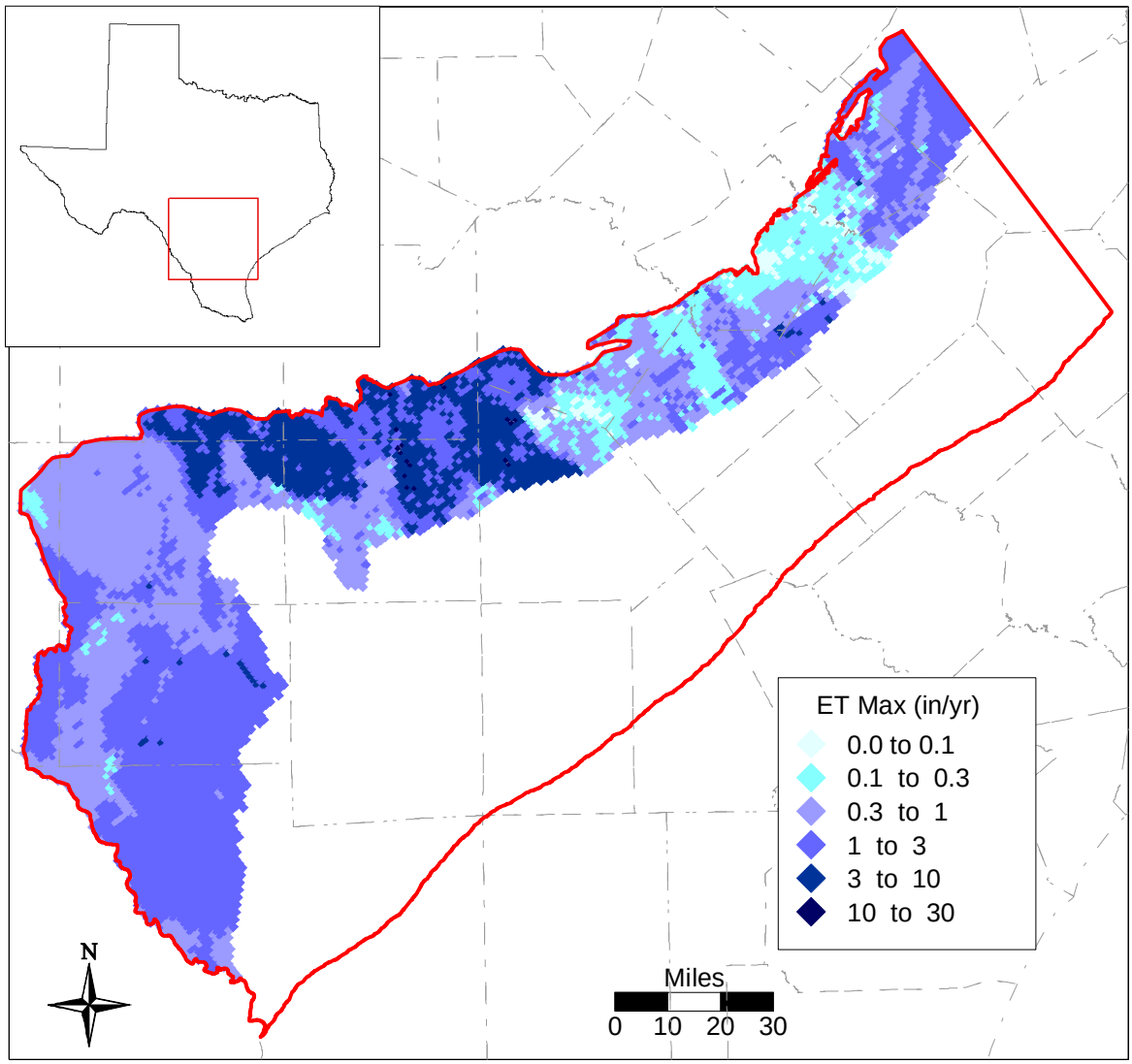

Figure 8.1.9 Steady-state groundwater ET maximum (in/year).

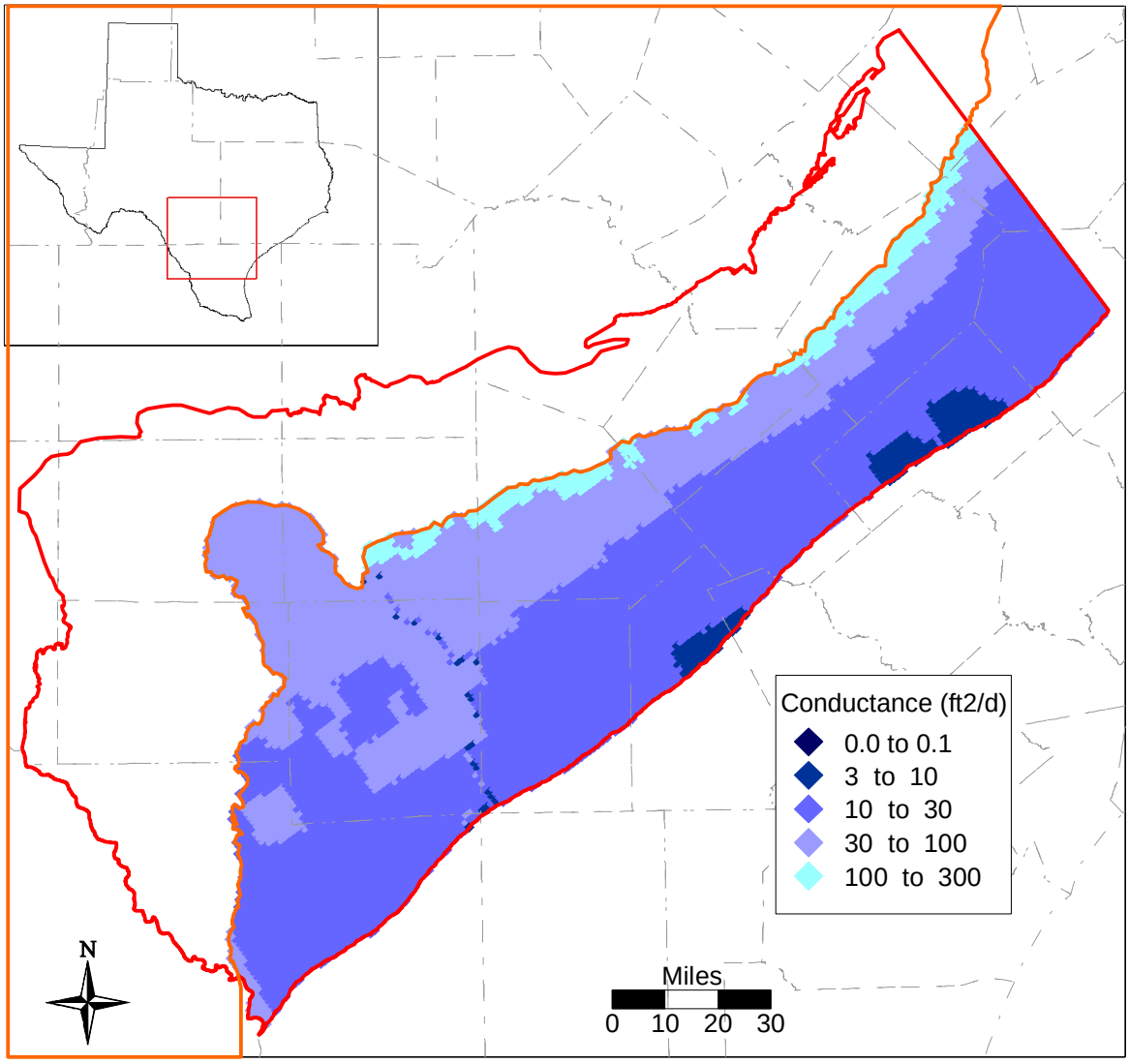

Figure 8.1.10 Steady-state calibrated GHB conductance.

8.2 Results

Steady-state model results are discussed in this section in terms of heads, stream flows, and the model water budget.

8.2.1 Heads

Figures 8.2.1-8.2.7 show the head surface results for the calibrated steady-state model. The residuals are plotted on the same figures, where residuals are defined as:

$$residual = head_{measured} - head_{simulated} \tag{8.1}$$

The RMS (Equation 7.3) for Layer 1 (Queen City/El Pico) in the steady-state model is 34.5 ft. The head range in this layer was 306 ft, giving an RMS/range of 0.11. The RMS in Layer 3 (Carrizo) was 26.9 ft and the range in head was 353.4 ft, giving an RMS/range of 0.076. The head calibration statistics are summarized in the Table 8.2.1.

Table 8.2.1 Steady-state head calibration statistics.

Layer	Count	ME (ft)	MAE (ft)	RMS (ft)	Range (ft)	RMS/Range
1	30	8.6	28.6	34.6	306.6	0.11
3	23	6.9	19.7	26.9	353.4	0.076

Figures 8.2.1 and 8.2.3 support these statistics where slightly more variation is evident in the scatter plot (Figure 8.2.1) for Layer 1 than in the scatter plot (Figure 8.2.3) for Layer 3. The scatter plots show a good distribution of residuals around zero. Figure 8.2.4 shows a comparison of the simulated steady-state Carrizo head surface and the estimated predevelopment Carrizo-Wilcox head surface (Section 4.4.1). Note that statistics could not be calculated for layers 2, 4, 5, and 6 where only one or two predevelopment targets were available. The simulated head surface for the Reklaw/Bigford (Layer 2) is included in Figure 8.2.2. The simulated head surfaces for the upper, middle, and lower Wilcox layers are included in Figures 8.2.5-8.2.7.

The Carrizo head surface in Figure 8.2.3 indicates that the gradient in the steady-state model is mostly east-southeast, moving downdip consistent with the observed heads. In the eastern portion of the model, there is a depression in the head surface in Gonzales County. This depression is considered the result of a large number of streams running through that area. The

Wilcox layers show similar trends in head distribution to the Carrizo (Figures 8.2.5 – 8.2.7), with gradients decreasing in the lower Wilcox layers. Heads increase in the lower layers for a given horizontal location, indicating an upward gradient in the downdip portion of the model. This upward gradient is consistent with the conceptual model discussed in Section 5.

Some cells went dry in the steady-state simulation. The rewetting option was not used in the steady-state, because it was unstable when combined with the ET package. Out of 6,892 outcrop cells, 259 were dry, or 3.7%. These dry cells can be indicative of model instability or actual subsurface conditions. Because no obvious discontinuities exist in the model predicted outcrop water table, these cells are likely indicative of actual subsurface conditions (i.e., small cell thickness, low water table). The small number of dry cells does not have a significant impact on model results.

8.2.2 Streams

We have no defined calibration targets for the streams for the predevelopment model because no gain/loss estimates are available for the modeled streams in the applicable time period (turn of the century or before). Based upon historical occurrence of flowing wells across the model area, intuitively we would expect the major streams to be gaining. This is consistent with the analysis performed in LBG-Guyton and HDR (1998).

Figure 8.2.8 shows the gain/loss values for the stream reaches in the steady-state model. As would be expected, the larger stream segments are more likely to be gaining than the smaller tributaries which are typically higher in shallower channels and higher in overall elevation. The streams in the eastern portion of the model are more gaining than those in the west, partially due to the higher amount of recharge in that region and the shallower water table.

8.2.3 Water Budget

Table 8.2.2 summarizes the water budget for the model. The mass balance error for the steady-state model was 0.71 percent. As would be expected, the predominant input source is recharge. Water discharging from the model is split between the streams, ET, and the GHBs in descending order. Groundwater ET removes about 36% of the recharge that goes into the model under predevelopment conditions. The majority of the water exiting the Carrizo leaves by cross-formational flow through the bottom of the Reklaw Formation which is consistent with our conceptual model detailed in Section 5. This rate is approximately equal to that leaving the

Reklaw through the top, and is also similar to the rate exiting Layer 1 through the GHBs. This indicates that most of the water that is flowing in the Carrizo in the confined section exits upward through the Reklaw and Queen City formations. Also, the Carrizo has groundwater flowing in through the bottom of the formation, although it is small in comparison to the amount coming in through recharge. The accuracy of this component of flow into the Carrizo from below is unknown because there were very few Wilcox wells in the confined section in historical times. However, it is hydraulically correct that flow is diverted towards higher permeability layers from less permeable layers.

Table 8.2.3 gives the various sources and sinks as percentages of the total water entering or leaving the model. The highest percentage of recharge occurs in the Queen City, due to its large outcrop. The highest percentage of ET occurs in this same layer, for the same reason. Recharge makes up 87% of the inflow to the model, with streams contributing 11%. Forty-three percent of the water leaving the aquifer exits through the streams, while 31% and 27% exit through groundwater ET and GHBs, respectively. Approximately two-thirds of the water that enters the model through recharge and losing streams ends up moving downdip and exiting the Carrizo-Wilcox via cross-formational flow.

In Atascosa County there is a study that allows us to check the Carrizo flow rates from the outcrop to the confined section. Pearson and White (1967) performed a groundwater age dating study in Atascosa County using Carbon-14 age dating techniques. Figure 8.2.9 shows their estimate of groundwater travel times from the outcrop to the confined section. Also included in Figure 8.2.9 is a particle track from the steady-state model run for 20,000 years. The model travel path and time of travel shows good agreement with the results of Pearson and White (1967) providing a good validation measure for flow in that portion of the model. Consistent with our conceptual model, the particle moves from the Carrizo and into the Reklaw in southern Atascosa County.

Table 8.2.2 Water budget for the steady-state model (AFY).

IN	Layer	GHBs	Recharge	Streams	Top	Bottom
	1	7,892	125,096	16,681		95,491
	2		37,677	11,341	18,610	99,316
	3		71,137	6,544	30,852	23,118
	4		893	105	9,350	16,390
	5		58,061	3,922	1,981	19,841
	6		33,852	3,607	8,683	
	Sum	7,892	326,716	42,199	69,477	254,156
OUT	**Layer**					
	1	100,523	57,496	68,937		18,610
	2		17,958	22,757	95,491	30,852
	3		7,200	17,256	99,316	9,350
	4		896	935	23,118	1,981
	5		19,934	38,736	16,390	8,683
	6		14,054	12,810	19,841	
	Sum	100,523	117,539	161,431	254,156	69,477

Table 8.2.3 Water budget for the steady-state model with values expressed as a percentage of inflow or outflow.

IN	Layer	GHBs	Recharge	Streams
	1	2.1	33.2	4.4
	2		10.0	3.0
	3		18.9	1.7
	4		0.2	0.0
	5		15.4	1.0
	6		9.0	1.0
	Sum	2.1	86.7	11.2

OUT	Layer	GHBs	ET	Streams
	1	26.5	15.2	18.2
	2		4.7	6.0
	3		1.9	4.5
	4		0.2	0.2
	5		5.3	10.2
	6		3.7	3.4
	Sum	26.5	31.0	42.5

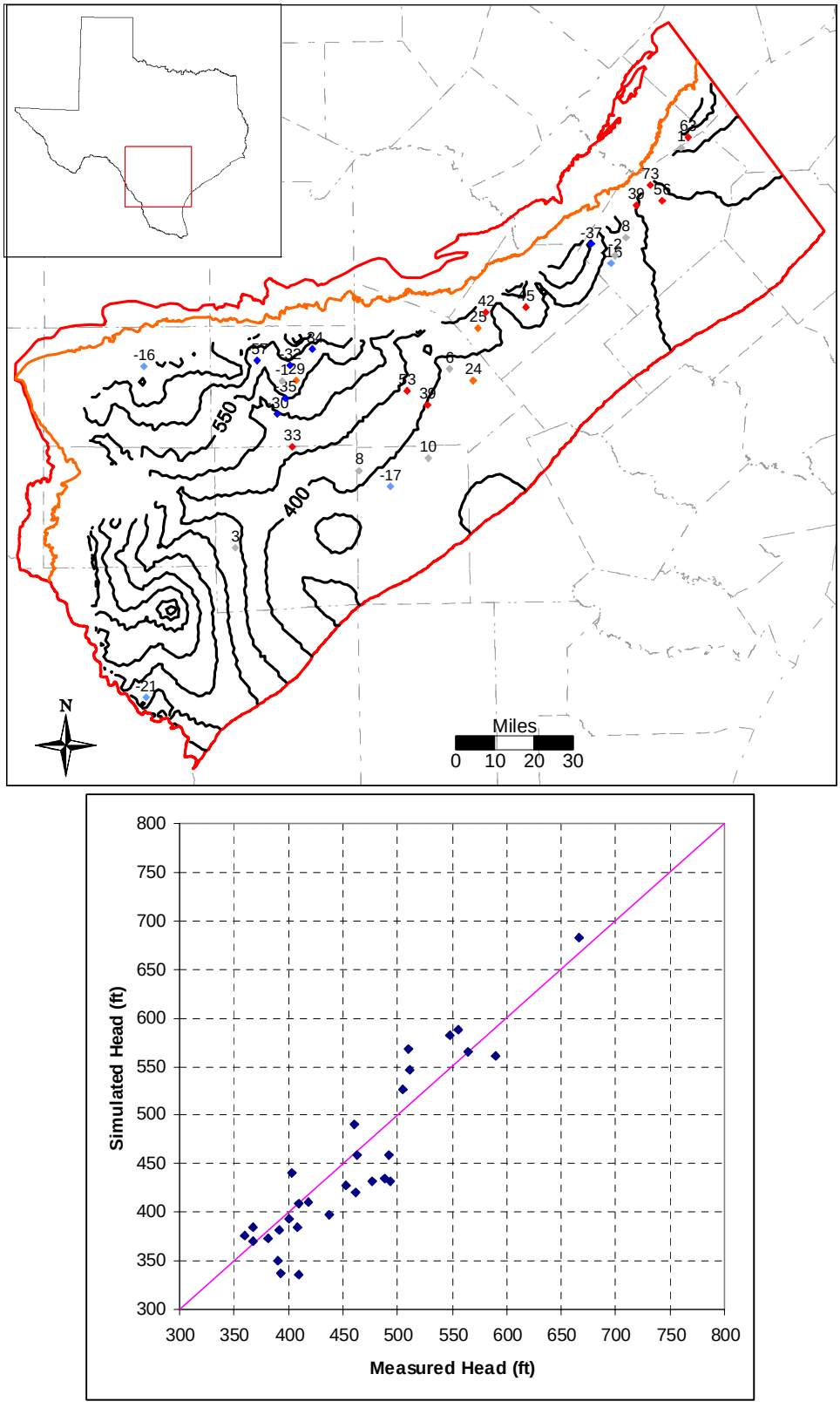

Figure 8.2.1 Simulated steady-state head surface, residuals and scatterplot for the Queen City/El Pico (Layer 1).

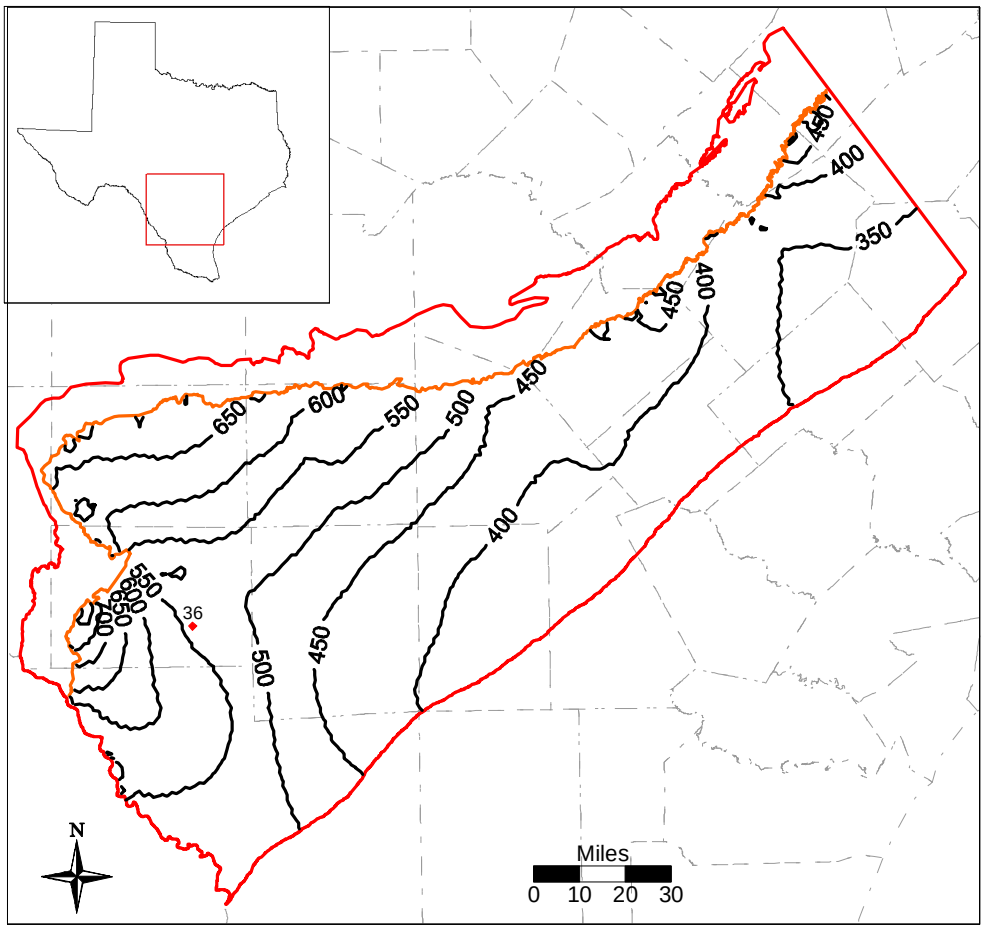

Figure 8.2.2 Simulated steady-state head surface and posted residuals for the Reklaw/Bigford (Layer 2).

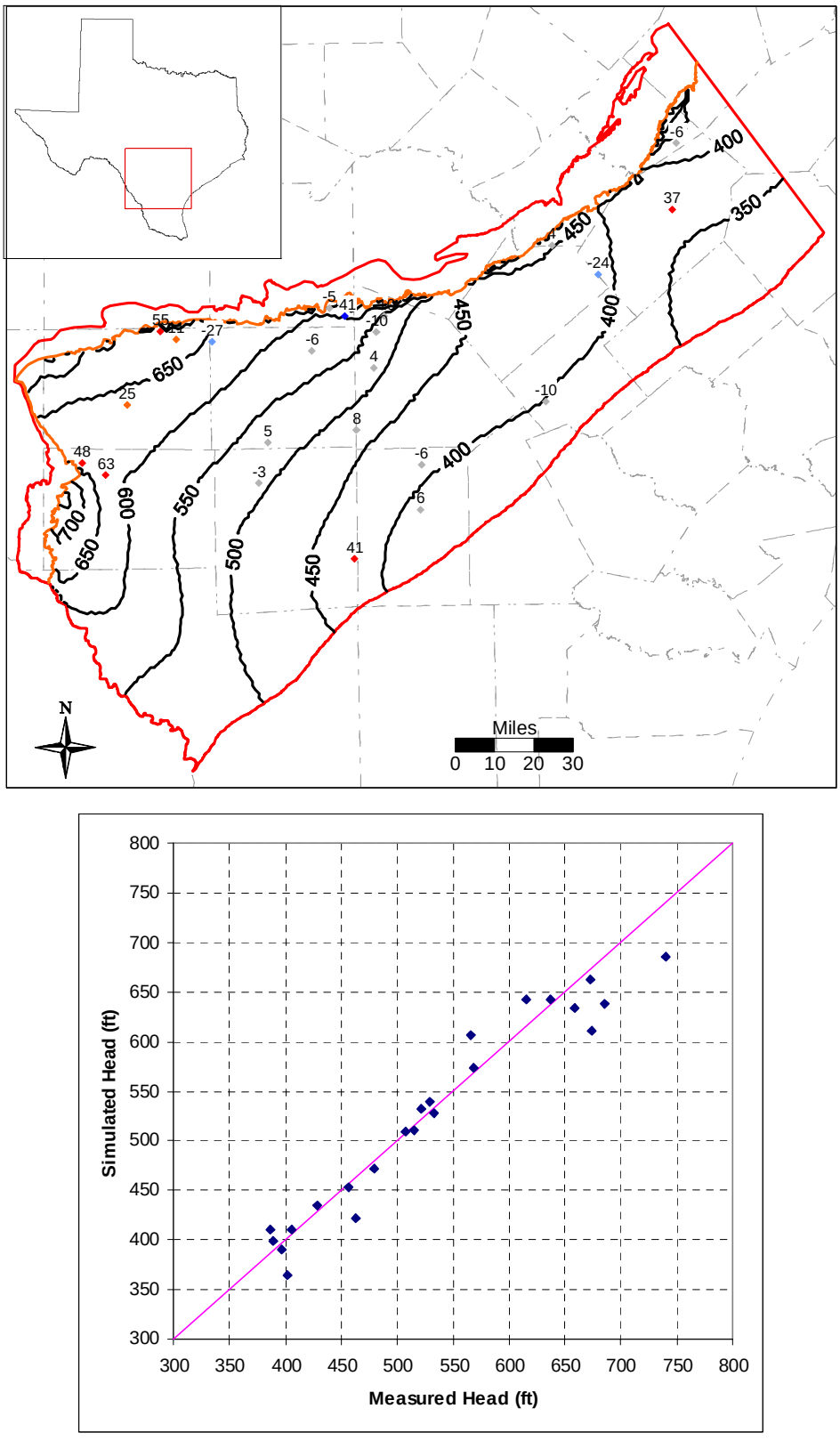

Figure 8.2.3 Simulated steady-state head surface, residuals and scatterplot for the Carrizo (Layer 3).

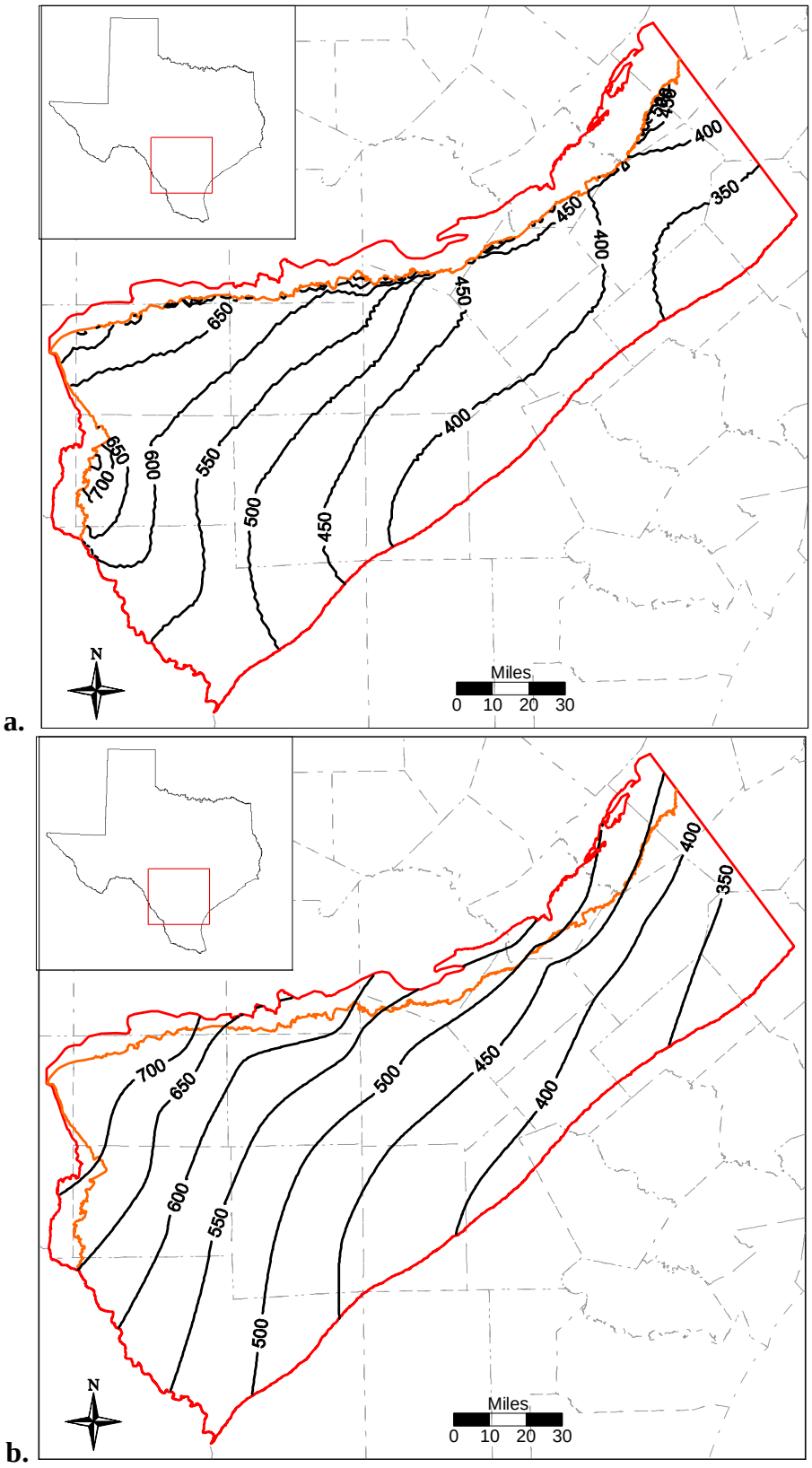

Figure 8.2.4 Simulated (a) and observed (b) steady-state head surfaces for the Carrizo (Layer 3).

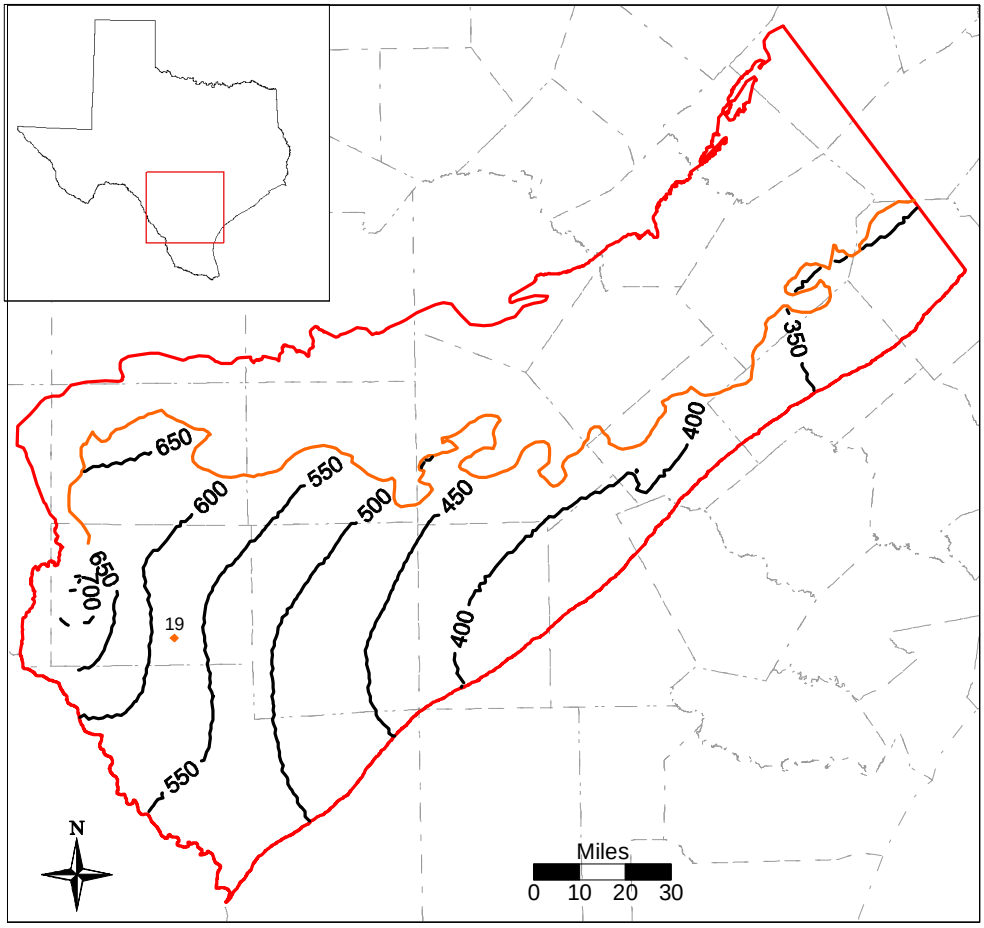

Figure 8.2.5 Simulated steady-state head surface and posted residuals for the upper Wilcox (Layer 4).

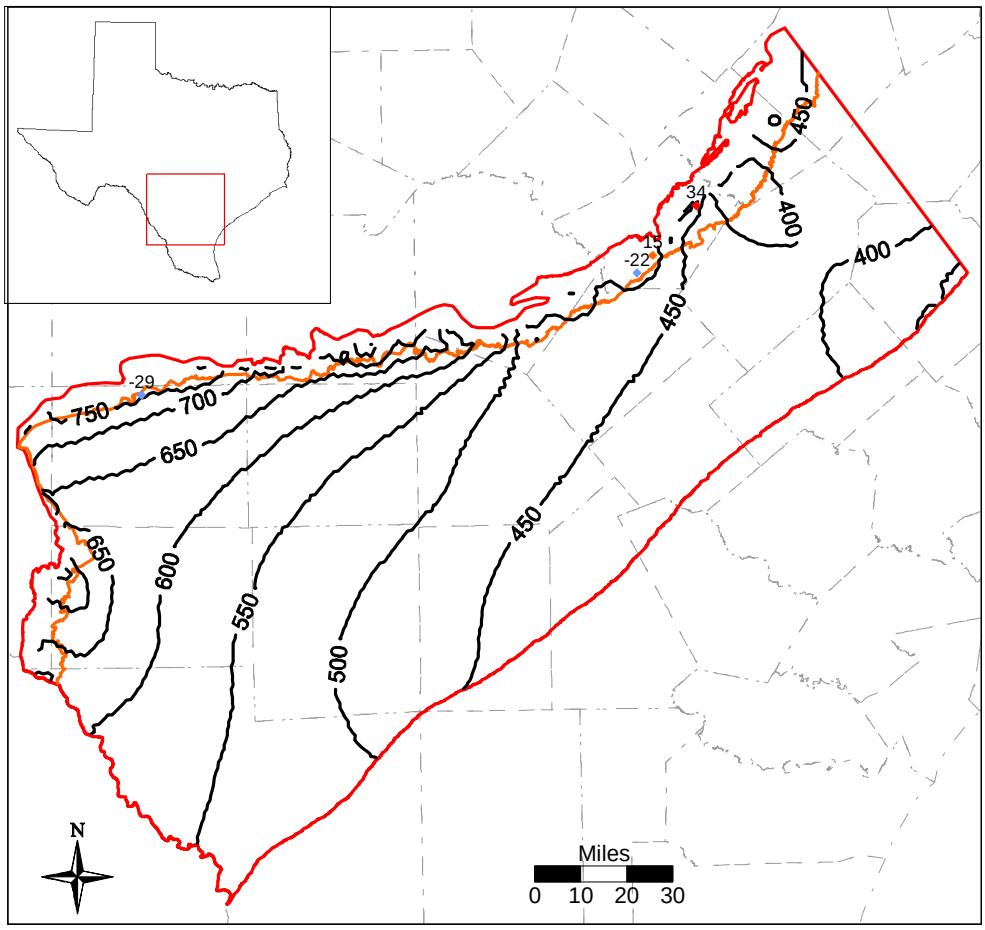

Figure 8.2.6 Simulated steady-state head surface and posted residuals for the middle Wilcox (Layer 5).

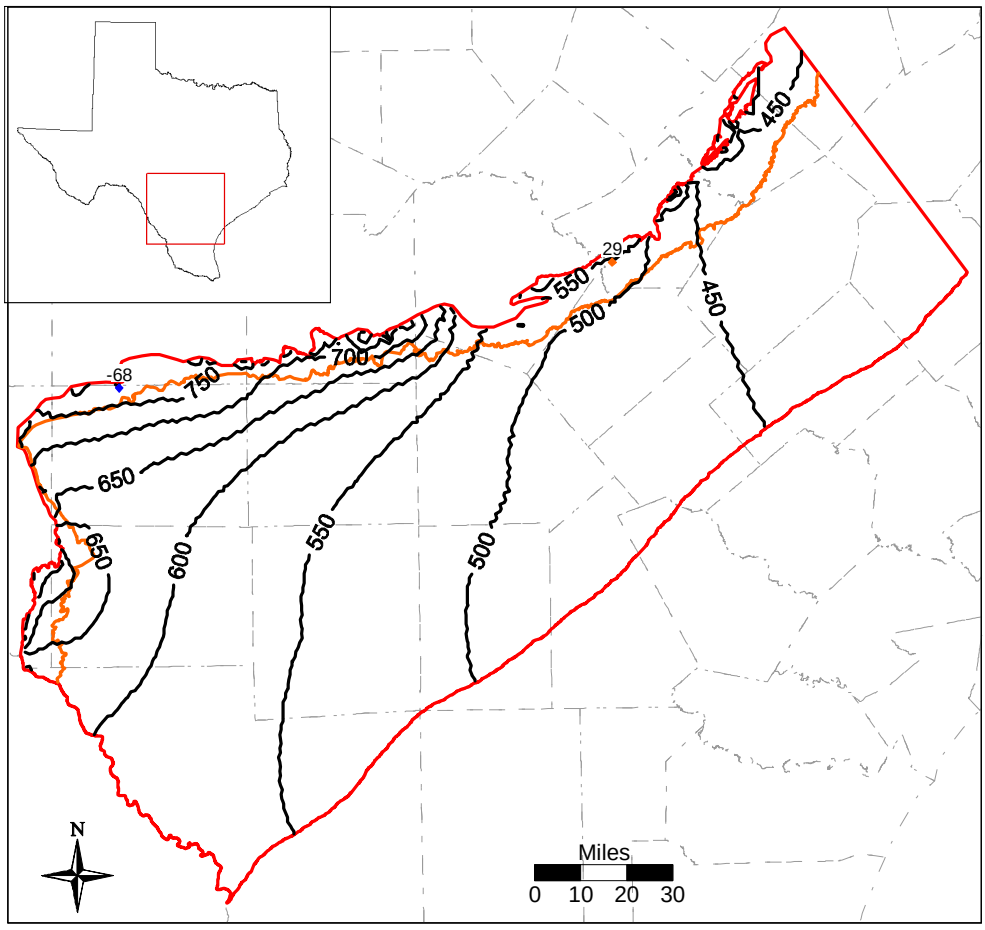

Figure 8.2.7 Simulated steady-state head surface and posted residuals for the lower Wilcox (Layer 6).

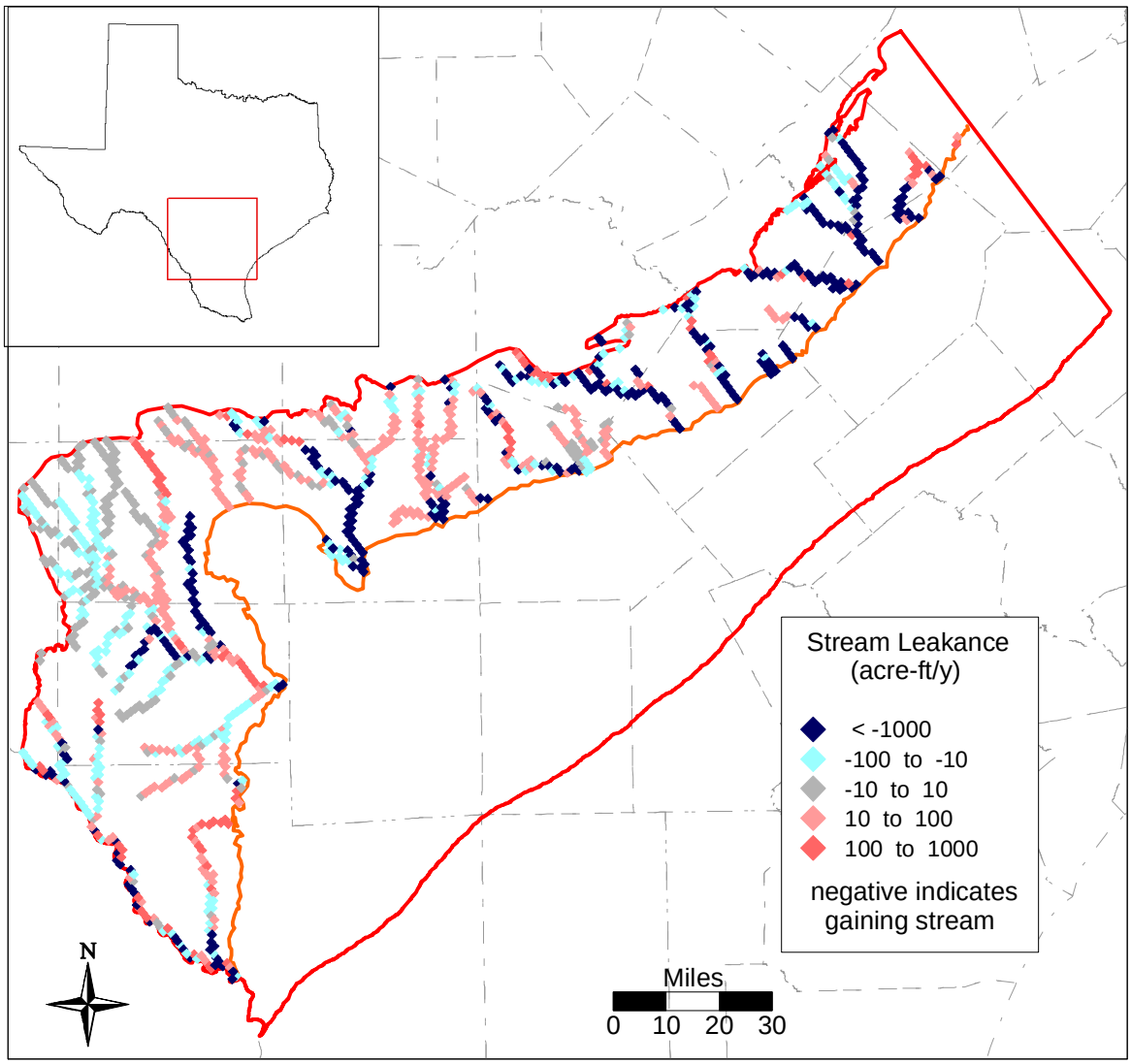

Figure 8.2.8 Steady-state model stream gain/loss (negative value denotes gaining stream).

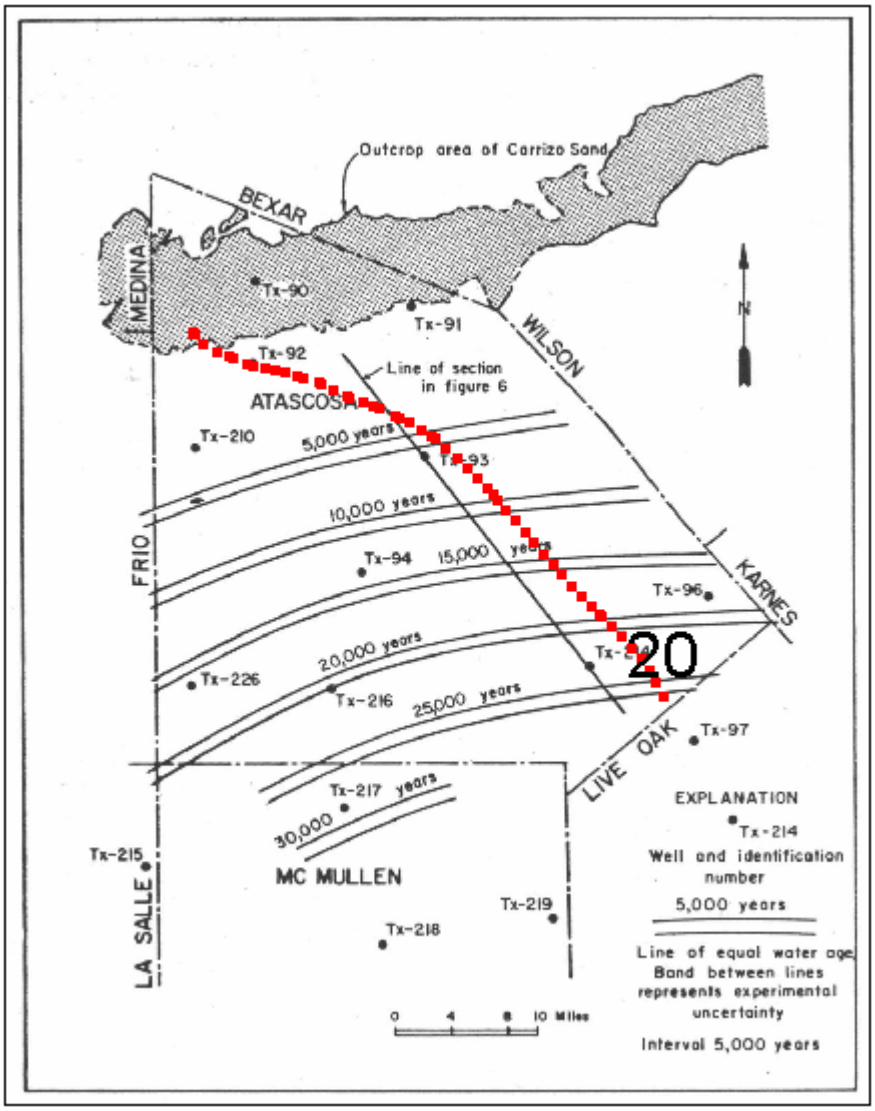

Figure 8.2.9 Steady-state particle travel path and travel time (20,000 years) compared to the groundwater age dating study of Pearson and White (1967).

8.3 Sensitivity Analysis

A sensitivity analysis was performed for the calibrated steady-state model. A sensitivity analysis provides a means of formally describing the impact of varying specific parameters or groups of parameters on model outputs. In this sensitivity analysis, input parameters were systematically increased and decreased from their calibrated values while the change in head was recorded. Four simulations were completed for each parameter varied, where the input parameters were varied either according to:

$$sensitivity\,value = (calibrated\,value)(factor) \tag{8-2}$$

$$sensitivity\,value = (calibrated\,value)(10^{factor-1}) \tag{8-3}$$

and the factors were 0.75, 0.9, 1.1, and 1.25. For parameters such as hydraulic conductivity, which typically vary by orders of magnitude and are usually lognormally distributed, equation (8-3) was used. Parameters such as recharge were varied linearly using equation (8-2). For the output variable, we calculated the mean difference (*MD*) between the base simulated head and the simulated head calculated for the sensitivity simulation for each layer. The equation for calculating the *MD* is:

$$MD = \frac{1}{n}\sum_{i=1}^{n}\left(h_{sens,i} - h_{cal,i}\right) \tag{8-4}$$

where

$h_{sens,i}$ = sensitivity simulation head at active grid block *i*

$h_{cal,i}$ = calibrated simulation head at active grid block *i*

n = number of grid blocks compared

We considered two approaches to applying Equation 8-4 to the sensitivity of output heads. First, we compared the heads in all active grid blocks between the sensitivity output and the calibrated output. Second, we compared the heads only at grid blocks where measured targets were available (i.e., n = number of targets in that layer). A comparison between these two methods can provide information about the bias in the target locations, i.e. a similar result indicates adequate target coverage. However, a drawback to the second method is that sensitivity results will not be available in layers containing an insufficient number of targets.

For the steady-state analysis, we completed 6 parameter sensitivities:

1. Horizontal hydraulic conductivity, model-wide (K_h)
2. Vertical hydraulic conductivity in Layer 2 (K_v-Reklaw, model leakance between layers 2-3)
3. Vertical hydraulic conductivity in Layers 4-6 (K_v-Wilcox, model leakance between layers 3-4, 4-5, and 5-6)
4. Recharge, model-wide
5. Streambed conductance, model-wide (K-Stream)
6. GHB conductance, model-wide (K-GHB)

Equation 8-2 was used for sensitivity to recharge (4), and Equation 8-3 was used for the remainder. Note that the head values assigned to the GHBs were not varied in the sensitivity analysis. These heads were estimated as water table elevations (Section 6.3.2), and variation would result in water levels above ground surface.

Figure 8.3.1 shows the sensitivity results for the Carrizo (Layer 3), with *MDs* calculated from just the gridblocks where targets were available. Figure 8.3.2 shows the sensitivity results for the Carrizo, with *MDs* calculated from all active cells in the layer. Note that the two figures indicate similar trends in sensitivities at 0.75 for the two most positive *MD*s [hydraulic conductivity of the GHBs (K-GHB) and vertical hydraulic conductivity of the Reklaw (K_v-Reklaw)] and the most negative *MD* (recharge). The two figures are less consistent for the *MD*s that were close to zero. However, the good agreement for the significant *MD* values indicates adequate target coverage in the Carrizo.

Figure 8.3.1 indicates that change in head in the Carrizo for the steady-state model is most positively correlated with recharge and most negatively correlated with the conductance of the GHBs. Also, the figure indicates that decreasing the Reklaw vertical hydraulic conductivity increases heads in the Carrizo, as would be expected given the upward cross-formational flow from the Carrizo to the Reklaw. Figures 8.3.3 and 8.3.4 show that Layers 1 and 2 are strongly influenced by the conductivity of the GHBs. Because the GHBs are present in a large portion of Layer 1, they have a large effect. This effect propagates through to the Carrizo (Layer 3), since the gradient between Layers 1 and 3 is important to determining Carrizo heads downdip. This effect is illustrated in Figure 8.3.5, which gives the sensitivity results for all layers when the

GHB conductivity was varied. The sensitivity decreases in order with increasing layer depth. A significant drop in sensitivity occurs between the Carrizo and middle Wilcox layers. Because of the low vertical conductivity of the middle Wilcox (Layer 5), the effect is dampened. This is illustrated again in Figure 8.3.6, where the sensitivity of the middle Wilcox to both recharge and vertical hydraulic conductivity is on the same order as the sensitivity to GHB conductance. Heads in the lower Wilcox (Layer 6) are most sensitive to the vertical hydraulic conductivity of the Wilcox, as shown in Figure 8.3.7. Because this layer is modeled as impermeable at the bottom, its connection to the rest of the model is through the middle Wilcox, or through recharge in the outcrop, which is the second most important factor. Recharge is an interesting sensitivity, because the relative *MD* for a layer appears to be dependent on the elevation of the outcrop. Figure 8.3.8 illustrates this, with the lower Wilcox (Layer 6) being most sensitive and the Queen City/El Pico (Layer 1) being least sensitive, even though Layer 1 has the largest outcrop. However, this could be due to the higher calibrated head values in Layer 6. Stated otherwise, a similar percent change in head leads to higher *MD*s in Layer 6 as compared to Layer 1 because *MD* is not scaled by calibrated head.

The sensitivity analysis determined that the two most important parameters to predicting heads in the Carrizo in the steady-state model are recharge and the vertical conductivity of the formations overlying the Carrizo (vertical hydraulic conductivity of the Reklaw and the GHBs).

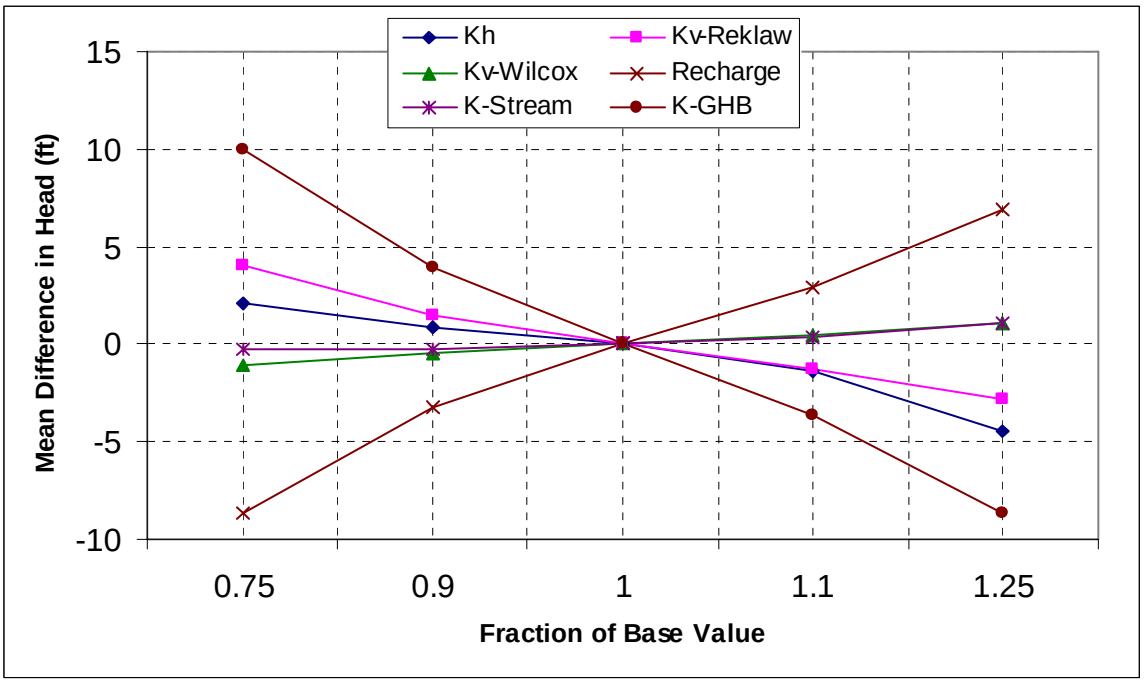

Figure 8.3.1 Steady-state sensitivity results for the Carrizo (Layer 3) using target locations.

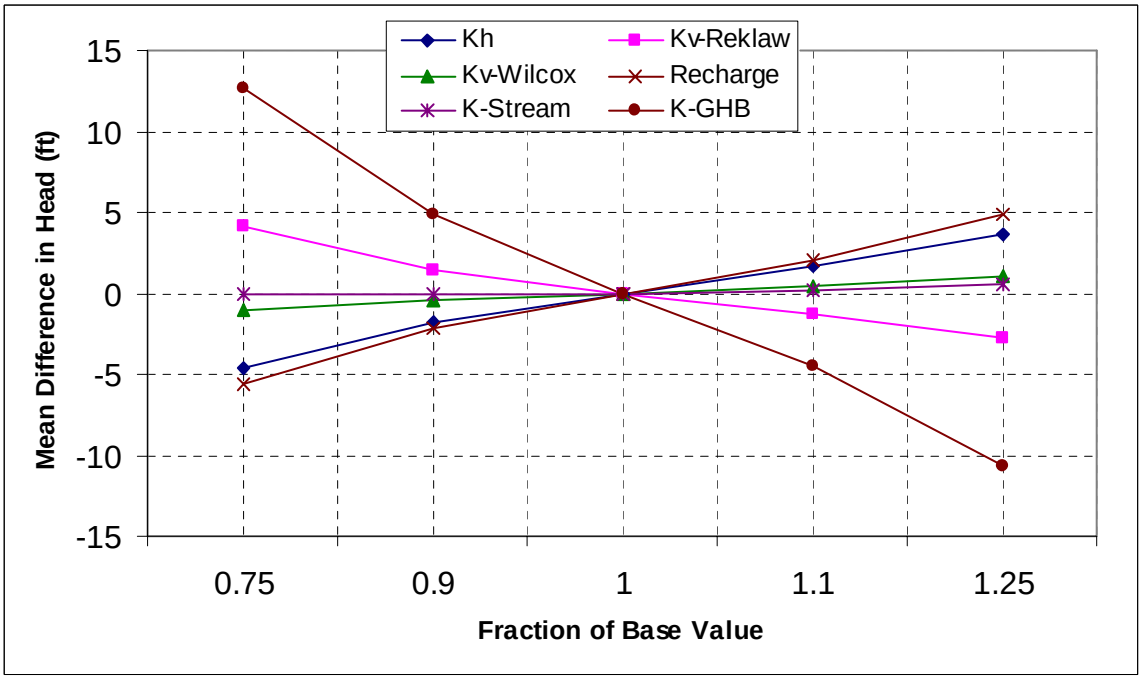

Figure 8.3.2 Steady-state sensitivity results for the Carrizo (Layer 3) using all active gridblocks.

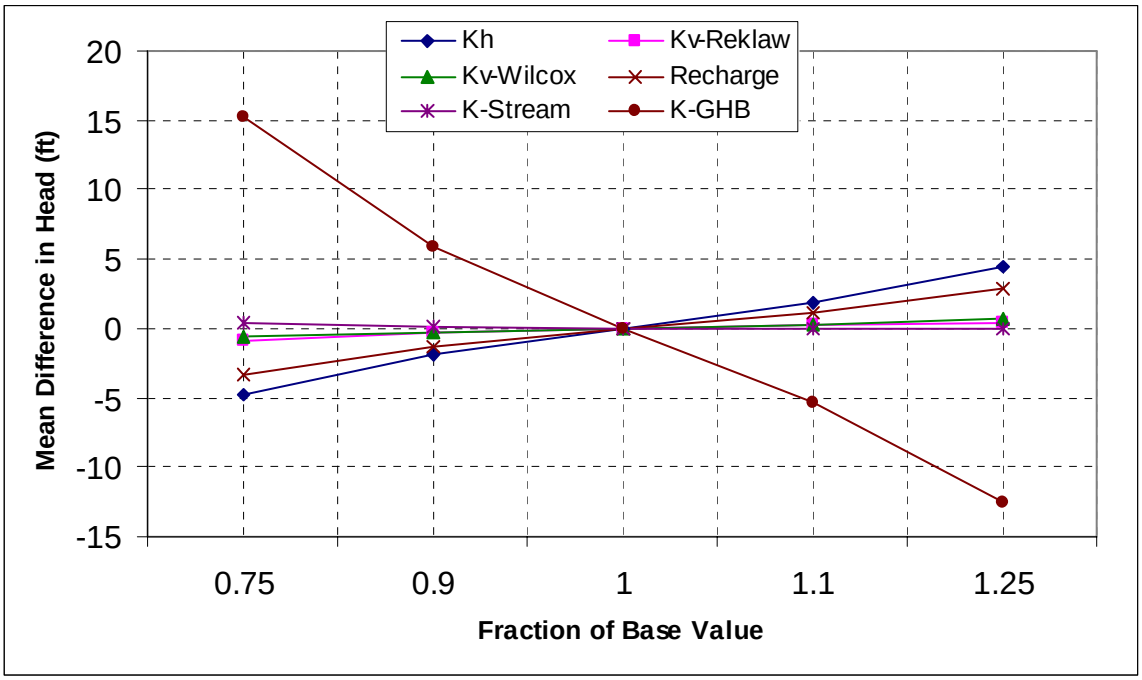

Figure 8.3.3 Steady-state sensitivity results for the Queen City/El Pico (Layer 1) using all active gridblocks.

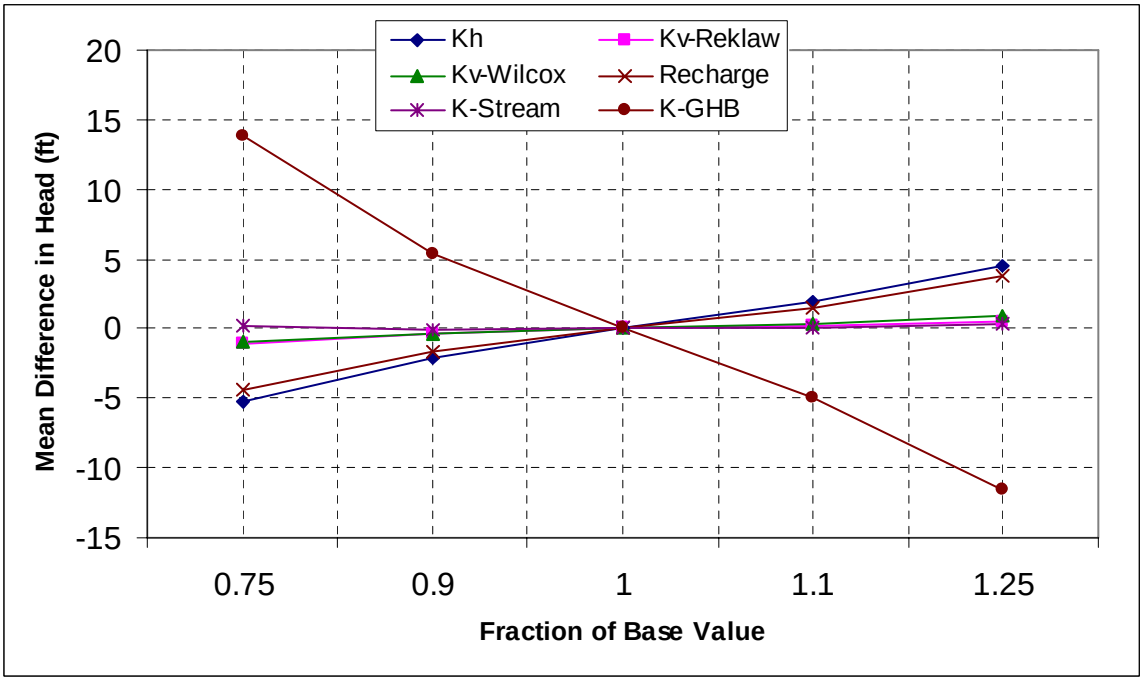

Figure 8.3.4 Steady-state sensitivity results for the Reklaw/Bigford (Layer 2) using all active gridblocks.

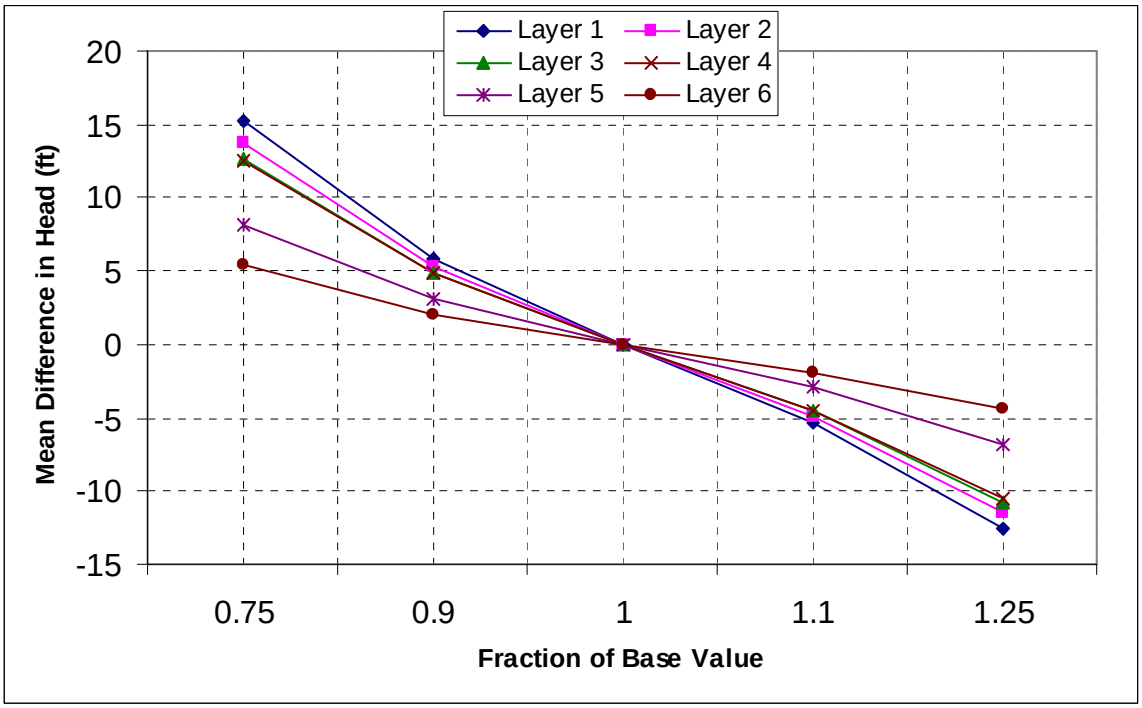

Figure 8.3.5 Steady-state sensitivity results where GHB conductivity is varied.

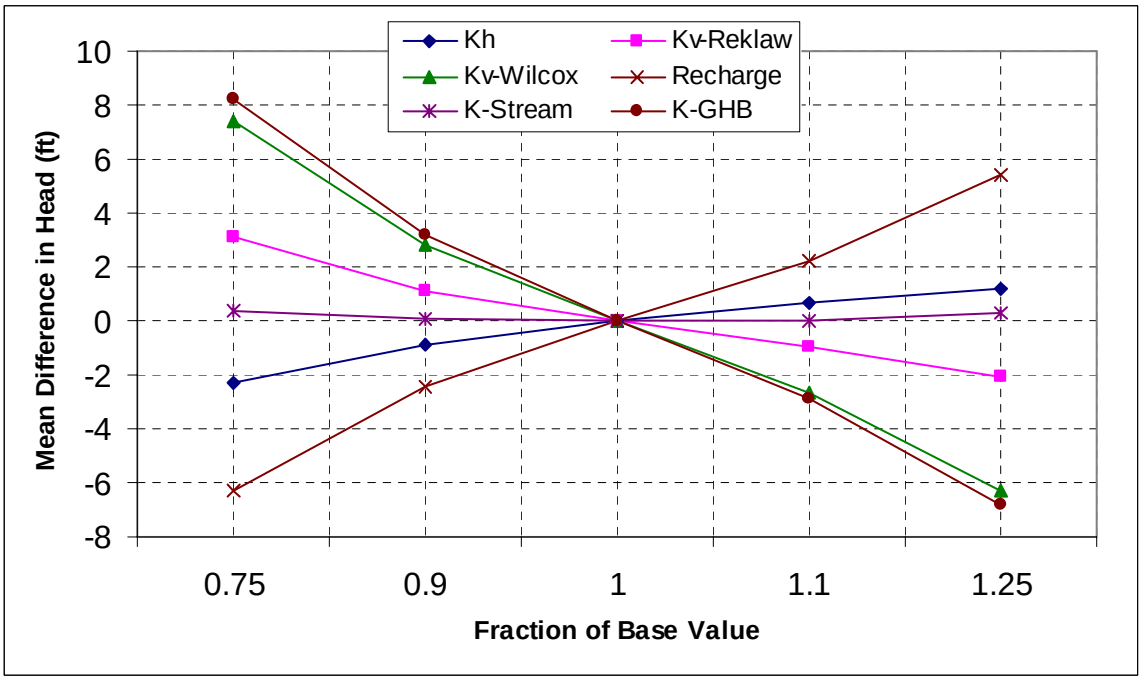

Figure 8.3.6 Steady-state sensitivity results for the middle Wilcox (Layer 5) using all active gridblocks.

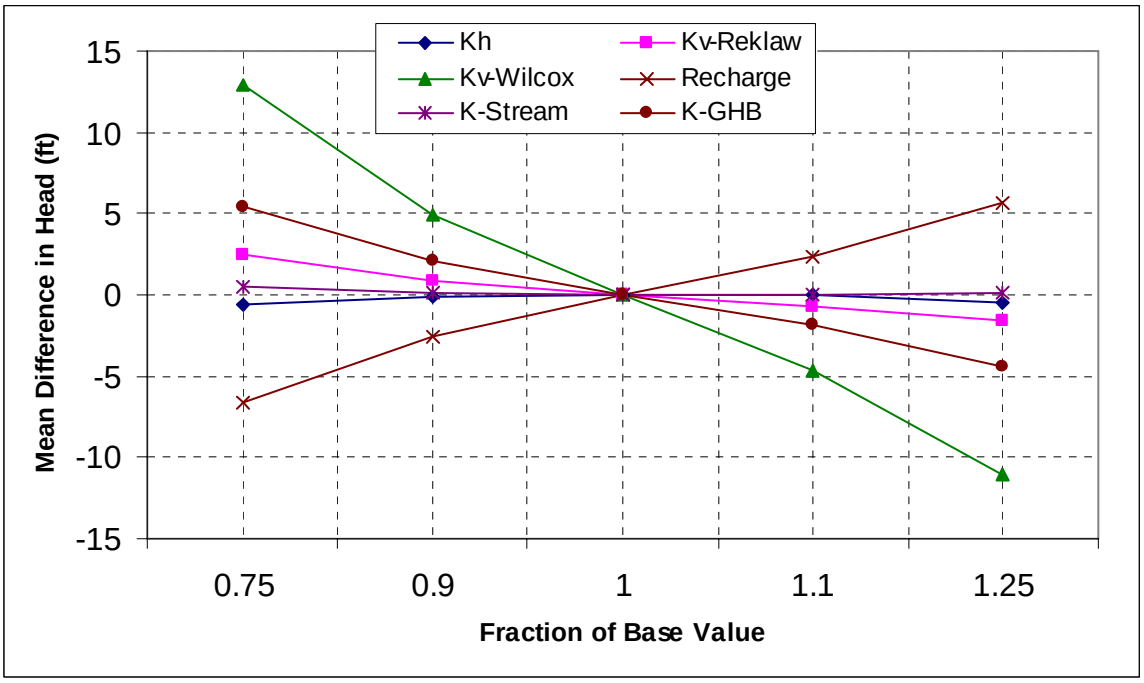

Figure 8.3.7 Steady-state sensitivity results for the lower Wilcox (Layer 6) using all active gridblocks.

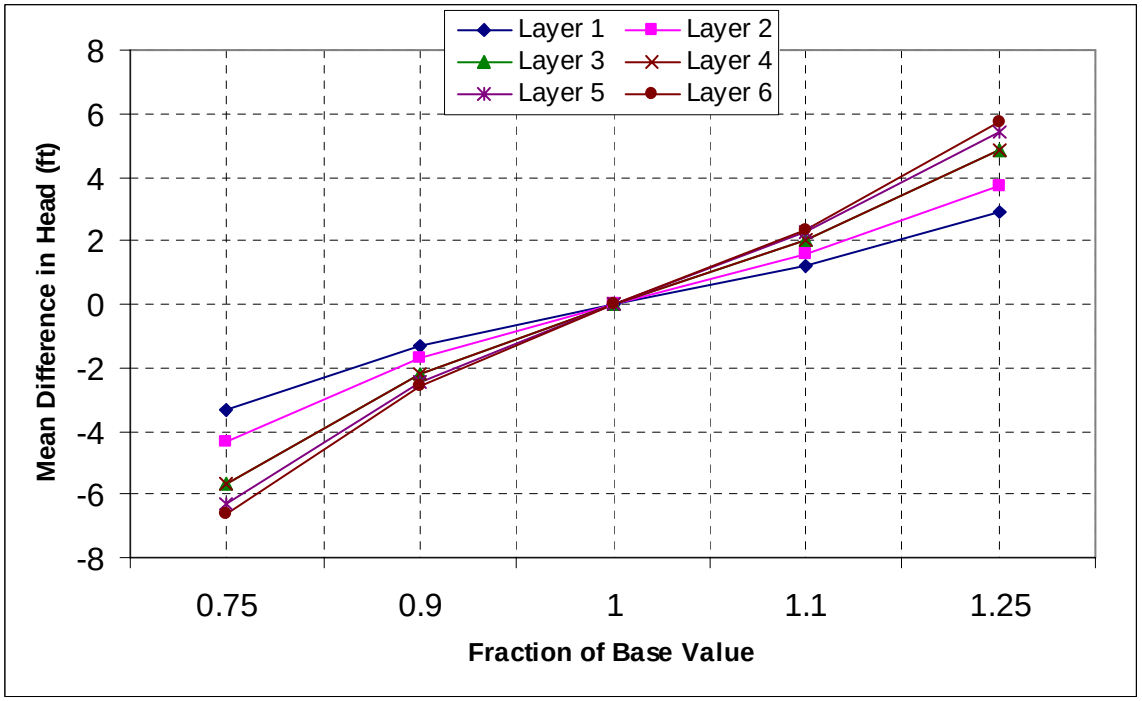

Figure 8.3.8 Steady-state sensitivity results where recharge is varied.

9.0 TRANSIENT MODEL

This section describes the calibration and verification of the transient model and presents the transient model results. This section also describes a sensitivity analysis for the transient model. The transient model was started in 1975 to allow any initialization effects to dampen by 1980, the start of the calibration period. This period from 1975 to 1980 was considered a "ramp up" period, and was not used for calibration. The model was calibrated for the time period from 1980 through 1989. The model was verified for the time period from 1990 through 1999. The model calibration is discussed in Section 9.1. The results from the calibration period and the verification period are discussed together in Section 9.2. A formal sensitivity analysis with the calibrated transient model is presented in Section 9.3.

9.1 Calibration

Because the groundwater model must be calibrated to steady-state and transient conditions using the same physical hydraulic properties, calibration is an iterative process between the conditions. As a result, the physical properties which are common between the steady-state model and the transient model are the same, as presented in Section 8.1. In addition, a transient model requires storage estimates for the aquifers and these are discussed in this section. Also, the calibration process is further discussed in light of the transient model.

The transient model played an important part in setting vertical anisotropy ratios (K_h/K_v) for the model. We initially set the anisotropy ratios of the Reklaw/Bigford (Layer 2) and the Wilcox Group (Layers 4-6) to values on the order of 100 to 1,000. However, during initial transient calibration, we found that water was flowing between the formations so freely that drawdowns resulting from pumping centers could not be maintained at the estimated pumping rates. Water was moving into the Carrizo from storage in the Wilcox and Reklaw/Bigford layers (or from storage in the El Pico/Queen City through the Reklaw/Bigford) due to the high vertical gradients initialized in pumping centers, especially in the Wintergarden area. We tried increasing the anisotropy ratios by decreasing the vertical hydraulic conductivity in the Reklaw/Bigford and the Wilcox to near the extremes of published values. This increase in anisotropy mitigated the "rebound" effect considerably in these areas. Figure 9.1.1 illustrates the impact in Wilson County of half an order of magnitude change in anisotropy in the Reklaw.

Figure 9.1.1 shows that the water level trend changes from basically flat to downward during the calibration period. During calibration, we reduced the vertical hydraulic conductivity (e.g. increased anisotropy) until an optimum match was attained. The final vertical hydraulic conductivities resulting from the calibrated anisotropy ratios (Table 8.1.1) are within published limits for these formation materials, but are lower in magnitude than we expected for a regional scale model.

Primary and secondary storage (also called storativity and specific yield) are properties of a transient model that are not required in a steady-state model. Specific storage was defined as 3.0×10^{-6} (1/ft) in all layers based upon a review of published data, prior models, and considering the materials of the formation. Specific storage was then multiplied by layer thickness to provide the storativity at each grid cell. Storativity has an impact upon the amplitude of head variation due to pumping. However, we did not find overall hydrograph trends to be strongly sensitive to storativity, and therefore did not make areal changes in storativity during calibration. Figure 9.1.2 is a hydrograph that illustrates the effect of an order of magnitude increase in storativity in Frio County. Note that the seasonal effect of pumping is dampened, but the overall trend of the hydrograph is very similar. When we reduced the storativity further, the response of simulated heads to seasonal variations in pumping increased to unreasonable levels. Figure 9.1.3 shows the variation of storativity in the Carrizo. The storativity of the Carrizo is generally less than 0.003 except for a thick portion of the aquifer in south Atascosa County and in the outcrop where it was set to one. A storativity of one in the outcrop overcomes the numerical limitation of MODFLOW when it calculates heads above ground surface in an unconfined section.

Because there are only two reservoirs in the model area, reservoirs did not play a significant role in the calibration. We initially assumed a hydraulic conductivity of 1 foot per day in the reservoir conductance calculation. This value resulted in too much aquifer-reservoir interaction, so we decreased the conductivity until a more reasonable amount of water passed between the reservoirs and the aquifer.

Because we lacked good targets for stream leakance, we made only coarse adjustments to streambed conductivity during the calibration. The streams exchange significant volumes of water with the aquifer, so they are important in the outcrop area. However, in the transient

model, the hydrology of the outcrop has little effect on downdip regions during the simulation period. We made comparisons between simulated stream leakances and some general reported estimates (Section 9.2.2).

As noted in the steady-state calibration Section 8.1.2, SWAT-predicted recharge was decreased in the eastern portion of the model so that recharge in that area was more consistent with the rest of the model. Recharge is still highest in the east, reaching values in excess of 3 inches per year.

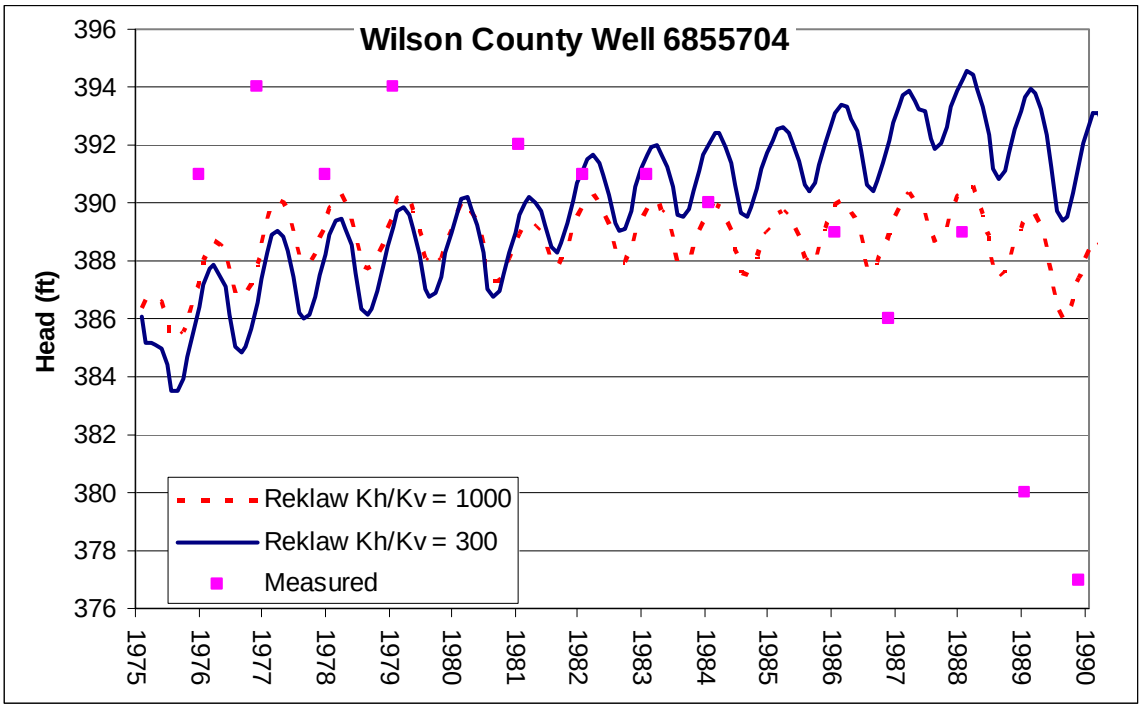

Figure 9.1.1 Example of head sensitivity to Reklaw vertical hydraulic conductivity.

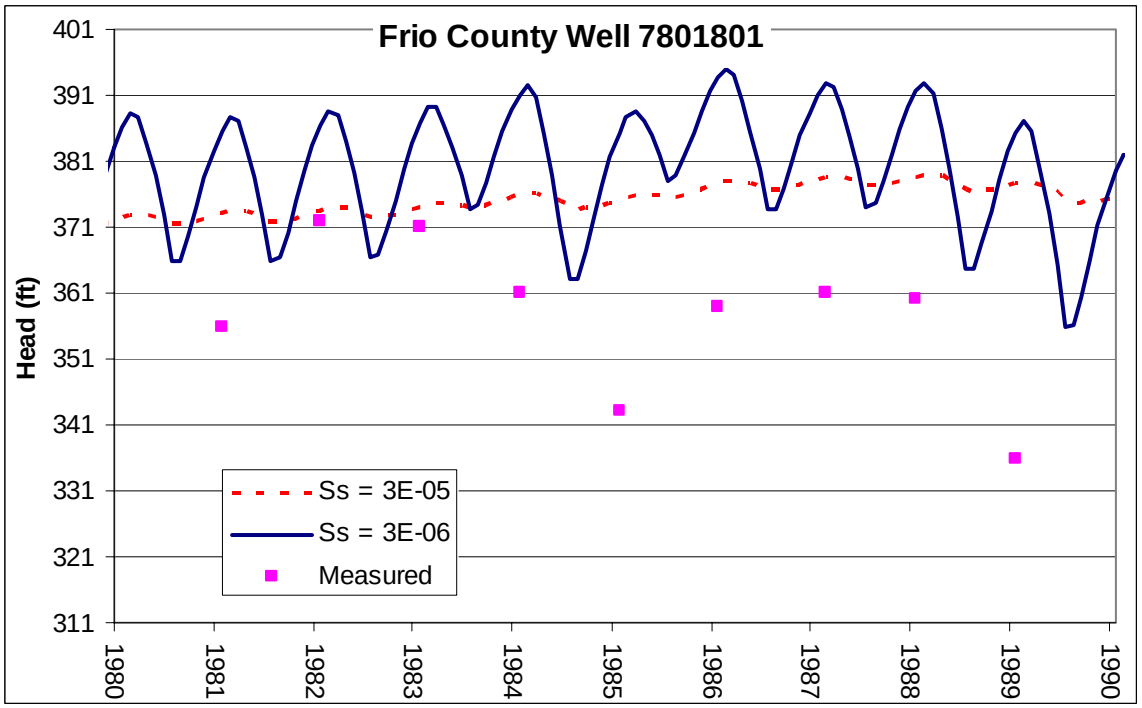

Figure 9.1.2 Example of head sensitivity to specific storage.

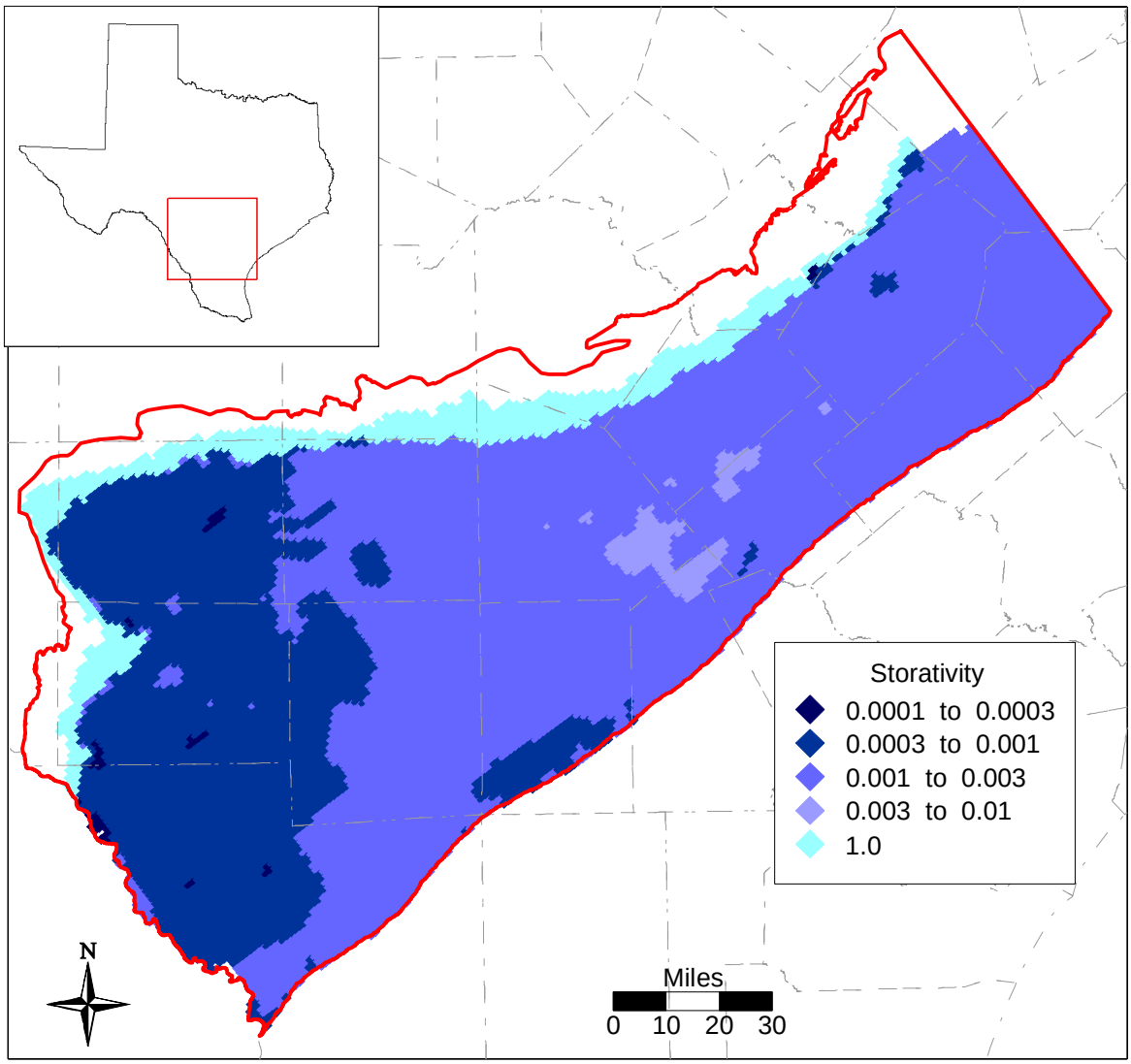

Figure 9.1.3 Storativity in the Carrizo Formation (Layer 3).

9.2 Results

The results of the transient calibrated model are compared to the available calibration targets in this section. The calibration measures were also applied to the verification period to provide an indication of the model's predictive capability.

9.2.1 Hydraulic Heads

Figures 9.2.1 and 9.2.2 show simulated head surfaces at the end of the transient calibration period (1989) and at the end of the verification period (1999) respectively. The measured and predicted heads are representative of December of those years. The general trends of the simulated and measured data are the same. However, the simulated heads do not show as pronounced a drawdown in portions of the western model region where significant water level declines have been observed. As noted in the previous section, during calibration we decreased the vertical hydraulic conductivity of the model layers above and below the Carrizo to help maintain drawdowns in the western portion of the model. However, without modifying either horizontal hydraulic conductivity or pumping, we were not able to sustain the largest drawdowns. Because well-distributed well test data exist for the Carrizo throughout most of the problem area, we did not feel that we could arbitrarily modify horizontal hydraulic conductivity. Similarly, we could not find objective evidence for re-distributing our pumping, even though we know that the distribution of pumping is uncertain. This problem with insufficient drawdowns in the largest drawdown centers in the Wintergarden area was also experienced by LBG-Guyton and HDR (1998). The fit in the west-central part of the model should be further investigated as discussed in the future improvements section of this report.

Figure 9.2.3 shows the distribution of available transient head targets for the model layers. The majority of the targets are in the Carrizo layer. Most of the targets had incomplete records over the simulated time period. As a result, calibration statistics have been calculated using all of the available data in time and space for the calibration and verification periods. Table 9.2.1 shows the mean error (ME), mean absolute error (MAE), root mean square error (RMS), range, and RMS/range for aquifer layers in the transient model for the calibration and verification periods. The RMS/range for the Carrizo (Layer 3) was 0.059 for the calibration period. The RMS/range increases to 0.092 in the verification period, which is still within the calibration criteria of 0.10. The increase in RMS during the verification period is largely due to

the aforementioned non-sustained drawdowns in the western portion of the model. This is evident in Figure 9.2.4 which shows a crossplot comparison for the Carrizo (Layer 3) between the calibration and verification periods. These crossplots compare all of the measured heads through each time period to their corresponding simulated heads. The tailing in the lower part of the verification period crossplot is a result of the inability of the model to maintain the largest drawdowns in the western region. Figures 9.2.5 and 9.2.6 show the crossplots for the calibration and verification periods, respectively, for the remainder of the model layers. Note the general scarcity of data in these layers compared to the Carrizo. In all cases where significant data are available, the crossplots show a good correlation between the measured and simulated heads.

Figures 9.2.7 – 9.2.13 show selected hydrographs by layer for the transient model. Table 9.2.2 provides the calibration statistics for these hydrographs. All hydrographs in this section are shown on a 100 ft vertical scale for consistency, unless the data range exceeds 100 ft. Figure 9.2.7 shows hydrographs for the Queen City/El Pico (Layer 1). In general, both the simulated and measured heads stay at nearly the same level throughout the simulation. Figure 9.2.8 shows the hydrographs for the Carrizo (Layer 3) in the western region of the model. Some of the hydrographs in Zavala and Dimmitt counties show considerable fluctuation with seasonal pumping. The measured data for these hydrographs typically show scatter in a similar range. This region is very difficult to simulate because some proximal hydrographs show opposite trends, as illustrated in Figure 9.2.8. Examples of both declining and recovering heads are shown for Zavala and Dimmitt counties. These trends emphasize the importance of having correct pumping, not only in magnitude but also in location. Figure 9.2.9 shows the hydrographs for the Carrizo (Layer 3) in the central region of the model. The figure shows declining hydrographs in Bexar and Atascosa counties that are matched well by the simulated heads. The recovering heads in LaSalle County are not matched as well, with the simulated heads flattening out while the measured heads continue to recover. Figure 9.2.10 shows the hydrographs for the Carrizo (Layer 3) in the eastern region of the model. The counties in this region generally do not have much pumping stress, and both the measured and simulated hydrographs are relatively flat. The exception is the hydrograph from Guadalupe County in which both the simulated and measured data are slowly declining over the course of the simulation. Figure 9.2.11 shows the few hydrographs in the upper Wilcox Formation. The measured data from Webb County and from one of the Dimmitt County hydrographs are erratic, making it difficult to judge the trend.

The Atascosa County hydrograph shows declining heads with a good fit for the simulated heads. The southern Dimmitt County measured hydrograph appears flat, while the simulated hydrograph is rising, resulting in a poor fit. Figure 9.2.12 shows transient hydrographs from the middle Wilcox formation. The simulated heads in both Wilson and Gonzales County hydrographs are increasing slightly over the course of the simulation. While this trend is not reflected in the measured data, the increase is less than 10 feet over the entire simulated time period. Given the scale of the model, and the model error discussed in Section 7.2, this trend is not significant. The Uvalde and Atascosa County graphs show stable simulated and measured heads. The Zavala County hydrograph is somewhat erratic, although the range of the scatter is similar to the amplitude of the simulated head, possibly indicating a good estimate of storativity for that region. Figure 9.2.13 shows transient hydrographs for the lower Wilcox. The measured and simulated heads in these hydrographs remain relatively stable throughout the simulated period.

Figure 9.2.14 shows the head residuals averaged for the verification period. In the figure, the blue indicates over prediction of heads, and orange or red indicates under prediction of heads. In general, there is a good mix of over and under prediction throughout the model. The area between Atascosa and Frio counties appears to have consistent over prediction which we were unable to correct during calibration, without modifying horizontal hydraulic conductivity or pumping.

More cells go dry in the transient simulation than in the steady-state simulation. This increase is expected since the transient simulation includes pumping, and also includes years where recharge is much lower than average. Dry cells are typically thin cells located at the farthest updip edge of layer outcrops. Because some of these cells are only 20 ft thick, the cells go dry if the water table is more than 20 ft below ground surface. The MODFLOW rewetting package is active, allowing these cells to resaturate given a subsequent increase of the water table elevation. Out of 6,892 outcrop cells, between 1400 and 1550 (20-22%) are dry during the transient simulation. The drying of these thin edge cells is a physically correct condition and we do not expect it to have an adverse impact on model results.

9.2.2 Stream-Aquifer Interaction

We performed direct comparisons of simulated streamflow to stream gages in the model area, and these compared well. However, this is expected because we defined headwater streamflow rates based upon the available gage data. The more important metric for aquifer-stream interaction is the gain/loss estimate. Therefore, we used two data sources for comparison to simulated stream gain or loss; (1) the Slade et al. (2002) study of stream gains and losses in Texas and (2) the average stream gain/loss estimates reported in LGB-Guyton and HDR (1998). Unfortunately, the Slade (2002) report does not contain measurements made within the simulated time period for our model area. The report contained several studies in the area (shown in Figure 4.6.1) completed earlier than the simulated period. The results of these studies are shown in Figure 9.2.15, represented by the solid circles. In addition, the 10^{th}, 50^{th}, and 90^{th} percentile average (1980-1999) simulated stream gain or loss for the same river reaches is shown on the plot, represented by the horizontal lines. Note that reach statistics are based on all stream cells in each reach, for all stress periods in the duration. So, this figure compares the simulated gain/loss estimates to those reported by Slade et al. (2002). The gain/loss studies are referenced by study number on the bottom horizontal axis consistent with Table 4.6.1 of this report and Slade et al. (2002). Studies 104, 349, and 350 were performed on Cibolo Creek. As would be expected, the measured data are predominantly gaining and consistent with the simulated results. Studies 325, 327, and 328 are on the Rio Grande. All of the measured data fall within the simulated data. However, the median of the simulated data is gaining, while all of the measured data are losing. The middle group of studies shown on Figure 9.2.15 were performed on the Nueces River. Most of the measured data fall within the simulated data, showing losing conditions. However, there are two studies that indicated gaining conditions which were not well represented by the model. Studies 165 through 175 are on the Leona River. The magnitude of variation in the measured data is larger than that of the simulated data. The measured data are also both losing and gaining, while the simulated data do not show significant gaining values. In study 130, on the Medina River, the one measurement is within the simulated data and very near the median.

We also compared the stream gain/loss to average estimates reported by LBG-Guyton and HDR (1998) for the period of time when the two models overlap (1980-1990). Table 9.2.3 shows the values taken from Figure 7-7 of LBG-Guyton and HDR (1998) compared to the simulated values. The simulated values are taken from the Carrizo-Wilcox outcrop. In all cases,

the current simulated values show gaining or losing concurrent with the reported simulated values. The largest difference is in the Frio River results, where LGB-Guyton and HDR (1998) simulated the Frio as more strongly losing by 400 acre-ft/yr-mi.

9.2.3 Water Budget

Table 9.2.4 shows the water budget for the transient model totaled for years 1980, 1988 (lowest annual precipitation in the calibration period), 1990, and 1999. In the overall model, the greatest influx of water consistently occurs from recharge, and the greatest outflow of water consistently occurs from pumping. Stream leakance accounts for a large amount of influx or outflow, depending on climatic conditions for the model. In 1980, pumping accounts for approximately 300,000 acre-feet of water extracted from the model, while recharge adds 193,000 acre-feet of water and 303,000 acre-feet of water is lost through the streams. Secondary to these are groundwater evapotranspiration, which removes 62,000 acre-feet and the GHBs, which add 38,000 acre-feet to the Queen City/El Pico. If we consider the outcrop only, 109,000 acre-feet discharge through the streams from storage in the outcrop. The remaining decrease in storage occurs downdip due to pumping. It is important to note when looking at the water budget that the majority of pumping occurs downdip, so most of the water being removed from storage by pumping will not be replenished during the simulation by recharge. The outcrop and downdip sections operate nearly independently over the simulation time period. The streams, recharge and, to a lesser extent, groundwater ET and pumping dominate outcrop hydrogeology. Pumping and storage are the main components of downdip hydrogeology.

The water budget for 1990 illustrates the effect of a wet year on the water budget in this model. Not only does recharge increase significantly, but the streams contain higher flows and higher stages (rising faster than groundwater levels), which leads to greater leakance into the aquifer from losing streams, and less leakance out of the aquifer in gaining streams. Note that if recharge increases groundwater heads above a previously losing stream stage, then the effect will be mitigated by the stream going from losing to gaining. In 1999, dry conditions lead to less recharge and less water in the streams, so the net stream leakance returns to negative.

The Carrizo layer as a single unit is most affected by pumping. Pumping in the Carrizo draws water from storage in the layer and from cross-formational flow from above and below. The net flow of water from the Reklaw to the Carrizo indicates that some of the gradients seen in

the steady-state model, where water was flowing up and out of the Carrizo through the Reklaw, have been reversed by pumping in the Carrizo.

Table 9.2.1 Calibration statistics for the transient model for the calibration and verification periods.

Calibration period (1980-1989)						
Layer	**Count**	**ME (ft)**	**MAE (ft)**	**RMS (ft)**	**Range (ft)**	**RMS/Range**
1	112	-5.1	15.5	19.0	142	0.13
3	1644	-6.8	25.5	33.7	571	0.059
4	95	-13.8	29.3	34.9	300	0.12
5	251	-0.2	18.7	25.5	471	0.054
6	77	4.0	16.1	22.5	303	0.074
Verification period (1990-1999)						
Layer	**Count**	**ME (ft)**	**MAE (ft)**	**RMS (ft)**	**Range (ft)**	**RMS/Range**
1	76	-10.5	23.1	28.9	112	0.26
3	1141	-11.8	38.3	50.8	553	0.092
4	69	-14.6	25.4	30.9	279	0.11
5	205	-1.1	17.4	24.4	465	0.052
6	72	2.2	20.4	25.7	299	0.086

Table 9.2.2 Calibration statistics for the hydrographs shown in Figures 9.2.7-9.2.13.

Well	Layer	Count	ME (ft)	MAE (ft)	RMS (ft)	Figure
7814203	1	9	15.6	15.6	15.9	9.2.7
7732501	1	11	3.5	3.7	4.7	9.2.7
6856804	1	17	-12.3	12.3	12.4	9.2.7
6721201	1	13	1.5	2.7	2.9	9.2.7
7715903	1	11	-6.7	6.7	7.1	9.2.7
6714801	1	17	3.9	3.9	4.0	9.2.7
7726605	3	108	-46.2	47.6	56.5	9.2.8
7608406	3	11	6.0	6.0	6.2	9.2.8
7722502	3	9	-47.3	47.3	52.1	9.2.8
6857402	3	12	-2.7	7.9	10.2	9.2.8
7733611	3	17	9.1	9.2	10.0	9.2.8
7711703	3	13	-11.0	19.6	23.5	9.2.8
6858302	3	14	-1.0	4.9	5.3	9.2.9
7826802	3	7	-32.8	32.8	35.3	9.2.9
7740305	3	12	12.4	12.4	12.7	9.2.9
7737301	3	15	64.9	66.3	69.8	9.2.9
7806507	3	7	-16.1	16.1	17.0	9.2.9
6853703	3	12	11.3	11.3	13.1	9.2.9
6721104	3	9	0.6	4.5	5.6	9.2.10
6727502	3	15	1.4	2.7	3.1	9.2.10
6856302	3	18	-2.4	3.9	4.5	9.2.10
6863101	3	16	2.2	8.1	9.8	9.2.10
6734402	3	8	10.3	10.3	10.3	9.2.10
7816601	3	13	-1.2	7.9	9.1	9.2.10
7737501	4	19	-49.4	49.4	53.6	9.2.11
7758301	4	5	7.5	21.4	22.4	9.2.11
7742801	4	17	-33.1	33.1	33.7	9.2.11
6859312	4	9	4.4	4.4	4.8	9.2.11
7704603	5	14	-36.4	41.8	50.4	9.2.12
6960201	5	13	4.0	5.0	5.6	9.2.12
6719608	5	16	1.8	3.1	3.6	9.2.12
6852713	5	26	10.2	10.3	11.7	9.2.12
6847601	5	11	9.0	9.1	9.7	9.2.12
6727806	5	33	-19.6	19.6	19.6	9.2.12
6733407	6	10	-17.9	17.9	18.4	9.2.13
6846902	6	6	-27.0	27.0	27.1	9.2.13
6712111	6	17	4.3	4.3	4.8	9.2.13
6955901	6	19	4.5	4.5	5.1	9.2.13

Table 9.2.3 Comparison of simulated stream leakance to LBG-Guyton and HDR (1998) simulated values (AFY per mile of stream)

Stream	LBG-Guyton / HDR		GAM	
	Gaining	*Losing*	*Gaining*	*Losing*
Cibolo Creek		100		31
Guadalupe River	50		62	
Nueces River		500		209
San Antonio River		325		108
San Marcos River	100		350	
San Miguel River		100		72
Frio River		500		104
Atascosa River		50		103

Table 9.2.4 Water budget for the transient model. All rates reported in AFY.

Year	Layer	GHBs	Reserv.	Wells	ET	Top	Bottom	Rech.	Streams	Storage
1980	**1**	37,679	0	-7,142	-51,703	0	-54,293	115,689	-193,735	152,555
	2	0	0	-13,264	-3,325	54,293	-30,954	18,379	-60,455	33,974
	3	0	0	-215,491	-76	30,954	-27,502	20,912	932	190,281
	4	0	0	-32,896	-139	27,502	2,797	1,055	-3,635	5,245
	5	0	3,050	-16,833	-2,761	-2,797	1,659	22,499	-23,679	18,851
	6	0	0	-14,748	-4,269	-1,659	0	14,476	-22,301	28,500
	Sum	37,679	3,050	-300,373	-62,272	108,293	-108,293	193,009	-302,872	429,407
1988	**1**	22,622	0	-6,604	-40,312	0	-50,983	55,416	-443,820	462,699
	2	0	0	-11,986	-2,913	50,983	-38,183	10,469	-484,424	475,007
	3	0	0	-191,034	-65	38,183	-18,667	17,914	-39,595	193,276
	4	0	0	-26,784	-12	18,667	4,099	3,413	-36,959	37,512
	5	0	3,196	-15,913	-3,339	-4,099	1,247	19,490	-92,135	91,535
	6	0	0	-10,219	-3,272	-1,247	0	13,838	-90,785	91,679
	Sum	22,622	3,196	-262,540	-49,914	102,487	-102,487	120,539	-1,187,718	1,351,707
1990	**1**	21,253	0	-8,335	-6,683	0	-56,068	171,951	171,766	-294,074
	2	0	0	-12,570	-680	56,068	-50,911	81,838	297,279	-371,279
	3	0	0	-199,913	-11	50,911	-18,423	91,366	15,830	60,249
	4	0	0	-25,799	0	18,423	7,067	20,882	21,287	-41,871
	5	0	4,065	-16,131	-2,337	-7,067	3,196	54,406	15,526	-51,679
	6	0	0	-10,944	-1,591	-3,196	0	38,095	41,684	-64,060
	Sum	21,253	4,065	-273,693	-11,302	115,138	-115,138	458,539	563,372	-762,713
1999	**1**	16,219	0	-7,963	-24,002	0	-60,527	78,495	-285,584	283,289
	2	0	0	-10,184	-3,339	60,527	-61,059	14,684	-303,657	302,899
	3	0	0	-201,371	-119	61,059	-8,445	16,206	-49,437	182,117
	4	0	0	-19,319	-36	8,445	9,695	1,922	-24,294	23,583
	5	0	1,742	-13,936	-2,193	-9,695	2,920	11,188	-65,572	75,528
	6	0	0	-10,788	-1,654	-2,920	0	8,517	-55,197	62,032
	Sum	16,219	1,742	-263,560	-31,342	117,416	-117,416	131,013	-783,740	929,448

a.

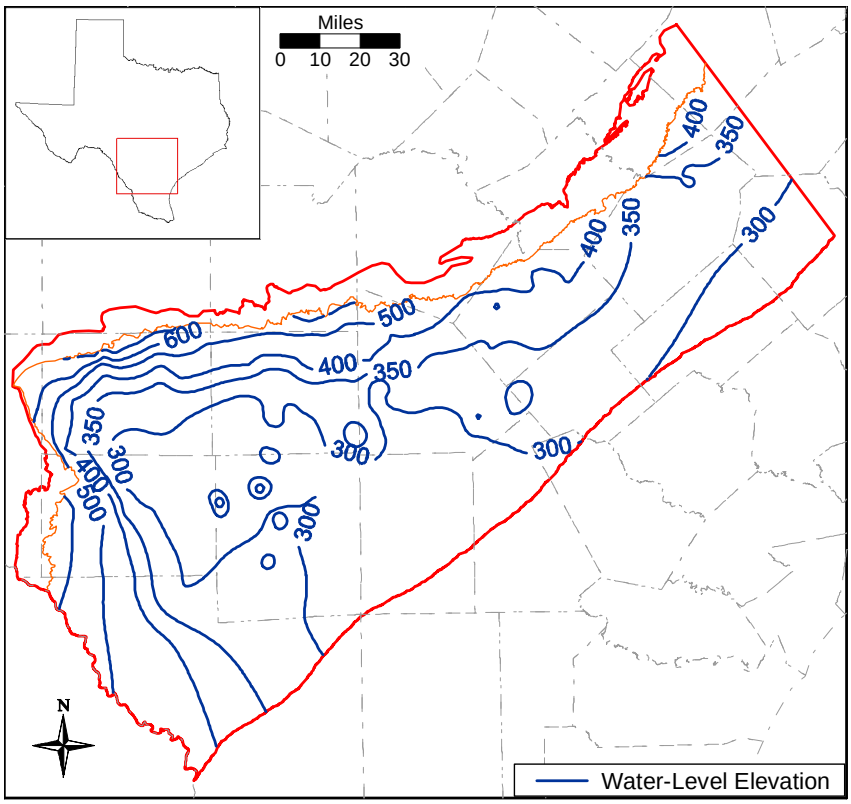

b.

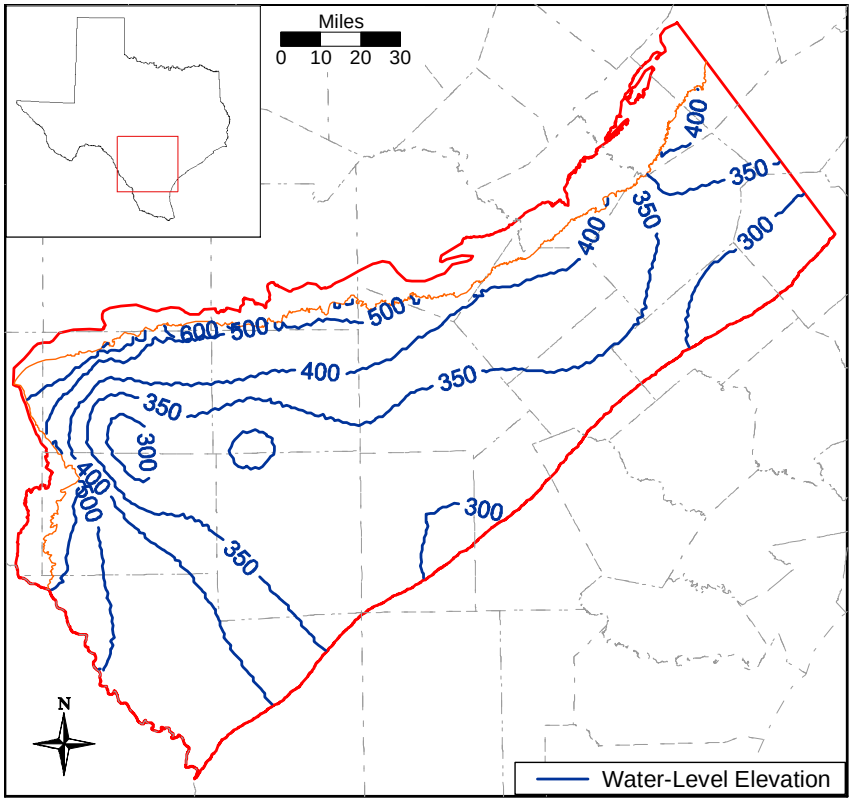

Figure 9.2.1 Comparison between 1989 measured (a) and simulated (b) heads in the Carrizo formation (Layer 3).

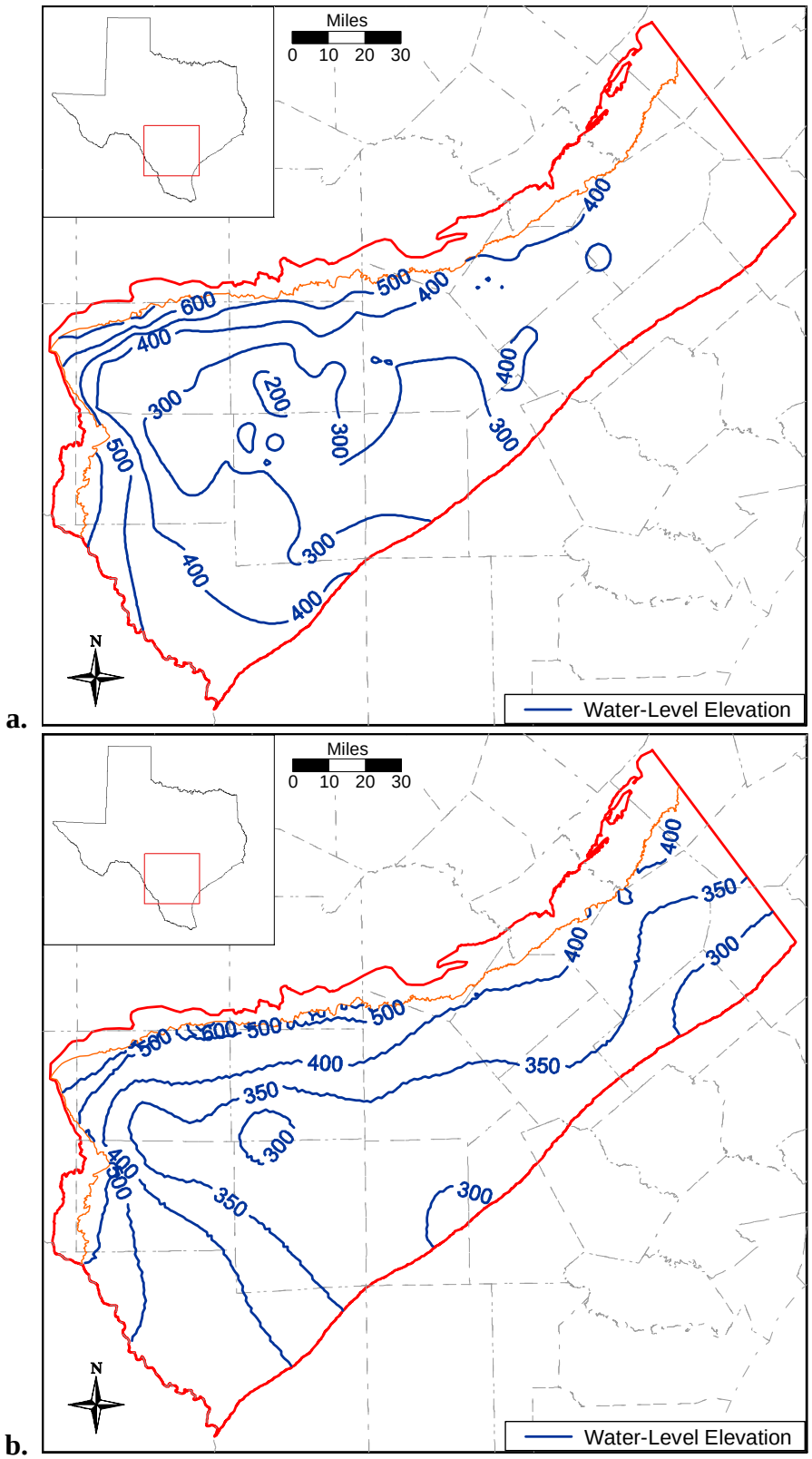

Figure 9.2.2 Comparison between 1999 measured (a) and simulated (b) heads in the Carrizo formation (Layer 3).

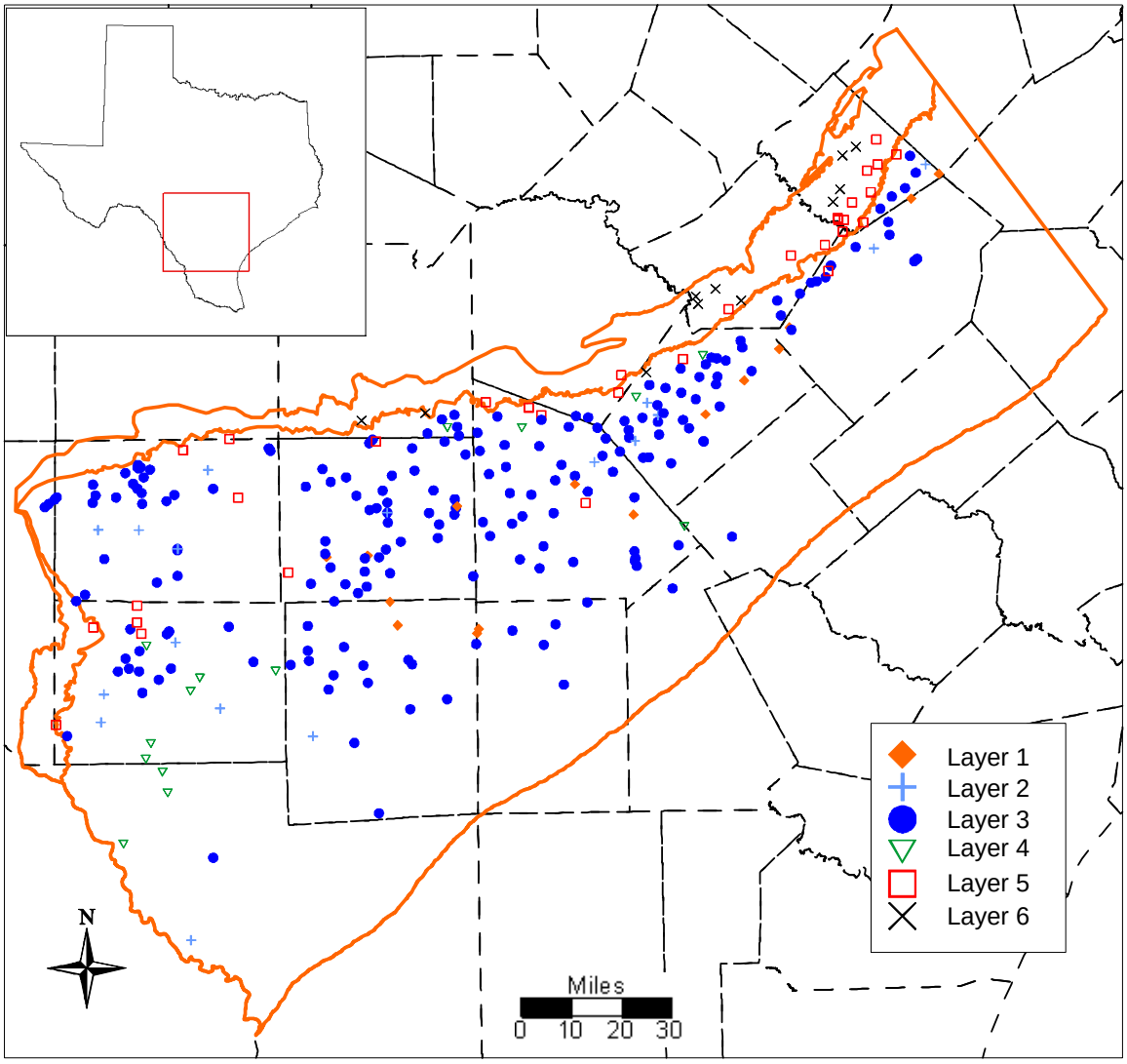

Figure 9.2.3 Locations of hydrograph wells for the transient model.

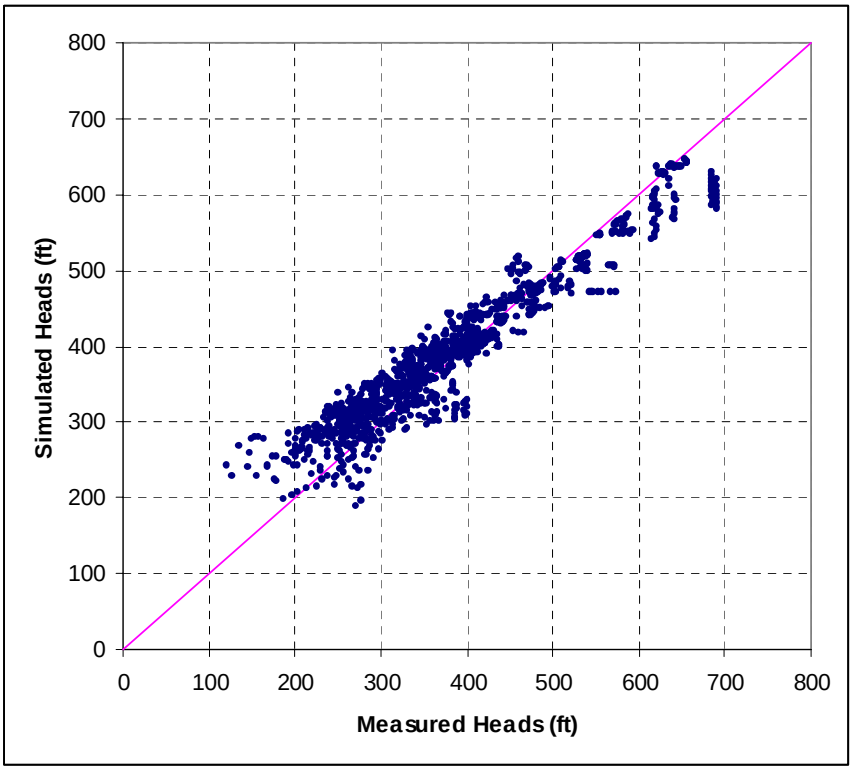

a.

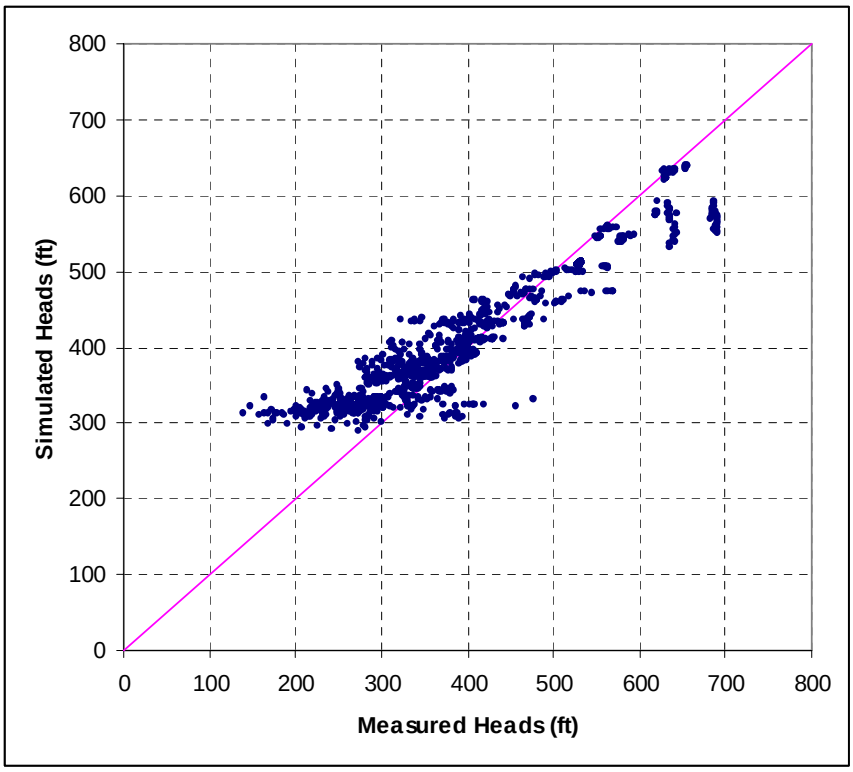

b.

Figure 9.2.4 Calibration period (a) and verification period (b) crossplots for the Carrizo formation (Layer 3) in the calibrated transient model.

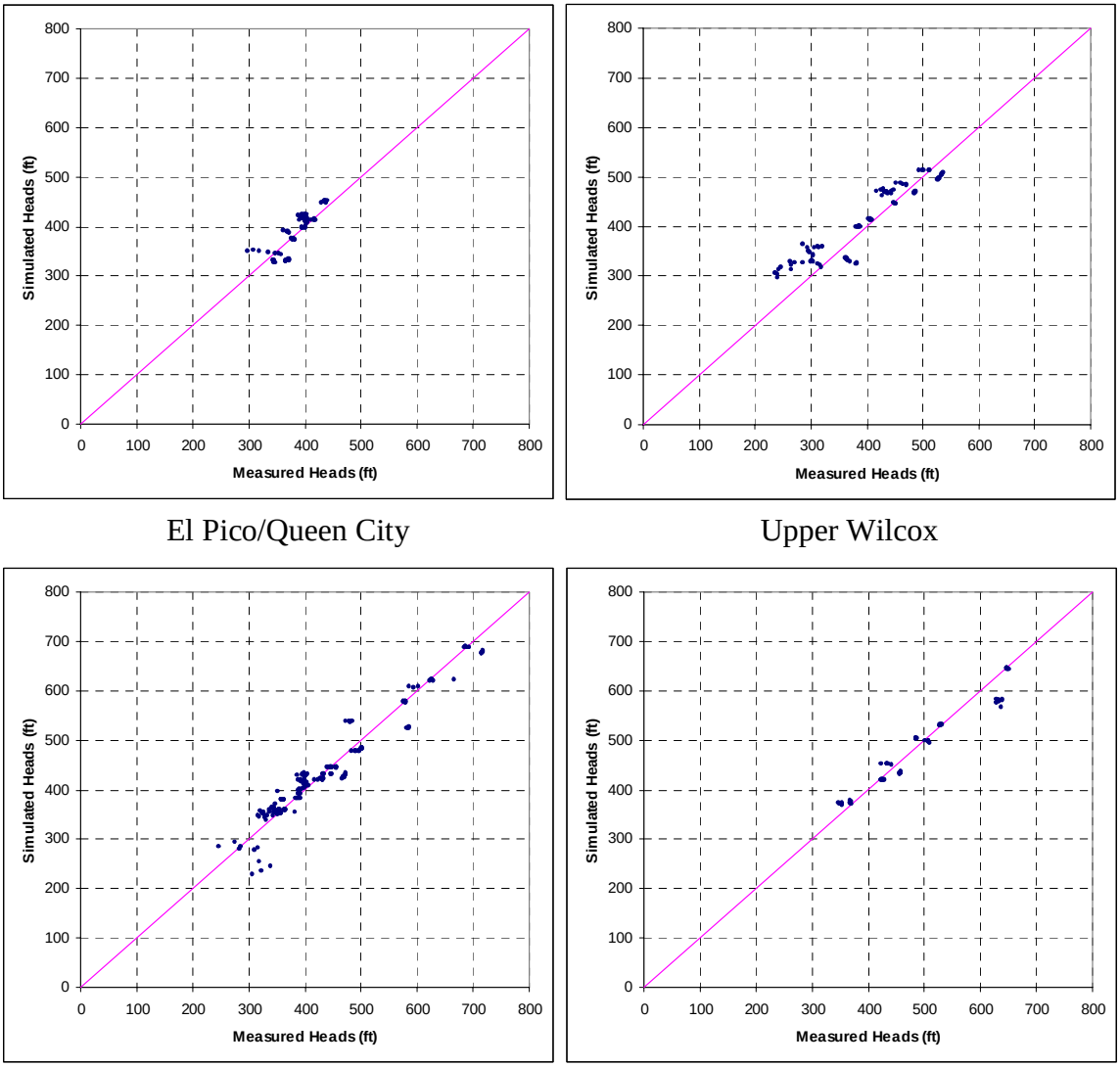

Figure 9.2.5 Calibration period crossplots for the calibrated transient model.

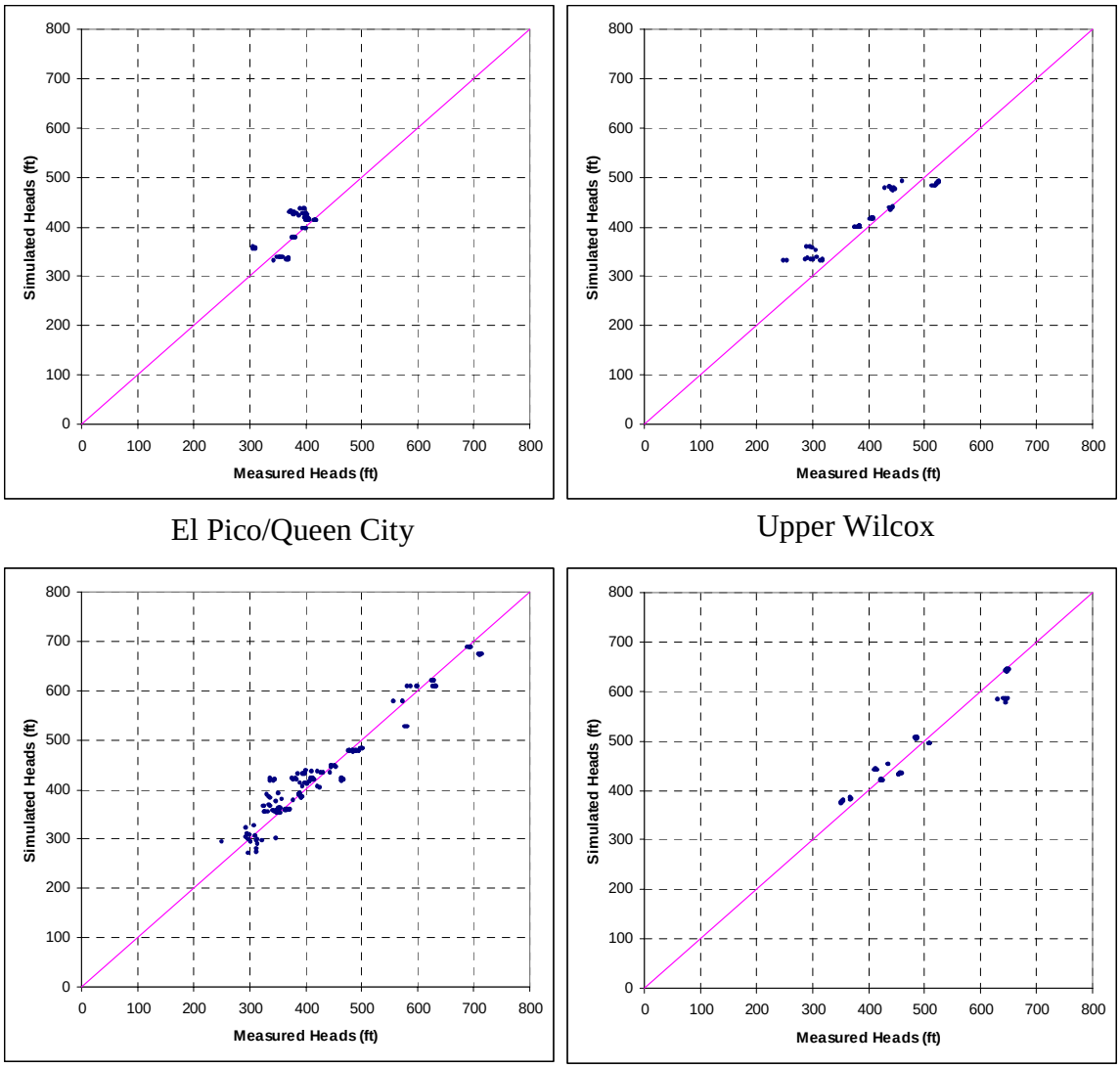

Figure 9.2.6 Verification period crossplots for the calibrated transient model.

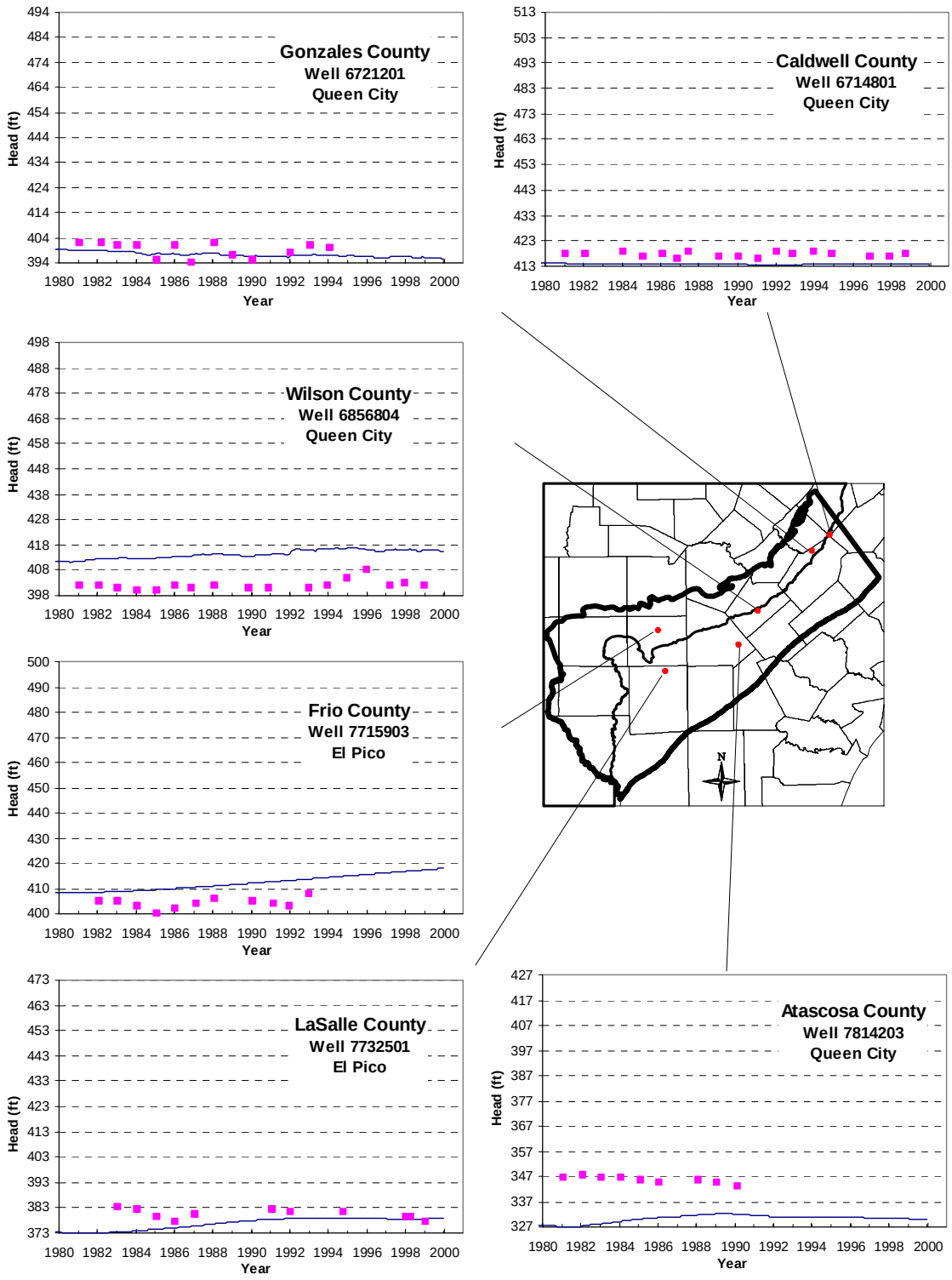

Figure 9.2.7 Transient model hydrographs from the Queen City/El Pico (Layer 1).

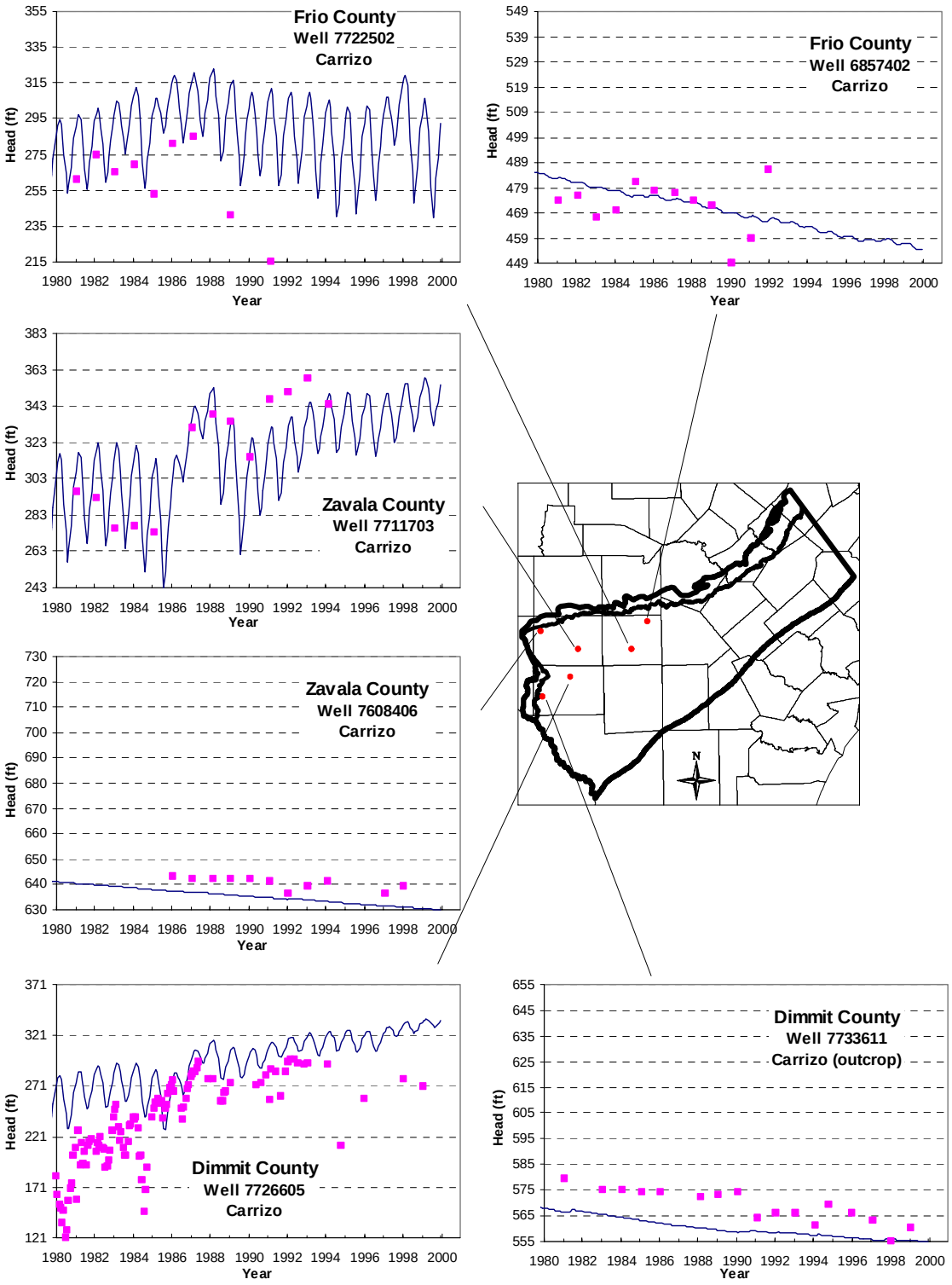

Figure 9.2.8 Transient model hydrographs from the Carrizo (Layer 3), West.

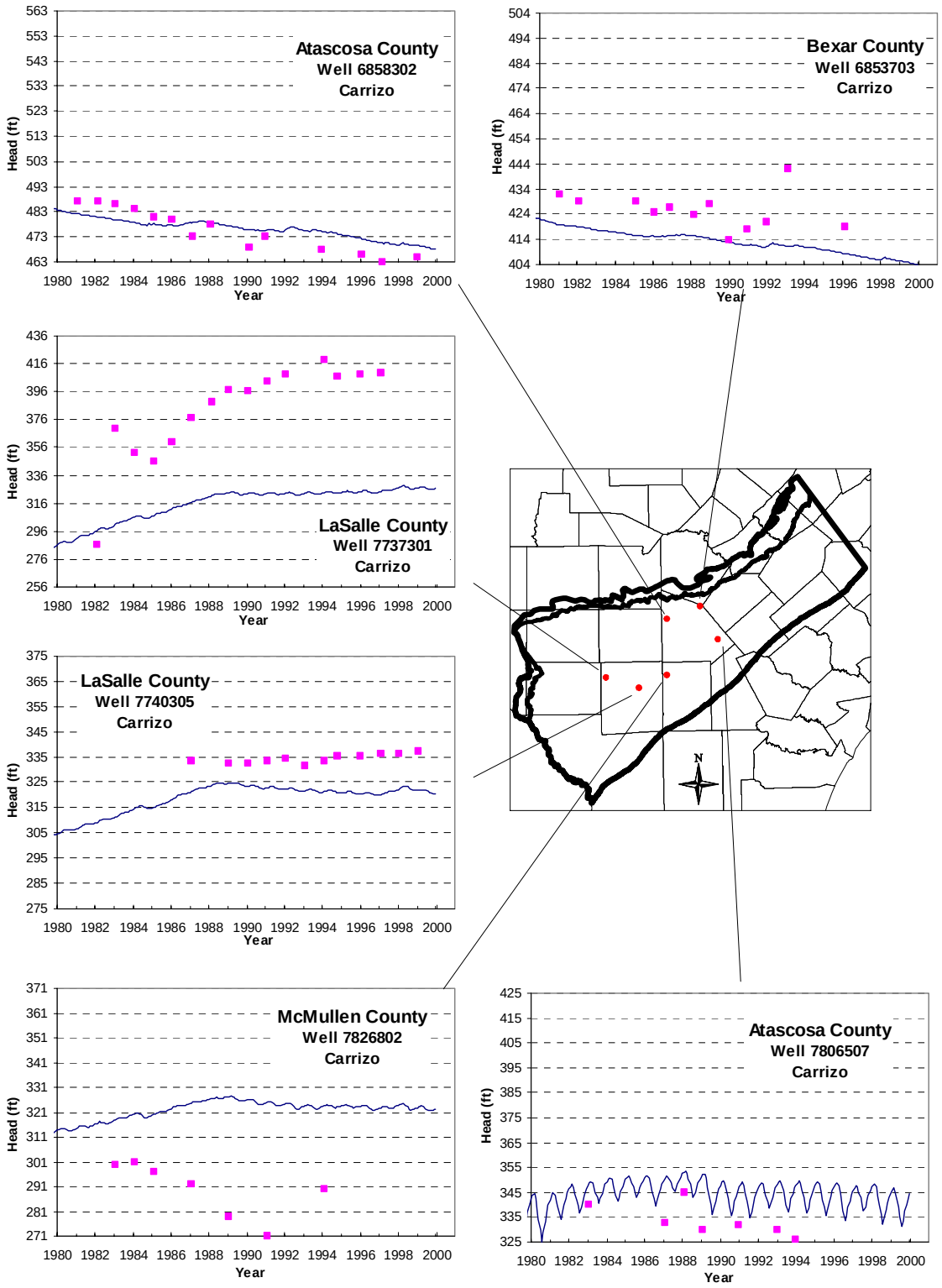

Figure 9.2.9 Transient model hydrographs from the Carrizo (Layer 3), Central.

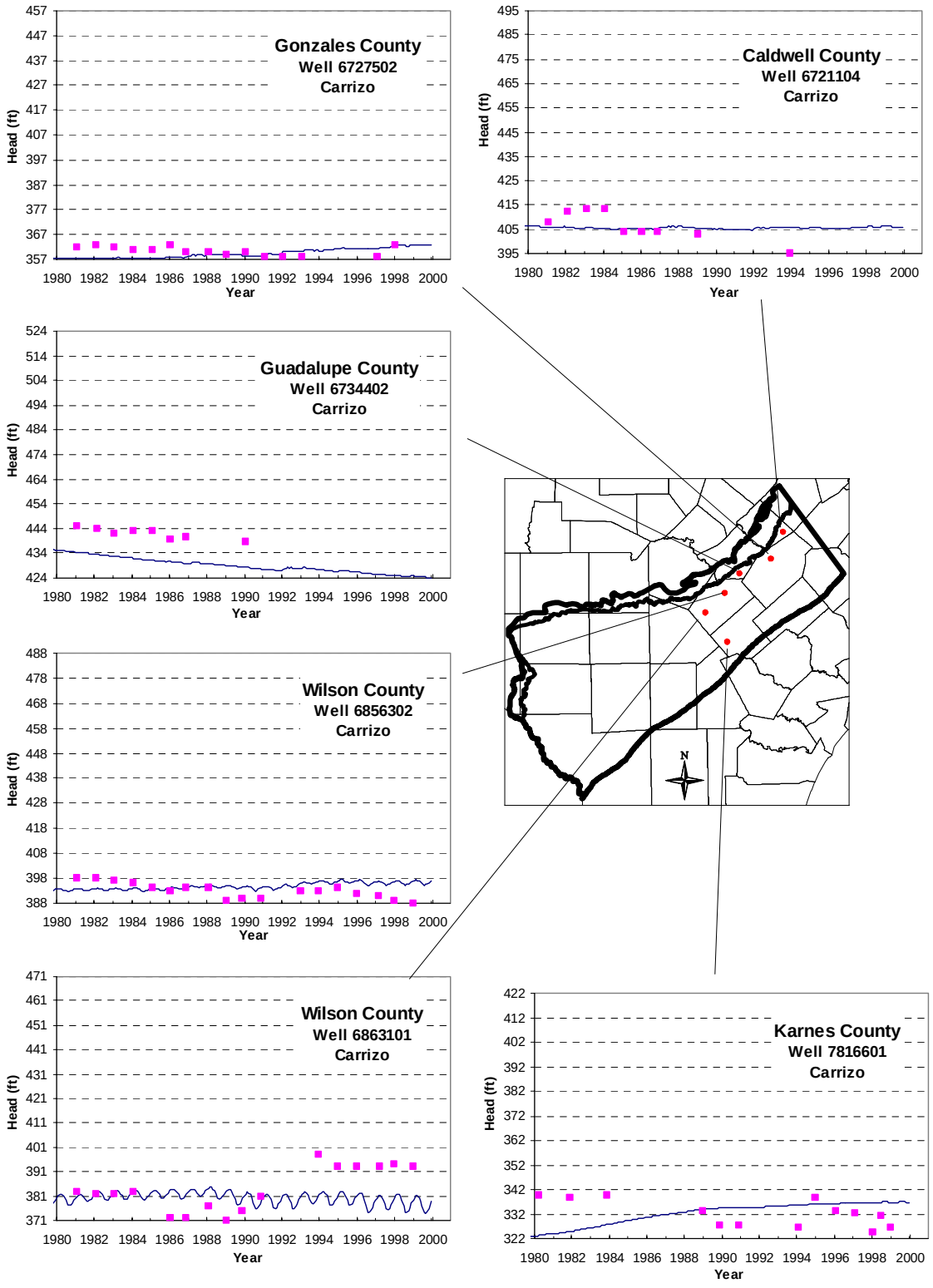

Figure 9.2.10 Transient model hydrographs from the Carrizo (Layer 3), East.

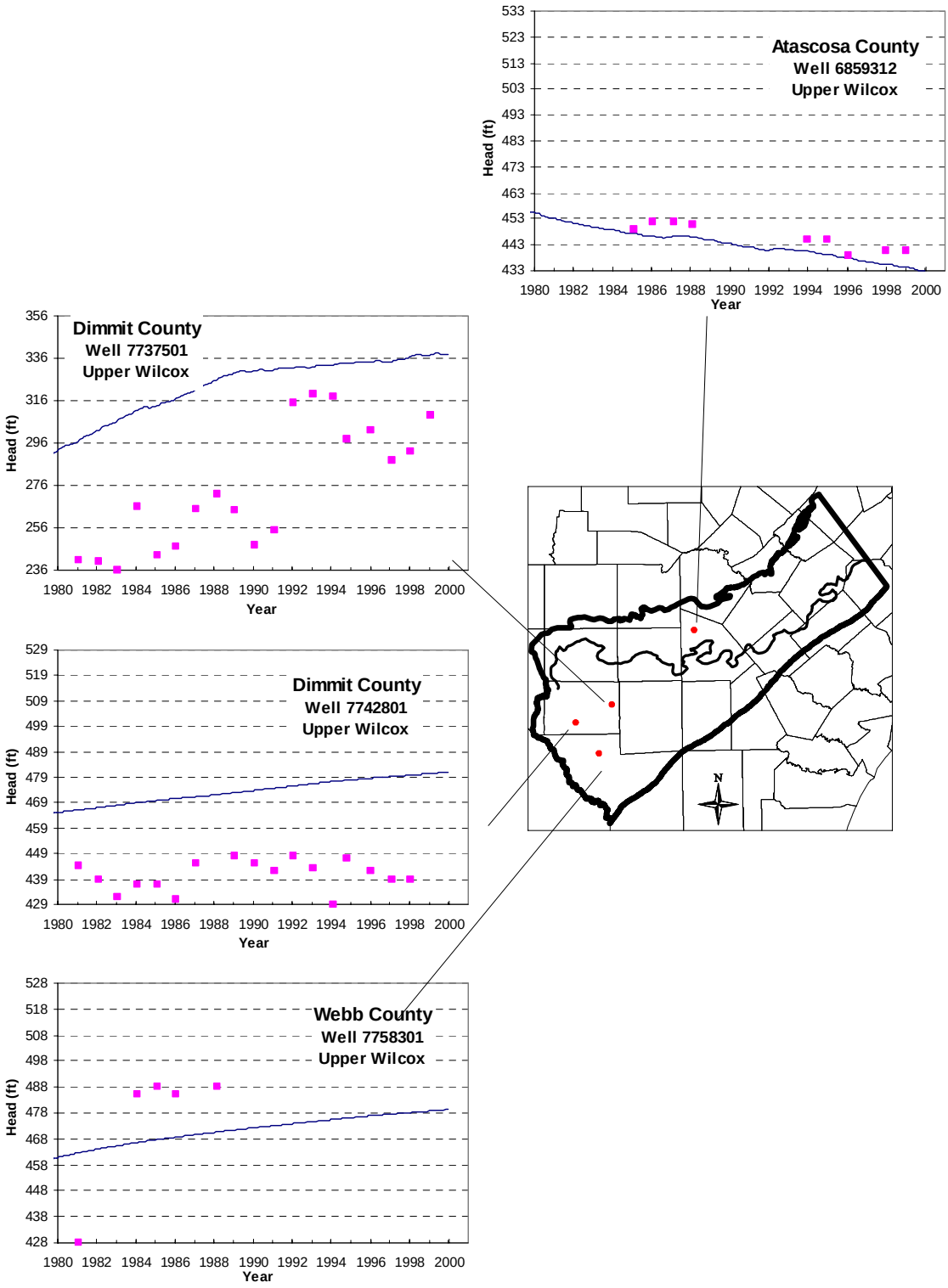

Figure 9.2.11 Transient model hydrographs from the upper Wilcox (Layer 4).

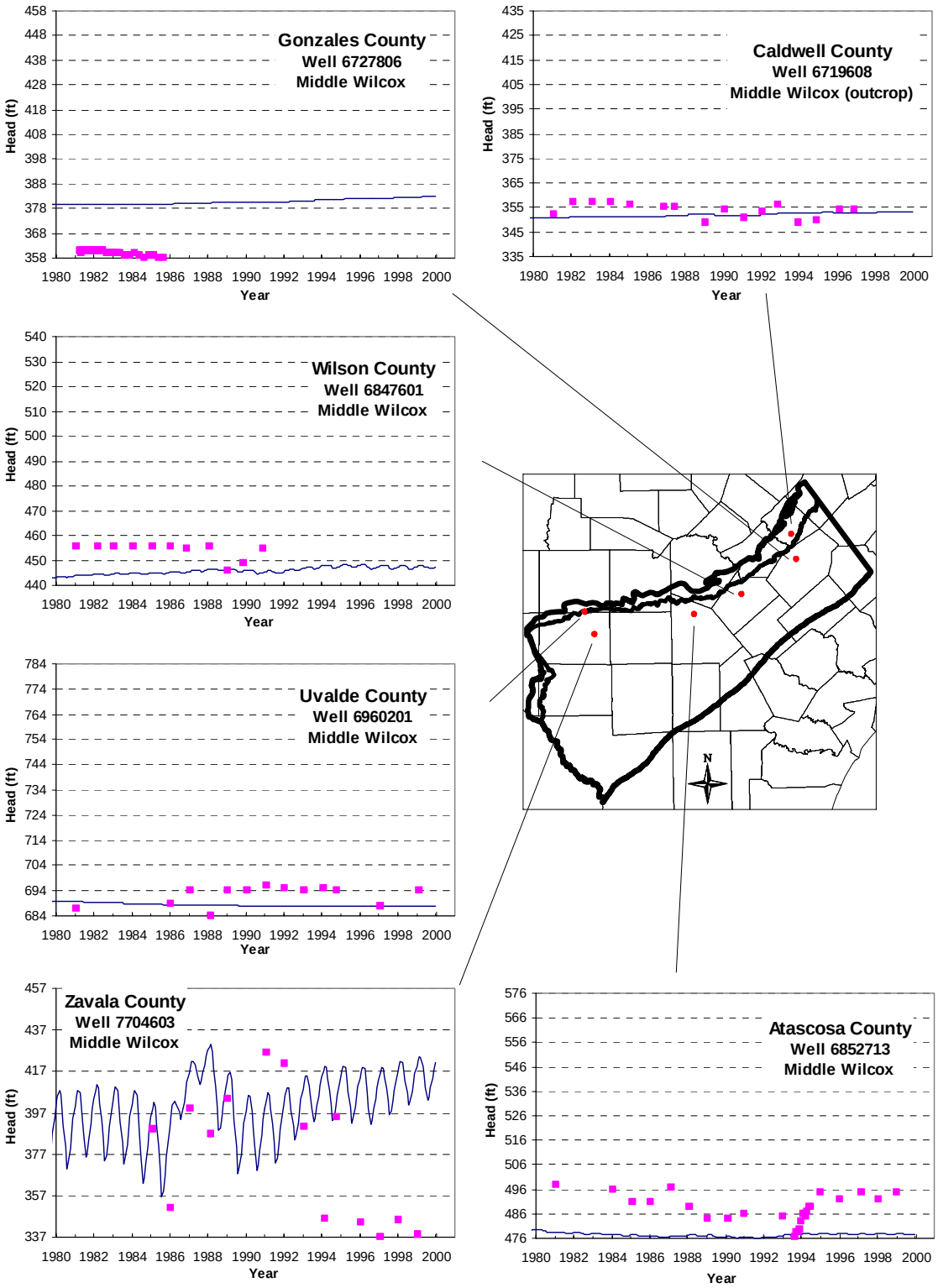

Figure 9.2.12 Transient model hydrographs from the middle Wilcox (Layer 5).

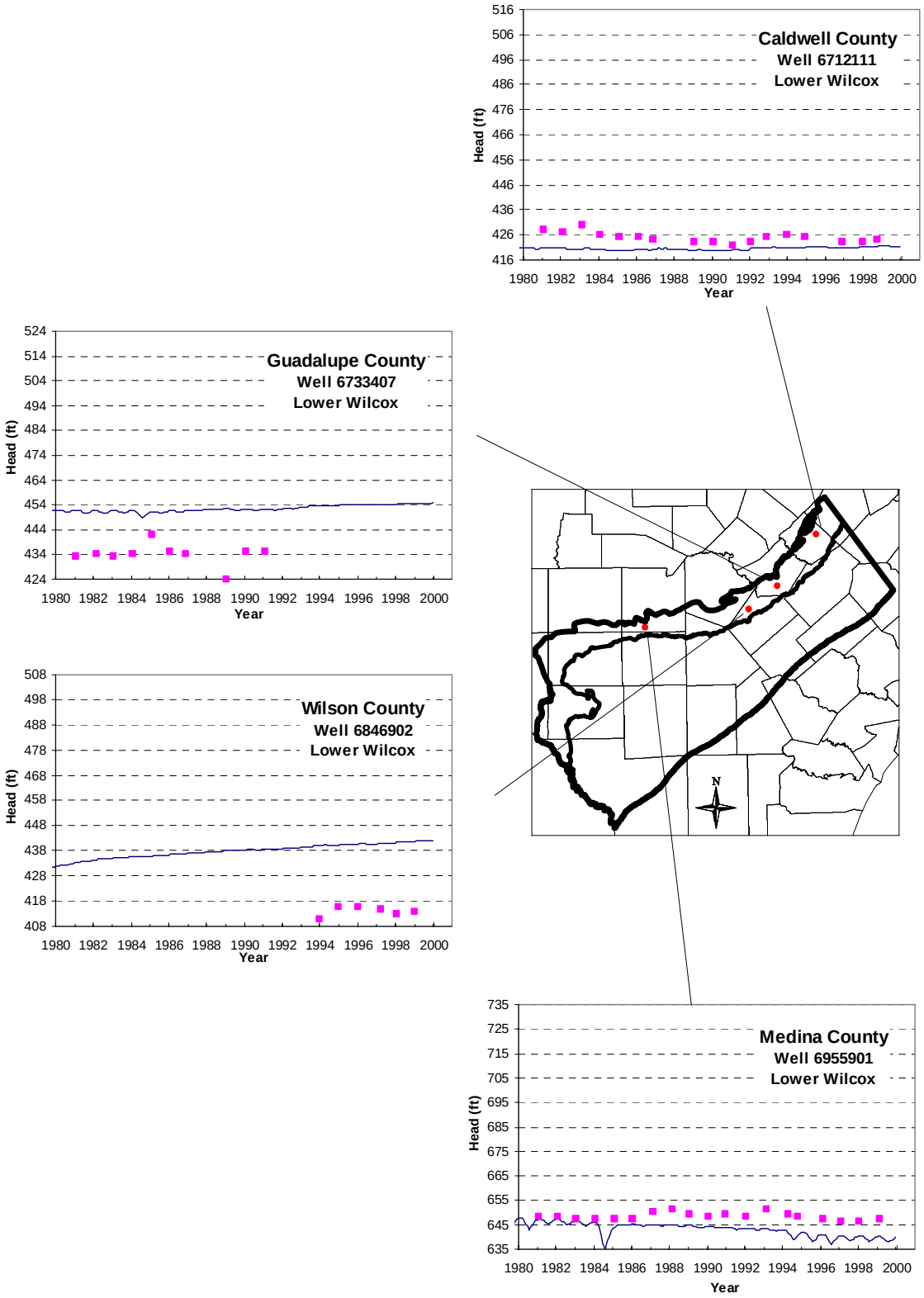

Figure 9.2.13 Transient model hydrographs from the lower Wilcox (Layer 6).

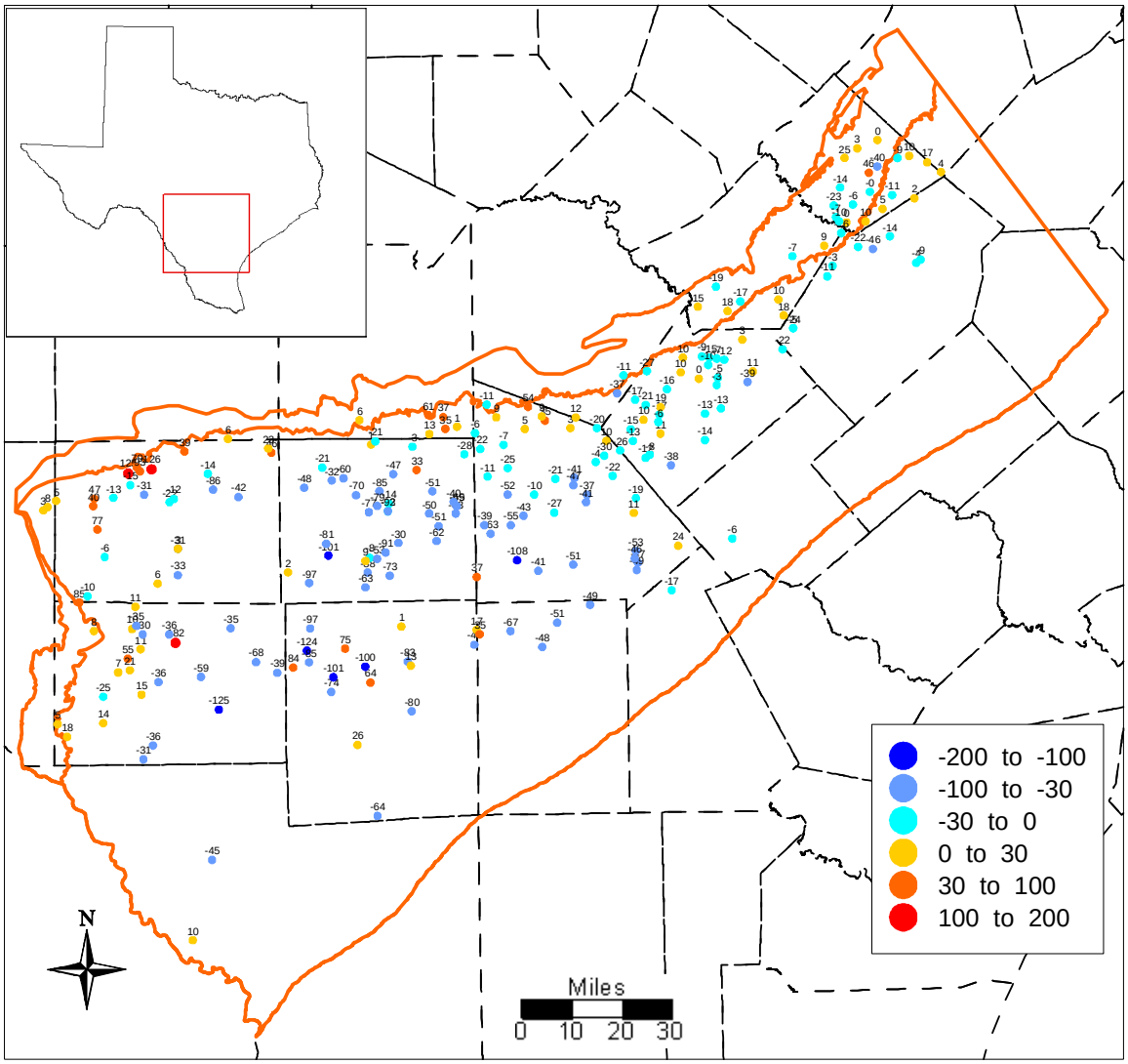

Figure 9.2.14 Average residuals for the verification period (1990-1999) in the Carrizo Formation (Layer 3).

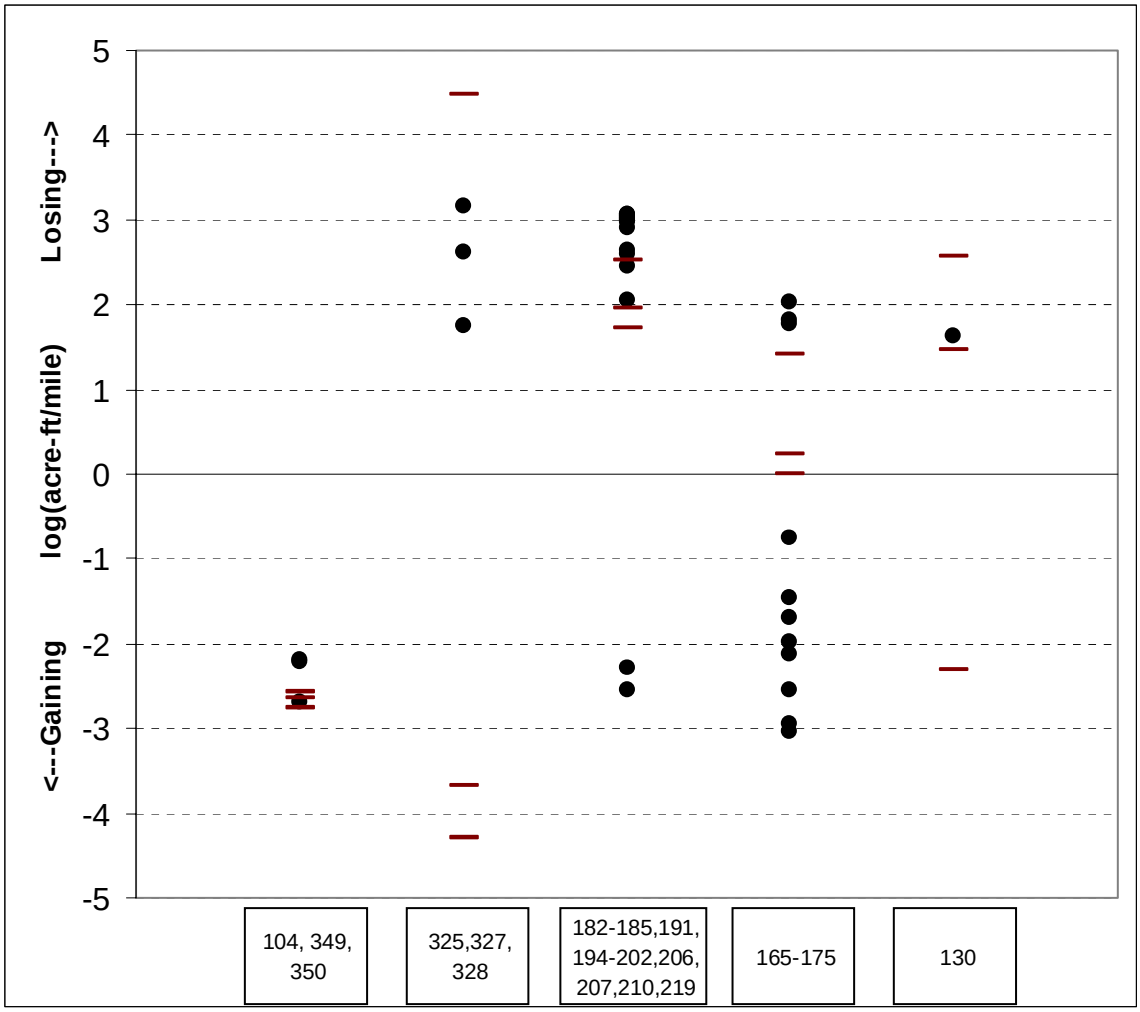

Figure 9.2.15 Comparison of Slade et al. (2002) with average simulated stream gain/loss.

Note: The horizontal lines represent the 10th, 50th, and 90th percentile simulated gains/losses, while the solid circles represent the Slade et al. (2002) measured values.

9.3 Sensitivity Analysis

Section 8.3 discusses the approach for the sensitivity analysis for the steady-state model. The sensitivity analysis for the transient model was performed similar to the steady-state model. However, some additional sensitivity simulations were added for the transient model to account for the addition of storage and pumping as model parameters.

Ten parameter sensitivity simulations were performed for the transient model. These are listed below.

1. Horizontal hydraulic conductivity, model-wide (K_h)
2. Vertical hydraulic conductivity in Layer 2 (K_v-Reklaw, model leakance between Layers 2 and 3)
3. Vertical hydraulic conductivity in Layers 4-6 (K_v-Wilcox, model leakance between layers 3-4, 4-5, and 5-6)
4. Recharge, model-wide
5. Streambed conductance, model-wide (K-Stream)
6. GHB conductance, model-wide (K-GHB)
7. Storativity in the Carrizo (S-Carrizo)
8. Specific yield, model-wide (Sy)
9. Pumping rate
10. Reservoir conductivity (K-Reservoir)

Equation 8-2 (varying linearly) was used for sensitivities 4, 8, and 9, and Equation 8-3 for the rest of the sensitivities listed above.

As with the steady-state model, we checked the difference between applying equation 8-4 at all grid blocks or only at grid blocks where targets were present. Figure 9.3.1 shows the transient sensitivity results for the Carrizo (Layer 3) calculated for the target gridblocks and Figure 9.3.2 shows the transient sensitivity results for the Carrizo (Layer 3) calculated at all gridblocks. As with the steady-state model, the order of the first four most sensitive parameters is the same for both methods. This indicates an adequate target coverage in this layer. Figure 9.3.2 shows that the most positively correlated parameter for the Carrizo is horizontal hydraulic conductivity. The most negatively correlated parameter for the Carrizo is pumping.

This is an important result because these parameters were changed very little during calibration (Section 9.2.1). The third most important parameter is the vertical hydraulic conductivity of the Reklaw/Bigford (Layer 2). This parameter was significantly adjusted during calibration. Contrast the results of this sensitivity with that of the steady-state model. In the steady-state model, recharge and GHB conductivity were the dominant parameters. In the transient model, hydraulic heads are much less sensitive to these parameters. This difference is another indication of the importance of calibrating to different hydrologic scenarios to improve the uniqueness of the calibrated parameter values.

Figure 9.3.3 shows the transient sensitivity results for Layer 1. The results are similar to the Carrizo, except that the GHB conductance has a significant *MD*. Since the GHBs are all attached directly to Layer 1, this is an expected result. Figure 9.3.4 shows the transient sensitivity results for the Reklaw/Bigford (Layer 2), which are similar to the Carrizo. Figures 9.3.5 and 9.3.6 show the transient sensitivity results for the upper Wilcox (Layer 4) and the middle Wilcox (Layer 5), which are also similar to the Carrizo. In the sensitivity results for the lower Wilcox (Layer 6), which are shown in Figure 9.3.7, the vertical conductivity of the Wilcox appears as a sensitive parameter with a significant *MD*. The lower Wilcox can only communicate with the rest of the model through the middle Wilcox, as the lower Wilcox is simulated as impermeable on the base of the formation at the Midway contact. So this sensitivity result is expected.

Figure 9.3.8 shows the sensitivity results for all layers, where horizontal hydraulic conductivity is varied. The layer with the greatest mean head difference is the Carrizo, indicating that this is the layer that is most affected by horizontal flow. We noted previously in this section that drawdowns in the Carrizo were most sensitive to pumping and horizontal hydraulic conductivity. During initial attempts at calibration, the Reklaw and Wilcox were more vertically conductive and heads in the Carrizo were far less sensitive to pumping or horizontal hydraulic conductivity. Reducing the vertical conductivity in the layers above and below the Carrizo brought the model to an inflection point with respect to its sensitivity to horizontal flow parameters. This sensitivity indicates that the model is currently better constrained than during initial calibration.

Figures 9.3.9 and 9.3.10 show the results for all layers for the recharge and specific yield sensitivities. Note that the maximum mean difference for both of these sensitivities is less than 1 ft. These figures indicate that recharge and specific yield, which should be most important in the outcrop, do not have a large overall effect on the heads in the model.

Figure 9.3.11 shows the effect of varying horizontal hydraulic conductivity on several Carrizo (Layer 3) hydrographs. In general, these hydrographs show a trend that is similar to Figure 9.3.8, i.e. hydraulic head decreases when horizontal hydraulic conductivity is decreased. This trend occurs where pumping is a significant stress. The hydrograph that is an exception to this trend is from Well 6858302 in Atascosa County. This hydrograph shows an increased head with decreased hydraulic conductivity. This trend is likely due to a combination of two factors: (1) head near this well is only weakly affected by pumping, and (2) the well is near the outcrop, where water flows in from recharge and losing streams, so decreasing horizontal hydraulic conductivity causes hydraulic head to build up. Figure 9.3.12 shows the effect of varying pumping rate on several Carrizo (Layer 3) hydrographs. All of these hydrographs display the trend of decreased hydraulic head with increased pumping. Hydrographs from wells in the western portion of the model show a larger change than hydrographs from wells in the eastern portion, simply due to the higher amount of pumping in the west during the simulated period.

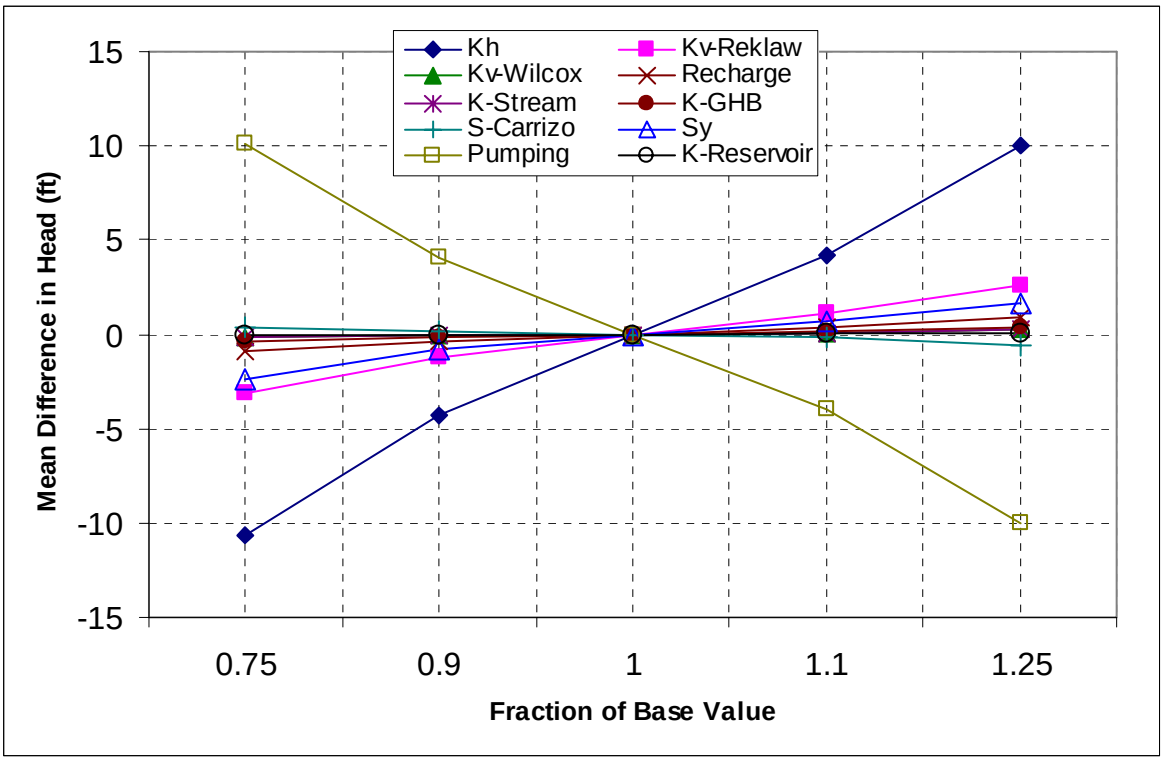

Figure 9.3.1 Transient sensitivity results for the Carrizo (Layer 3) using target locations.

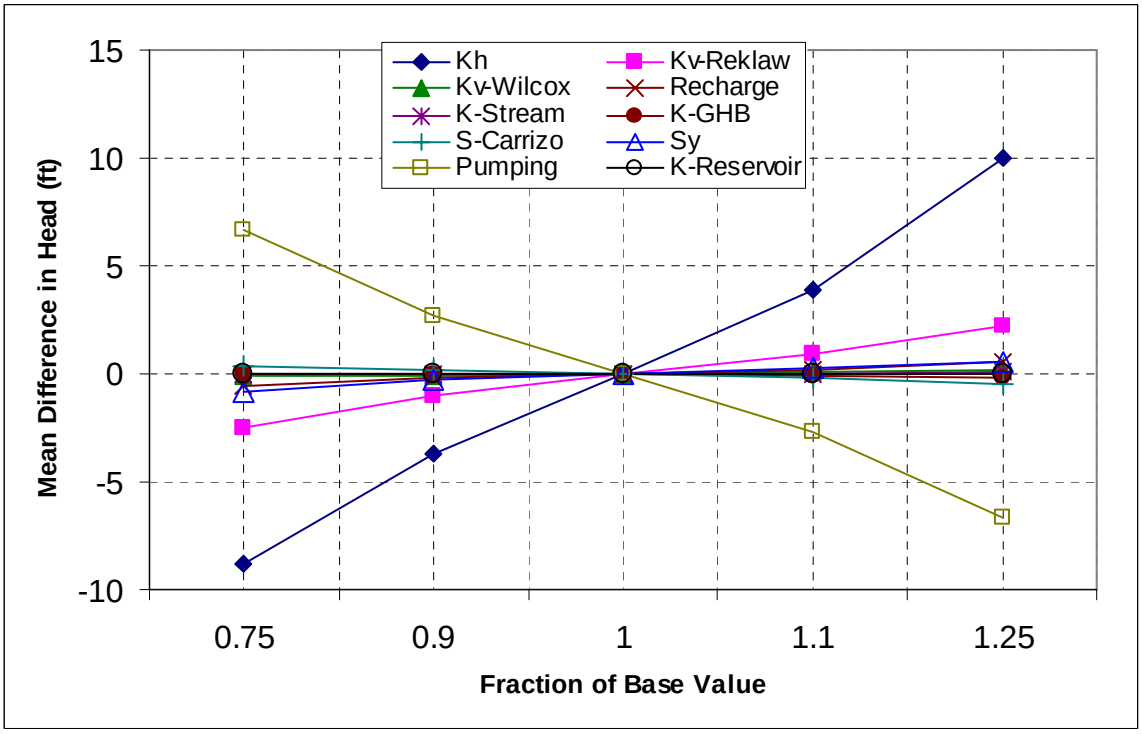

Figure 9.3.2 Transient sensitivity results for the Carrizo (Layer 3) using all active gridblocks.

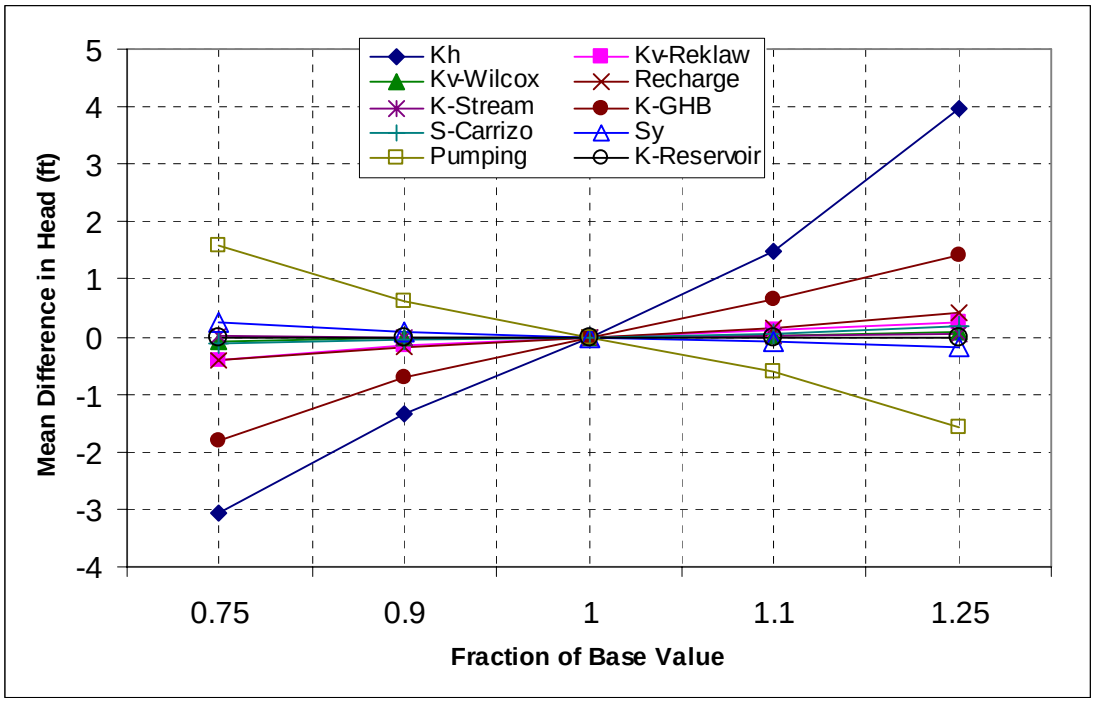

Figure 9.3.3 Transient sensitivity results for the Queen City/El Pico (Layer 1) using all active gridblocks.

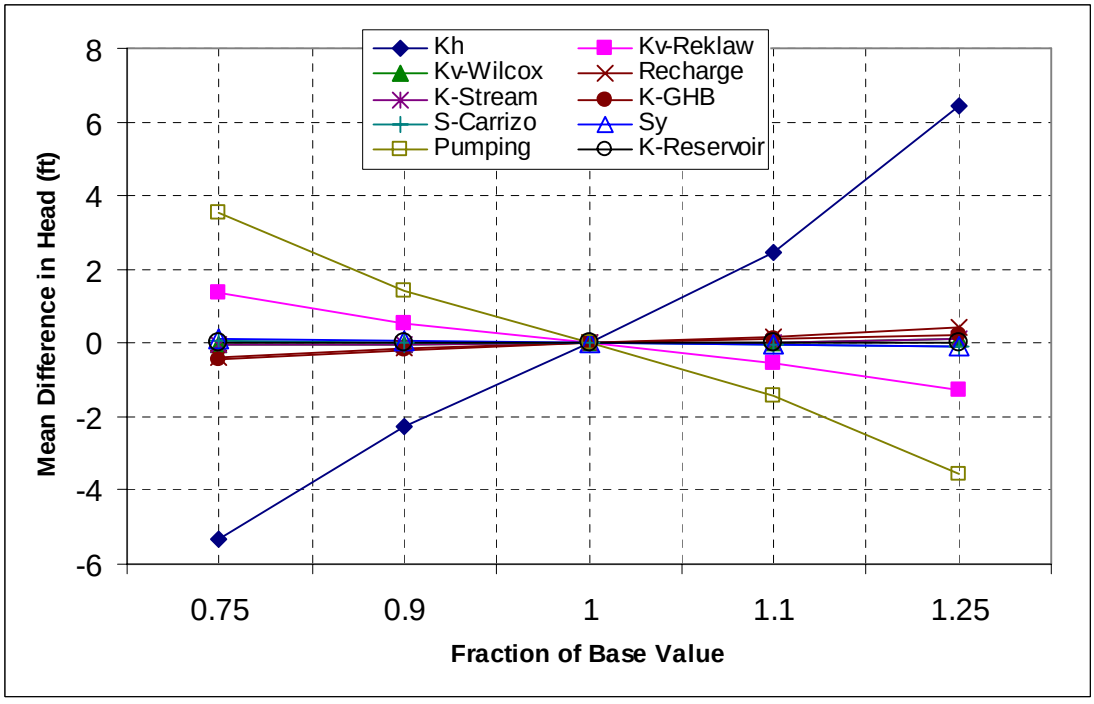

Figure 9.3.4 Transient sensitivity results for the Reklaw/Bigford (Layer 2) using all active gridblocks.

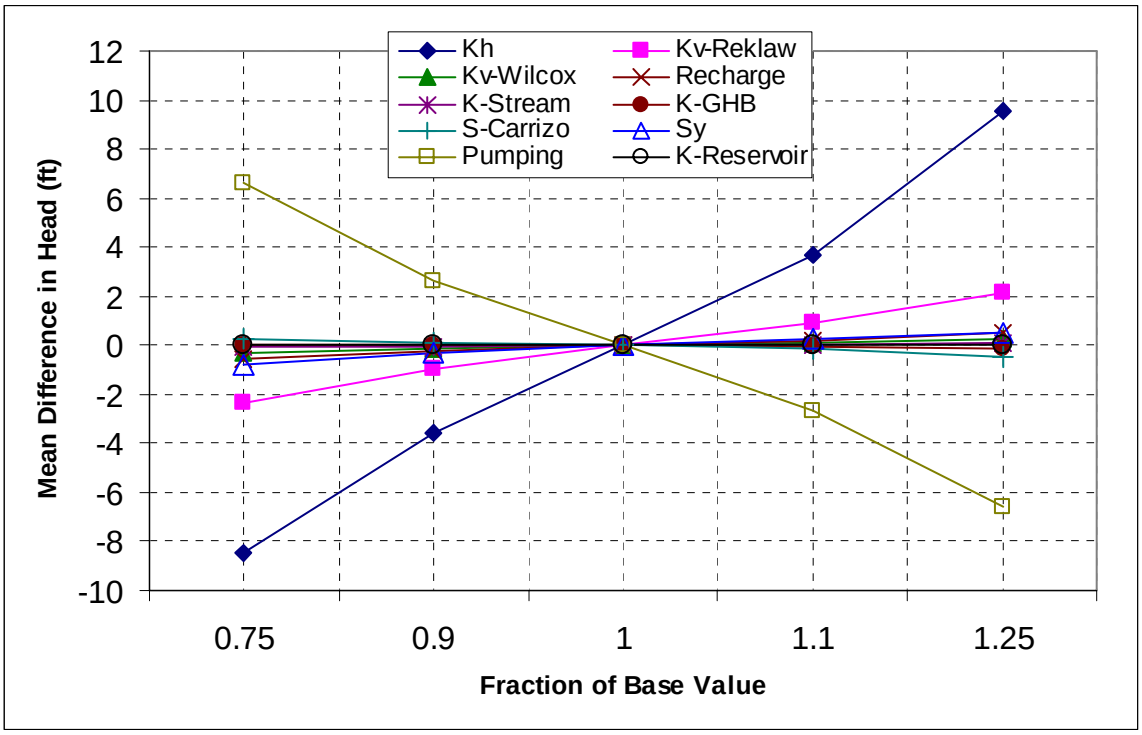

Figure 9.3.5 Transient sensitivity results for the upper Wilcox (Layer 4) using all active gridblocks.

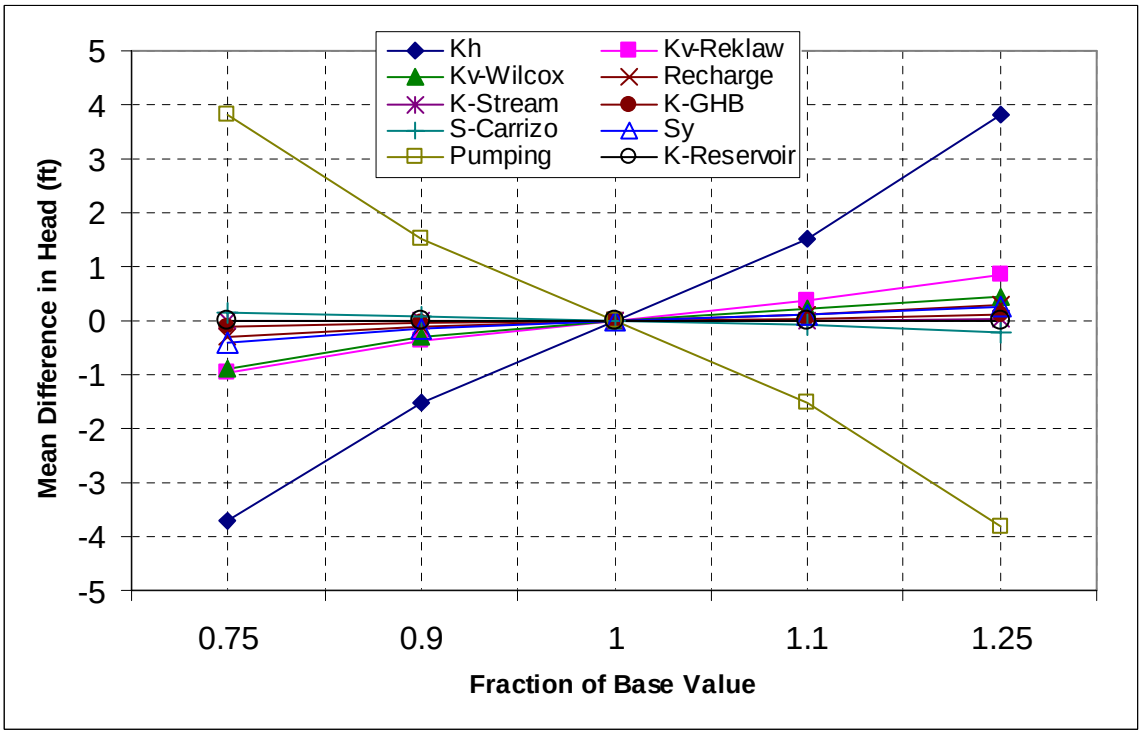

Figure 9.3.6 Transient sensitivity results for the middle Wilcox (Layer 5) using all active gridblocks.

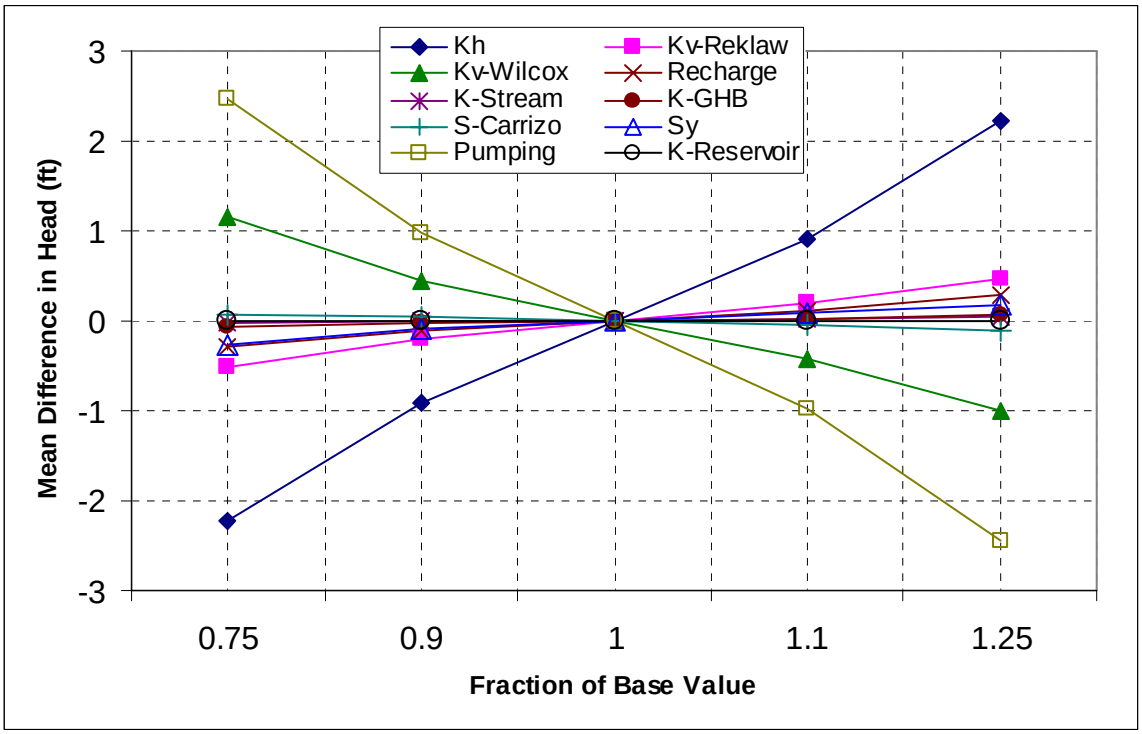

Figure 9.3.7 Transient sensitivity results for the lower Wilcox (Layer 6) using all active gridblocks.

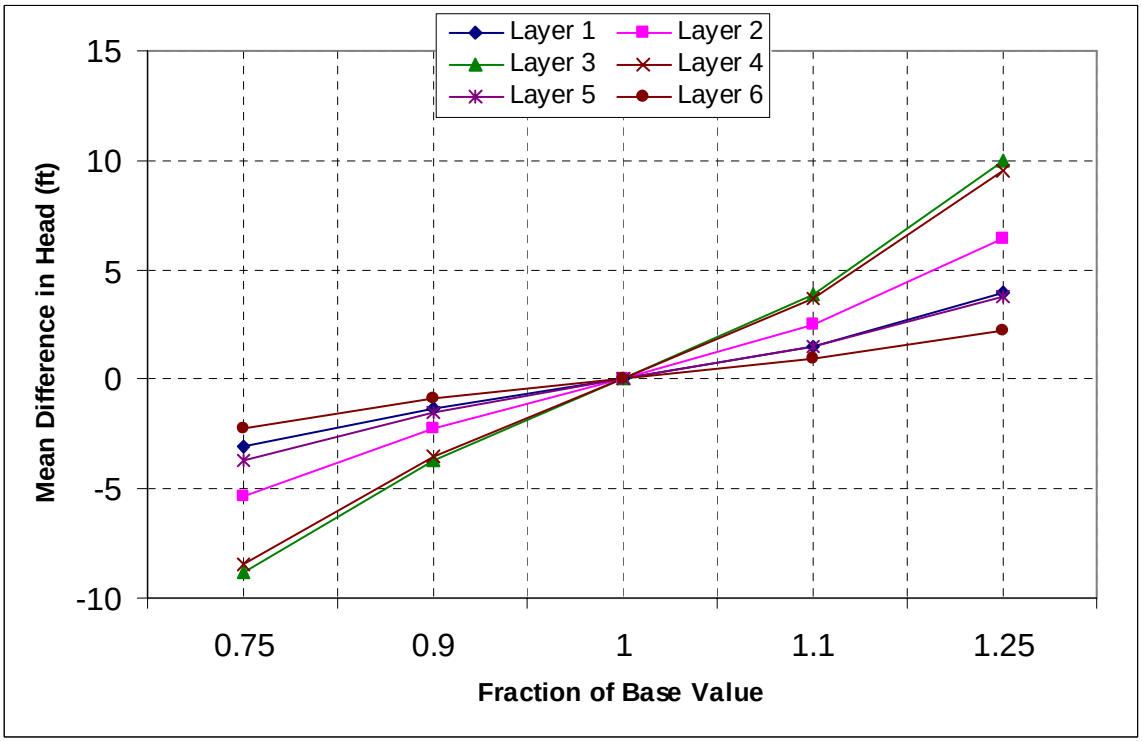

Figure 9.3.8 Transient sensitivity results where the horizontal hydraulic conductivities for all layers are varied.

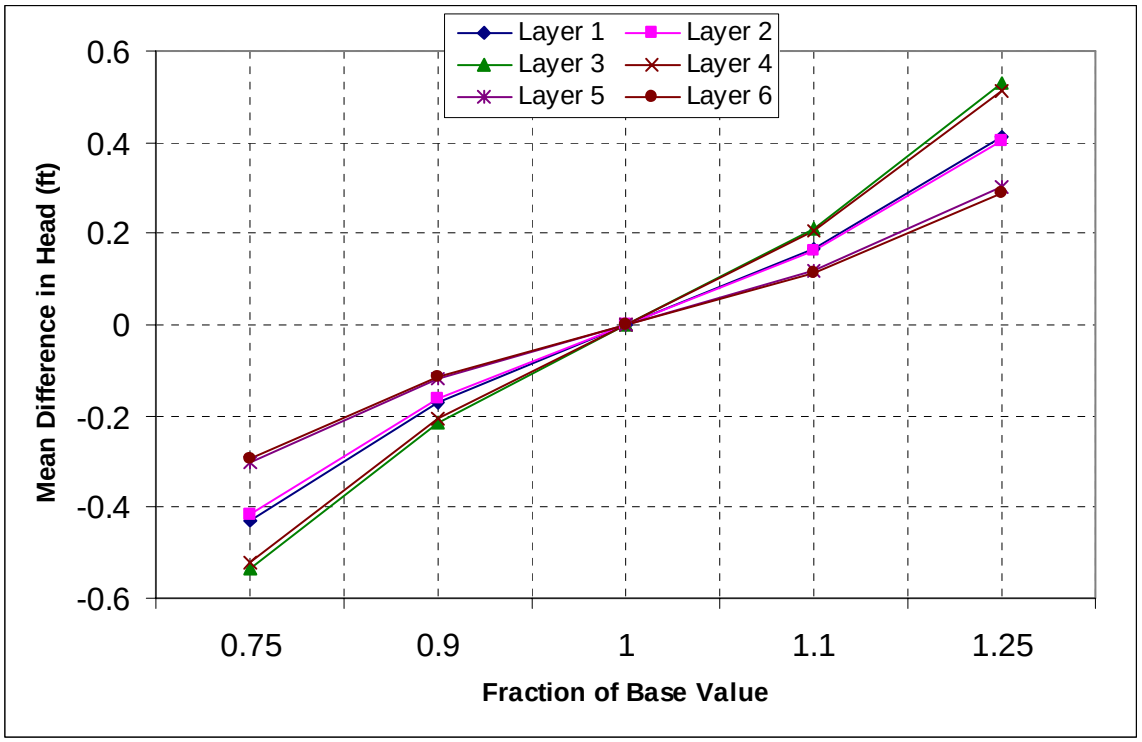

Figure 9.3.9 Transient sensitivity results where recharge is varied.

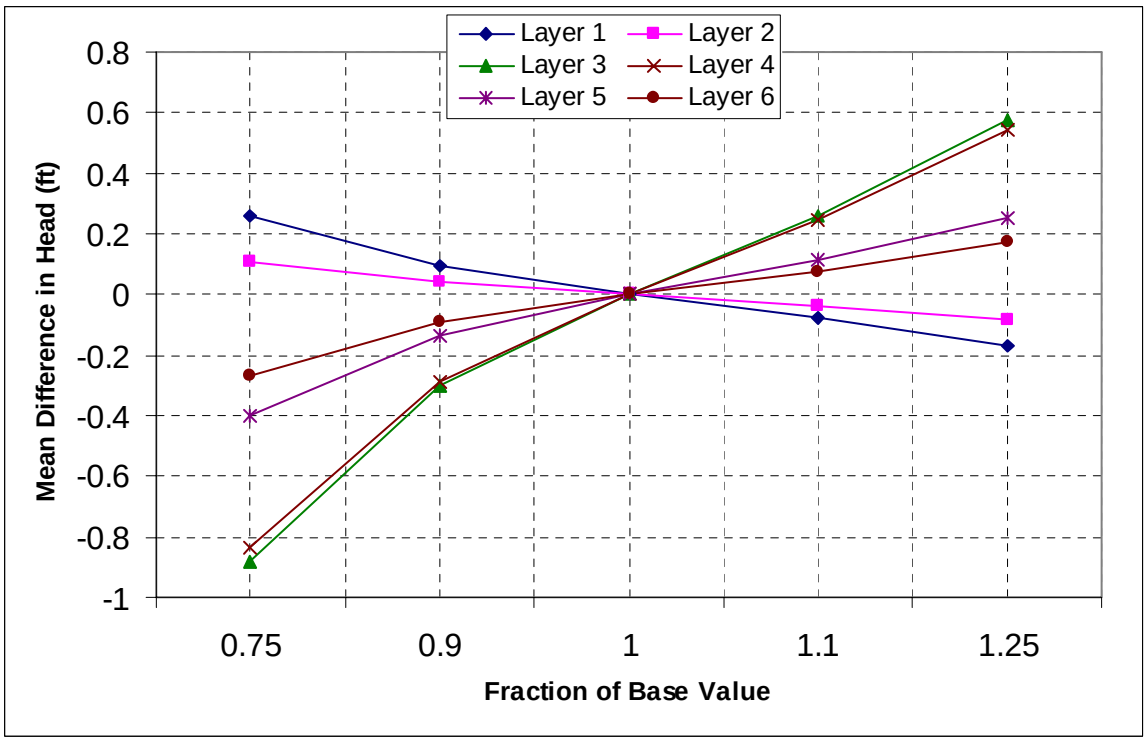

Figure 9.3.10 Transient sensitivity results where specific yield is varied.

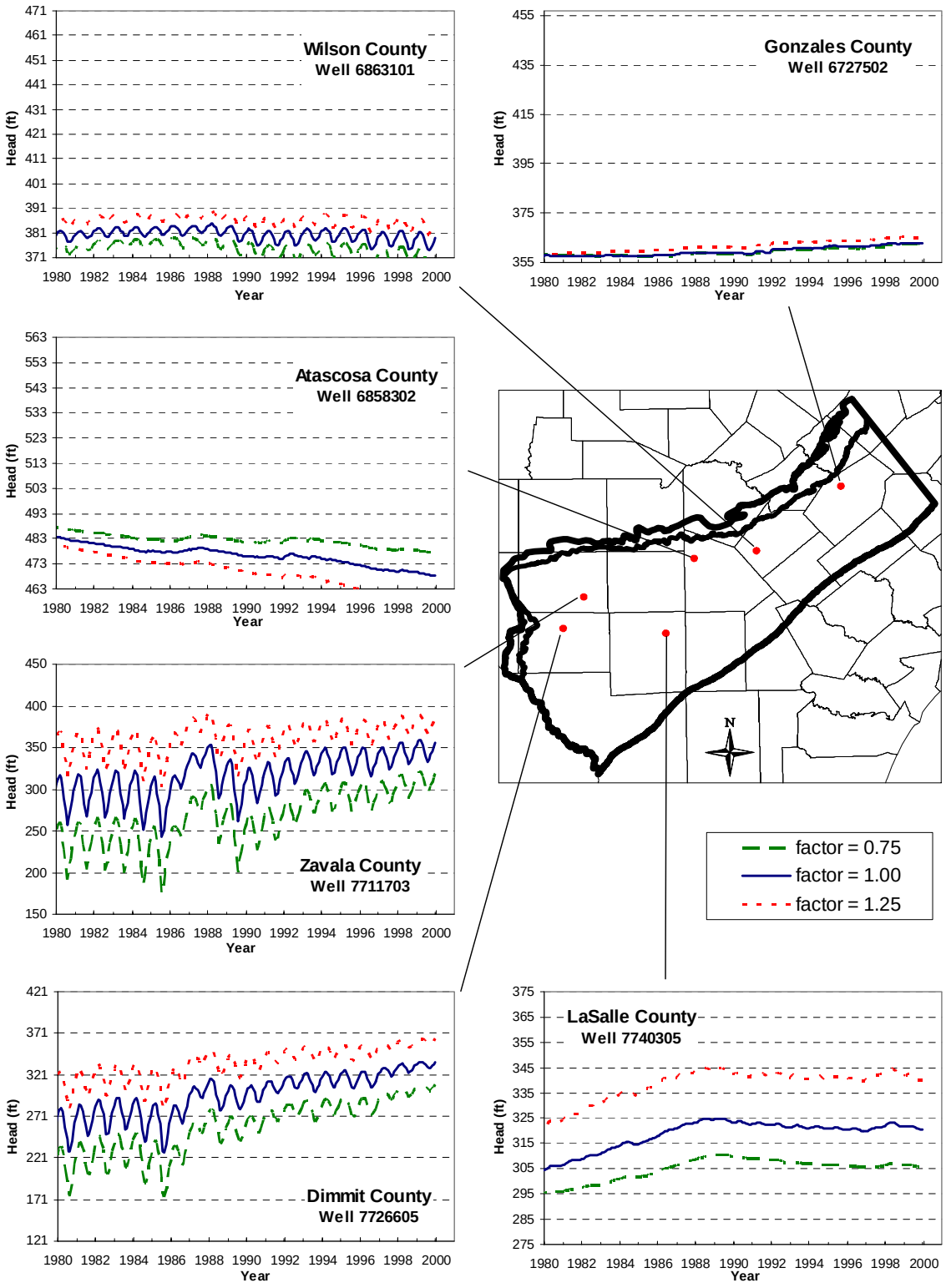

Figure 9.3.11 Transient sensitivity hydrographs from the Carrizo (Layer 3) where the horizontal hydraulic conductivities for all layers are varied.

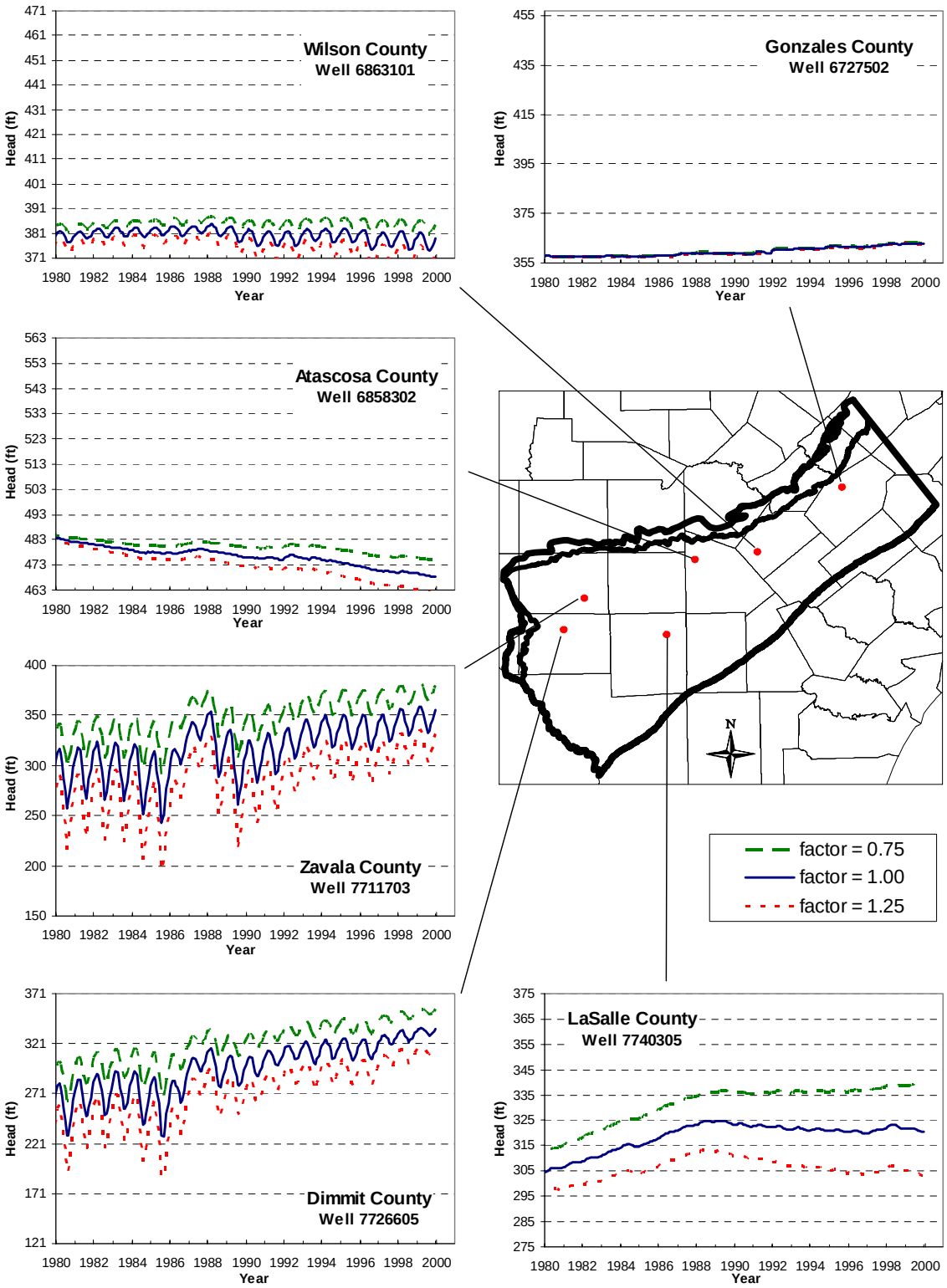

Figure 9.3.12 Transient sensitivity hydrographs from the Carrizo (Layer 3) where pumping rate is varied.

10.0 MODEL PREDICTIVE SIMULATIONS

The purpose of the GAM is to assess groundwater availability within the modeled Southern Carrizo-Wilcox GAM region over a 50-year planning period (2000-2050) using Regional Water Planning Group (RWPG) water-demand projections under drought-of-record (DOR) conditions. The GAM will be used to predict changes in regional groundwater water levels (heads) and fluxes related to baseflow to major streams and rivers, springs, and cross-formational flow.

Six basic predictive model runs are presented and documented: (1) average recharge ending with the DOR in 2010, (2) average recharge ending with the DOR in 2020, (3) average recharge ending with the DOR in 2030, (4) average recharge ending with the DOR in 2040, (5) average recharge ending with the DOR in 2050, and (6) average recharge through 2050 without including the DOR. In addition, a model run to 2010 that includes an estimated implementation of the Twin Forks project (7) is presented.

To complete the predictive simulations, estimates of pumping, recharge and groundwater evapotranspiration (ET), and streamflow must be completed for both an average future condition and a DOR. Predictive pumping demands from the RWPGs are used in the predictive simulations assuming that the pumping distribution (as determined in Appendix C) for the year 1999 applies in the future (2000-2050). Section 6.3.4 discusses the estimation of recharge and ET for the future conditions. In short, transient estimates from the calibration/verification period were averaged by month to maintain seasonality and used for the predictive simulations. For the DOR, additional SWAT runs were made over the time of the DOR to determine recharge and ET. Additional streamflow estimates (Section 6.3.3) were also made using gage records from the time period of the DOR. The following discusses the development of a DOR.

10.1 Drought of Record

GAM specifications require that the DOR used for model predictions be representative for the past 100 years and be defined by severity and duration. Drought is considered a normal, recurring climatic event. It is conceptually defined by the National Drought Mitigation Center as a protracted period of deficient precipitation resulting in extensive damage to crops with loss of yield. Operational definitions of drought are typically used to define the beginning, end, and

severity of a drought over a given historical period. Operational definitions typically quantify the departure of precipitation, or some other climatic variable, from average conditions over a defined time window (typically 30 years).

Drought indices are quantitative measures that assimilate raw data into a single value that defines how precipitation has varied from a specific norm. As discussed above, drought is a phenomenon related directly to available moisture from precipitation. Precipitation is the primary variable controlling recharge in the model region. Accordingly, we used precipitation data as the raw data for defining the DOR in the Southern Carrizo-Wilcox GAM region.

There are many drought indices available to measure the degree that precipitation has deviated from historical norms. The typical measure is "percent of normal", which is calculated by dividing the measured annual precipitation depth by the average annual precipitation depth and multiplying by 100. This calculation could be performed over a range of time scales but is typically annualized. The average annual precipitation depth is usually a long-term arithmetic mean. The available precipitation records within the model domain were analyzed to calculate the percent of normal as an indicator of drought. Figure 2.12 shows a select set of long-term annual precipitation records in the model region. Inspection of these shows particularly dry periods in 1917 and 1954 and 1956. The drought of 1917 is consistently measured by the nine available gages at that time and 1917 represents yearly minimum precipitation depths for five out the nine available gages. The average precipitation, as measured in percent of normal averaged across all available gages in the model area was equal to 42% in 1917 and 66% for the three year period from 1915 to 1917.

The 1950's represents a period of historical drought in Texas and the Rio Grande Basin including the region being modeled. The drought peaked in 1954 and continued through 1956. By the 1950s the available number of rain gages in the model area increased to 38. The severe drought conditions in the 1950s were consistently recorded by the model region precipitation gage records with 27 of 38 gages recording their period of record low annual precipitation depths between 1954 and 1956. The average precipitation, as measured in percent of normal averaged across all available gages in the model area, is equal to 70% from 1950 through 1956. The same metric calculated for the peak drought years from 1954 through 1956 is 56% of normal.

A secondary drought index that can be used to quantify the DOR is the Standardized Precipitation Index (SPI). This index was developed to define precipitation deficits over multiple time scales (McKee et al., 1993). The SPI is calculated based upon the precipitation record for a given location. The long-term precipitation record is fitted to a general probability distribution (typically the Gamma distribution). This distribution is then normally transformed and standardized so that the mean SPI for that location over the time period of interest is equal to zero. When the SPI is equal to zero, it signifies median precipitation conditions for that location based upon the time integration window specified (Edwards and McKee, 1997). Because the index is normalized, comparison of SPI values between locations (i.e., across our model domain) is simplified in that an SPI of –1 represents a similar magnitude deficit for all stations. Monthly precipitation averages are used as the raw data for the SPI calculation. A one-month SPI would represent normalized precipitation data without temporal averaging. The SPI is backward-averaged over some user-specified duration, typically between six months and three years. By lengthening this time integration window, one investigates longer term precipitation trends less subject to short-term variations. Short-term deficit conditions or anomalies are of less concern for predicting groundwater conditions. Figure 10.1.1 shows the SPI for precipitation gage 412458 in Frio County calculated using one year, two year, and three year averaging windows. Current SPI index maps are available online for the State of Texas for multiple time averaging periods from one month through three years at the following URL: http://www.txwin.net/Monitoring/Meteorological/Drought/spi.htm

McKee et al. (1993) defined a classification system for defining drought conditions using the SPI. This classification is taken from (Hayes, 2001) and presented in the table below. McKee et al. (1993) defined a drought event as any time period over which the SPI is continuously negative and reaches a magnitude of –1.0 or less.

Table 10.1 SPI Precipitation Deficit Classification System (Hayes, 2001).

SPI Value	Precipitation Deficit Condition
2.0 and above	Extremely wet
1.5 to 1.99	Very wet
1.0 to 1.49	Moderately wet
-0.99 to 0.99	Near normal
-1.0 to –1.49	Moderately dry
-1.5 to –1.99	Severely dry
-2.0 and less	Extremely dry

Figure 10.1.2 plots SPI curves for five representative long-term precipitation gages in the model area. A two year time window was used for the analysis. Drought occurs most consistently in these gages in the period from 1915 to 1920 and in the 1950s. The drought in the 1950s is of longer duration, and is supported by more available data. The SPI analysis gives a consistent result to the analysis of percent normal. The DOR is, therefore, considered to have occurred in the mid-1950s.

With the DOR picked to occur in the mid-1950s, we next reviewed the monthly data to define the month the DOR began and ended. For picking the beginning and end of the DOR, one would like to use a measure that represents climate conditions across the entire mode domain. To meet this need, records from all of the precipitation stations in the model area were averaged for each month to provide input to a "model-wide" SPI. Figure 10.1.3 shows the SPI calculated for this average dataset for several time integration windows. The longer duration (2- and 3-year) integration windows dip well below -1 starting in July 1954. However, the monthly data show that the below-average precipitation that started this downward trend began in October 1953. The consistently below-normal precipitation continued until February 1957, when a wet-dry-wet period occurred, followed by more normal precipitation trends. Therefore, we chose the DOR to have occurred between October 1953 and February 1957 for this model region.

To implement the drought of record in the predictive scenarios, we replaced the end of the scenario with the drought of record data, while maintaining the seasonality of the dataset. For instance, for the 2010 scenario, September 2006 marks the end of the averaged predictive dataset. From that point, climatic data calculated for October 1953 through February 1957 were used for the remainder of the simulation to estimate recharge. The simulation then ends in February 2010.

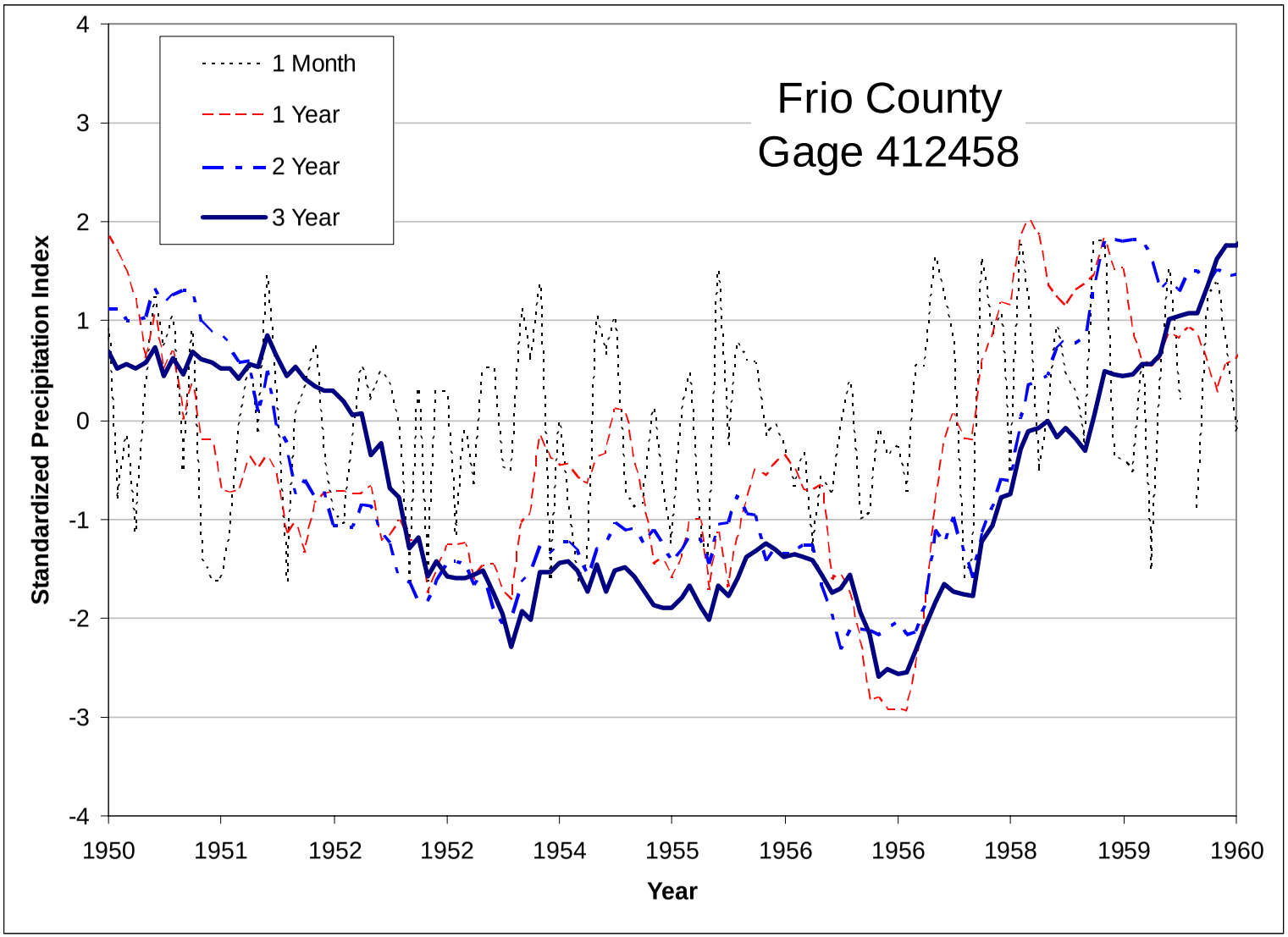

Figure 10.1.1 Standard precipitation index (SPI) curves for the Dilley rain gage (#412458-Frio Co.) for 1 month, 1 year, 2 year, and 3 year time periods.

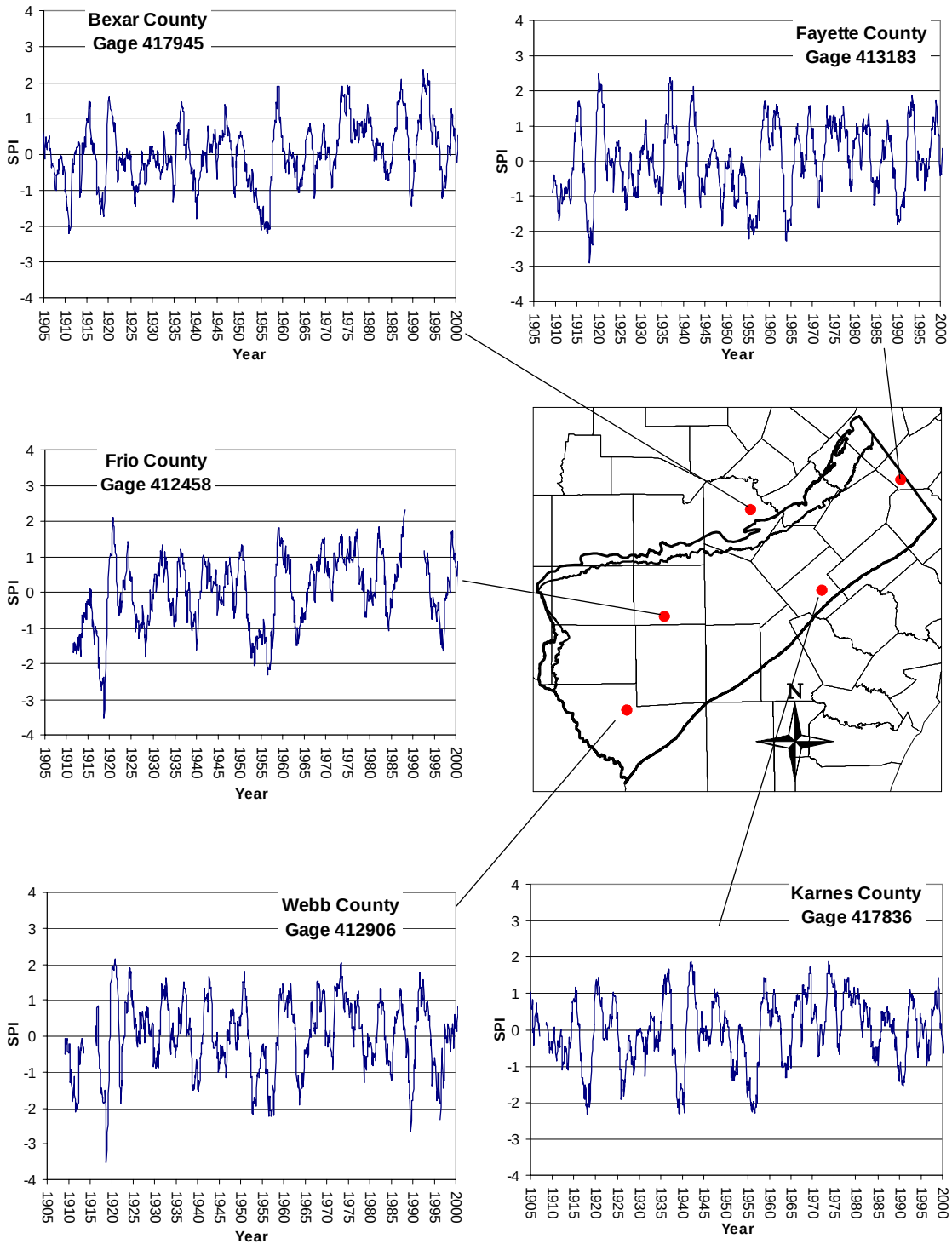

Figure 10.1.2 Standardized precipitation indices for precipitation gages in the region.

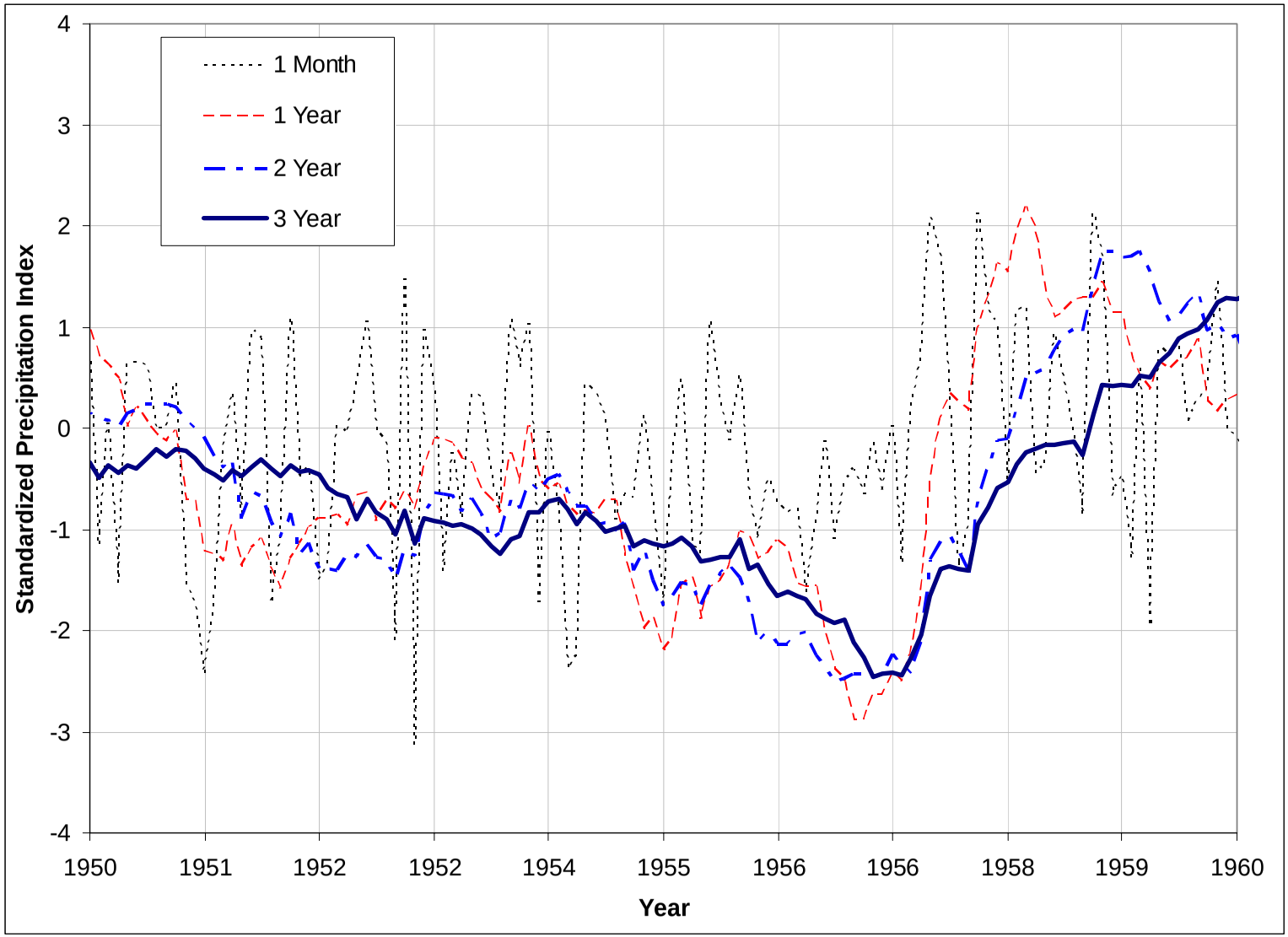

Figure 10.1.3 Standardized precipitation index averaged for all gages in the region from 1950-1960.

10.2 Predictive Simulation Results

In this section, we present the head and drawdown surfaces from the predictive simulation results. We also discuss a comparison between the average recharge condition simulation and the simulation with a drought of record (DOR).

Figure 10.2.1 shows the simulated 2000 and 2050 head surfaces for Layer 1. The direction of the gradient does not change significantly from 2000 to 2050. The contour lines have smoothed somewhat in the western portion of the model, with not as pronounced a depression in LaSalle county as had previously been present. Figure 10.2.2 shows that heads decreased slightly in the eastern portion of the model, but increased more than 25 ft in a region that includes parts of Frio, Atascosa, LaSalle, and McMullen counties.

Figure 10.2.3 shows the simulated 2000 and 2050 head surfaces for the Carrizo (Layer 3). This figure shows that the most pronounced drawdown has moved from between Frio and LaSalle counties down to northern Webb county. This drawdown is the result of including pumping for one of the options in the Rio Grande region (Region M) water plan for the City of Laredo. This option is a groundwater development project in the Carrizo aquifer in northern Webb County that would serve the city of Laredo in southern Webb County. The drawdown plot in Figure 10.2.4 shows the two main phenomena occurring over the simulated time period, the increase in heads in the Wintergarden area primarily due to relocated or decreased pumping, and the drawdown in northwest Webb County. Also, some drawdown occurred in the eastern portion of the model, where pumping is projected to increase over time. What is shown in this figure is the projected trend of shifting pumping from the west to the east in this region.

Figure 10.2.5 shows the simulated 2000 and 2050 head surfaces for the upper Wilcox (Layer 4). The upper Wilcox is strongly affected by heads in the Carrizo, so it mimics many of the changes occurring in the Carrizo that directly overlies it. The drawdown plot for the upper Wilcox (Layer 4) shown in Figure 10.2.6 demonstrates this, with increasing heads in the Wintergarden area and decreasing heads in northern Webb County. Figure 10.2.7 shows the simulated 2000 and 2050 head surfaces for the middle Wilcox (Layer 5). This figure illustrates the change in gradient direction occurring over the simulated period. In the 2000 head surface in the western portion of the model, gradients are primarily south with Dimmitt, Webb, and

southern La Salle counties showing a northeast gradient, as everything feeds into the depression in the Wintergarden area that continues downdip to the growth faults. By 2050, the rebound in heads has changed the gradients to predominantly southeast, directly downdip. Along the western boundary, the gradients have shifted to the east. The drawdown plot shown in Figure 10.2.8 indicates that in the middle Wilcox (Layer 5) heads are increasing in the Wintergarden area. The drawdown in the eastern portion of the model that was seen in the shallow layers is not evident in the middle Wilcox. Figure 10.2.9 shows the simulated 2000 and 2050 head surfaces for the lower Wilcox (Layer 6). Because the lower Wilcox is hydrologically separated from the rest of the model by the middle Wilcox, which has a low vertical hydraulic conductivity, many of the effects seen in the shallower layers are dampened in the lower Wilcox. This figure indicates that the direction of flow has not changed much in the lower Wilcox, although Figure 10.2.10, which shows the drawdown plot, does indicate more than 50 ft of head increase beneath the Wintergarden region.

Figures 10.2.11 through 10.2.14 show the simulated head results in the Carrizo for the remaining predictive runs. These simulations ended with a drought of record in 2010, 2020, 2030, and 2040, respectively. These figures show a consistent trend of drawdown in northern Webb County, increasing heads in the Wintergarden area, and slight decreases in heads in the eastern region of the model. Figures 10.2.15 through 10.2.19 show the 2010, 2020, 2030, and 2040 simulated head surfaces for the upper and middle Wilcox layers. The head surfaces for the Queen City and Lower Wilcox layers are not shown for all cases because the change in head in these layers is small (less than about 50 ft) at 2050. In all layers, we examined the drawdowns with respect to the assumed boundary conditions in the model (Section 6.3.1). Drawdowns at the lateral no-flow boundaries to the northeast, southwest, and downdip are within estimated model head error, so the boundaries are considered appropriate for the predictive simulations. In one investigative simulation, we found that replacing the northeast no-flow boundary with a general head boundary had little effect on the resulting head surfaces, further validating the suitability of the northeast no-flow boundary.

The trends in the simulated Carrizo hydraulic heads through time are further exemplified in Figure 10.2.19 which shows selected hydrographs from the predictive simulation from 2000 to 2050 ending with the drought of record. In the eastern region of the model, illustrated by the hydrographs from Wilson and Gonzales counties, the trend after 2000 is a slight decrease in

head. In the Gonzales County hydrograph, the decrease is steady over time. In the Wilson County hydrograph, the decrease is most evident in the first few predictive years, (i.e. 2000-2010), then the heads level off for the rest of the simulation period. In both cases, the decrease in heads is not dramatic. The previous figures 10.2.11 and 10.2.14 also show the trend from Wilson County where there is slight drawdown in 2010 which has not increased significantly by 2040. The hydrograph for Atascosa County shown in Figure 10.2.19 shows the increase in heads that results from decreased pumping in the area. The effect is more dramatic if the well is near an area of historically greater pumping than in the predictive simulation period (2000-2050). This is evident in the hydrograph for Frio County. In 2000, the amplitude of the seasonal cycling decreases dramatically and the head increases more than 50 feet over the simulated period. See Table 4.7.1 for a summary of the predictive and historical pumping by county. The hydrograph from Dimmit County shows a steady downward trend throughout the simulation, from the calibration/verification period through the predictive period. This is likely the result of the increased pumping in the northern Webb County area.

Figures 10.2.20 through 10.2.22 show the differences between the simulated head surfaces for 2050 with average recharge and the simulated head surfaces for 2050 with the DOR for the Carrizo through the lower Wilcox (Layers 3 through 6). In all of these layers there is a maximum head difference of less than 10 ft. All of the simulated head difference is in or near the outcrop, where recharge has the most impact. These figures emphasize an important point about the hydrology of this aquifer system. Recharge does not have a significant impact on downdip heads over the timescale of these simulations. One aspect of these simulations that is misleading is that simulated pumping does not increase during the DOR. The DOR only impacts climate data and subsequently, recharge and ET. Therefore, the effect of a DOR will be seen predominantly in the updip and outcrop areas. The hydrographs for Gonzales and Wilson counties (Figure 10.2.19) show a slight effect of the drought of record for heads near the outcrop. The slight increase in negative slope of the hydrograph in the last years of the simulation is concurrent with the drought of record.

Figures 10.2.23 and 10.2.24 show the saturated thickness in the outcrop for 2000 and 2050, respectively. Note that the figures show the saturated thickness for each layer outcrop, without combining any layers. The Carrizo-Wilcox aquifer is primarily confined and the layers are thin in the narrow outcrop region, so the model does not provide great resolution for

saturated thickness. These figures indicate that little change has occurred in the saturated thickness between years 2000 and 2050.

An additional predictive simulation was performed to add the expected pumping associated with the Twin Oaks Project in southern Bexar County. Approximately 14,000 AFY of pumping was added to a 5 square mile area in southern Bexar County. The simulation was identical to the 2010 predictive simulation, except that the additional pumping was started in 2003. Figure 10.2.25 shows the difference between the base 2010 simulation and the simulation that includes the Twin Oaks Project. The additional pumping causes a maximum of about 20 ft of drawdown in southern Bexar County.

a.

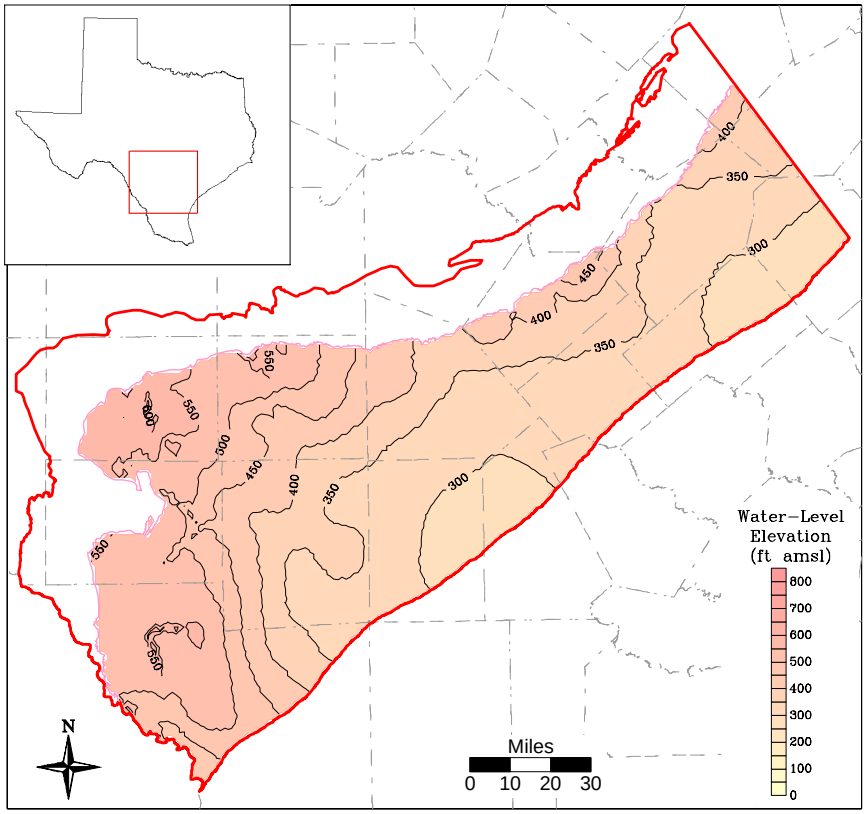

b.

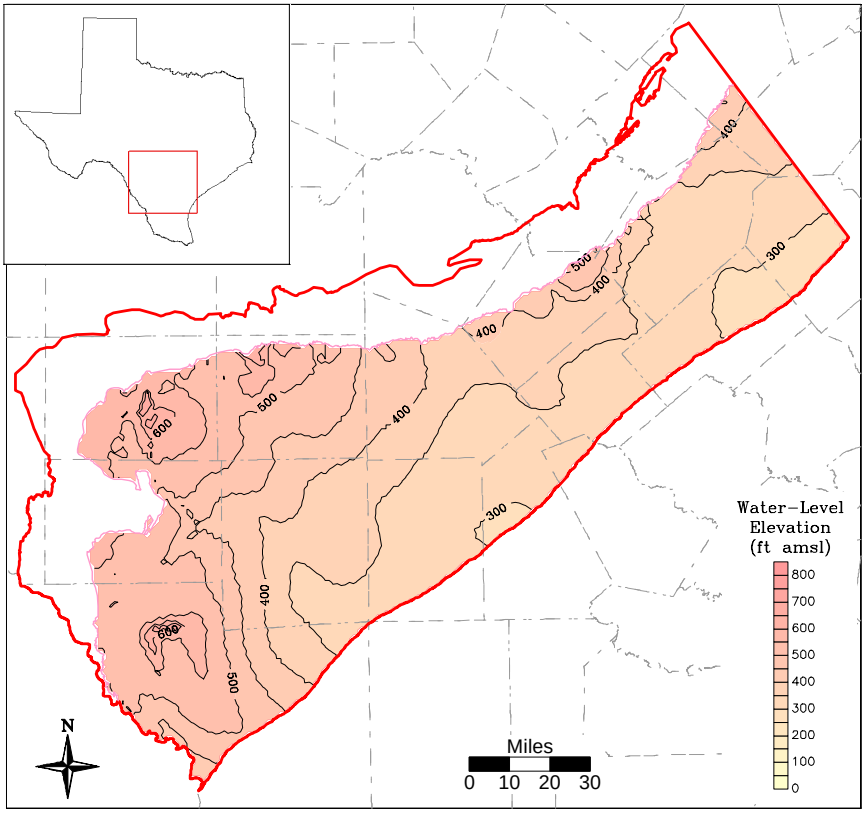

Figure 10.2.1 Simulated 2000 (a) and 2050 (b) head surfaces, Queen City/El Pico (Layer 1).

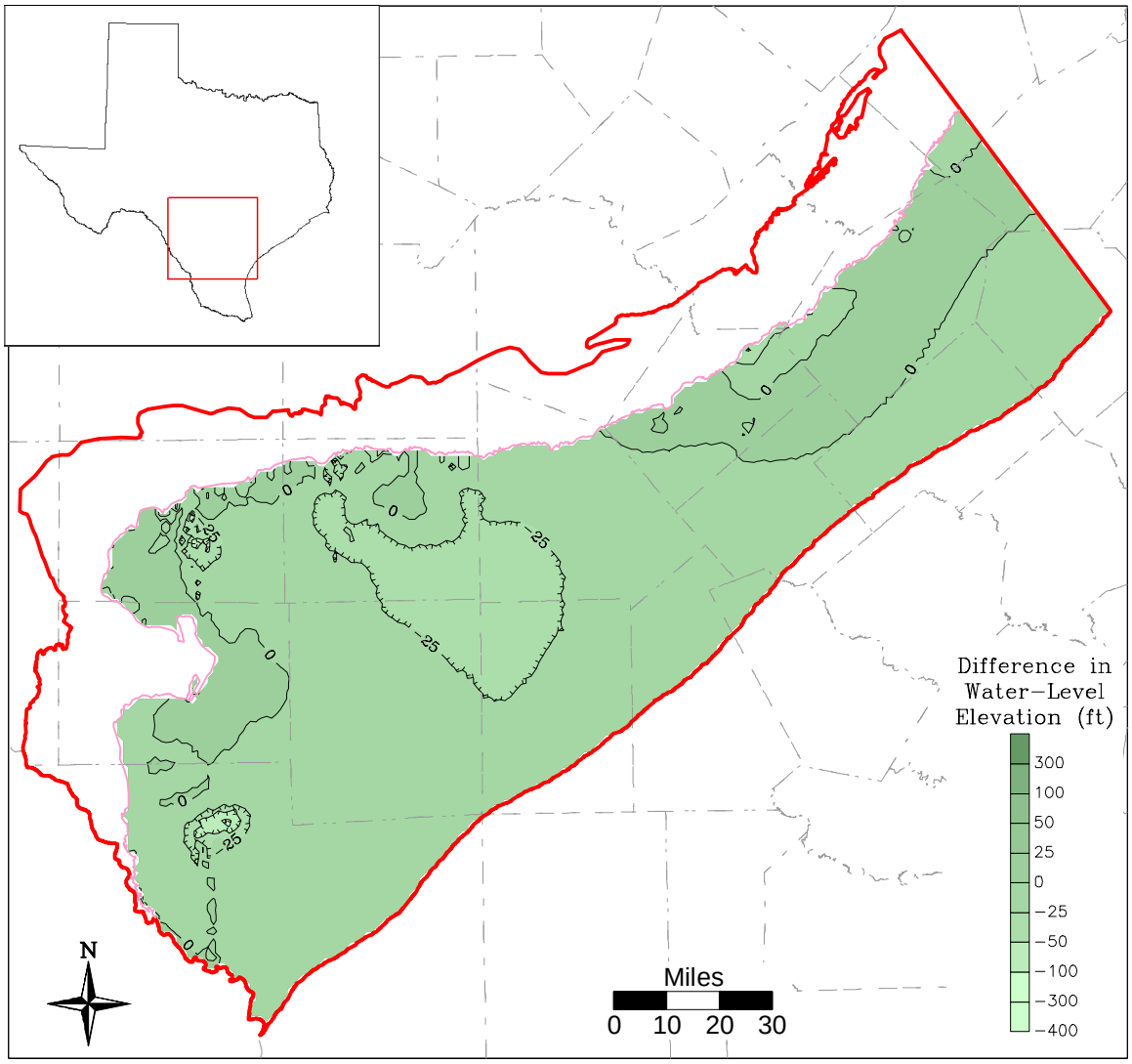

Figure 10.2.2 Difference between 2000 and 2050 simulated head surfaces, Queen City/El Pico (Layer 1).

a.

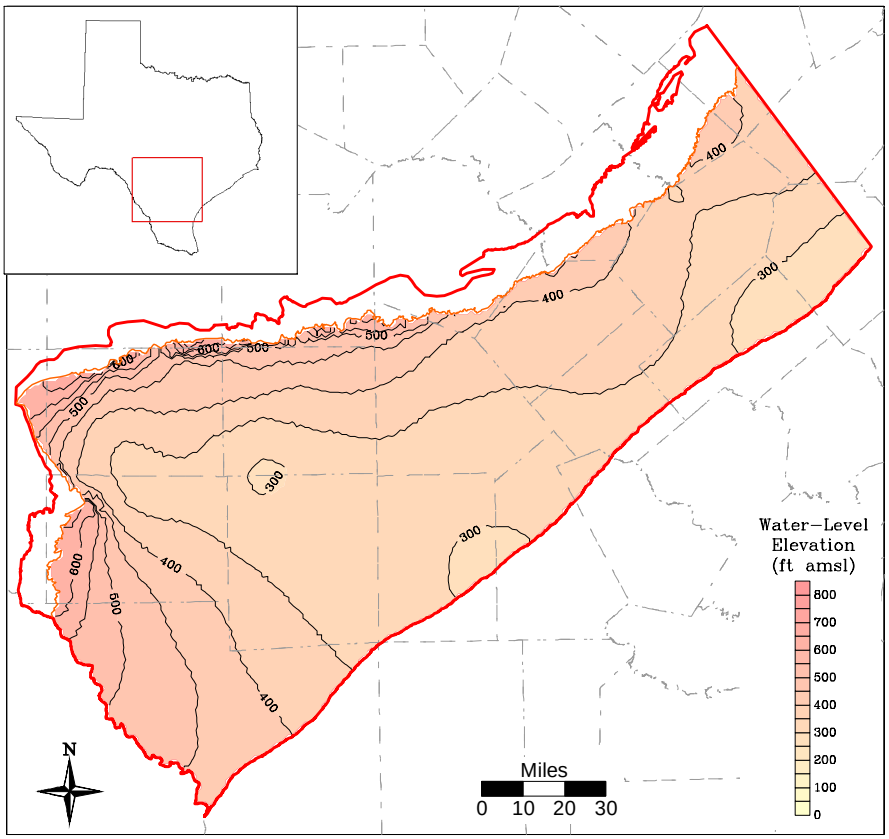

b.

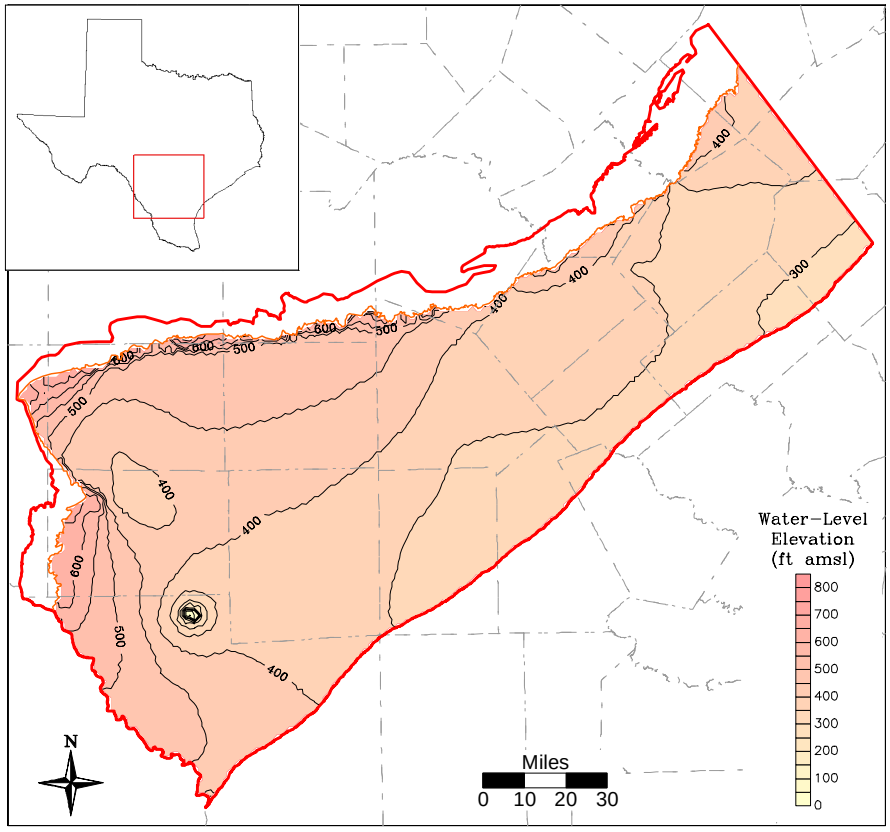

Figure 10.2.3 Simulated 2000 (a) and 2050 (b) head surfaces, Carrizo (Layer 3).

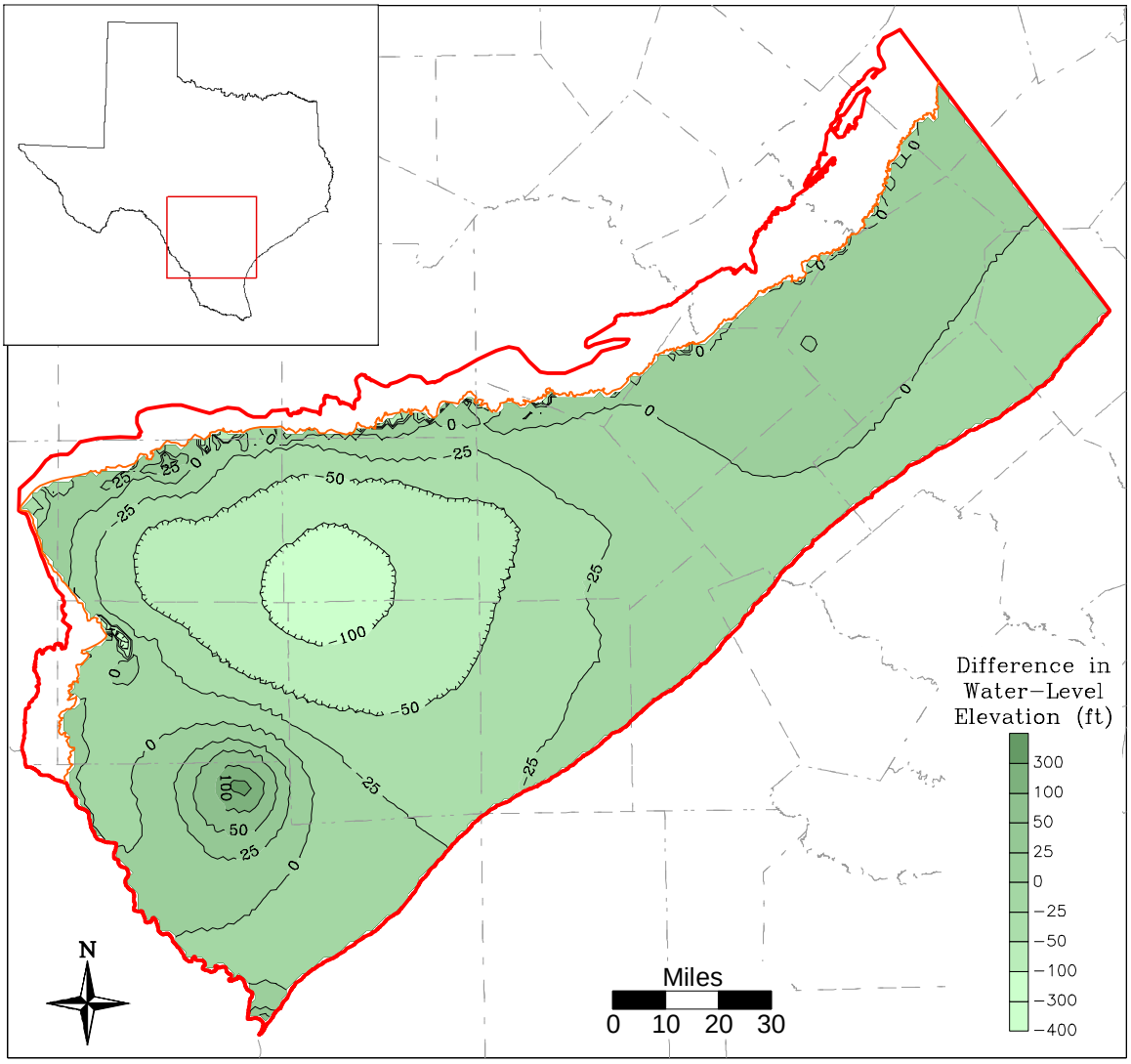

Figure 10.2.4 Difference between 2000 and 2050 simulated head surfaces, Carrizo (Layer 3).

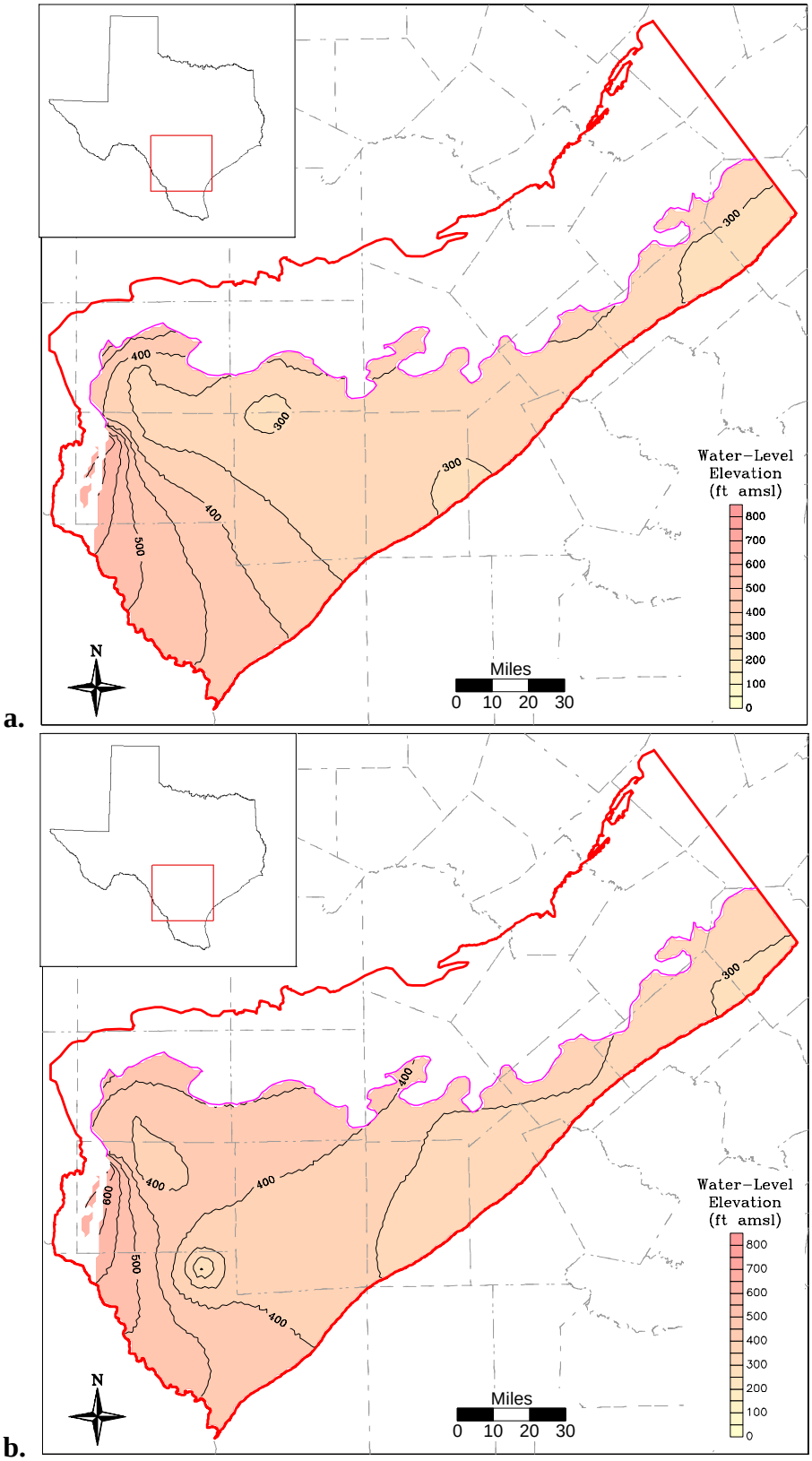

Figure 10.2.5 Simulated 2000 (a) and 2050 (b) head surfaces, upper Wilcox (Layer 4).

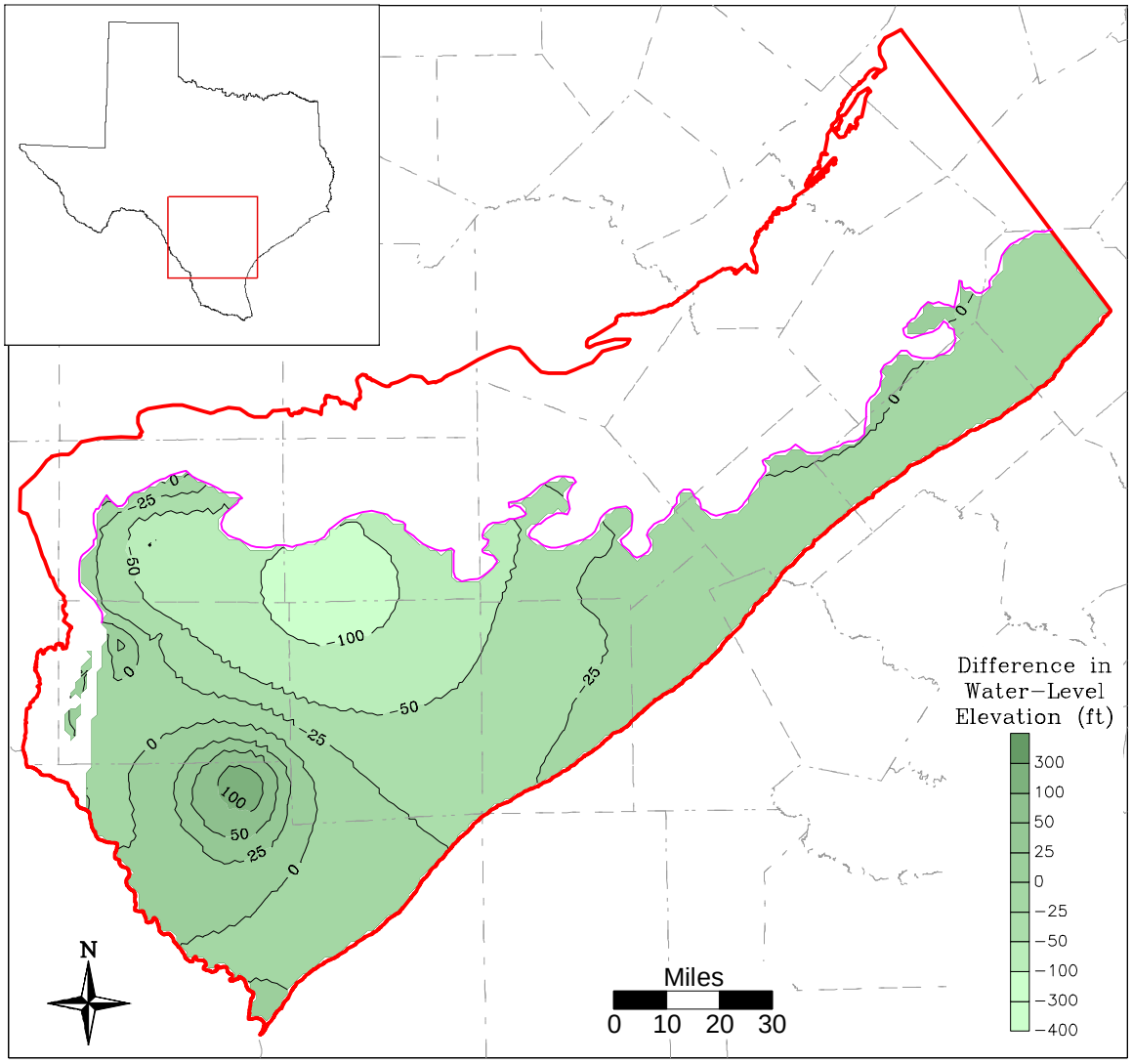

Figure 10.2.6 Difference between 2000 and 2050 simulated head surfaces, upper Wilcox (Layer 4).

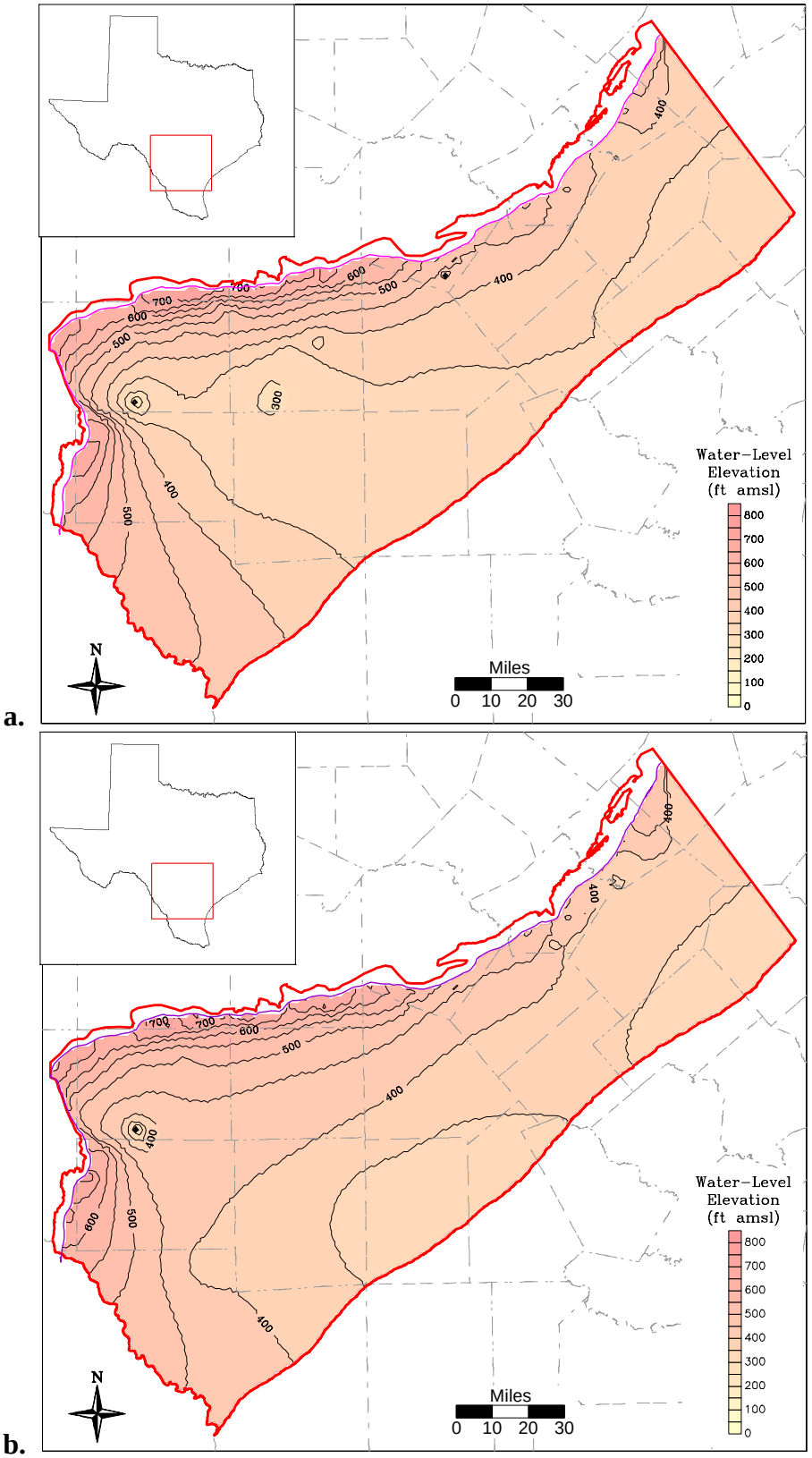

Figure 10.2.7 Simulated 2000 (a) and 2050 (b) head surfaces, middle Wilcox (Layer 5).

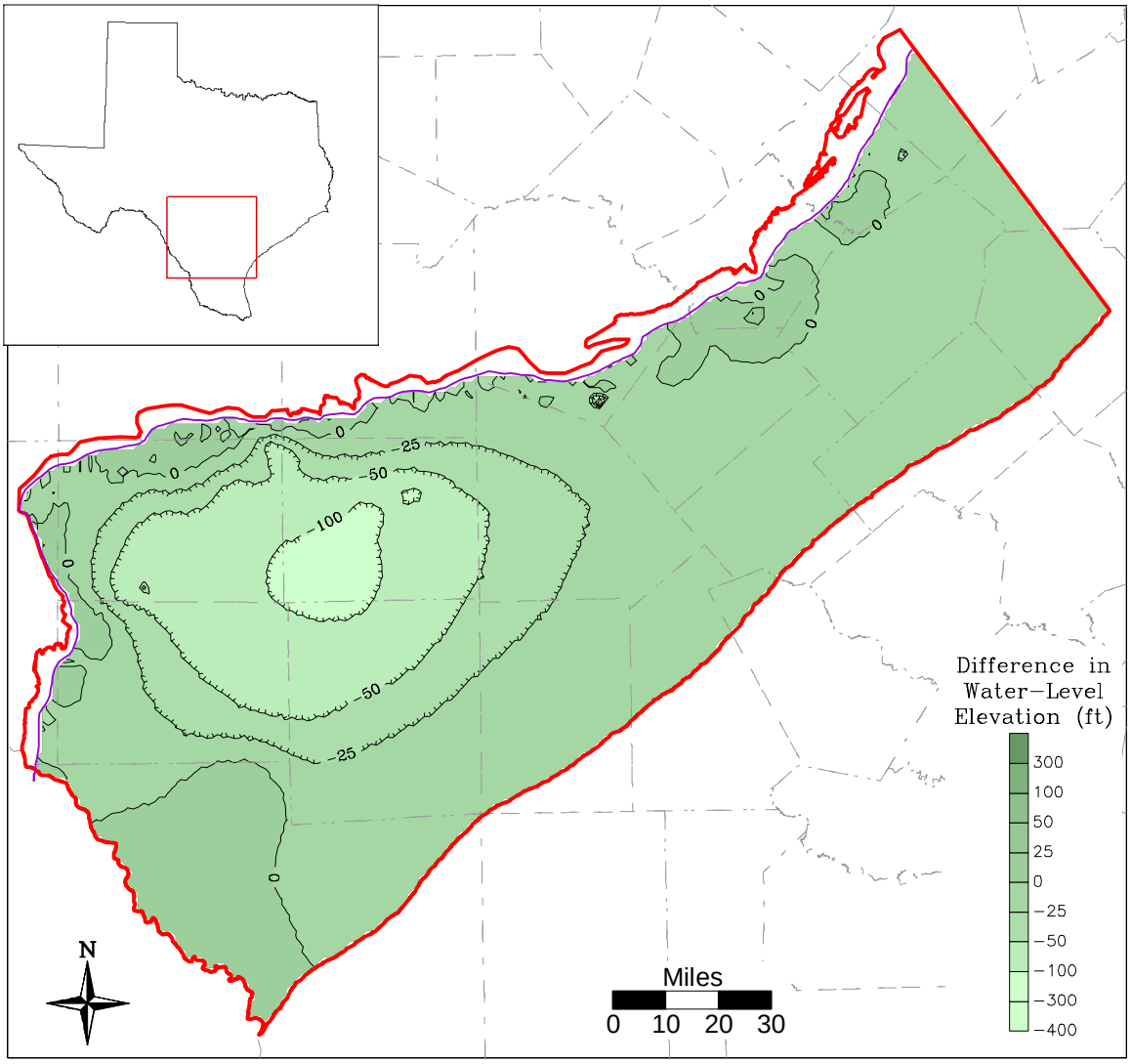

Figure 10.2.8 Difference between 2000 and 2050 simulated head surfaces, middle Wilcox (Layer 5).

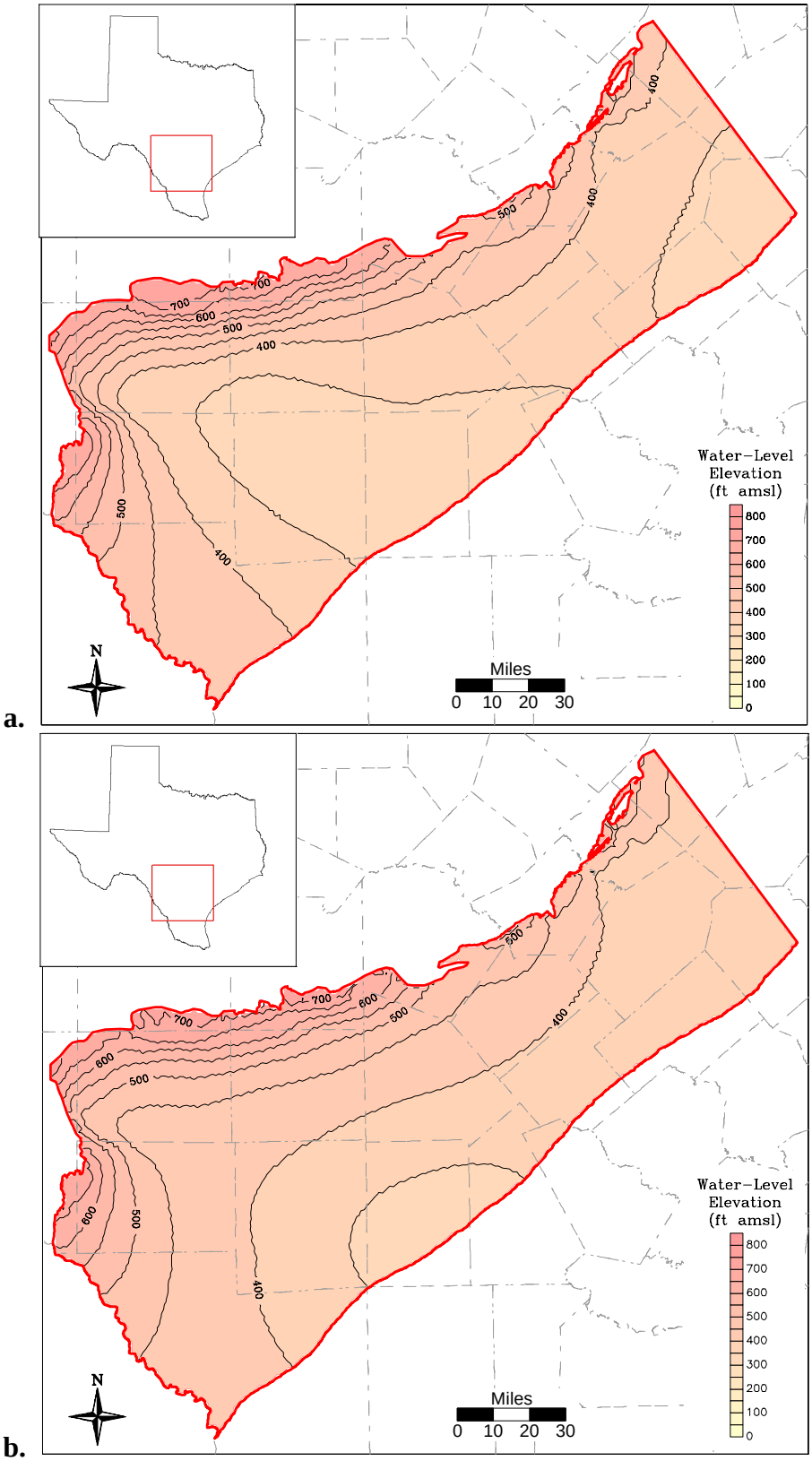

Figure 10.2.9 Simulated 2000 (a) and 2050 (b) head surfaces, lower Wilcox (Layer 6).

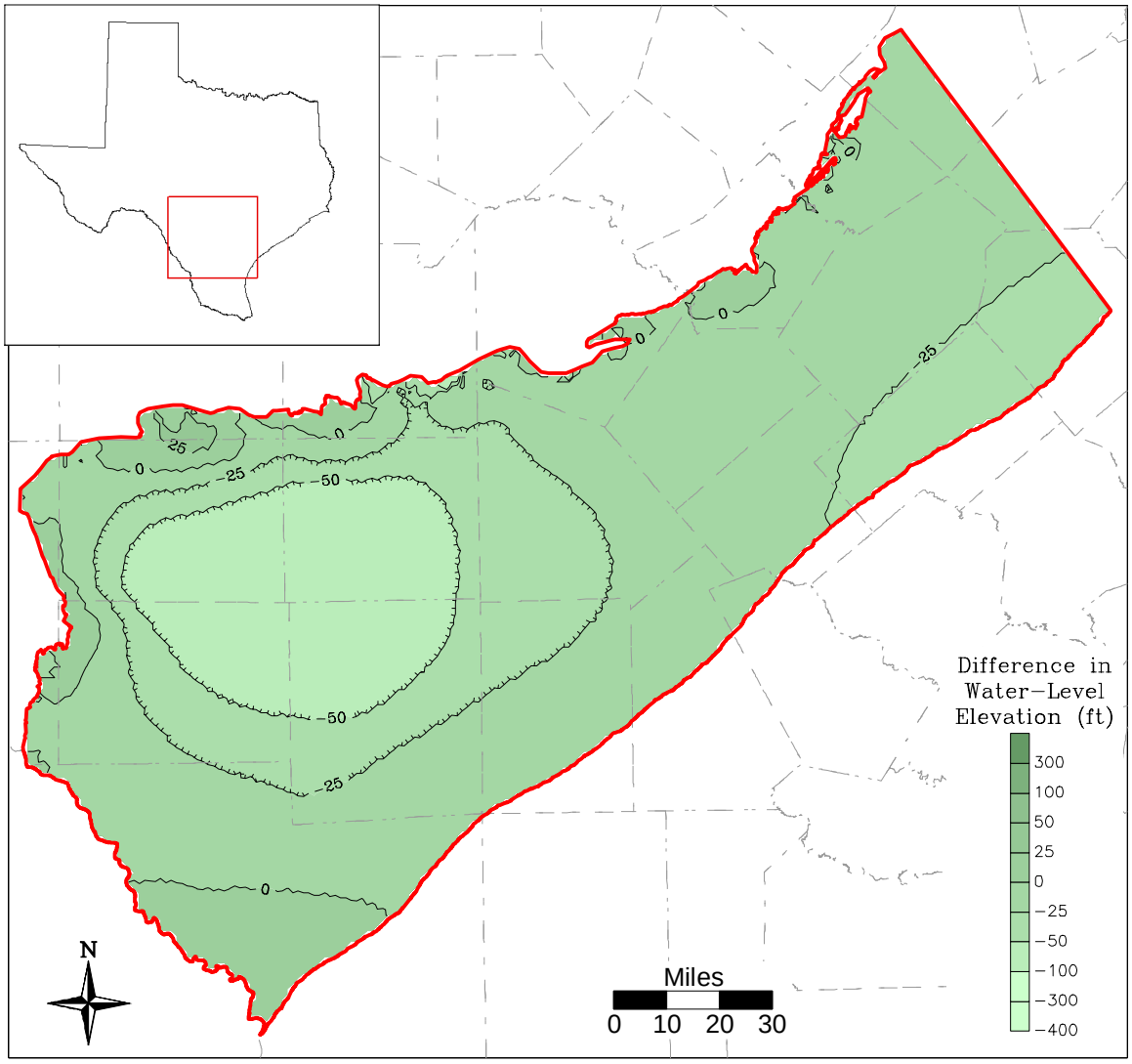

Figure 10.2.10 Difference between 2000 and 2050 simulated head surfaces, lower Wilcox (Layer 6).

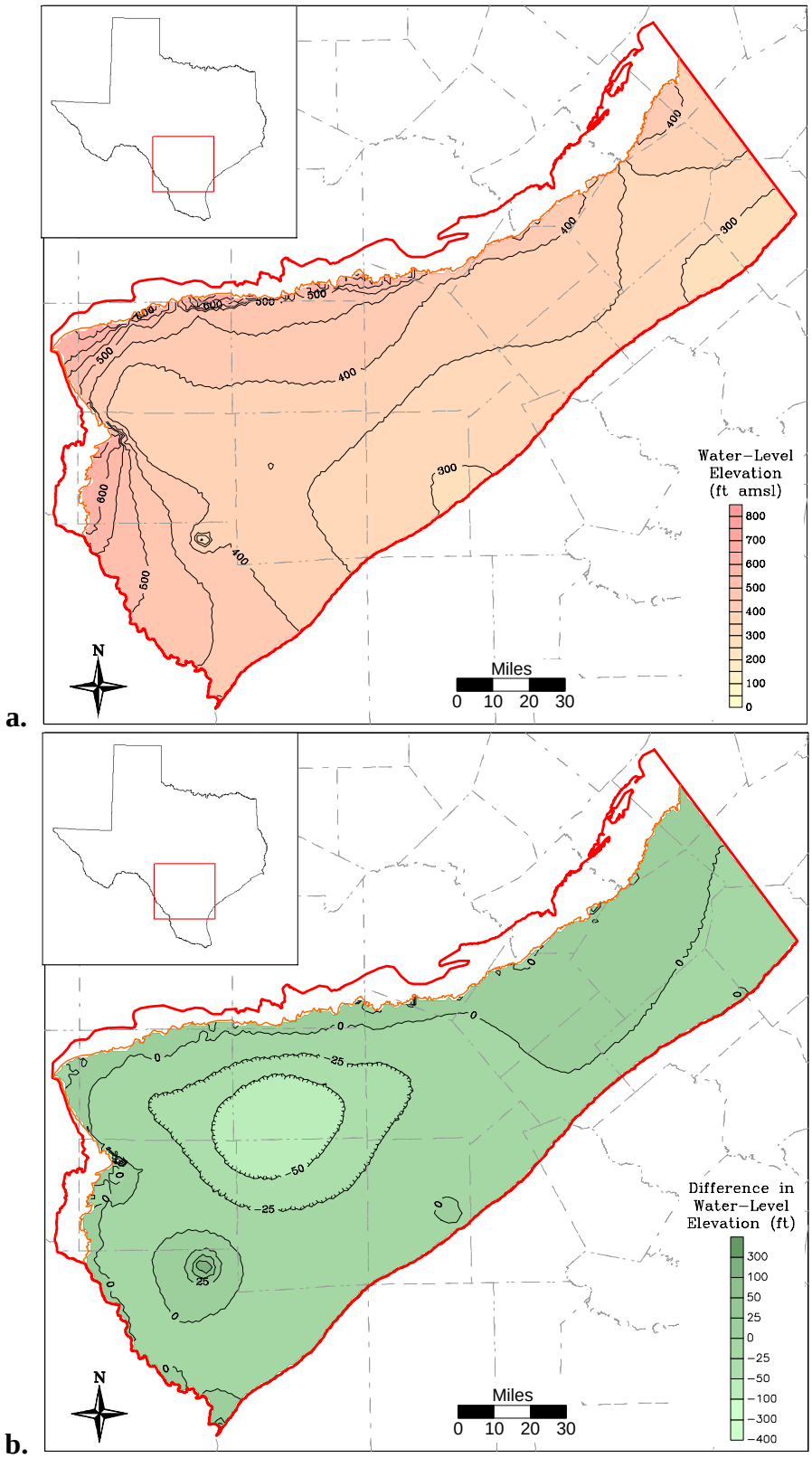

Figure 10.2.11 Simulated 2010 head surface (a) and drawdown from 2000 (b) for the Carrizo (Layer 3).

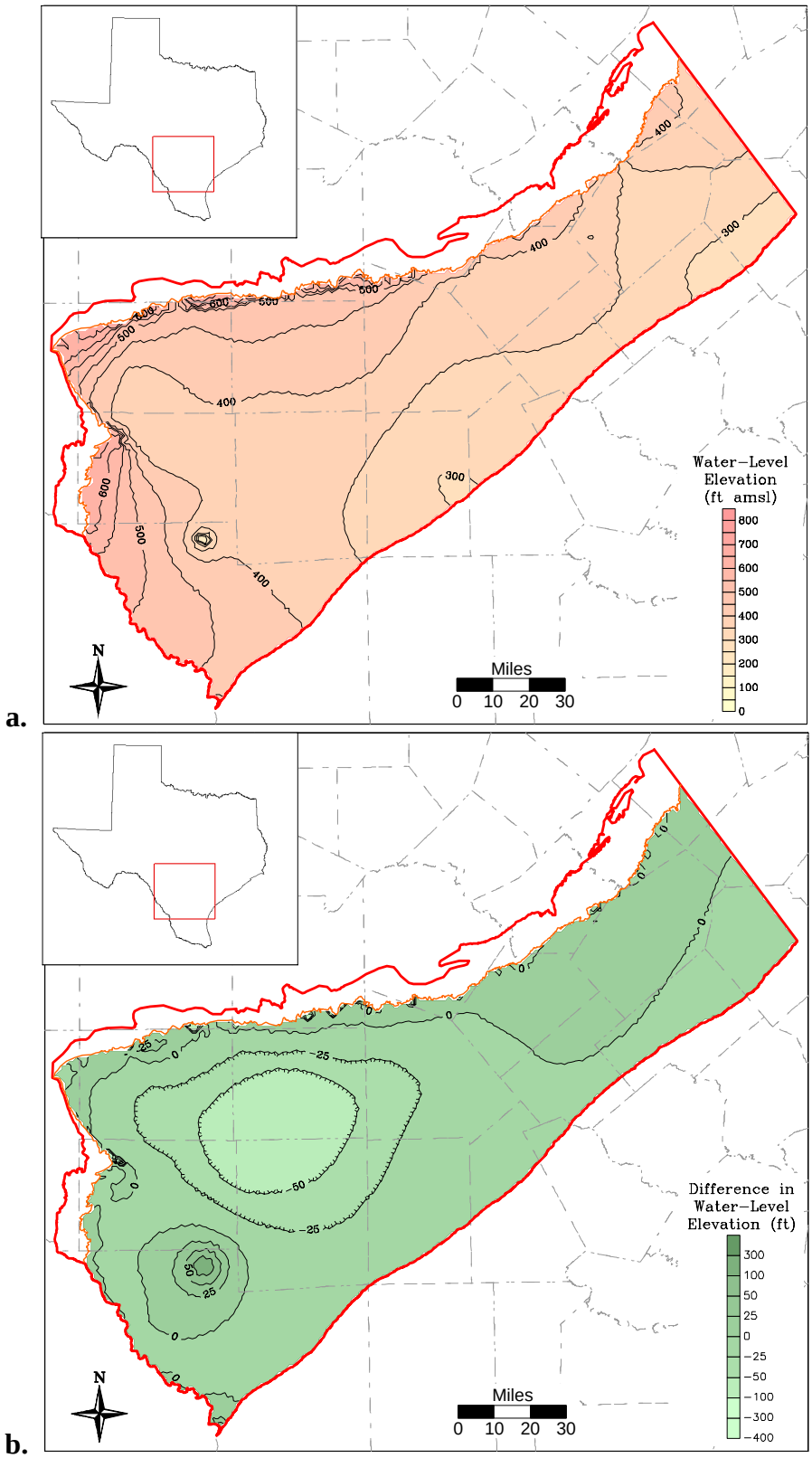

Figure 10.2.12 Simulated 2020 head surface (a) and drawdown from 2000 (b) for the Carrizo (Layer 3).

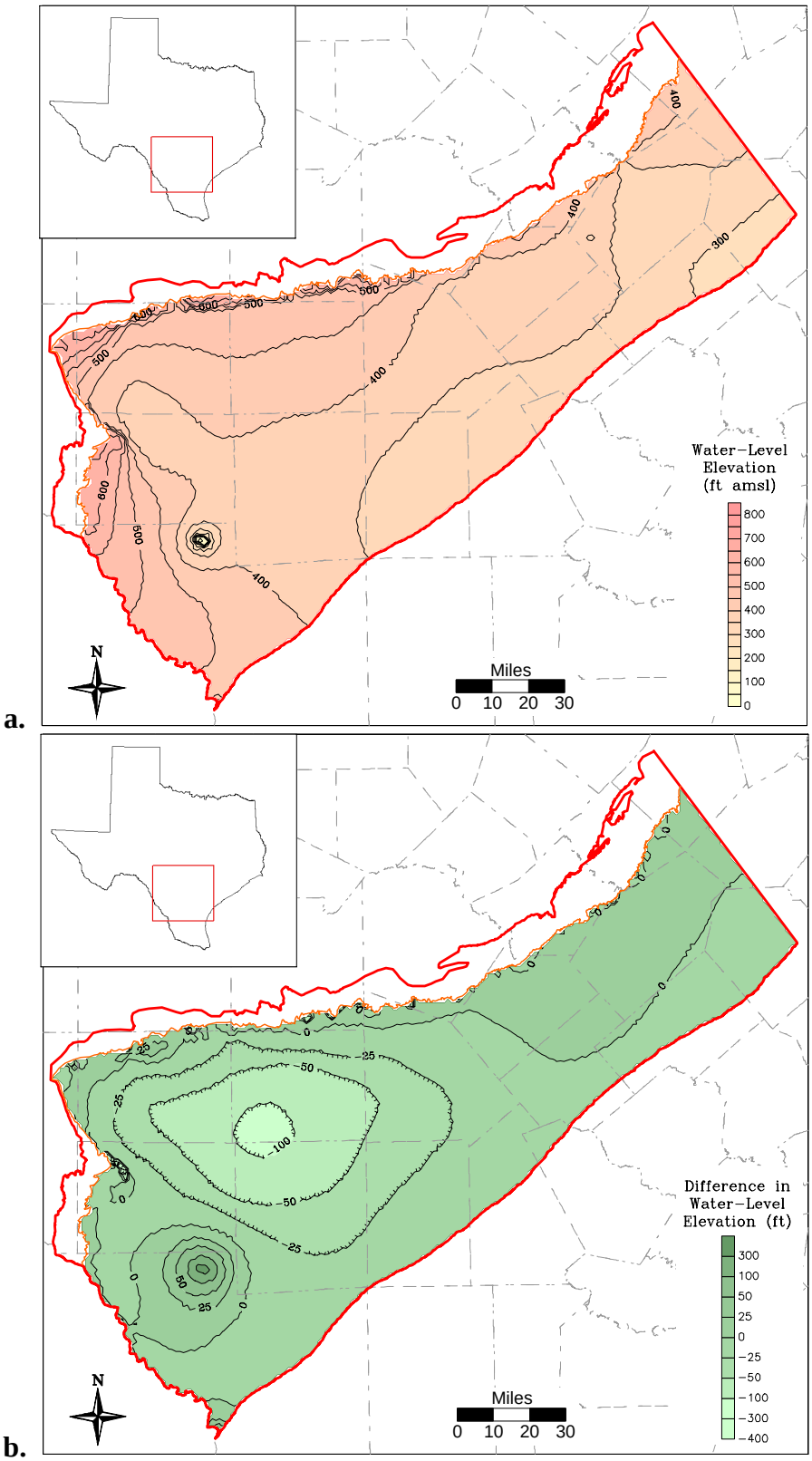

Figure 10.2.13 Simulated 2030 head surface (a) and drawdown from 2000 (b) for the Carrizo (Layer 3).

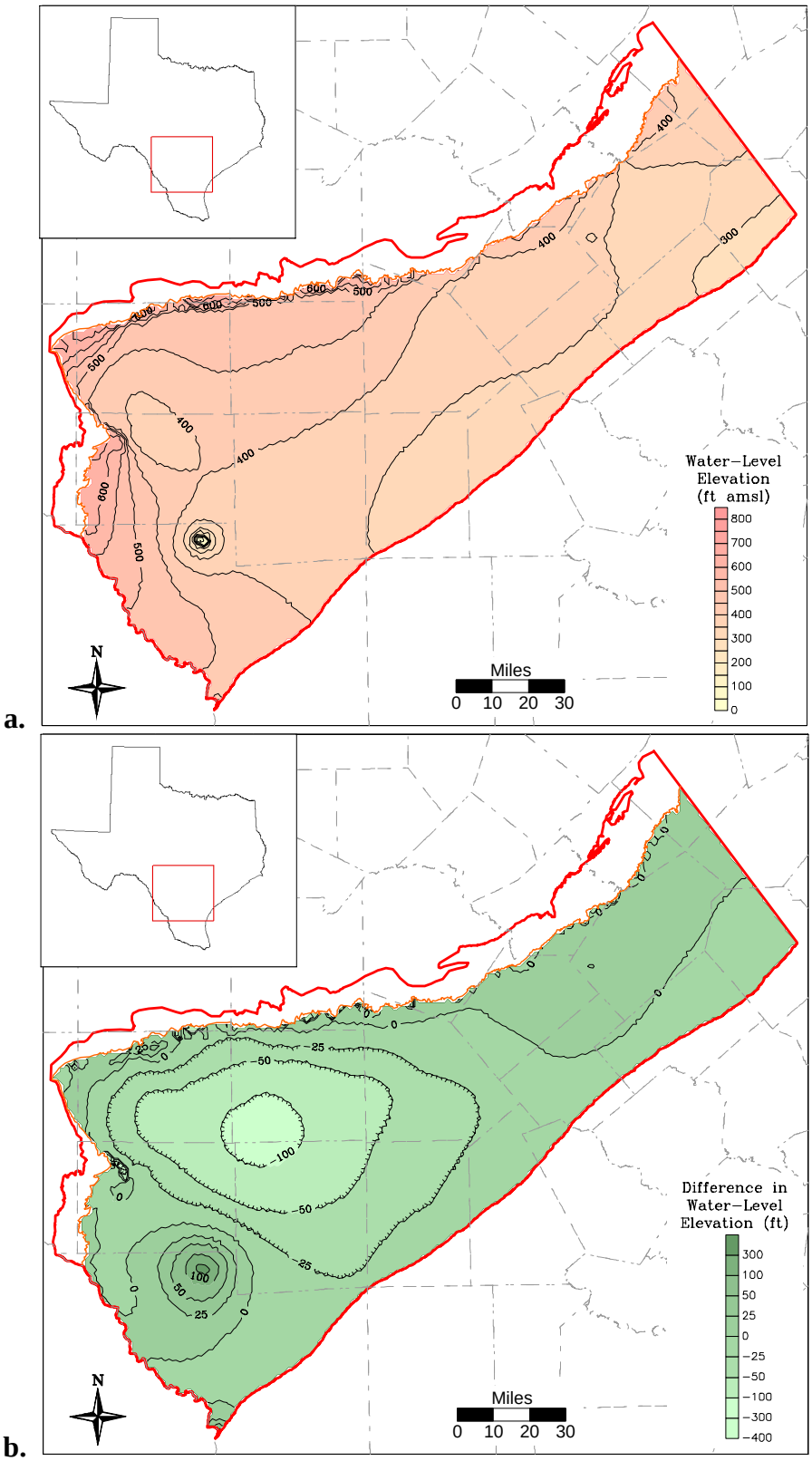

Figure 10.2.14 Simulated 2040 head surface (a) and drawdown from 2000 (b) for the Carrizo (Layer 3).

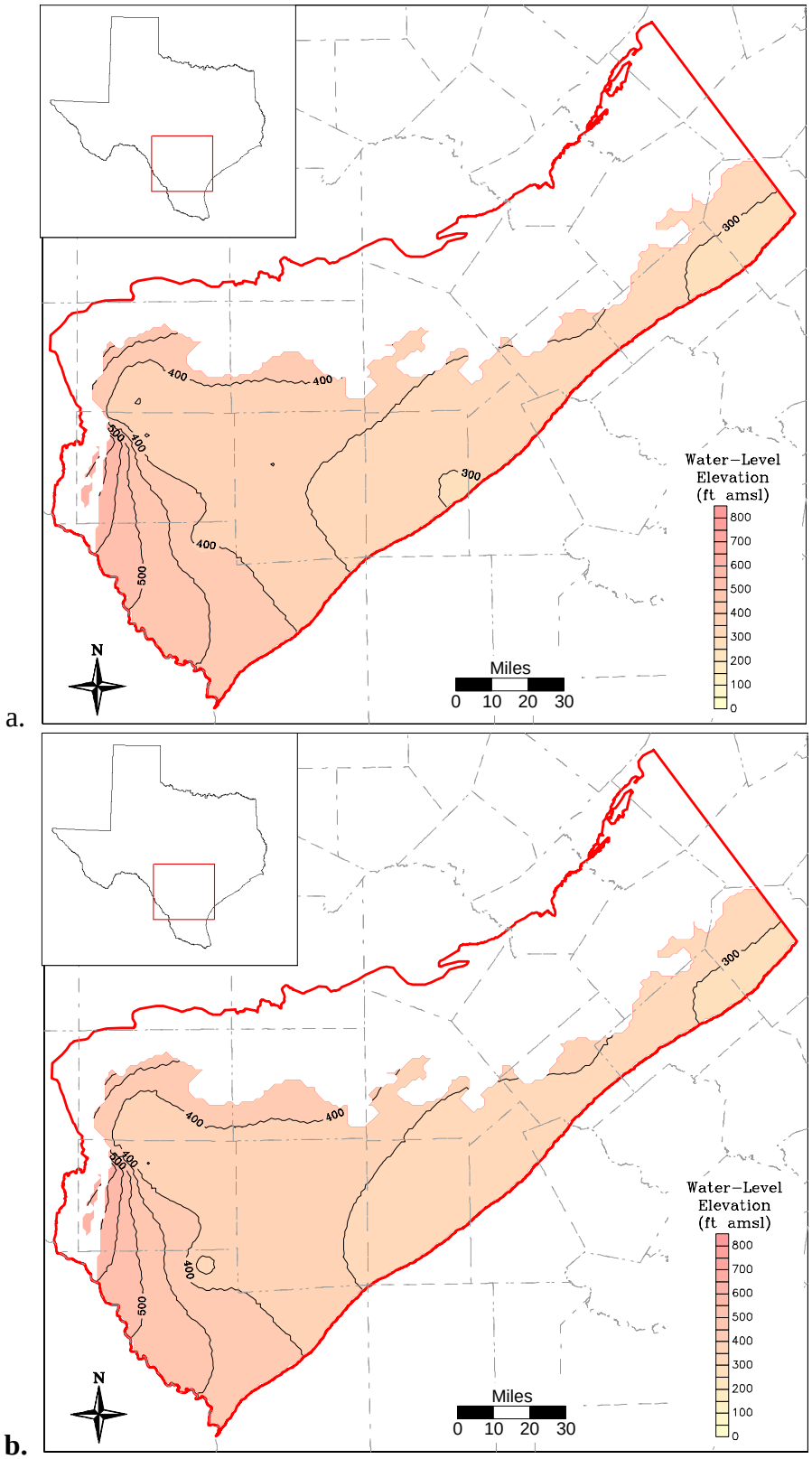

Figure 10.2.15 Simulated 2010 (a) and 2020 (b) head surface, upper Wilcox (Layer 4).

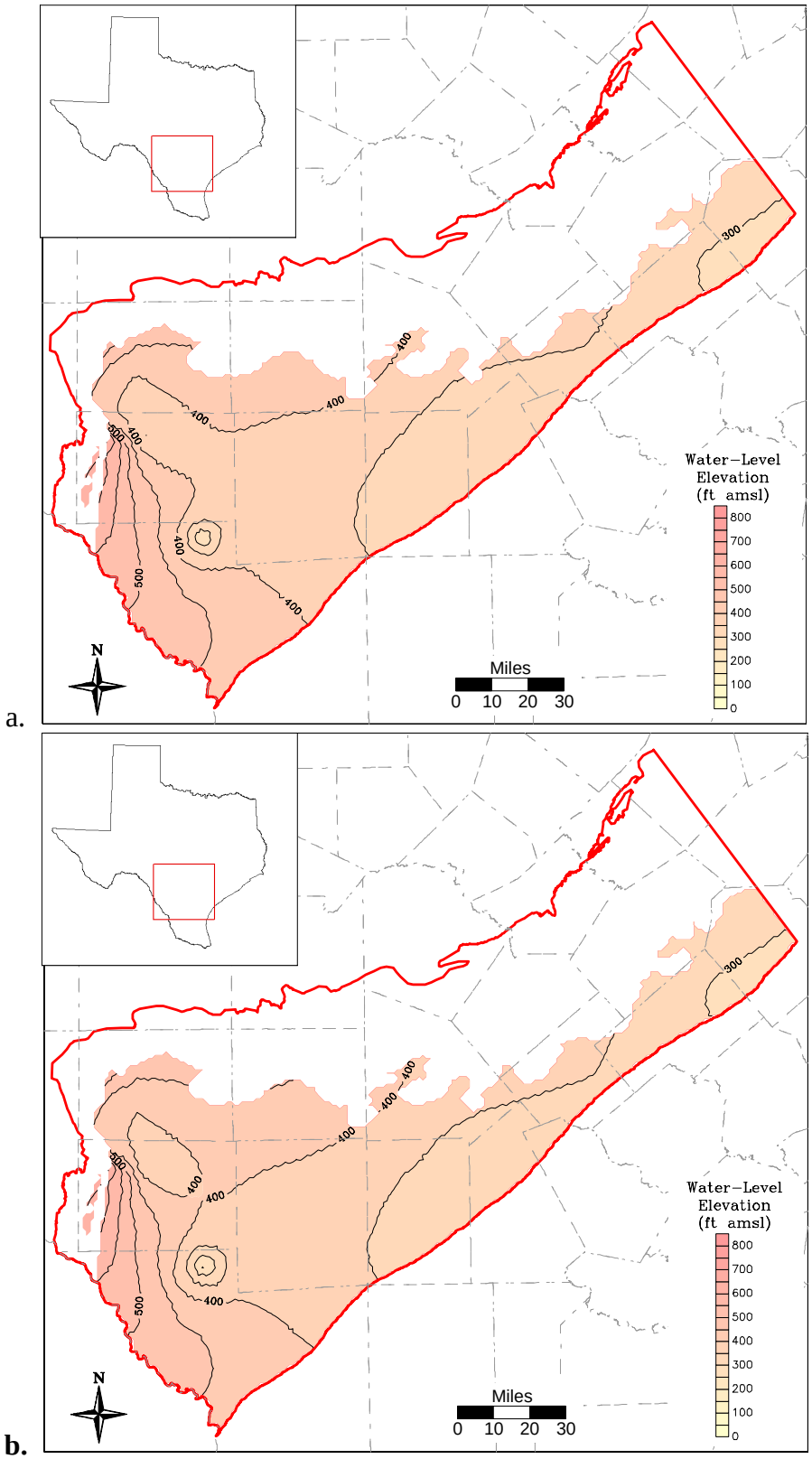

Figure 10.2.16 Simulated 2030 (a) and 2040 (b) head surface, upper Wilcox (Layer 4).

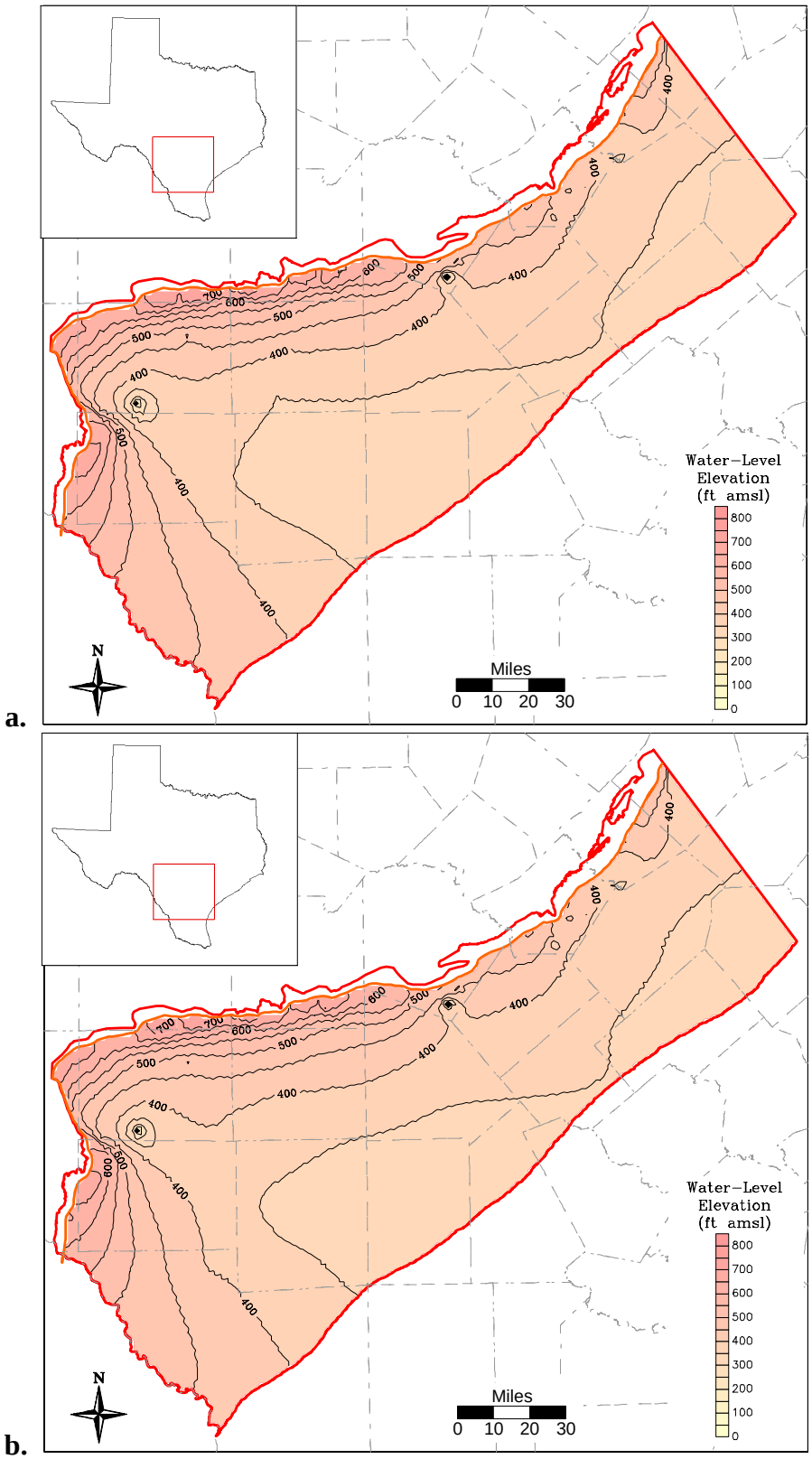

Figure 10.2.17 Simulated 2010 (a) and 2020 (b) head surface, middle Wilcox (Layer 5).

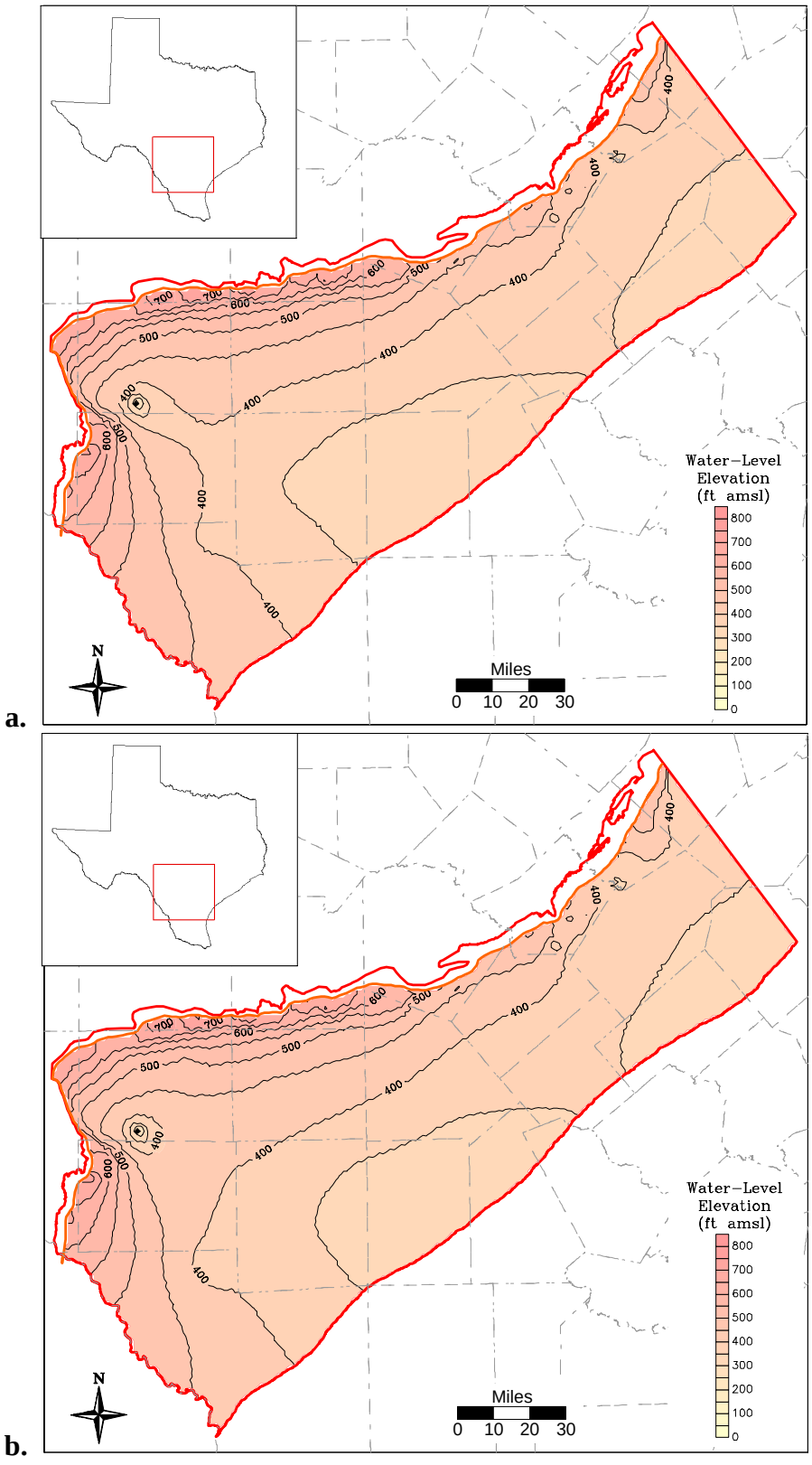

Figure 10.2.18 Simulated 2030 (a) and 2040 (b) head surface, middle Wilcox (Layer 5).

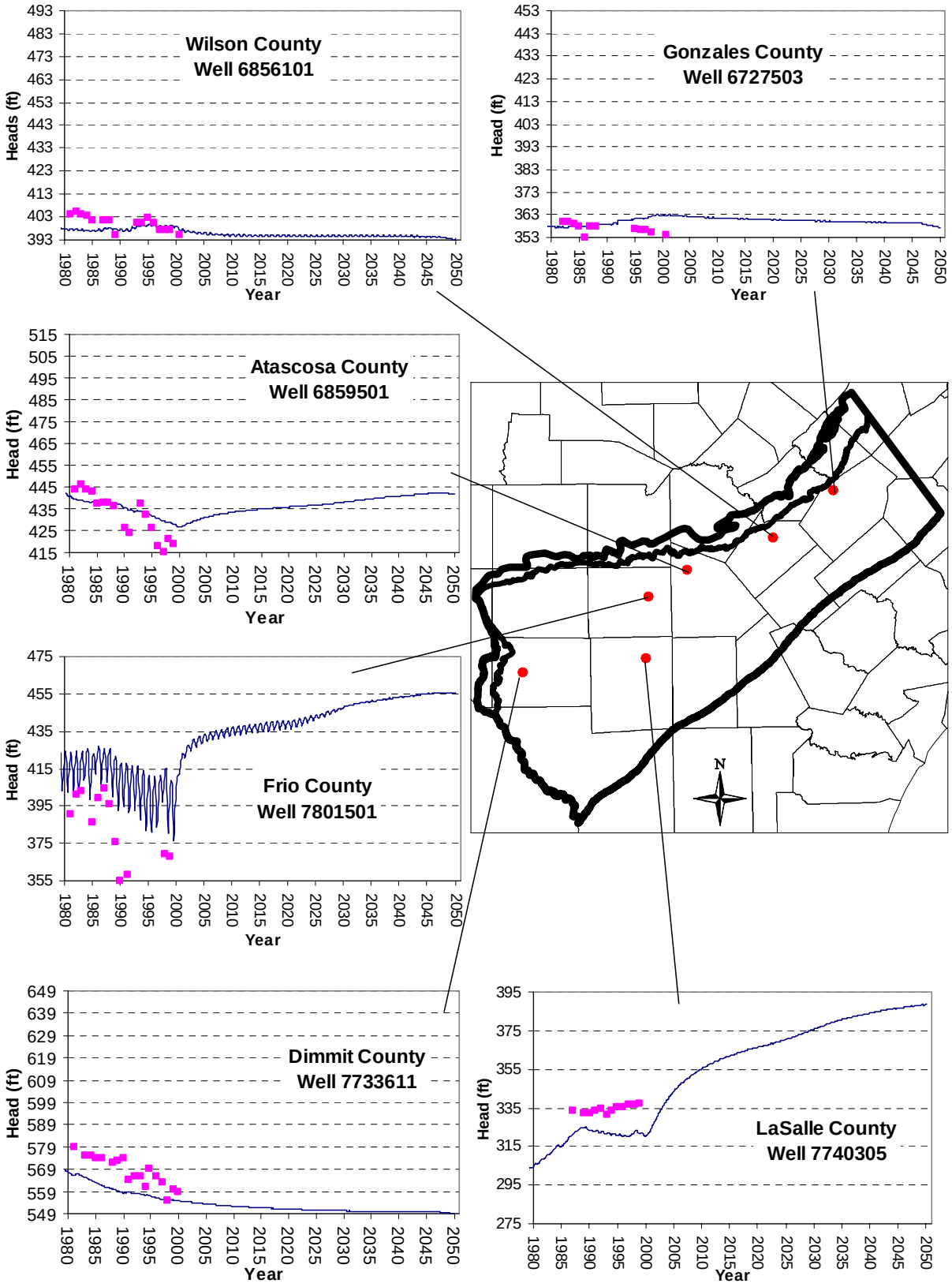

Figure 10.2.19 Selected hydrographs from predictive simulation to 2050 with the DOR.

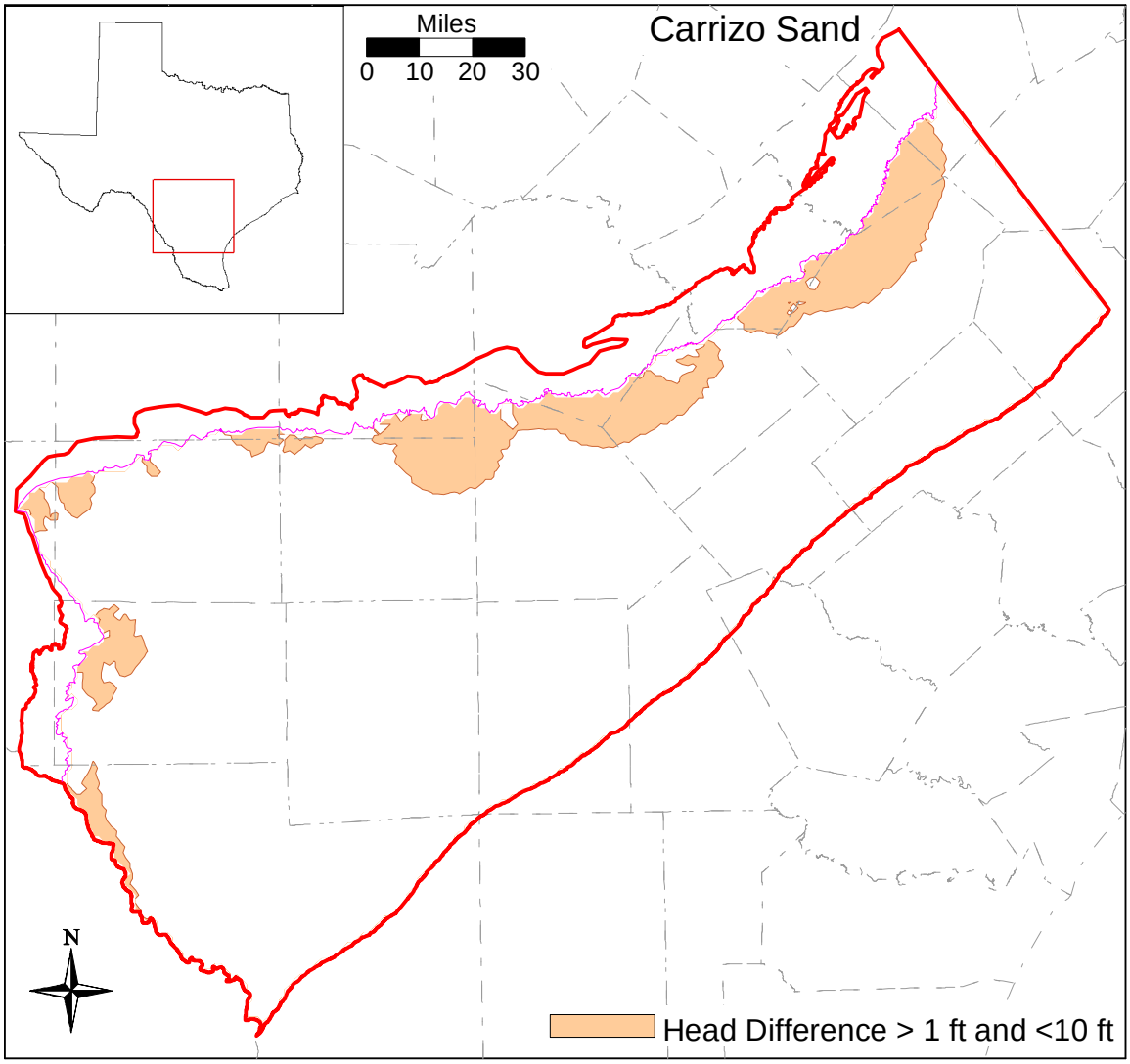

Figure 10.2.20 Simulated difference in head surfaces for the Carrizo between the average condition 2050 simulation and the drought of record 2050 simulation.

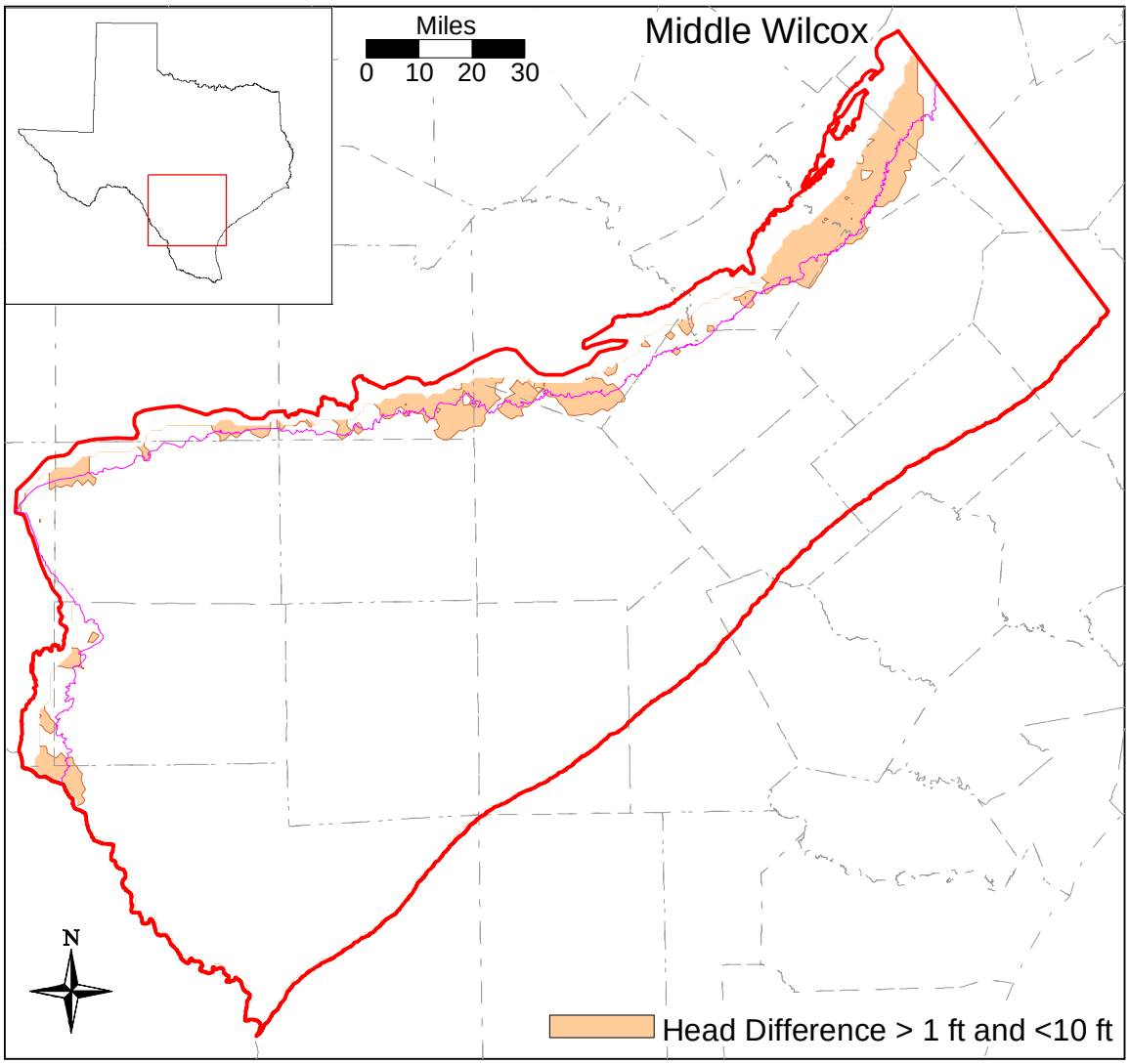

Figure 10.2.21 Simulated difference in head surfaces for the middle Wilcox between the average condition 2050 simulation and the drought of record 2050 simulation.

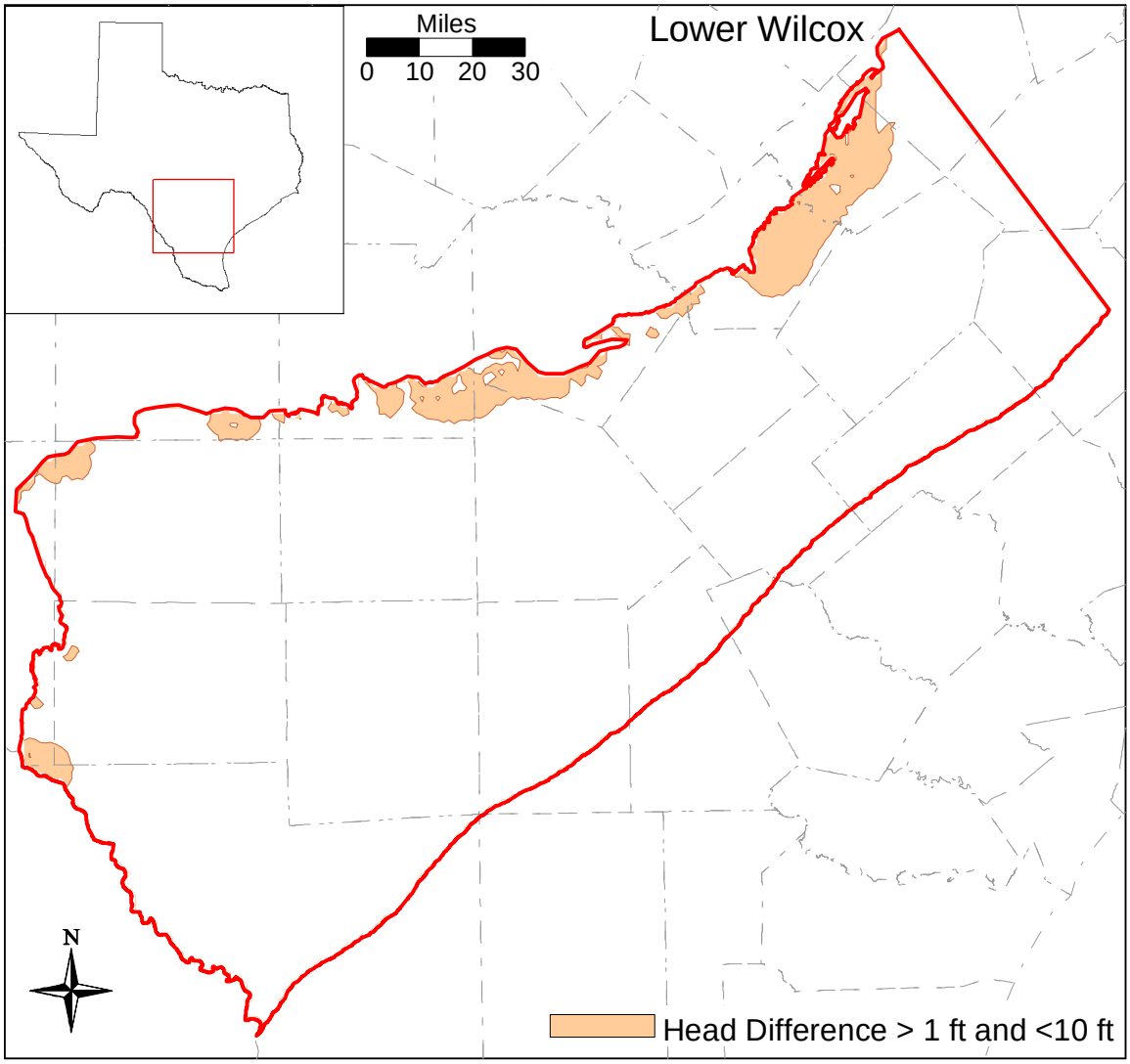

Figure 10.2.22 Simulated difference in head surfaces for the lower Wilcox between the average condition 2050 simulation and the drought of record 2050 simulation.

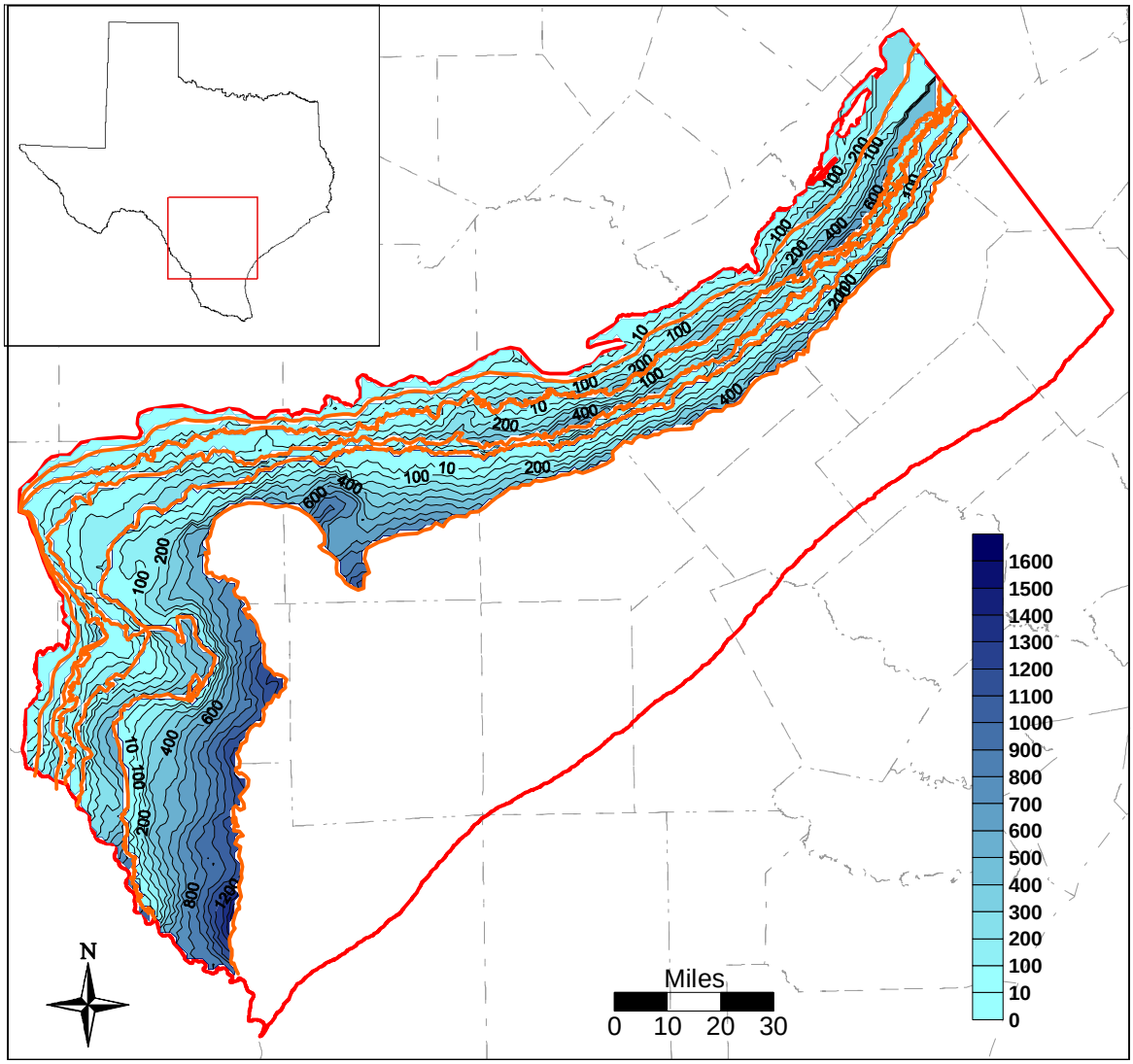

Figure 10.2.23 Simulated saturated thickness in the outcrop at year 2000.

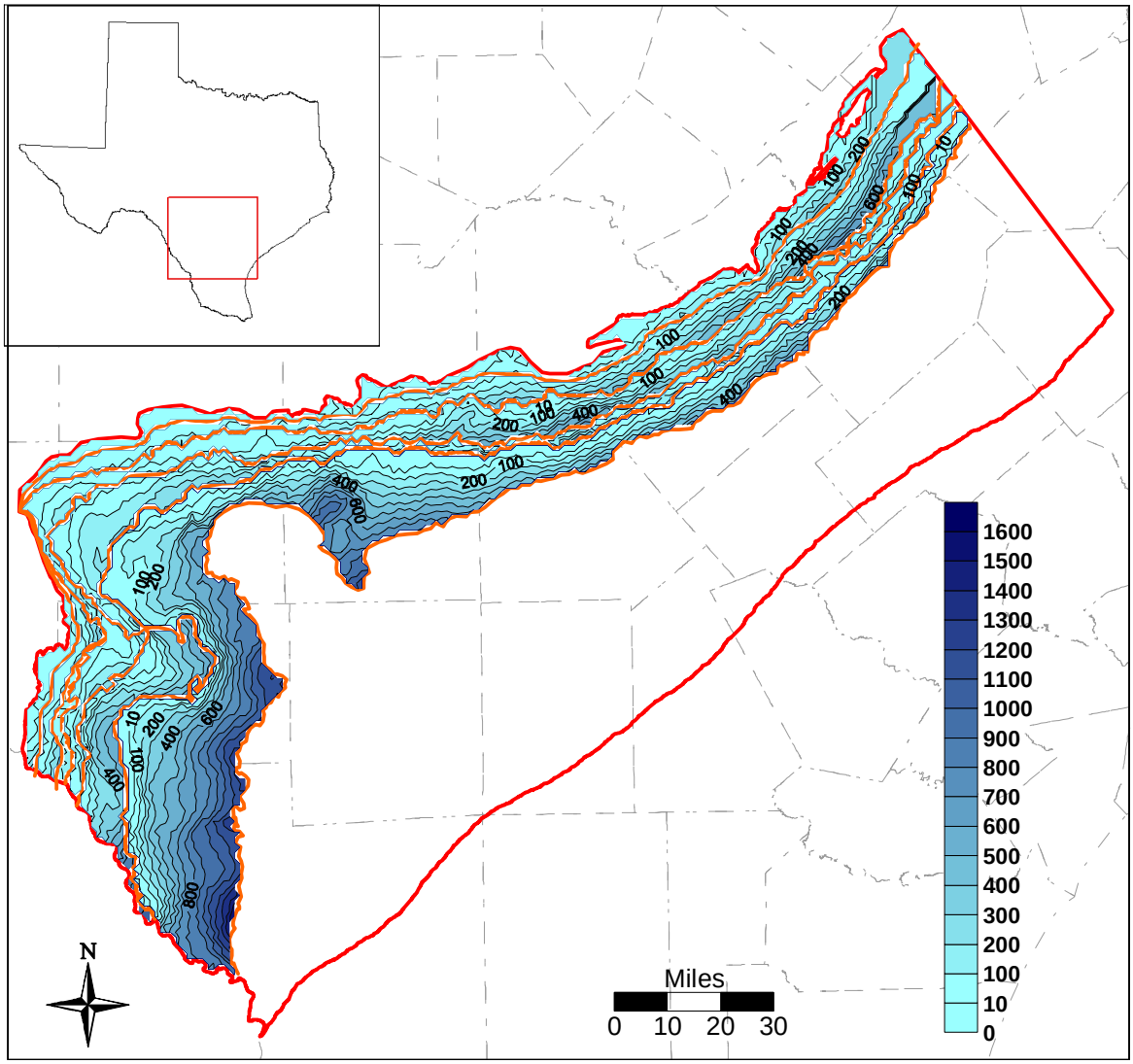

Figure 10.2.24 Simulated saturated thickness in the outcrop at year 2050.

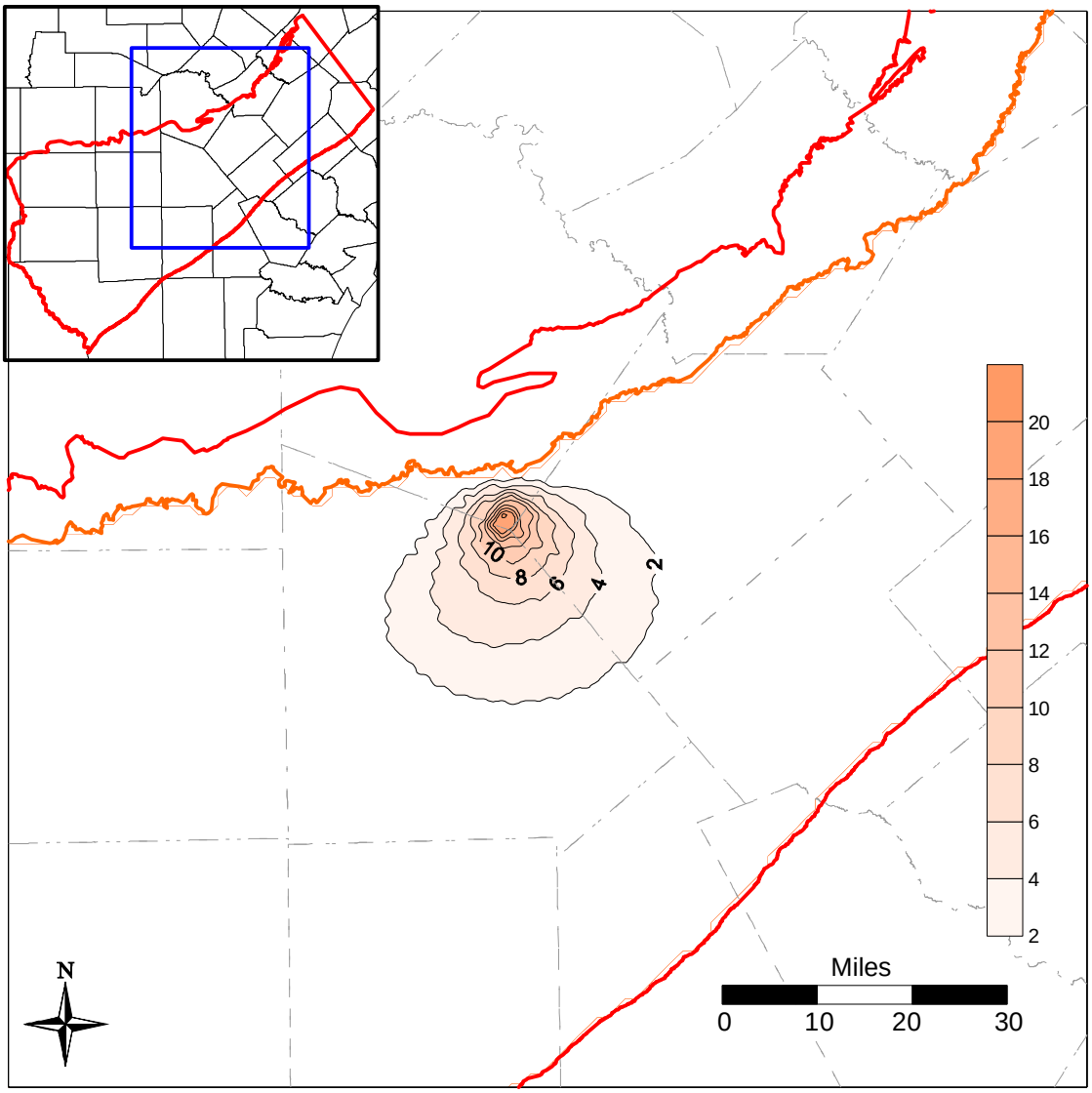

Figure 10.2.25 Difference between the 2010 base simulation and the 2010 simulation including the Twin Oaks Project in Bexar County.

10.3 Predictive Simulation Water Budget

Table 10.3.1 shows the water budget for the predictive simulations. The table shows the water budget for the final year of each of the predictive simulations. Because the simulations ended in February (defined by the drought of record), these balances are from February of the previous year to February of the given year. For example, the water budget for 2010 extends from February 2009 to February 2010. In general, the predictive simulation water budget shows similar trends to that of the calibration/verification simulations. However, a major difference in the predictive simulations is the decrease in pumping. Table 10.3.1 shows that the pumping decreases by 44% from 1990 to 2010. The pumping decreases further to 130,427 AFY in 2030 and is relatively stable for the remainder of the simulation. Most of the increase in heads seen in the predictive simulations, discussed in the previous section, can be attributed to this decrease in pumping. The most significant pumping decreases are in the Carrizo, where historically most of the pumping has occurred. As with the calibration/verification simulations, the amount of leakance from the streams varied significantly through the predictive period. In all years shown in the table, the streams are gaining more water than they are losing. As discussed in Section 9.2.3, this is likely due to the drought of record which has decreased the amount of flow in the streams to the point where the losing streams are not contributing as significantly to the aquifer. Note that in the 2050 run with average recharge (i.e., no DOR), the net gain of the streams is at least an order of magnitude less than in all of the drought years. Also, comparing the 2050 run with average recharge to the DOR years shows the difference between average and drought condition recharge, which in the case of the 2050 simulation is approximately 232,000 AFY, or more than half of the average recharge. Groundwater evapotranspiration is also higher in the 2050 DOR simulation than in the 2050 average condition simulation.

The Carrizo aquifer behaves similarly in the predictive runs, with most of the outflow from the aquifer due to pumping. However, as pumping decreases in the predictive simulations, less water is directed across the Reklaw Formation into the Carrizo. For example, in 1990, when pumping is 303,154 AFY, 50,412 AFY of water comes into the Carrizo from the Reklaw. In 2010, when pumping is 170,747 AFY, 29,817 AFY flows in through the top. So, as pumping decreases, the gradient across the Reklaw decreases, and by 2050 the inflow from the top seems stable at approximately 25,000 AFY.

Table 10.3.1 Water budget for predictive simulations, AFY.

Year	Layer	GHBs	Reservoirs	Wells	ET	Top	Bottom	Recharge	Streams	Storage
1990	**1**	21,575	0	-7,228	-31,897	0	-54,422	102,478	-97,276	64,941
	2	0	0	-13,989	-1,742	54,422	-50,412	21,747	-31,279	19,029
	3	0	0	-223,628	-20	50,412	-16,618	25,865	4,246	159,753
	4	0	0	-29,546	-10	16,618	7,338	5,676	-1,783	1,569
	5	0	4,925	-17,754	-4,210	-7,338	3,002	24,736	-24,670	21,288
	6	0	0	-11,009	-3,144	-3,002	0	17,914	-7,972	7,204
	Sum	21,575	4,925	-303,154	-41,023	111,112	-111,112	198,416	-158,734	273,785
2000	**1**	16,185	0	-7,884	-24,002	0	-60,693	116,840	-231,968	191,441
	2	0	0	-10,030	-3,339	60,693	-61,387	27,310	-237,867	224,480
	3	0	0	-200,091	-119	61,387	-8,705	36,551	-28,422	139,411
	4	0	0	-19,299	-36	8,705	9,778	4,192	-19,224	15,879
	5	0	2,255	-15,077	-2,193	-9,778	2,984	30,349	-57,843	49,289
	6	0	0	-11,671	-1,660	-2,984	0	20,006	-45,922	42,224
	Sum	16,185	2,255	-264,053	-31,348	118,023	-118,023	235,247	-621,245	662,723
2010	**1**	6,854	0	-6,885	-57,704	0	-39,843	89,581	-135,466	142,334
	2	0	0	-6,227	-4,241	39,843	-29,817	13,514	-111,055	96,531
	3	0	0	-104,592	-118	29,817	-6,119	15,994	-1,414	66,498
	4	0	0	-13,145	-745	6,119	6,370	531	-7,670	8,398
	5	0	3,104	-22,516	-2,607	-6,370	1,129	22,721	-33,354	37,871
	6	0	0	-17,382	-3,436	-1,129	0	10,460	-17,167	28,640
	Sum	6,854	3,104	-170,747	-68,851	68,280	-68,280	152,800	-306,126	380,271
2020	**1**	618	0	-6,382	-57,799	0	-38,111	90,806	-138,703	148,050
	2	0	0	-6,147	-4,317	38,111	-31,967	12,525	-111,428	101,777
	3	0	0	-110,559	-120	31,967	-2,125	15,954	-1,356	66,251
	4	0	0	-13,191	-861	2,125	8,968	474	-8,329	10,728
	5	0	2,992	-23,850	-2,631	-8,968	1,949	22,973	-33,488	41,000
	6	0	0	-17,871	-3,521	-1,949	0	10,388	-17,468	30,406
	Sum	618	2,992	-178,000	-69,250	61,287	-61,287	153,121	-310,772	398,212

Table 10.3.1 (continued)

Year	Layer	GHBs	Reservoirs	Wells	ET	Top	Bottom	Recharge	Streams	Storage
2030	**1**	-4,638	0	-5,525	-58,092	0	-33,062	92,518	-140,031	147,217
	2	0	0	-2,890	-4,261	33,062	-24,283	10,814	-111,355	97,469
	3	0	0	-84,017	-130	24,283	1,452	16,110	-1,353	43,667
	4	0	0	-9,342	-862	-1,452	9,663	318	-8,637	10,224
	5	0	2,874	-14,650	-2,411	-9,663	1,942	23,009	-34,422	33,299
	6	0	0	-14,004	-3,616	-1,942	0	10,492	-17,923	26,980
	Sum	-4,638	2,874	-130,427	-69,372	44,289	-44,289	153,260	-313,722	358,856
2040	**1**	-9,713	0	-5,394	-58,564	0	-30,820	92,519	-142,424	152,682
	2	0	0	-2,964	-4,308	30,820	-21,910	10,813	-111,353	97,458
	3	0	0	-85,455	-153	21,910	3,578	16,111	-1,413	45,460
	4	0	0	-9,002	-862	-3,578	11,019	398	-8,796	10,706
	5	0	2,763	-15,250	-2,603	-11,019	2,577	23,336	-34,925	35,101
	6	0	0	-14,005	-3,981	-2,577	0	10,156	-18,270	28,662
	Sum	-9,713	2,763	-132,070	-70,471	35,556	-35,556	153,333	-317,180	370,069
2050	**1**	-11,981	0	-5,344	-59,587	0	-32,606	92,542	-144,405	160,299
	2	0	0	-4,386	-4,267	32,606	-24,137	10,791	-111,439	99,389
	3	0	0	-93,093	-175	24,137	5,275	16,265	-1,377	49,083
	4	0	0	-9,089	-862	-5,275	11,985	461	-8,891	11,479
	5	0	2,667	-15,596	-2,838	-11,985	3,154	23,117	-35,340	36,800
	6	0	0	-13,335	-4,314	-3,154	0	11,671	-18,670	27,786
	Sum	-11,981	2,667	-140,843	-72,042	36,330	-36,330	154,848	-320,122	384,836
2050*	**1**	-12,348	0	-5,344	-32,694	0	-33,043	164,603	-27,664	-53,501
	2	0	0	-4,386	-2,448	33,043	-25,186	41,870	17,274	-60,173
	3	0	0	-93,094	-408	25,186	3,985	73,466	7,881	-16,919
	4	0	0	-9,089	-429	-3,985	11,597	4,927	230	-3,323
	5	0	2,367	-15,596	-2,743	-11,597	2,412	61,866	-18,258	-18,456
	6	0	0	-13,383	-3,635	-2,412	0	40,471	-1,114	-19,924
	Sum	-12,348	2,367	-140,893	-42,357	40,235	-40,235	387,203	-21,651	-172,295

* Does not include DOR.

11.0 LIMITATIONS OF THE MODEL

A model can be defined as a representation of reality that attempts to explain the behavior of some aspect of it, but is always less complex that the real system it represents (Domenico, 1972). As a result, limitations are intrinsic to models. Model limitations can be grouped into several categories including: (1) limitations in the data supporting a model, (2) limitations in the implementation of a model which may include assumptions inherent to the model application, and (3) limitations regarding model applicability. The limitations of this modeling study are discussed in the following consistent with the grouping provided above.

11.1 Limitations of Supporting Data

Developing the supporting database for a regional model at this scale and with this large a number of grid cells is a challenge. An adequate database was available from published sources for estimation of the structural surfaces for the Carrizo-Wilcox aquifer at the scale of the model. Because the model is at a regional scale, structural data will not have every bend and discontinuity found at a local scale. However, we did find that the regional projection of our structure through a smaller scale structural data set made available by the Gonzales Underground Water Conservation District showed very good agreement even at the local scale.

Our discussion will now focus on the parameters which were found to be important in the sensitivity analyses and the quality of the targets used to assess calibration and verification. For the steady-state model, the primary parameters controlling model behavior are recharge and vertical conductivity. For the transient model, the primary parameters controlling model behavior are pumping and the horizontal hydraulic conductivity. Recharge in the Carrizo-Wilcox aquifer has been studied by many and Scanlon et al. (2002) provide a good summary of the available recharge estimates in the study area. Estimates of recharge for the Carrizo-Wilcox vary from less than an inch per year to up to five inches per year. The Southern Carrizo-Wilcox GAM steady-state model provides a good means for estimating viable recharge estimates for the aquifer. However, because of the correlation between recharge and vertical conductance of the formations, recharge cannot be uniquely determined. The vertical conductance of the modeled aquifers can only be estimated regionally by models such as this GAM. The conundrum is that in the steady-state model, the vertical conductance of the aquifers is inversely related to recharge

which means that unique determination of these two parameters is not possible. To take advantage of this, we estimated recharge with a forward model (SWAT), and considered the recharge to be fixed, for the most part, during calibration. Estimates of recharge are important to the GAM modeling process because they provide a means of constraining the vertical conductance terms in the model especially when calibrating to steady-state and transient conditions. Recharge studies should be continued in the Carrizo-Wilcox aquifer.

For the transient model, the most important parameter through the calibration process was the vertical conductivity of the Carrizo-Wilcox aquifer and the Reklaw/Bigford formations. At the end of calibration, the sensitivity analysis showed that the most important parameters at the final calibration state were pumping and the horizontal hydraulic conductivity. The pumping estimates were derived through a detailed process (see Appendices B and C), however they must be considered uncertain. Because the southern Carrizo-Wilcox aquifer is most heavily developed in the confined portion of the aquifer, errors in pumping rates make a significant impact on simulated water levels. Not unlike the situation with recharge and vertical conductance in the steady-state model, horizontal hydraulic conductivity and pumping are correlated parameters and unique determination of them is not possible. We were reticent to adjust the horizontal conductivities and could not find good evidence for adjusting/moving pumping.

Pumping estimates in the Wintergarden area should be revisited relative to the results of this model and the LBG-Guyton and HDR (1998) model. Likewise, applicability of aquifer test data to estimate regional effective hydraulic conductivity in the Wintergarden area should be further investigated. At this time, we do not know if our lack of model performance in the Wintergarden area is a result of pumping or horizontal hydraulic conductivity. This issue must be addressed to improve model predictions in that local area of the model.

The model also lacks horizontal hydraulic conductivity data for the Queen City/El Pico and the Wilcox Group. This is especially true in the downdip confined portions of the aquifer where there is a total lack of data. Hydraulic conductivity data for the Carrizo is also lacking in the deeper portions of the aquifer. The model was not strongly sensitive to the Wilcox hydraulic conductivity but this is probably because of a general lack of Wilcox head targets. With improved control on hydraulic conductivity data in the confined portions of the aquifer, estimates

of vertical conductance in the aquifer system would be better constrained. Carrizo hydraulic conductivity data would be of great benefit in the area of the model north of Laredo where development of the Carrizo-Wilcox is being considered. There is little hydraulic conductivity data available to support predictions in that area of the model.

The primary type of calibration target is hydraulic head. There is a general lack of heads representative of the predevelopment for all model layers. However, we believe the steady-state model is important to the constraint of the model calibration and accept the uncertainty in predevelopment conditions. Head calibration targets for the transient (historical model) are also lacking in the Wilcox and in the eastern Carrizo for the confined portions of the model. The model calibration could be improved by an increased density of head targets in these areas. Many of the groundwater conservation districts have implemented or are in the process of implementing monitoring programs. This effort should be continued and supported.

The other type of calibration target used was stream gain/loss estimates. There are limited stream gain/loss estimates in the model area. There were also a limited number of stream gages in the outcrop that were amenable to estimation of losses or gains through the study region. Because the MODFLOW stream routing package does not model runoff, direct comparison to stream gages is problematic. It would be beneficial if publicly available surface water models were developed for the outcrop regions in the study area. These would provide better estimates of the hydrography of the area and could be coupled with MODFLOW.

11.2 Limiting Assumptions

There are several assumptions that are key to the model regarding construction, calibration, and prediction. These are briefly discussed below with a discussion of the potential limitations of the assumption.

We modeled the lower boundary of the model as a no-flow boundary at the base of the Wilcox Group. This assumption is consistent with other regional models in the area and is probably a good assumption for the model in the overall sense. However, as the model moves to the outcrop, the no-flow nature of the base of the lower Wilcox creates some problems with recharge rates where the lower Wilcox is thin. This is not considered a significant limitation to the model since it causes only limited-area edge effects.

The lateral model boundaries were also modeled as no-flow boundaries. The western model boundary is the Rio Grande and probably does not limit the models performance in the west. The east boundary is in a region where significant pumping could occur in the future. We used a no-flow boundary because we assumed that the boundary provided a conservative reflective boundary as long as pumping east of the boundary was equal to or less than pumping west of the boundary. We reviewed the Central Carrizo-Wilcox GAM transient heads and concluded that drawdowns were not significant enough (less than 30 feet) to use a transient boundary condition for the historical period.

Another assumption used in our model is that the recharge estimated from SWAT was applicable to the region. As discussed earlier, we made few modifications to the SWAT output. We believe that the model provided defensible regional estimates of recharge in the model region using physical models and parameters representative of the area. We did not model the interflow zone in SWAT. We used MODFLOW to reject recharge to the stream networks. We consider this approach successful in this region because rejected recharge is less important to the model region as a whole than it would be in the eastern part of Texas.

In the predictive simulations, we assumed (in accordance with TWDB's GAM requirements) that the pumping estimates available from the Regional Water Planning Group database tables were representative of the future demands. This resulted in a 100,000 AFY decrease in pumping at the juncture between 1999 and 2000, prompting a significant head recovery in the Wintergarden area. The State Water Plan (TWDB, 2002) estimates that Region L, which is not entirely coincident with our model area, will meet 25 percent of their water needs in 2050 with new groundwater (approximately 200,000 AFY). This is in addition to 157,000 AFY from existing groundwater in 2050. The region is looking to the Carrizo-Wilcox aquifer as a source for water (strategies CZ-10C and CZ-10D). The current predictive simulations do not appear to bracket a worst case scenario of demand for the region. However, this does not limit the models applicability.

Finally, predictive pumping demand estimates provided by the RWPGs are based upon DOR conditions. As a result, pumping does not increase at the end of each predictive simulation when the DOR occurs. It is expected that we would see greater water level declines in the

aquifer system as a whole if the pumping and climate (recharge) were impacted as a result of the DOR.

11.3 Limits for Model Applicability

The model was developed on a regional scale and is only capable of predicting aquifer conditions at the regional scale. The model is applicable for assessing regional aquifer conditions resulting from groundwater development over a fifty-year time period.

The model itself was developed at a grid-scale of one square mile. The model is not capable of being used in its current state to predict aquifer responses at specific points such as a particular well at a particular municipality. The aquifer is accurate at the scale of tens of miles which is adequate for understanding groundwater availability at the scale of the southern Carrizo-Wilcox aquifer.

The model is ideal for refinement for more local scale issues related to specific water resource questions. Questions regarding local drawdown to a well should be based upon analytical solutions to the diffusion equation or a refined numerical model. The GAM produces water levels representative of large volumes of aquifer (e.g., 5,280 ft X 5,280 ft X aquifer thickness in feet). The model was built to determine how regional water levels will respond to water resource development in an area smaller than a county and larger than a square mile.

The GAM model provides a first-order approach to coupling surface water to groundwater which is adequate for the GAM model purposes and for the scale of application. However, this model does not provide a rigorous solution to surface water modeling in the region and should not be used as a surface water modeling tool in isolation.

The GAM model as developed does not simulate the transport of solute (water quality). As a result, the model cannot be used in its current form to explicitly address water-quality issues. The study and model did not delineate specific regions within the Carrizo-Wilcox aquifer having poorer water quality and thus potentially not being suitable as a groundwater resource. The study only documents a limited assessment of water quality in the study area.

12.0 FUTURE IMPROVEMENTS

To use models to predict future conditions requires a commitment to improve the model as new data becomes available or when modeling assumptions or implementation issues change. This GAM model is no different. Through the modeling process one generally learns what can be done to improve the model's performance or what data would help better constrain the model calibration. Future improvements to the model will be discussed below.

12.1 Supporting Data

Several types of data could be collected to better support the GAM model development process. These include recharge studies, surface water-groundwater studies and basic addition of stream gages, and water level monitoring in the confined portion of the Carrizo-Wilcox aquifer.

Estimates of recharge are important to the GAM modeling process because they provide a means of constraining the vertical hydraulic conductivity of the aquifer system when calibrating to steady-state and transient conditions. Studies should be continued into the nature of recharge in the Carrizo-Wilcox aquifer.

Characterization of surface water groundwater interaction requires a good coverage of stream gages in the model outcrop areas, preferably immediately upstream and downstream of the outcrop areas. The model predicts that stream-aquifer interaction is significant in the model region. It would be beneficial if publicly available surface water models were developed for the outcrop regions in the study area. These would provide better estimates of the hydrography of the area and could be coupled with MODFLOW in future model improvement.

Additional water-level monitoring in the Wilcox Group and downdip portions of the Carrizo Formation is also important for future model development. Nearly all available Wilcox water-level measurements are from the outcrop regions of the aquifer. Although the Wilcox may be non-potable in portions of the confined section, it is still advantageous to monitor these deep areas to improve aquifer understanding and to implement those improvements into the model. It is also important to increase water-level monitoring in areas that are potential areas of future development but which are currently not greatly developed. Two regions that fit this description in the model area are northern Webb County and the Gonzales, Wilson, and southern Bexar County area. These areas have not been heavily produced in the past. If monitoring begins prior

to increased development, the GAM can be calibrated against the aquifer response to improve model predictive capability in those regions.

Currently, horizontal hydraulic conductivity data are lacking for the Queen City/El Pico and the Wilcox Group in the model area. This is especially true in the downdip confined portions of the aquifer where there is a total lack of data. Hydraulic conductivity data for the Carrizo is also lacking in the deeper, more confined portions of the aquifer. Any additional hydraulic conductivity estimates and storativity estimates from pump tests will further help parameterize future improvements to this model.

12.2 Future Model Improvements

Pumping estimates in the Wintergarden area should be revisited relative to the results of this model and the LBG-Guyton and HDR (1998) model. Likewise, applicability of aquifer test data to estimate regional effective hydraulic conductivity in the Wintergarden area should be further investigated. The model exhibits a poorer fit in the largest drawdown cones in the Wintergarden area. At this time, we do not know if this is the result of errors in historical pumping or horizontal hydraulic conductivity, or both. This issue should be addressed in future model improvements.

The lateral model boundaries were modeled as no-flow boundaries. The east boundary is in a region where significant pumping could occur in the future. We used a no-flow boundary because we assumed that the boundary provided a conservative reflective boundary as long as pumping east of the boundary was equal to or less than pumping west of the boundary. The applicability of the eastern boundary should be reviewed with the finalization of the Central and Southern Carrizo-Wilcox GAMs. If the boundary condition should be transiently applied as a head-dependent flow boundary, these changes can be made when the Queen City-Sparta aquifers are added to the model.

The current predictive simulations, although based upon pumping in the Regional Water Planning Group tables, do not appear to bracket a worst case scenario of demand for the region. An upper–end estimate of pumping should be developed in cooperation with the TWDB and the RWPGs and run with the Southern Carrizo-Wilcox GAM model.

13.0 CONCLUSIONS

This report documents a three-dimensional groundwater model developed for the southern Carrizo-Wilcox aquifer to the GAM standards defined by the TWDB. This regional-scale model was developed using MODFLOW with the stream-routing package to simulate stream-aquifer interaction and the reservoir package to model groundwater interaction with lakes and reservoirs. The model divides the Carrizo-Wilcox aquifer into four layers: the Carrizo, and the upper, middle, and lower Wilcox. The Reklaw/Bigford formations and the Queen City/El Pico formations are also modeled as individual model layers.

The purpose of this GAM is to provide predictions of groundwater availability through the year 2050 based on current projections of groundwater demands during drought-of-record conditions. This GAM provides an integrated tool for the assessment of water management strategies to directly benefit state planners, Regional Water Planning Groups (RWPGs), and Groundwater Conservation Districts (GCDs).

This GAM has been developed using a modeling protocol which is standard to the groundwater model industry. This protocol includes: (1) the development of a conceptual model for groundwater flow in the aquifer, (2) model design, (3) model calibration, (4) model verification, (5) sensitivity analysis, (6) model prediction, and (7) reporting.

The model has been calibrated to predevelopment conditions (prior to significant resource use) which are considered to be at steady state. The steady-state model reproduces the predevelopment aquifer heads well and within the uncertainty in the head estimates. The median recharge rate estimated for the steady-state model was 0.51 inches per year. In the pre-development model, recharge accounted for approximately 87% of the aquifer inflow and streams and ET discharged approximately 43% and 30% of aquifer flow, respectively. Approximately 27% of the aquifer inflowing water passed from the outcrop through to the confined aquifer and exited vertically through the GHBs attached to the confined portion of the Queen City/El Pico. A sensitivity analysis was performed to determine which parameters had the most influence on aquifer performance and calibration. The two most sensitive parameters for the steady-state model were recharge and vertical hydraulic conductivity of all units younger (overlying) the Carrizo.

The model was also satisfactorily calibrated to transient aquifer conditions from 1980 through December 1989. The model did a good job of reproducing aquifer heads and available estimates of aquifer-stream interaction. The transient-calibrated model was verified by simulating to aquifer conditions from 1990 through December 1999. Again, the model satisfactorily simulated observed conditions. However, the model did have problems matching the very low heads in the Wintergarden area which has experienced extreme water level declines. This issue is considered to be either the result of lower hydraulic conductivities in the area than are measured or the result of an inadequate accounting of pumping in the area. Regionally, the model reproduces model heads to within head target errors. A sensitivity analysis was performed on the transient model. The two most sensitive parameters for the transient model were pumping and the Carrizo horizontal hydraulic conductivity.

Model predictions were performed to estimate aquifer conditions for the next 50 years based upon projected pumping demands under DOR conditions as developed by the Regional Water Planning Groups. The pumping demand estimates developed from the regional water plans predicted a significant decline in Carrizo-Wilcox pumping starting in 2000. This decline is approximately 100,000 AFY. As a result of the significant pumping declines predicted, the Carrizo-Wilcox rebounds significantly in the western model region where groundwater pumping was predicted to decrease. The eastern portion of the model showed a slight gradual water level decline as pumping demand generally increased in that part of the model. Pumping associated with potential future Laredo development (14,000 AFY) of the Carrizo-Wilcox in northern Webb County created a significant local drawdown of over 100 feet by 2050.

This model, like all models, has limitations and can be improved. However, this calibrated GAM provides a documented, publicly-available tool for the assessment of future groundwater availability in the southern Carrizo-Wilcox region. The GAM is capable of reproducing the natural (predevelopment) and historical conditions of the aquifer measured by multiple calibration measures.

14.0 ACKNOWLEDGEMENTS

The Southern Carrizo-Wilcox GAM was developed with the participation of a committed group of stakeholders representing varied interests within the model region. Interaction with these stakeholders was performed through a series of Stakeholder Advisory Forums (SAF) held across the model region. In these meetings, stakeholders were solicited for data and were provided updates on a regular basis. The model described in this report has benefited from the stakeholders involvement and interest. In addition, we would like to specifically thank those members of the SAF who have hosted meetings across the model region, including: Barry Miller at the Gonzales Underground Water Conservation District, Steve Raabe and Ronnie Hernandez at the San Antonio River Authority, Mike Mahoney at the Evergreen Underground Water Conservation District, and Ed Walker at the Wintergarden Underground Water Conservation District.

We would also like to thank the TWDB GAM staff led by Robert Mace for their support during this modeling exercise. We would like to thank Ted Angle who has managed our contract with professionalism. We would also like to thank Grant Snyder of URS Corporation and Bill Klemt of LBG-Guyton and Associates for providing aquifer test results and data in the study region. We would also like to thank Rick Hay from Texas A&M Corpus for his help in understanding previous modeling studies in the area.

We would like to thank our senior technical reviewers for this project; Dr. Steve Gorelick (Stanford University) and Dr. Graham Fogg (University of California, Davis). The model was greatly improved by their recommendations. We would also like to thank Jeannie Gibbs of INTERA for her efforts in compiling and organizing the tremendous amount of data collected for this study and her GIS support. Finally, we would like to thank Judy Ratto of INTERA for her efforts above and beyond the call of duty in developing this report.

15.0 REFERENCES

Alexander, W.H., Jr., B.N. Myers, and O.C. Dale, 1964. Reconnaissance investigation of the ground-water resources of the Guadalupe, San Antonio, and Nueces River Basins, Texas. Texas Water Commission, Bulletin 6409.

Alexander, W.H., and White, D.E., 1966. Ground-water resources of Atascosa and Frio Counties, Texas: Texas Water Development Board Report 32, 99 p.

Anders, R.B., 1960. Ground-water geology of Karnes County, Texas. Texas Board of Water Engineers, Bulletin 6007.

Anders, R.B., and E.T. Baker, Jr., 1961. Ground-Water Geology of Live Oak County, Texas. Texas Board of Water Engineers, Bulletin 6105.

Anders, R.B., 1967. Ground-water resources of Sabine and San Augustine Counties, Texas: Texas Water Development Board Report 37, 115 p.

Ashworth J.B., and J. Hopkins, 1995. Aquifers of Texas. Texas Water Development Board, Report 345.

Anderson. M.P., and W.W. Woessner, 1992. *Applied Groundwater Modeling*. Academic Press, San Diego, CA, 381 p.

Ayers, W.B., Jr., and A.H. Lewis, 1985. The Wilcox Group and Carrizo Sand (Paleogene) in East-Central Texas: Depositional Systems and Deep-Basin Lignite: The University of Texas at Austin, Bureau of Economic Geology Special Publication, 19p., 30 pls.

Bebout, D.G., B.R. Weise, A.R. Gregory, and M.B. Edwards, 1982. Wilcox Sandstone reservoirs in the deep subsurface along the Texas Gulf Coast; their potential for production of geopressured geothermal energy: : The University of Texas at Austin, Bureau of Economic Geology Report of Investigations No. 117, 125 p.

Borrelli, J., C.B Fedler, and J.M. Gregory, 1998. Mean Crop Consumptive Use and Free-Water Evaporation for Texas. Report for TWDB Grant 95-483-137. Feb. 1, 1998.

Broom, M.E., 1968. Ground-water resources of Wood County, Texas: Texas Water Development Board Report 79, 84 p.

Broom, M.E., and B.N. Myers, 1966. Ground-water resources of Harrison County, Texas: Texas Water Development Board Report, 27, 73 p.

Broom, M.E., W.H. Alexander, Jr., and B.N. Myers, 1965. Ground-water resources of Camp, Franklin, Morris, and Titus Counties, Texas: Texas Water Development Board Bulletin 6517, 153 p.

Brune, G., 1975. Springs of Texas, Volume I. Branch-Smith, Inc., Texas.

Bureau of Economic Geology, 1996. River Basin Map of Texas. Bureau of Economic Geology , The University of Texas at Austin.

Chiang, W.-H., and W. Kinzelbach, 1998. Processing Modflow- A simulation system for modeling groundwater flow and pollution: software manual, 325 p.

de Marsily, G., 1986. Quantitative Hydrogeology, Groundwater Hydrology for Engineers. Academic Press, Orlando, FL, p. 440.

Domenico, P.A., 1972. Concepts and Models in Groundwater Hydrology, McGraw Hill, New York, 405 pp.

Domenico, P. A., and Schwartz, F. W., 1990. Physical and chemical hydrology: John Wiley & Sons, New York, 824 p.

Duffin, G.L., and G.R. Elder, 1979. Variations in specific yield in the outcrop of the Carrizo Sand in South Texas as estimated by seismic refraction. Texas Department of Water Resources, Report 229.

Dutton A.R., 1999. Groundwater availability in the Carrizo-Wilcox aquifer in Central Texas – numerical simulations of 2000 through 2050 withdrawal projections. The University of Texas at Austin, Bureau of Economic Geology, Report of Investigations No. 256.

Edwards, D.C., and T.B. McKee, 1997. Characteristics of 20th Century drought in the United States at multiple time scales. Climatology Report Number 97-2, Colorado State University, Fort Collins, Colorado.

Fenske, J.P., S.A. Leake, and D.E. Prudic, 1996. Documentation of a computer program (RESI) to simulate leakage from reservoirs using the modular finite-difference ground-water flow model (MODFLOW). U.S. Geological Survey, Open-File Report 96-364.

Fisher W.L., and J.H. McGowen, 1967. Depositional systems in the Wilcox Group of Texas and their relationship to occurrence of oil and gas. Transactions-Gulf Coast Association of Geological Societies, Vol. XVII.

Fogg, G.E., 1989. Stochastic analysis of aquifer interconnectedness: Wilcox Group, Trawick area, East Texas: The University of Texas at Austin, Bureau of Economic Geology, Report of Investigations No. 189, 68 p.

Fogg, G.E., 1986. Groundwater flow and sand-body interconnectedness in a thick, multiple-aquifer system: Water Resources Research, v. 22, no. 5, p. 679-694.

Fogg, G.E., and W.R. Kaiser, 1986. Regional hydrogeologic considerations for deep-basin lignite development in Texas, in Kaiser, W. R., and others, Geology and ground-water hydrology of deep-basin lignite in the Wilcox Group of East Texas: The University of Texas at Austin, Bureau of Economic Geology Special Publication, p. 57-59.

Fogg, G.E., and C.W. Kreitler, 1982. Ground-water hydraulics and hydrochemical facies in Eocene aquifers of the East Texas Basin: The University of Texas at Austin, Bureau of Economic Geology Report of Investigations No. 127, 75 p.

Fogg, G.E., S.J. Seni, and C.W. Kreitler, 1983. Three-dimensional ground-water modeling in depositional systems, Wilcox Group, Oakwood salt dome area, east Texas. The University of Texas at Austin, Bureau of Economic Geology Report of Investigations No. 133, 55 p.

Follett, C.R., 1966. Ground-Water Resources of Caldwell County, Texas. Texas Water Development Board, Report 12.

Follett, C.R., 1970. Ground-Water Resources of Bastrop County, Texas. Texas Water Development Board, Report 109.

Freeze, R.A., 1969. The mechanism of natural ground-water recharge and discharge. 1. One-dimensional, vertical, unsteady, unsaturated flow above a recharging or discharging ground-water flow system: Water Resources Research, Vol. 5, No. 1, p. 153-171.

Freeze, R.A., 1971. Three-dimensional, transient, saturated-unsaturated flow in a groundwater basin: Water Resources Research, Vol. 7, No. 2, p. 347-366.

Freeze, R.A., 1975. A stochastic-conceptual analysis of one-dimensional ground-water flow in nonuniform homogeneous media: Water resources Research, Vol. 11, No. 5, p. 679-694.

Freeze, R.A., and J.A. Cherry, 1979. Groundwater: Prentice-Hall, Inc., New Jersey, 604 p.

Galloway, W.E., X. Liu, D. Travis-Neuberger, and L. Xue, 1994. References high-resolution correlation cross sections, paleogene section, Texas Coastal Plain. The University of Texas at Austin, Bureau of Economic Geology.

Gelhar, L.W., and C.L. Axness, 1983. Three-dimensional stochastic analysis of macrodispersion in aquifers: Water Resources Research, v. 19, no. 1, p. 161-180.

Grubb, H.F., 1997. Summary of hydrology of the regional aquifer systems, Gulf Coastal Plain, south-central United States. U.S. Geological Survey, Professional Paper 1416-A.

Gutjahr, A.L., L.W. Gelhar, A.A. Bakr, and J.R. MacMillan, 1978. Stochastic analysis of spatial variability in subsurface flows-2, Evaluation and application. Water Resources Research, v. 14, no. 5, p. 953-959.

Hamlin, H.S., 1988. Depositional and ground-water flow systems of the Carrizo-Upper Wilcox, South Texas. The University of Texas at Austin, Bureau of Economic Geology, Report of Investigations No. 175.

Harbaugh, A.W., and M.G. McDonald, 1996. User's documentation for MODFLOW-96, an update to the U.S. Geological Survey modular finite-difference ground-water flow model: U.S. Geological Survey Open-File Report 96-485, 56 p.

Harden and Associates, Inc., 2000. Brazos G Regional Water Planning Area, Carrizo-Wilcox ground water flow model and simulations results.

Harris, H.B., 1965. Ground-Water Resources of La Salle and McMullen counties, Texas. Texas Water Commission, Bulletin 6520.

Hayes, M., 2001. Drought Indices. National Drought Mitigation Center, Available online at http://enso.unl.edu/ndmc/enigma/indices.htm.

HDR Engineering, Inc., 2000. Preliminary feasibility options to deliver ALCOA/CPS groundwater to Bexar County: technical report prepared for San Antonio Water Systems, variously paginated.

Helm, D.C., 1976. One-dimensional simulation of aquifer system compaction near Pixley, California-2, Stress-dependent parameters, Water Resources Research, Vol. 12, No. 3, p. 375-391.

Henry, C.D., J.M. Basciano, and T.W. Duex, 1980. Hydrology and water quality of the Eocene Wilcox Group; significance for lignite development in East Texas: The University of Texas at Austin, Bureau of Economic Geology Geological Circular 80-3,9p.

Hibbs, B.J., and J.M. Sharp, Jr., 1991. Evaluation of underflow and the potential for instream flow depletion of the lower Colorado River by high capacity wells in adjoining alluvial systems : final report for the Lower Colorado River Authority, Water Resources Division, 126p.

Isaaks, E.H., and R.M. Srivastava, 1989. An Introduction to Applied Geostatistics. Oxford UniversityPress, New York.

Kaiser, W.R., 1990. The Wilcox Group (Paleocene-Eocene) in the Sabine Uplift area, Texas: Depositional systems and deep-basin lignite: The University of Texas at Austin, Bureau of Economic Geology Special Publication, 20p.

Kaiser, W.R., M.L. Ambrose, W.B. Ayers, Jr., P.E. Blanchard, G.F. Collins, G.E. Fogg, D.L. Gower, C.L. Ho, C.S. Holland, M.L. W. Jackson, C.M. Jones, A.H., Lewis, G.L. Macpherson, C.A. Mahan, A.H. Mullin, D.A. Prouty, S.J. Tewalt, and S.W. Tweedy, 1986. Geology and ground-water hydrology of deep-basin lignite in the Wilcox Group of East Texas: The University of Texas at Austin, Bureau of Economic Geology Special Publication, 182 p.

Kaiser, W.R., 1974. Texas lignite: near-surface and deep-basin resources: The University of Texas at Austin, Bureau of Economic Geology Report of Investigations No. 79, 70 p.

Kaiser, W.R., 1978. Depositional systems in the Wilcox Group (Eocene) of east-central Texas and the occurrence of lignite, *in* Kaiser, W.R., ed., Proceedings, 1976 Gulf Coast Lignite Conference: geology, utilization, and environmental aspects. The University of Texas at Austin, Bureau of Economic Geology, Report of Investigations No. 90.

Klemt, W.B., G.L. Duffin, and G.R. Elder, 1976. Ground-water resources of the Carrizo aquifer in the Winter Garden area of Texas, Volume 1: Texas Water Development Board, Report 210.

Kreitler, C.W., 1979. Ground-water hydrology of depositional systems, *in* Galloway, W.E., and others, Depositional and ground-water flow systems in the exploration for uranium, a research colloquium. The University of Texas at Austin, Bureau of Economic Geology.

Kuiper, L.K., 1985. Documentation of a numerical code for the simulation of variable density ground-water flow in three dimensions. U.S. Geological Survey, Water-Resources Investigations Report 84-4302.

LBG-Guyton Associates and HDR Engineering Inc., 1998. Interaction between ground water and surface water in the Carrizo-Wilcox aquifer.

Mace, R.E., R.C. Smyth, L. Xu, and J. Liang, 2000a. Transmissivity, hydraulic conductivity, and storativity of the Carrizo-Wilcox Aquifer in Texas, The University of Texas at Austin, Bureau of Economic Geology Final Report submitted to the Texas Water Development Report, 76p.

Mace, R.E., A.H. Chowdhury, R. Anaya, and S.C. Way, 2000b. Groundwater availability of the Middle Trinity aquifer in the Hill Country area of Texas – Numerical simulations through 2050: Texas Water Development Board Report, 174p.

Maidment, D.R., 1992. Handbook of Hydrology. McGraw-Hill, Inc.

Mason, C.C., 1960. Geology and ground-water resources of Dimmit County, Texas. Texas Board of Water Engineers, Bulletin 6003.

McDonald, M.G., and A.W. Harbaugh, 1988. A modular three-dimensional finite-difference ground-water flow model. U.S. Geological Survey, Techniques of Water-Resources Investigations, book 6, chapter A1.

McKee, T.B., N.J. Doesken, and J. Kleist, 1993. The relationship of drought frequency and duration to time scales. Preprints, 8th Conference on Applied Climatology, 17-22 January, Anaheim, CA, pp. 179-184.

Moulder, E.A., 1957. Development of Ground Water from the Carrizo Sand and Wilcox Group in Dimmit, Zavala, Maverick, Frio, Atascosa, Medina, Bexar, Live Oak, McMullen, La Salle, and Webb counties, Texas. USGS Open-File Report.

Opfel, W.J., and G.R. Elder, 1978. Results of an infiltration study on the Carrizo Sand outcrop in Atascosa County, Texas. Texas Department of Water Resources, LP-61.

Payne, J.N., 1975. Geohydrologic significance of lithofacies of the Carrizo Sand of Arkansas, Louisiana, and Texas and the Meridian Sand of Mississippi: U.S. Geological Survey Professional Paper, P 0569-D, 11p.

Pearson, F.J., Jr., and D.E. White, 1967. Carbon 14 ages and flow rates of water in Carrizo Sand, Atascosa County, Texas, Water Resources Research, Vol. 3, No. 1, p. 251-261.

Prudic, D.E., 1988. Documentation of a computer program to simulate stream-aquifer relations using a modular, finite-difference, ground-water flow model, U.S. Geological Survey, Open-File Report 88-729, Carson City, Nevada.

Prudic, D.E., 1991. Estimates of hydraulic conductivity from aquifer-test analyses and specific capacity data, gulf coast regional aquifer systems, south-central United States., U.S. Geological Survey, Water- Resources Investigation Report 90-4121, Austin, Texas.

Ritchey, J.D. and J.O. Rumbaugh, 1996. Subsurface fluid flow (ground-water and vadose zone) modeling. ASTM Special Technical Publication 1288.

Ryder, P.D., 1988. Hydrogeology and Predevelopment Flow in the Texas Gulf Coast Aquifer Systems. USGS Water-Resources Investigations Report 87-4248.

Ryder, P.D., and A.F. Ardis, 1991. Hydrology of the Texas Gulf Coast aquifer systems. U.S. Geological Survey, Open-File Report 91-64.

Sandeen, W.M., 1987. Ground-water resources of Rusk County, Texas: Texas Water Development Board Report 297, 121 p.

Scanlon, B.R., A. Dutton, and M. Sophocleus, 2002. Groundwater recharge in Texas.

Shafer, G.H, 1965. Ground-water resources of Gonzales County, Texas. Texas Water Development Board, Report 4

Slade, R.M., Jr., J.T. Bentley, and D. Michaud, 2002. Results of streamflow gain-loss studies in Texas, with emphasis on gains from and losses to major and minor aquifers, Texas, 2000. U.S. Geological Survey, Open-File Report 02-068.

Texas Water Development Board (TWBD), 1972. Survey of the subsurface saline water of Texas, Report 157.

Texas Water Development Board (TWBD), 1997. Water for Texas, A Consensus-Based Update to the State Water Plan, Volume II, Technical Planning Appendix, August 1997, Document No. GP-6-2.

Texas Water Development Board (TWBD), 2002. Water for Texas – 2002, January, 2002, 155 p.

Theis, C.V., 1940. The source of water derived from wells - essential factors controlling the response of an aquifer to development: Civil Engineering, American Society of Civil Engineers, p. 277-280.

Thompson, G.L., 1972. Ground-water resources of Navarro County, Texas: Texas Water Development Board Report 160, 63 p.

Thorkildsen, D, R. Quincy, and R. Preston, 1989. A digital model of the Carrizo-Wilcox aquifer within the Colorado River Basin of Texas. Texas Water Development Board, Report 332.

Thorkildsen, D., and Price, R.D., 1991. Ground-water resources ff the Carrizo-Wilcox aquifer in the Central Texas Region: Texas Water Development Board Report 332, 59p.

Turner, S.F., T.W. Robinson, and W.N. White., revised by D.E. Outlaw, W.O. George, and others, 1960. Geology and Ground-Water Resources of the Winter Garden District Texas, 1948. USGS Water-Supply Paper 1481.

Warren, J.E., and H.S. Price, 1961. Flow in heterogeneous porous media, Society of Petroleum Engineers Journal, Vol. 1, p. 153-169.

White, D.E., 1973. Ground-water resources of Rains and Van Zandt counties, Texas. Texas Water Development Board, Report 169.

White, W.N., and O.E. Meinzer, 1931. Ground-Water in the Winter Garden and Adjacent Districts in Southwestern Texas. USGS Open-File Report.

Williams, T.A., and A.K. Williamson, 1989. Estimating water-table altitudes for regional ground-water flow modeling. U.S. Gulf Coast: National Water Well Association, Ground Water, v. 27, no. 3, p. 333-340.

Williamson, A.K., H.F. Grubb, and J.S. Weiss, 1990. Ground-water flow in the Gulf Coast aquifer systems, South Central United States – A preliminary analysis. U.S. Geological Survery, Water-Resources Investigations Report 89-4071.

Wilson, T.A., and R.L. Hossman, 1988. Geophysical well-log data base for the gulf coast aquifer systems, south-central United States. U.S. Geological Survey, Open-File Report 87-677.